EMISSION CROSS-SECTIONS OF N_2 IN THE VACUUM ULTRAVIOLET BY ELECTRON IMPACT

by

Joseph Michael Ajello

EMISSION CROSS-SECTIONS OF N_2 IN THE

VACUUM ULTRAVIOLET BY ELECTRON IMPACT

by

Joseph Michael Ajello

B.S., Southwestern at Memphis, 1962

M.S., Rensselaer Polytechnic Institute, 1964

A thesis submitted to the Faculty of the Graduate School

of the University of Colorado in partial fulfillment of

the requirements for the degree of

Doctor of Philosophy

Department of Astro-Geophysics
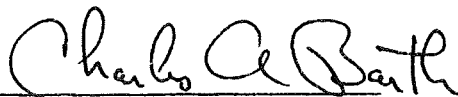
1969

This Thesis for the Doctor of Philosophy Degree by

Joseph Michael Ajello

has been approved for the

Department of

Astro-Geophysics

by

_____
Charles A. Barth

_____
Gordon Dunn

_____
T. W. Speiser

_____
A. Ian Stewart

_____
Manfred Rees

_____
Gary Thomas

Date Oct 22, 1969

Ajello, Joseph Michael (Ph.D., Astro-Geophysics)

Emission Cross-Sections of N_2 in the Vacuum

Ultraviolet by Electron Impact

Thesis directed by Professor Charles A. Barth

An electron beam excitation chamber was designed and con-
structed for the measurement of emission cross-sections by electron
impact excitation of gases. The electron beam excitation spectrum
of N_2 at low pressure (0.12 microns to 0.18 microns) in the wave-
length range 1200 Å to 2000 Å was recorded for monoenergetic
electron impact energies from 10 eV to 208 eV. The spectral fea-
tures observed were the Lyman-Birge-Hopfield vibrational transi-
tions $(a^1\Pi_g \rightarrow X^1\Sigma_g^+)$ and several atomic nitrogen lines produced by
dissociative excitation of N_2. The radiation detection system con-
sisted of a McPherson 218 monochromator and a 541 G-08-18 EMR
photomultiplier.

The emission cross-sections of the vibrational transitions of the
$a^1\Pi_g$ state of molecular nitrogen were measured. The transition is
predominantly magnetic dipole. The emission cross-sections of the
vibrational transitions were summed to give total emission cross-
sections for each of the first seven vibrational levels and for the
total electronic transition. The measured cross-sections were

apparent cross-sections, uncorrected for cascading   The peak cross-section was at 15.5 ± 1.5 eV and had a value of 3.85×10^{-17} cm^2 for the total electronic transition. The maximum cascade contribution was estimated to be 29%. The actual cascade contribution was probably much less.

The geometrical problem of determining the fraction of the Lyman-Birge-Hopfield (LBH) spontaneous radiation detected was solved. An N$_2$ molecule excited to a vibrational level of the $a^1\Pi_g$ state can travel several centimeters before radiating, because of the long lifetime of the state (80 microseconds).

The atomic nitrogen transitions studied were the multiplets at 1200 Å ($^4P \rightarrow {}^4S^o$), 1493 Å ($^2P \rightarrow {}^2D^o$) and 1743 Å ($^2P \rightarrow {}^2P^o$). These transitions in atomic nitrogen were caused by dissociative excitation of molecular nitrogen, one of the products being an excited nitrogen atom in a ^4P or ^2P state. The transitions were permitted electric dipole transitions. The emission cross-sections of these multiplets of atomic nitrogen were measured. The cross-sections typically had two thresholds, one at about 20 eV due to dissociative excitation of N$_2$ into two nitrogen atoms, and the other at about 35 eV because of dissociative ionization excitation of N$_2$ into a nitrogen atom and a once ionized nitrogen atom. The sum of the two types of dissociative excitation cross-sections was the measured quantity. The peak cross-section for these dissociatively excited transitions was at about 110 eV.

The results of the experiment were applied to the photoelectron excited dayglow and to the aurora to determine emission rate factors.

This abstract is approved as to form and content.

I recommend its publication.

_____
Faculty member in charge of thesis

ACKNOWLEDGEMENT

TABLE OF CONTENTS

List of Tables

List of Figures

CHAPTER I

INTRODUCTION

1.1 Historical Review

The Lyman-Birge-Hopfield $(a\,^1\Pi_g \longleftrightarrow X\,^1\Sigma_g)$ band system of nitrogen extends from 1200 Å to 2600 Å. It was first observed in emission by Lyman (1911) in a high voltage discharge lamp. It was later identified as a new band system by Birge and Hopfield (1928). Herzberg (1946) has shown the upper state must be $^1\Pi_g$, and the transition must be permitted by magnetic dipole selection rules. It has since been studied under high resolution by Loftus (1956) and Wilkinson and Mulliken (1957), who found the presence of quadrupole lines (S and O branches). The electric quadrupole contribution to the intensity was estimated to be about 13% of the total.

In 1965, McEwen measured the relative intensities of the bands of the Lyman-Birge-Hopfield (LBH) system. The results showed the electronic transition moment is a constant over the band system. Thus, the band strengths are directly proportional to the Franck-Condon factors for the band system. Franck-Condon factors for the LBH system were calculated

numerically, using Rydberg-Klein-Rees potential functions, by
Benesch, Vanderslice, Tilford and Wilkinson (1966), and by Zare,
Larsson and Berg (1965).

One of the first measurements of the lifetime of the LBH
state was made by Lichten (1957). He used a collimated molec-
ular beam, a small fraction of which had been excited by an elec-
tron beam. The excited molecules struck a moveable detector and
ejected electrons. The number emitted varied as a function of
distance. The distance function was used to calculate an average
lifetime of the various states. The lifetime was 170 microseconds.
In a similar experiment, Olmstead, Newton and Street (1965) ob-
tained a lifetime of 120 microseconds.

More recently, Ching, Cook and Becker (1967) have used
absorption measurements of N_2 to determine absorption band os-
cillator strengths, $f_{v''=0,v'}$ for the LBH system. Their results in-
dicate a lifetime of approximately 37 microseconds. Holland (1969),
in an electron beam excitation experiment, measured the total in-
tensity of the LBH band system versus distance from an electron
beam with a photometer and obtained a lifetime, uncorrected for
slow cascade, of 80 microseconds.

Holland also measured excitation cross-sections from 100
eV to 2 keV for the LBH band system. Possible electronic transi-
tions that might cascade to the LBH state and contribute to the

apparent cross-section are the $^1\Sigma_u^+$ and $^1\Pi_u \longleftrightarrow a^1\Pi_g$ transitions. Both are permitted electric dipole transitions.

Direct excitation of the $a^1\Pi_g$ transition by electrons, in an inelastic scattering experiment, has been observed by Lassettre and Krasnow (1964). By measuring the small angle inelastic scattering of electrons, the generalized oscillator strength for the LBH transition was determined at an accelerating voltage of 522 eV. Recently, Lassettre, Skerbele and Meyer (1966), and Lassettre, Skerbele, Dillion and Ross (1968) made a thorough study of excitation of the $a^1\Pi_g$ vibrational levels by observing at various scattering angles, the energy loss of a primary electron beam and found no change in the relative intensity of the vibrational levels of the $a^1\Pi_g$ state from 60 eV to 400 eV. Furthermore, the probabilities for direct excitation of the vibrational levels of the $a^1\Pi_g$ state were directly proportional to the (v',o) Franck-Condon factors.

A 'first principles' approach to the inelastic cross-section of the $a^1\Pi_g$ state of molecular nitrogen was a basic quantum mechanical calculation made by Rozsnyai (1967). He investigated inelastic electron scattering using the first Born approximation for homonuclear diatomic molecules. Two transitions in molecular nitrogen were investigated: the optically allowed $^1\Sigma_g \rightarrow {}^1\Pi_u$ (Birge-Hopfield) transition, and the optically forbidden $^1\Sigma_g \rightarrow {}^1\Pi_g$ (Lyman-Birge-Hopfield) transition. Both transitions involved a general type $\sigma \rightarrow \pi$ molecular orbital transition.

Another approach to inelastic cross-sections has been via the Born approximation at high energies and the modified Born approximation at low energies. Green and Barth (1965) and Stolarski et al. (1967) have calculated nitrogen excitation and ionization cross-sections in an attempt to organize systematically inelastic cross-sections for atmospheric computations. For example, they used the generalized oscillator strengths of Lassettre and Krasnow (1964) and phenomenological empirical formulas to obtain high energy cross-sections for the LBH transition. It was interesting to note that their calculated cross-sections differed by about a factor of 2 at 522 eV. This might have been due to the necessity of extrapolating the generalized oscillator strengths to scattering angles beyond the 3° to 10.5° measurement of Lassettre and Krasnow. At high energy (100 eV or greater) their formulation of excitation cross-sections for permitted transitions, reduced to the familiar $1/\epsilon \ln \epsilon$ dependence of the Born approximation (where ϵ is the incident electron energy). However, any extrapolation to low energies by empirical formula can be a hazardous procedure, especially for a forbidden transition such as the $a\,^{1}\Pi_{g}$ transition.

The low energy region is extremely important, since virtually all the photoelectron excitation of the atmospheric species in

the dayglow occurs between the threshold for the process and 60 eV. The photoelectrons are produced by solar XUV ionization of the atmospheric constituents. The ejected photoelectrons initially have a kinetic energy equal to the solar photon energy minus the ionization potential. Similarly in the aurora, the major part of the excitation of neutral species occurs in the low energy region by the secondary electrons. The secondary electrons are produced by ionization of the neutral species by the primary electrons in inelastic collisions, resulting in the ejection of electrons. For example, Green and Barth (1965) found that an incident primary auroral flux of electrons at 30 keV can produce 262 secondaries with an average secondary energy of 87.6 eV. This, coupled with the fact that inelastic cross-sections peak at about 2 to 4 times threshold and fall by factors of 3 to 50 at primary auroral electron energies, illustrate the importance of knowing low energy excitation cross-sections.

In the last few years, the advances in instrument equipped rockets and satellites has led to direct observations of the aurora and the dayglow, and to measurements of the atmospheric composition and temperature. These data, combined with solar XUV flux measurements (Hinteregger, Hall and Schmidtke, 1964), electron energy distributions in the aurora (Westerlund, 1968 and Rees, 1969) and electron energy distributions in the dayglow (Dalgarno, McElroy and Stewart, 1969) make it possible to propose theories of the

electron excited dayglow and aurora. In both the dayglow and the

aurora, the volume emission rate of the i-th transition of the k-th

molecular species of number density n_k may be written,

$$I_{ik}(z) = n_k(z) \, g_{ik}(z) \, \frac{photons}{cm^3 \; sec} \, , \qquad (1.1)$$

where:

I_{ik} is the volume emission rate at altitude z of the i-th

         transition of the k-th species,

g_{ik} is the emission rate factor–it directly relates the volume

         emission rate of an individual emission to the volume

         density of the emitter.

For excitation by photoelectrons or auroral electrons, g_{ik} may be

written as,

$$g_{ik}(z) = \int_{\epsilon_T}^{\infty} \Phi(\epsilon,z) \, Q_{ik}(\epsilon) \, d\epsilon \; \frac{photons}{sec \; molecule} \, , \qquad (1.2)$$

where:

ϵ_T is the threshold energy for process i in eV,

$\Phi(\epsilon,z)$ is the steady-state differential electron flux at altitude

         z and energy ϵ in units of electrons/sec cm^2 eV,

$Q_{ik}(\epsilon)$ is the emission cross-section of the i-th transition of

         species k in units of cm^2. (The emission cross-section

         is the cross-section for excitation to a level or state un-

         corrected for cascading).

Thus, in order to make this calculation, to compare theory with rocket and satellite measurements of electron excited atmospheric phenomena quantitatively, and to determine the energy deposition of electrons into the atmosphere, there is a need to have laboratory measurements of emission cross-sections. The expression for g_{ik} is actually the number of excitations per molecule per second. Since there is negligible deactivation in the region of interest (120 km to 300 km) for atmospheric electron excited spectral emissions of N_2 in the vacuum ultraviolet, except for the Vegard-Kaplan transition, the expression for g_{ik} is necessarily equal to the emission per molecule per second. In the case of the dayglow, the emission rate factor is a function of the solar zenith angle and the solar cycle, in addition to altitude, since the photoelectron flux is determined primarily by the intensity and the depth of penetration of the solar XUV radiation into the atmosphere. In the dayglow there are also other mechanisms for excitation of the atmospheric species, including resonant and fluorescent scattering, chemical and ionic reactions and photodissociative excitation.

Consider the ultraviolet aurora. The most prominent molecular emission features consist of the Lyman-Birge-Hopfield band system, with the most intense bands at 1325 Å, 1353 Å and 1383 Å, the (4,0), (3,0) and (2,0) bands, respectively (Barth, 1968). The process is very simple,

$$N_2 + e \rightarrow N_2^* + e \quad (\text{direct excitation and cascade}), \quad (1.3)$$

followed by,

$$N_2^* \rightarrow N_2 + h\nu_{LBH} ,$$ (1.4)
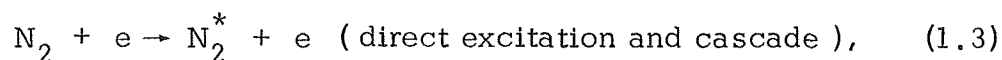
Where N_2^* refers to a nitrogen molecule, electronically excited to a

particular vibrational energy level of the LBH state.

The calculation of the emission rate of the LBH transition is

determined by Eqns. 1.1 and 1.2 and involves a knowledge of in-

elastic cross-sections of electrons for nitrogen molecules from

threshold to about 10 keV.

Barth (1968) has made a calculation of the electron impact

excitation of the auroral spectrum between 1200 Å and 1500 Å.

By considering 4 keV monoenergetic electrons impinging on the

atmosphere, and using empirical cross-sections, a comparison of

theory and the atmospheric measurement of Fastie (1967) was made.

The predicted intensities were higher than the rocket measured in-

tensities by factors of 2 to 6.

At the time of Barth's calculation, it was assumed that the

intense atomic nitrogen lines of the aurora, at 1200 Å, 1493 Å and

1743 Å, were caused by direct excitation of atomic nitrogen of

atmospheric abundance of about 0.1%. The predicted intensities

were too low by factors of 2 to 4. The reason for this discrepancy

was that the excitation mechanism assumed is less important than

a dissociative excitation mechanism, whose excitation cross-section

was measured in this experiment. This was one of the most impor-

tant results of the experiment.

The excitation mechanism is,

$$N_2 + e \rightarrow N^* + N + e \text{ (direct excitation + cascade)}, \quad (1.5)$$

and

$$N_2 + e \rightarrow N^* + N^+ + 2e , \quad (1.6)$$
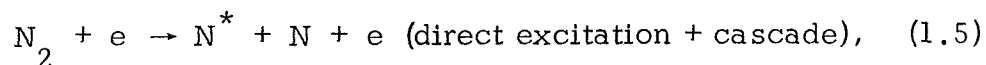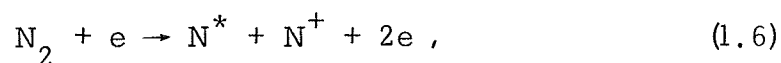
where N^* refers to electronically excited nitrogen. Eqn. 1.5 is a dissociative excitation process and Eqn. 1.6 is a dissociative ionization excitation process.

The emission mechanism is

$$N^* \rightarrow N + h\nu_{1200, 1493, \text{ or } 1743} . \quad (1.7)$$
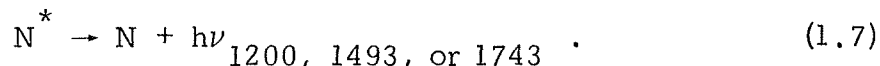
In the atmosphere, the emission rate of these atomic nitrogen multiplets is determined by Eqns. 1.1 and 1.2, where the emission cross-section is the total dissociative excitation cross-section. It is determined by adding the emission cross-section for dissociative excitation and the emission cross-section for dissociative ionization excitation for each transition.

In the dayglow, the atomic nitrogen lines emission are caused by photoelectrons. In addition, it is possible there may be a contribution by photodissociative excitation of molecular nitrogen. The cross-section for this process has not been measured. It is also of interest to point out that the dissociative excitation of molecular

nitrogen provides a minor source of atomic nitrogen atoms in the

upper atmosphere in the region 120 km to 250 km. The major source

probably is dissociative recombination of NO^+ with an electron.

For the LBH bands, the primary excitation mechanism in the day-

glow is photoelectron excitation.

1.2   Experimental Objectives.

It was intended to measure the apparent excitation cross-

section of nitrogen for the Lyman-Birge-Hopfield electronic tran-

sition from 10 eV to 208 eV, thus, extending the cross-section

measurement made by Holland from 100 eV to 2 keV. Cross-

sections are presented for the first seven vibrational levels of the

$a^1\Pi_g$ state and for the total electronic transition of the $a^1\Pi_g$ state.

It was expected that the higher levels would be weak, or absent,

from predissociation (Herman and Herman, 1942). In addition,

excitation functions were measured for each of the LBH vibronic

transitions. This cross-section was the cross-section for ex-

citation to the vibrational level multiplied by the branching ratio.

Furthermore, the apparent cross-section for dissociative

excitation of nitrogen by electrons, leading to the atomic nitrogen

multiplets at 1200 Å, 1493 Å and 1743 Å, were measured. It was

ascertained that two processes contribute to the emission cross-

section of the nitrogen lines. These processes were dissociative

excitation and dissociative ionization excitation. In addition,

the contribution of the (3,3) LBH emission cross-section to the 1493 Å nitrogen line multiplet was determined.

It was established that all of these measurements were made in the range where the measured flux of radiation depended linearly on pressure and electron beam current.

It was necessary to design, construct and calibrate an electron beam excitation chamber, composed of electron gun, electron collector, vacuum system, electronics and vacuum ultraviolet spectrometer. The cross-section was determined by simultaneously monitoring the steady-state ultraviolet radiation (1200 Å to 2000 Å), electron beam current, electron energy and nitrogen pressure. With molecular nitrogen in the flow regime (about 0.1 microns pressure) an electron beam was fired across a chamber, and excited, dissociated, or ionized the nitrogen molecules. The subsequent radiation from the excited nitrogen molecules and nitrogen atoms was monitored by the monochromator and photomultiplier tube. By assuming the excitation per unit length of the beam equaled the emission per unit length, and that all processes are linear with pressure and electron beam current, the emission cross-section was determined. Because of the long lifetime (80 microseconds) of the LBH state, account was made for the fraction of excited molecules that diffused out of the field of view.

The application of these measurements to the electron excited dayglow and aurora is discussed.

1.3   A Summary of the Presentation.

In Chapter II the design and construction of the electron beam excitation chamber is described. The necessity to build a large excitation chamber, using a monochromator with a fast optical system, capable of measuring the emission cross-sections of the nitrogen multiplets, as well as the emission cross-section of the LBH transition, which is a magnetic dipole transition, prompted the design.

In Chapter III the calibration technique for the optical system is discussed. The calibration results for the separate parts of the optical system--the photomultiplier, the monochromator and the lithium fluoride window, are presented.

In Chapter IV the theory of the electron beam excitation of N_2 is discussed. The various reactions that occur when an electron beam is incident on a neutral nitrogen gas at low pressure are summarized. In addition, the geometrical and physical factors determining the fraction of the emitted radiation from the excited nitrogen atoms and molecules detected are discussed.

In Chapter V the experimental results are presented. First, the preliminary measurements that determine the range of electron beam currents and molecular nitrogen pressures, for

which the measured flux of radiation is linear in these two parameters, are summarized. Secondly, the observational technique and experimentally derived emission cross-sections as a function of energy are presented.

In Chapter VI the results are applied to the atmosphere. Emission rate factors are determined for the LBH band system and the atomic nitrogen multiplets in the electron excited dayglow as a function of altitude, and in the auroral oval at 150 km.

CHAPTER II

INSTRUMENTATION

2.1   Introduction

The instrumentation for this experiment consisted basically
of a source, the electron beam excitation chamber, and a detector,
the monochromator with photomultiplier. Each was designed accord-
ing to the specific needs of this particular experimental problem.
It was necessary to build the electron beam chamber so that the
characteristic lengths in the chamber were larger than the distance
a nitrogen molecule, excited to the Lyman-Birge-Hopfield state,
would travel before radiating. With the lifetime of the order of
80 microseconds, and a gas temperature of 293 °K, an excited
molecule could travel about two inches before radiating. Since
the interaction of excited molecules with walls was unknown, walls
had to be placed out of the interaction region. This requirement
was met by providing a six-inch electron beam in a cylindrical
chamber eight inches in diameter. The atomic nitrogen lines, being
permitted electric dipole transitions, did not have this problem but
could be studied with this particular design. The ultraviolet radi-
ation of the Lyman-Birge-Hopfield band system was confined to a
glow region around the beam, whose intensity fell off a little faster

than 1/r, where r is the distance from the electron beam. See the calculation of the glow distribution in Chapter IV. It was obvious from these considerations that it was desirable to have a fast optical system of very low f number in order to collect as much of the radiation as possible. For this reason, it was decided to use the McPherson 218 monochromator of f/5.3. Furthermore, studies in the vacuum ultraviolet required the use of vacuum systems so that the monochromator could be kept at very low pressure. This was due to the fact that air is very opaque to radiation in the wavelength region less than 2000 Å.

2.2   The Electron Beam Excitation Chamber and Vacuum System.

The electron beam excitation chamber was cylindrically shaped and made of stainless steel. It is shown in Figures 2.1 and 2.2. A complete description of the excitation chamber is given in Appendix A.

2.3   The Vacuum System.

The vacuum system is displayed in Figure 2.3. It consists essentially of a liquid nitrogen baffled diffusion pump and forepump. The ultimate pressure obtainable in the system was 8×10^{-8} torr without the electron gun in operation and 1×10^{-7} torr with the gun in operation. The chamber was submitted to a mild bakeout before each experimental use by a heating coil.

4½" OD CONFLAT FLANGE

'C' VALVE

2" ELBOW UNFLANGED

½ OD × .049 × 8 TUBE

2¼ OD CONFLAT ROT. FLANGE

8 WIRE FEEDTHRU

8" OD × .120 WALL × 8" TUBE

10" OD CONFLAT FLANGE

10" OD CONFLAT BLANK

MILLITORR NUDE GUAGE

UHV NUDE GUAGE

4½ OD FLANGE BLANK

2½ VIEW PORT

4½" OD CONFLAT FLANGE

4½" OD CONFLAT ROT. FLANGE

ADAPTER, MCPHERSON FLANGE

2" L VALVE

DUAL RANGE IG CONTROLLER

AUTOMATIC PRESSURE CONTROLLER

2" PUMPING STATION

WALLACE & TIERNAN GUAGE

ELECTRON BEAM EXCITATION CHAMBER & PUMPING STATION

FIGURE 2.1
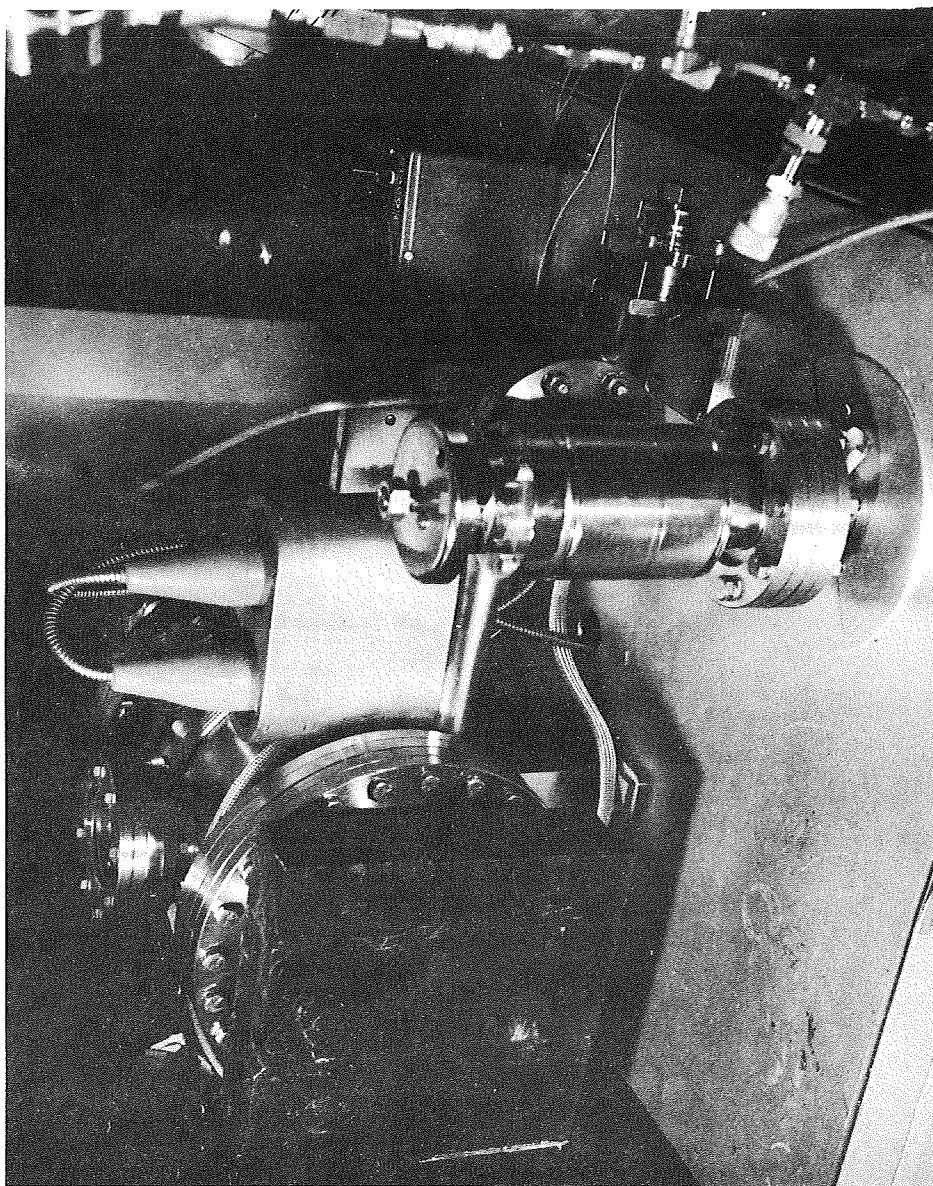
FIG. 2.2 THE ELECTRON BEAM EXCITATION CHAMBER
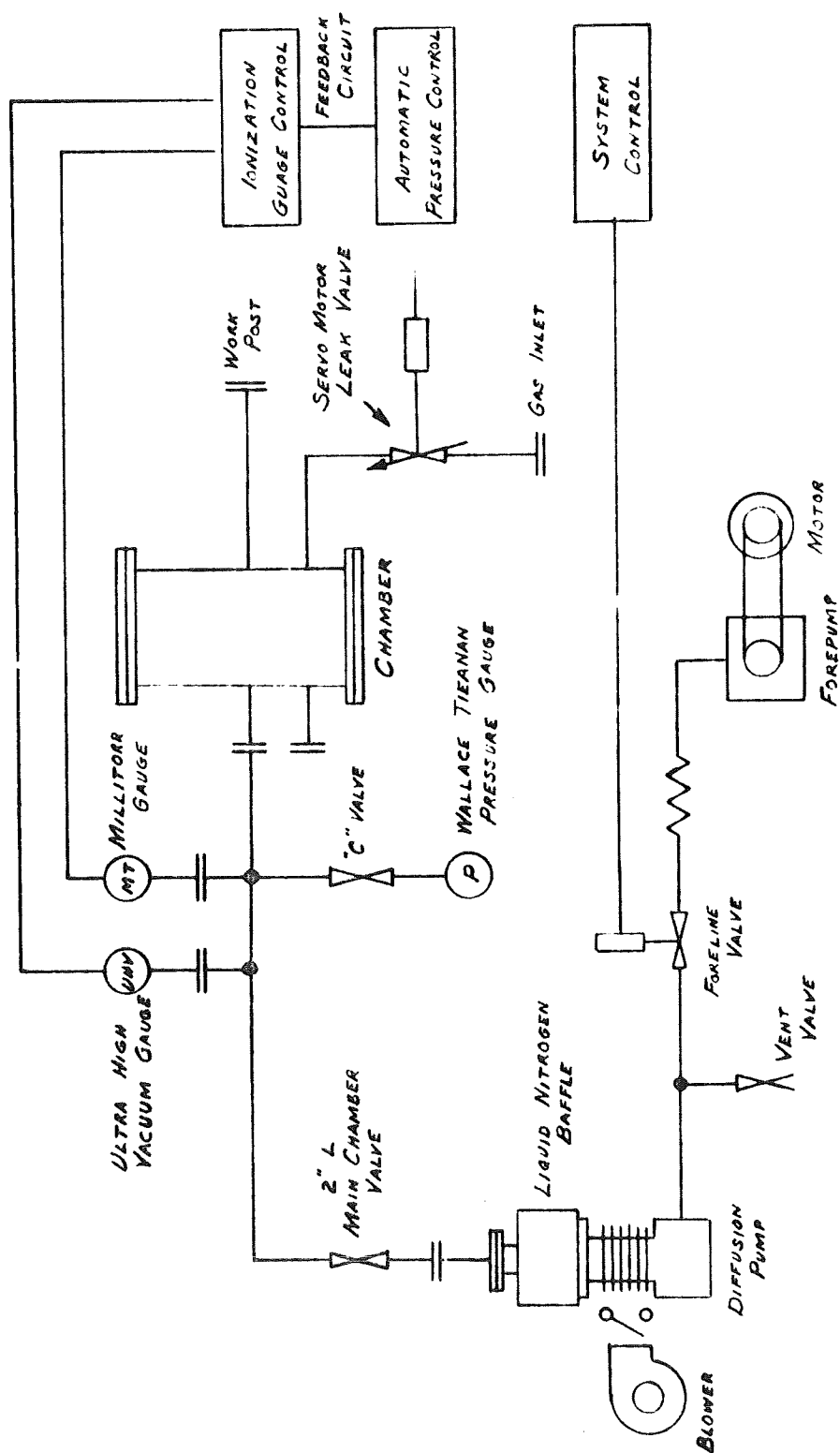
ELECTRON BEAM EXCITATION
CHAMBER VACUUM SYSTEM

FIGURE 2.3

2.3.1 The Pumping System.

The pumping system was a Granville Phillips 2 inch, series 225, ultra-high vacuum pumping station. It consisted of a 2 inch diffusion pump and mechanical fore-pump. The diffusion pump was air cooled and had a cyrosorb cold trap to prevent any back-streaming of oil. The trap was automatically filled by a Delta Engineering automatic liquid nitrogen controller.

2.3.2 The Gate Valve.

The gate valve was a 2 inch gold seal ultra-high vacuum valve. It was manually operated and had a maximum conductance of 60 liters/sec and a minimum conductance of 10^{-13} liters/sec.

2.3.3 Pressure Measuring Instrumentation.

The pressure in the chamber was monitored with a dual range ionization gauge and control unit. For high pressure, a millitorr nude gauge read from 1×10^{-5} torr to 1 torr. For low pressure, a Varian ultra-high vacuum gauge read from 2×10^{-11} torr to 10^{-3} torr.

During the experiment the millitorr gauge was used to monitor the pressure. It was operated at very low emission currents (11 microamps) and produced electron paths of very short lengths. The electrons collided with the gas molecules and produced ions, which were collected and indicated the pressure. The millitorr gauge was calibrated for nitrogen gas molecules by Ball Brothers

Research Corporation of Boulder, Colorado, using a mercury

McLeod gauge; absolute pressures were given at seven points be-

tween 10^{-5} torr and 10^{-1} torr. The effect of thermal transpiration

did not enter into the pressure measurement. The instrument was

calibrated with the same geometrical configuration of gauge and

chamber as used in the experiment. The McLeod gauge measured

the pressure in the chamber and determined the absolute pressure

calibration for the millitorr gauge. Even though the nipple that

contained the millitorr gauge became approximately 4 0°C warmer

than the gas in the chamber, the effect of thermal transpiration

was not transferred into the measurement. It was found necessary

to magnetically shield the ionization gauges from the magnetic

plates used to guide the electron beam. The magnetic shield was

not used in the calibration, since the imposed magnetic field of

the magnetic plates was not present. Tests were run to insure

that the pressure readings were the same under conditions of no

imposed magnetic field and no magnetic shield to conditions of an

imposed magnetic field and a magnetic shield. The shield was

manufactured by Perfection Mica Corporation of Chicago, Illinois.

The magnetic shield was made of conetic material, 0.060 inches

thick and could attenuate the 160 gauss field to less than 1 gauss

inside the gauge. Without the shield, pressure readings were 30%

too high under conditions of the imposed magnetic field of the mag-

netic plates.

2.3.4 Automatic Pressure Controller.

An automatic pressure controller, manufactured by Granville Phillips Corporation, was used for precise control of the gas pressure in the chamber. The automatic pressure controller (APC) was an electro-mechanical instrument designed to regulate automatically the gas pressure in a system. When combined with a pressure transducer, the APC could accurately maintain the gas pressure by automatically and continuously admitting the gas to a dynamic system to compensate for gas being removed by pumps. The millitorr gauge output (0 to 100 millivolts) served as the transducer. The APC constantly monitored the signal from the ionization gauge and subtracted it from the control point desired; thus, providing an error signal to either open, close, or maintain the valve opening in the leak valve between the chamber and the gas source.

2.4 The Electron Gun and Electron Collector.

2.4.1 The Electron Gun.

The electron gun used in this experiment is shown in Figure 2.4. It was provided by Superior Electronics Corporation of Clifton, New Jersey, who modified their SE-63M gun design for use in this experiment. The electrodes were made of stainless steel, .005 inches thick and 5/8 inch diameter. The electrodes were rigidly maintained in place by an insulated ceramic mounting rod. The
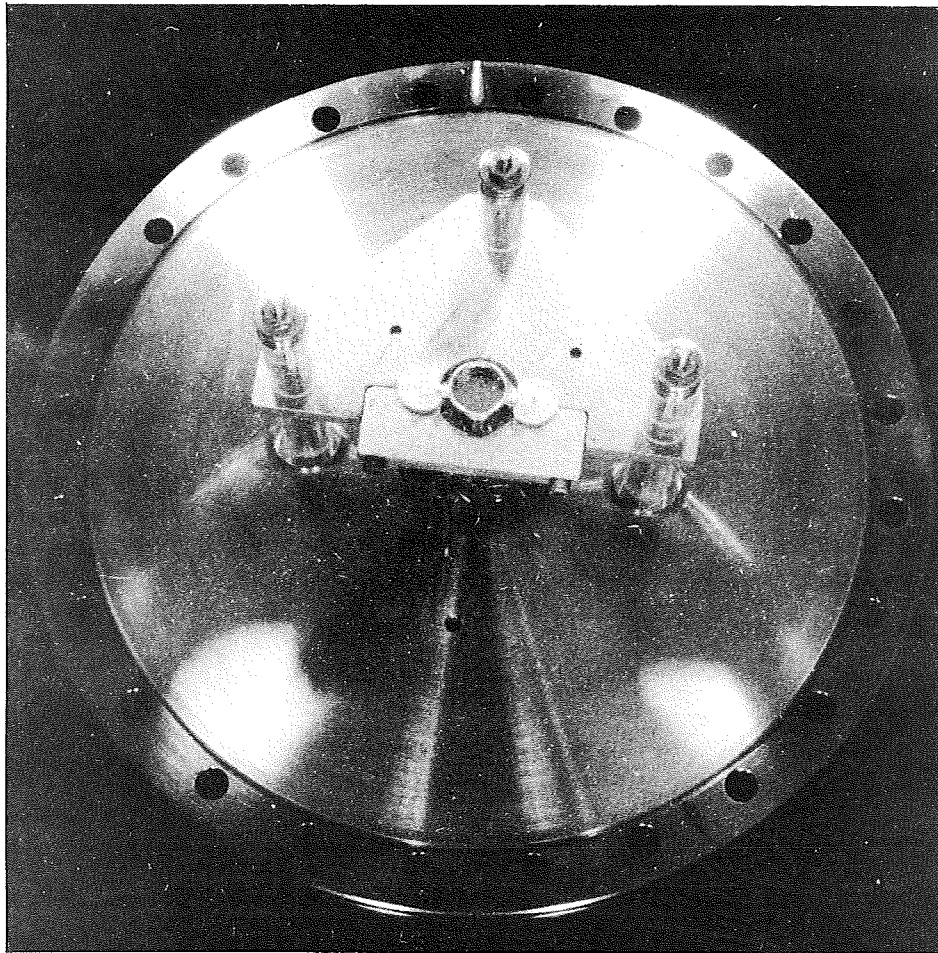
FIG. 2.4   THE ELECTRON GUN

entire assembly was fastened to a stainless steel plate, which kept the electron gun apertures on the center line of the chamber. The coaxially mounted electrodes consisted of an anode, a current control grid, and the cathode. The holes in the electrodes were 1 mm in diameter. Each electrode was spaced about .008 inches apart. Two types of cathodes were used. One was an indirectly heated nickel oxide coated cathode, and the other was a directly heated thoriated tungsten cathode. The nickel oxide coated cathode had to be activated in a high vacuum. During the exhaust pumping of the electron gun, it was necessary to employ a schedule of various applied voltages to the heater of the tube and the electrodes. The purpose of applying this power was to heat the cathode through a cycle which accomplishes the following items:

(1)   Chemically decompose the carbonates to oxides

        with the release of CO_2.

(2)   Start a reaction between the oxides and the materials in

        the cathode base nickel to reduce the oxides and create

        free alkaline earch materials (barium, strontium, and

        calcium). It is the availability of the first two ele-

        ments which causes the phenomenon of electron emission.

While the above processes were carried out, the vacuum system was pumped rapidly enough to remove the by-products of the reaction, as well as outgassing material. The voltage on the heater was gradually increased until a rapid evolution of gases

was noted by a sharp increase in pressure. This was the so-called activation region and the voltage increments thence must be applied slowly enough to maintain a high vacuum (5 x 10^{-6} torr or less). After passing through the activation region, the heater voltage was returned to between 6.5 and 7 volts. Voltages were put on the control grids to give the electron beam the desired energy and current.

The measurement of cross-section for energies less than 30 eV was made with the oxide coated cathode. It provided ample electron emission of up to 1 ma. In the experiment, electron beam currents from 25 microamps to 250 microamps were used.

The tungsten gun was used for pressure versus intensity measurements and high energy measurements (30 eV to 208 eV). It did not need to be activated and stabilized readily to pressure changes during the intensity versus pressure measurements. Both types of guns had long lifetimes of 100 hours or more. The electron gun was operated with the anode grounded and the chamber grounded so as to make the interaction region field free. The beam was collimated by a 160 gauss magnetic field provided by two large magnetic plates made of barium ferrite, provided by Bux Shrader Company of Los Angeles. The plates were 8 1/2 inches square and 2 1/4 inches thick and 12 inches apart. The ceramic magnets were epoxy encapsulated for rigidity and epoxied to a

hot rolled steel plate for support on the end flange of the chamber.
Most of the fringing tendency of the field was contained by a horse-
shoe arrangement of hot rolled steel, 1/4 inch thick and 3 inches
wide. The top of the horseshoe was 24 inches above the chamber.
The field lines were intended to be straight at the center of the
chamber and magnet. There was no measurable spreading or curv-
ing of the 1 mm in diameter beam across the 6 inch path length,
as observed by the blue light of the permitted transition of the
first negative bands of N_2^+.

2.4.2   The Electron Beam Collector Cup.

The electron beam collector cup was made of stainless
steel and OFHC copper. It consisted of two parts--a cylindrical
bias plate and a collector cone. The cylindrical bias plate was
2 1/2 inches long and 1/2 inch in diameter. It is desirable to
have a large length to diameter ratio. At the end of the cylinder
was attached a cone of 90° apex angle and a 1/2 inch depth. The
cylinder was normally held at +30v with respect to the grounded
anode and grounded excitation chamber. It served to refocus the
beam to the center of the cone where the electrons were trapped
by the cone which had a +100v potential. The primary electrons
were trapped in the cone by being forced to make a number of
collisions with the surface of the cone, if they were reflected.
The positive potentials also served to collect any ejected

secondaries. When the electrons collided with the copper cone, they penetrated the surface of the metal, the depth of penetration depending on the primary energy. As the result of interactions with the nuclei and electrons in the target material, the electrons lost energy. Some secondaries were ejected from the target by the ionization produced by the primaries. Furthermore, some primary electrons were inelastically scattered back to the surface with lower energy. If either the scattered primaries or ejected secondaries had enough energy to cross the potential barrier of the metal, they may have escaped back into the chamber. Thus, the main reason for the cone was to cause many collisions with the surface and to produce few electrons with enough energy to escape. At very low energies (up to 20 eV) and very high energies (75 eV and greater), few escaping secondaries were ejected. At very low primary energies, the energy of the secondaries was less than the work function of the target. At very high primary energies, the secondaries were produced deep within the target and lost a great deal of energy in collisions. Finally, there were the elastically scattered or reflected primaries (as much as 20% reflection coefficient per collision with a copper surface at 300 eV per collision, [McDaniel, 1964]), the cone caused these reflected primaries to make a number of collisions and minimized any escape into the chamber.

A grounded plate with a hole 1/2 inch in diameter was placed in front of the collector to minimize any field leakage into the interaction chamber. The high charge density of the electron beam also prevented any significant field penetration into the beam.

2.4.3   The Electronics for the Electron Gun and Collector.

The electronics schematic for the electron gun and collector is shown in Figure 2.5.

The dc power supplies were ABC model Kepco-power supplies regulated to 0.05% and with a stability of 3 millivolts. The voltages were monitored with calibrated Hewlett-Packard dc vacuum tube voltmeters, model 412A. The electron beam current was monitored by a Keithly model 602 electrometer. Both the power supplies and the electrometer were capable of operating off ground, since the dc terminals were isolated from the chasis. One leg of the filament was tied to the cathode, which was at a negative potential with respect to the anode. The filament was thus operated at a negative potential close to that of the cathode, preventing any discharge between filament and cathode. The current control grid was operated at a few volts above or below the cathode, depending on the electron beam current desired, which was usually between 50 and 250 microamps. The current going to the anode was about 1 microamp, for accelerating voltages greater than 25 eV, and was of the order of 10 microamps for operating voltages less than 25 eV. This current was due to the mode of emission of the electron gun.

ELECTRONIC SCHEMATIC FOR ELECTRON
GUN & COLLECTOR

P_1 — Filament Pwr. Supply

P_2 — First Grid To Cathode Pwr. Supply

P_3 — First Grid To Anode Pwr. Supply

P_4 — Bias Cylinder To Cone Pwr. Supply

P_5 — Cone To Ground Pwr. Supply

FIGURE 2.5

ELECTROMETER (TO MEASURE ELECTRON BEAM CURRENT)

P_5

P_4

.005 MICA INSULATION

GROUNDED ELECTRON BEAM EXCITATION CHAMBER

FILAMENT

CATHODE

ELECTRON BEAM

MAGNETIC FIELD

GROUNDED PLATE

FIRST GRID

ANODE

ELECTROMETER (TO MEASURE ACCELERATING VOLTAGE)

P_1

P_2

P_3
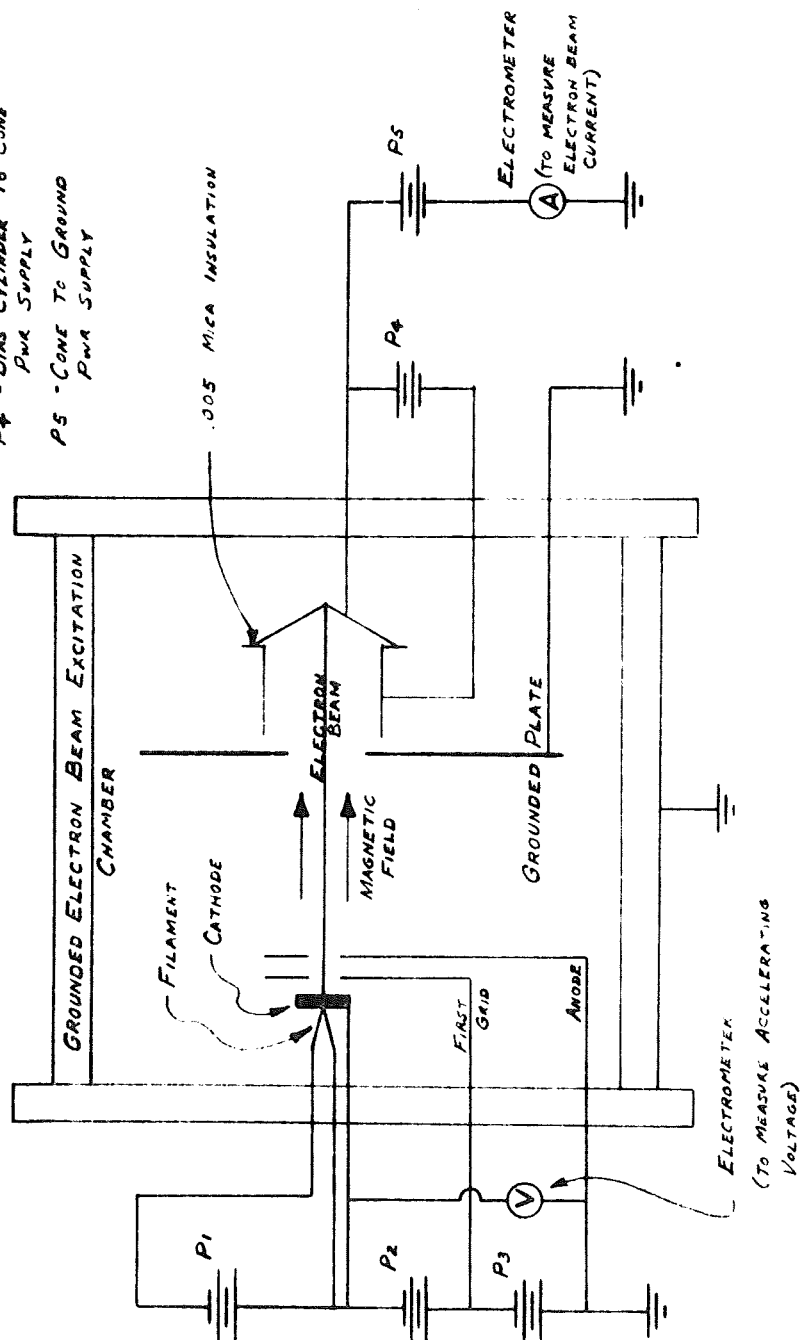
For high accelerating voltages the emission was temperature limited, since the voltages were strong enough to pull off all electrons leaving the cathode. At low voltages, it was space charge limited, since the accelerating voltages were not strong enough to pull off all the electrons. The current going to the grounded plate was less than 1 microamp. Furthermore, it was found that if the collector voltage is decreased below 50 volts, a substantial number of electrons were reflected from the collector as determined by an increase in anode current and a corresponding decrease in collector current. This phenomenon serves as a test for electron collection, since above 50 volts collector cone potential, no change in either collector current or anode current was noted. The anode current can even be 1 or 2 microamps positive corresponding to a small positive ion current.

2.5   The Monochromator.

2.5.1   Description of the Monochromator.

The monochromator used was a McPherson 0.3 meter, f/5.3, plane grating, capable of vacuum or atmospheric scanning. It was designed to operate in the wavelength range of 1050 Å to 16 microns by interchanging snap-in gratings and photomultiplier tubes. It is shown in Figure 2.6. The wavelength range from 1200 Å to 2000 Å was investigated by evacuating the spectrometer with an oil diffusion pump and liquid nitrogen baffle. The optical
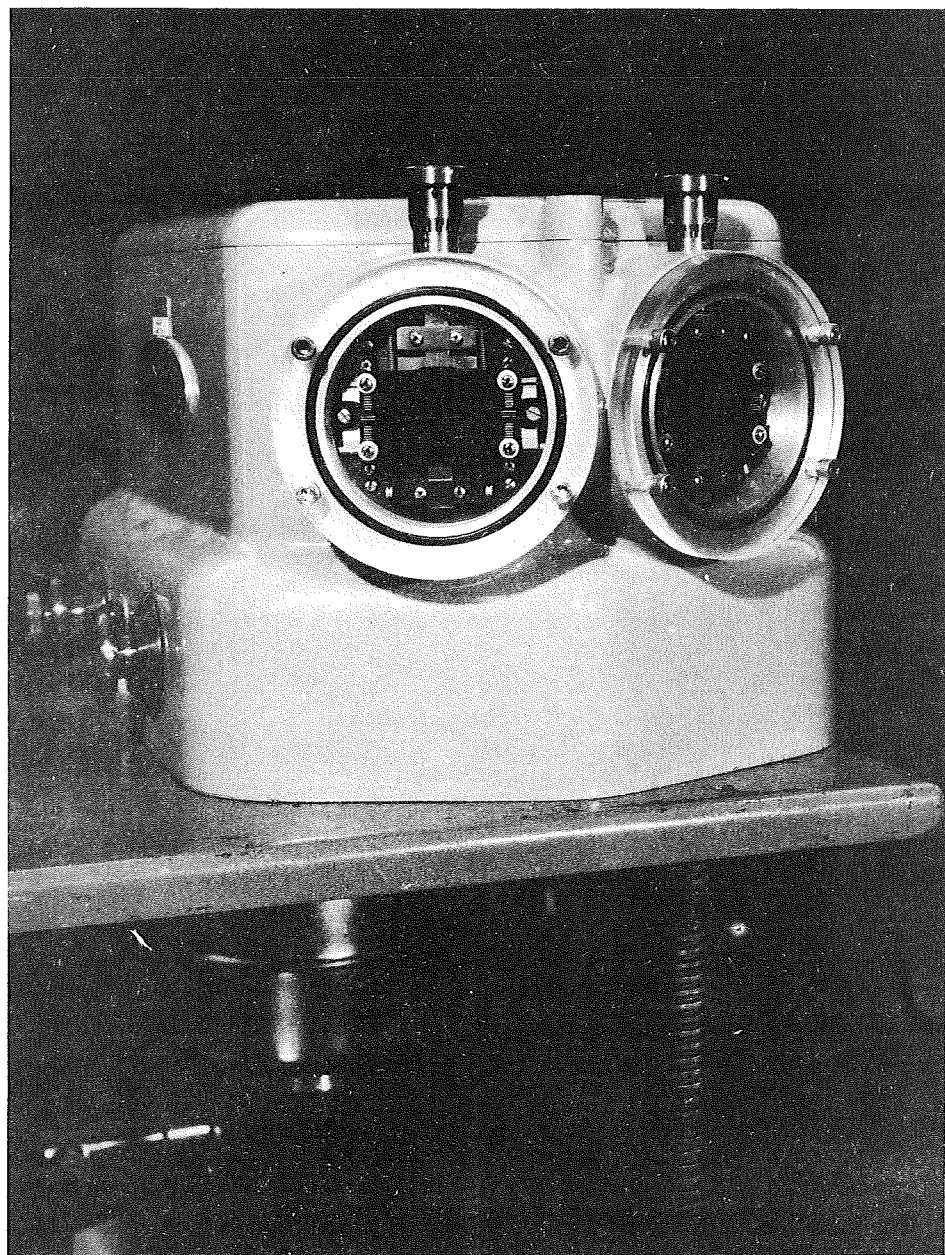
FIG. 2.6   THE McPHERSON 218 MONOCHROMATOR

system was a standard Czerny-Turner mount. It consisted of two concave mirrors and a plane diffraction grating. The monochromatic action was accomplished by a rotation of the plane grating about its center. With this optical system, off-axis aberrations, produced by reflection from the first concave mirror, were cancelled by reflection from the second concave mirror. It seems the limit of resolution was determined by imperfections in the grating and not by aberrations of the optical system. The combination of aluminum and magnesium fluoride coatings on mirrors and grating gave excellent reflecting power down to 1200 $\overset{\circ}{A}$. The coating of Mg F_2 on a freshly aluminized surface has been shown to greatly enhance the reflectance of the surface at short wavelengths by interference effects. The grating used in the experiment was a 2400 lines per millimeter replica grating. The grating was blazed at 1500 $\overset{\circ}{A}$ and its ruled area was 52 mm x 52 mm. The 2 inch aperature stop around the mirrors gave an effective focal ratio of f/5.3. The slit was set at a height of 4 mm. The slit width employed for the spectral scans was normally 200 microns. In addition, scans were made at a slit width of 100 microns for high resolution studies of overlapping bands and at a slit width of 400 microns for study of weak bands. The grating equation for this optical system is

$$n \lambda = 2 d \sin \theta \cos \alpha ,$$ (2.1)

where:

d   is the grating (groove) separation,

α is the ray separation half-angle and is equal to

       14° for this monochromator,

θ is the grating shaft angle.

The dispersion or plate factor for the instrument, using the 2400 lines/mm grating, was $d\lambda/dl = 13.9$ Å/mm. This equation gave a dispersion of 2.78 Å at a 200 micron slit width. The resolving power and dispersion are closely related quantities. Since the instrumental resolving power was much less than 2.78 Å, the monochromator can resolve two wavelengths of about 3 Å separation. Since most of the spectral scans were made between 1200 Å and 2000 Å at a speed of 50 Å/min., the entire spectrum was recorded in 16 minutes. This time was short enough that the electron beam excitation source remained constant to within a few per cent. During the scan the electron beam current and nitrogen gas pressure of the source were recorded in 30 second intervals.

The electron beam excitation chamber and monochromator were separated by a lithium fluoride window with a vacuum tight seal. This arrangement was used for two reasons. First, it was calculated that the 2 inch diffusion pump of the monochromator did not have a fast enough pumping speed to keep an order of magnitude pressure differential between the excitation chamber and the monochromator without the lithium fluoride window. It was

desirable to keep the photomultiplier tube well away from its arcing region, which begins at about 10^{-3} torr pressure. Second, for safety reasons in case of a power failure, a sudden rise of pressure in the excitation chamber, which was not equipped with automatic fail-safe valves, would not be transmitted to the monochromator. The lithium fluoride window was 2 mm thick and 1 inch in diameter. The top view of the electron beam chamber and monochromator is shown in Figure 2.7.

The distance from the entrance slit of the monochromator to the electron beam was 9 13/16 inches. The advantage of this fast optical system was its large field of view--$9°40'$. This enabled the photomultiplier to detect radiation at a distance of 2.11 mm from the beam. Since the Lyman-Birge-Hopfield band system has a lifetime of about 80 microseconds, it appeared as a diffuse glow, strongest at the electron beam, and fell off in intensity a little faster than $1/r$, where r is the distance from the beam. (See Chapter IV for the calculation of glow intensity as a function of distance from the electron beam). The detector could see about 75% of the LBH emission and, of course, all of the permitted atomic nitrogen line emission.

2.5.2 Vacuum System of the McPherson 218 Monochromator.

The vacuum system is illustrated in Figure 2.8. The vacuum system consisted of a Welch forepump, a 2 inch Consolidated Vacuum Corporation diffusion pump, a Granville Phillips

TOP VIEW OF ELECTRON BEAM EXCITATION EXPERIMENT

VACUUM CHAMBER

INLET BAFFLE

DIRECTION OF MAGNETIC FIELD

GAS INLET

MAGNETIC PLATE

LYMAN-BIRGE-HOPFIELD EMISSION REGION

COLLECTOR

GOLD BLACK ABSORBING SURFACE

ELECTRON BEAM

U.H.V. GAUGE

ENTRANCE SLIT

TO PUMPS

FOCUSING MIRROR

-9°40'

MILLITORR GAUGE

MAGNETIC PLATE

ELECTRON GUN

DIRECTION OF MAGNETIC FIELD

PHOTO MULTIPLIER TUBE
& MAGNETIC SHIELD

COLLIMATING MIRROR

LITHIUM FLUORIDE WINDOW

.3 METER SCANNING MONOCHROMATOR

GRATING

EXIT SLIT

FIGURE 2.7

VACUUM SYSTEM SCHEMATIC
FOR McPHERSON 218 MONOCHROMATOR

THERMOCOUPLE GAUGE
(MAIN CHAMBER)

DISCHARGE OR
IONIZATION GAUGE

MAIN CHAMBER

ROUGHING VALVE

AIR INLET VALVE

MAIN CHAMBER VALVE

LIQUID NITROGEN
BAFFLE

MECHANICAL
PUMP

DIFFUSION PUMP

THERMOCOUPLE GAUGE (FORELINE)

FORELINE VALVE
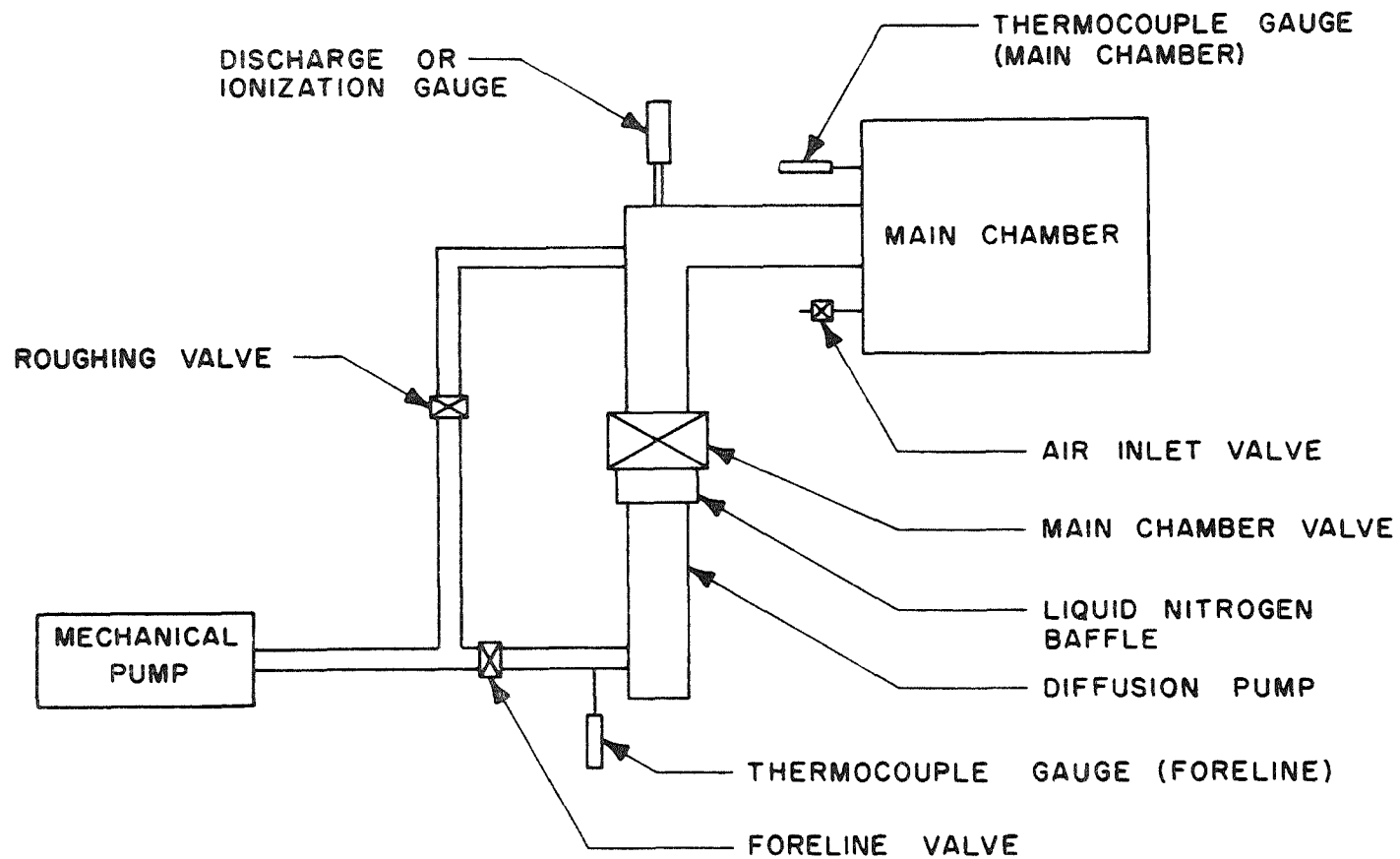
FIGURE 2.8

liquid nitrogen baffle, and a Delta Engineering automatic liquid

nitrogen controller. The pressure in the chamber was monitored

by a thermocouple gauge at high pressures and an ionization gauge

at low pressures. The monochromator had a valve for admitting air

to bring the system to atmosphere. The valves were all automati-

cally activated by push button controls on the main control panel.

The vacuum system was protected from overheating by a mercoid

control, which would close the main chamber valve and diffusion

pump, if the diffusion pump became too hot. The monochromator

was made of aluminum. The ultimate pressure in the monochromator

was designed for 1×10^{-5} torr. Lower pressures could not be

reached, and were not needed, since 1×10^{-5} torr pressure was

low enough for vacuum ultraviolet measurements, i.e., the optical

depth is much less than one in the ultraviolet for the transitions of

interest.

2.5.3   The Photomultiplier Tube.

The detector used in this experiment was an 18 stage, end

on, lithium fluoride window tube with a 10 mm diameter, semitrans-

parent cesium iodide photocathode. The response of this tube ex-

tended from 1050 Å, the cut-off of the cleaved lithium fluoride

window, to the photocathode threshold at 2500 Å. Thermionic

emission of the high work function photocathode was extremely

small, resulting in exceptionally low dark currents. Typical dark

currents were .1 and .2 picoamperes a half-hour after the 3000V high voltage was turned on. The peak response of this particular photomultiplier was at 1550 Å, falling to 40% of this value at 1200 Å and 1880 Å. The q'_λ g factor (quantum efficienty times gain for the photomultiplier) at 1216 Å, with 3000 volts across the photomultiplier, was 7.54 x 10^3 electrons/photons. The photosensitive cathode was located 11/16 inch away from the exit slit of the monochromator. The slit height was 4 mm, giving a 6.8 mm image height of the photocathode. The photomultiplier, which was physically very close (about 3 inches at closest approach) to the magnetic plates used to guide the electron beam, was shielded by a magnetic shield made especially for reducing a 160 gauss field to less than 1 gauss inside the tube. This accessory was necessary in order not to perturb the path of the electrons from dynode to dynode. The photomultiplier shield was made specifically for this experiment by the Magnetic Shield Division of Perfection Mica Corporation of Bensonville, Illinois. The material for the magnetic shield was 0.060 inch thick conetic material, high permeability, low reluctance material that shunted the magnetic field around the surface and reduced the magnetic field at the photocathode by 50 db. It was a rolled cylinder, heli-arc welded and annealed at 2000 °F.

2.5.4 Electronics for the Detection System.

The high voltage supply for the photomultiplier was a Fluke
Engineering power supply, model 408A, which was periodically cal-
ibrated. It was regulated to within 0.01% and ripple was maintain-
ed at less than 4 m.v.R.M.S. The supply was run with the nega-
tive terminal at -3000v and the positive terminal at ground. All
cables were shielded. The output of the photomultiplier went to a
Kiethly model 417 picoammeter equipped with damping controls and
suppression current offsets to offset the dark current. Typical
currents from the stronger LBH bands were of the order of 0.5×10^{-11}
amps. The three scales used for the experiment were $.3 \times 10^{-11}$
amps, 1×10^{-11} amps and 3×10^{-11} amps full-scale readings. The
output of the picoammeter went to a Brush recorder, Mark 280,
of the Clevite Corporation of Cleveland, Ohio. The output was
run at 50 mv/line and at 1 mm/sec chart speed. The picoammeter
and Brush recorder combination were periodically calibrated with a
picoampere source. The corrections applied were less than 1%.
During the calibration the scales used were the 10^{-8} and 10^{-9}
amps, full-scale ranges of the picoammeter. These scales were
also calibrated with the picoampere source. The corrections ap-
plied were less than 3%. The damping control on the picoam-
meter was used to filter out photomultiplier noise. The bucking
current supply of the picoammeter was used to offset the

photomultiplier dark current. The value of dark current stabilized

to 0.1×10^{-12} amps, a half-hour after the high voltage was turned

on. The chart speed of 1 mm/sec, used in conjunction with the 50

$\overset{\circ}{A}$/min drum speed of the monochromator, resulted in an output

that separated the bands for convenient integration to determine

the resultant intensity. Thus, the spectrum from 1200 $\overset{\circ}{A}$ to 2000 $\overset{\circ}{A}$

was displayed on a chart 42 inches long. The amplifier setting of

50 mv/line on the Brush recorder gave sizable peak heights of

about 3 inches above the zero setting on the recording. The full-

scale output of the picoammeter was 3 volts. The accuracy of the

picoammeter is $\pm 3\%$ on the 3×10^{-9} to 1×10^{-13} ampere ranges.

Fast response resulted from a circuit using a high gain dc am-

plifier and a critically damped feedback network, which conve-

niently adjusted the response speed. This helped achieve a bal-

ance of response speed and noise, thus minimizing the effect of

60 c.p.s. and other external noise pick-up. Tests were run to

ensure that the area under each band was independent of the damp-

ing control setting. Zero drift was less than 1% of full-scale per

8 hours. The electronics schematic for the detection system is

shown in Figure 2.9. The electronic rack is shown in Figure 2.10.
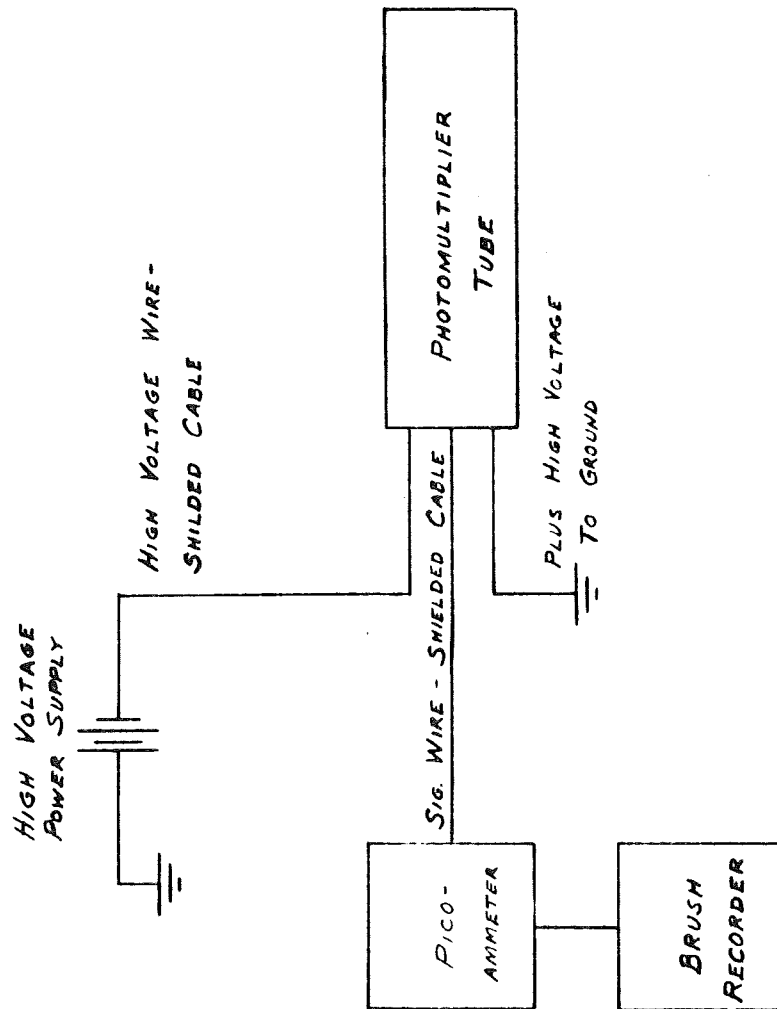
ELECTRONIC SCHEMATIC FOR PHOTO-
MULTIPLIER DETECTION SYSTEM

FIGURE 2.9
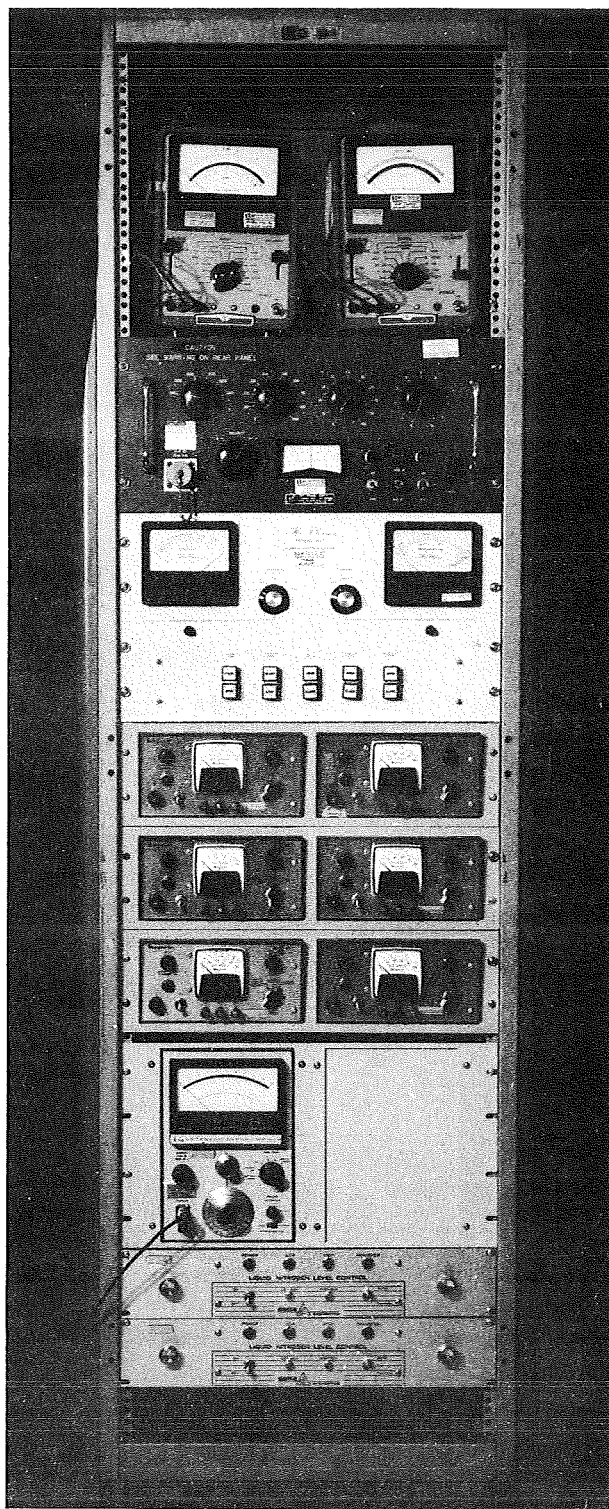
FIG. 2.10   THE ELECTRONIC   RACK

CHAPTER III

CALIBRATION

3.1   Introduction

In order to determine the absolute cross-section in an electron beam excitation experiment by optical measurements, it is necessary to know the absolute response of the detector and monochromator as a function of wavelength. Such a determination is conceptually straightforward in the visible and near ultraviolet regions where black body radiation can be used as a radiation standard. In the vacuum ultraviolet there is no satisfactory intensity standard to determine the relationship between the response of the spectrometer and the true intensity distribution of the radiation incident upon the spectrometer.

Before discussing the calibration techniques employed in the present study, it is useful to review the individual parameters which determined the overall absolute wavelength response of the spectrometer and detector. The parameters are:

1)   The transmission of the lithium fluoride window between the spectrometer and electron beam chamber.

2)   The efficiency of the monochromator-grating and two mirrors.

3)   The photomultiplier response.

To measure the absolute intensity of radiation at any wave-
length, it is necessary to have a detector whose response is known
in absolute units. This detector must be calibrated against a stan-
dard source, such as a black body source, or it must be an abso-
lute detector, whose response to the radiant intensity can be cal-
culated. The emission of black body furnaces are confined to wave-
lengths greater than 2700 Å, and thus, cannot serve as a standard
source in the wavelength range of interest, 1200 Å - 2000 Å.
According to Samson (1967) the most accurate and reproducible
method of measuring absolute intensities is based on the photo-
ionization of a suitable gas. The photoionization yield of a gas is
defined as the number of ions produced per photon absorbed. Thus
if an ionization chamber is filled with an appropriate gas until all
of the incident photons are absorbed, the number of photons per
second incident times the photoionization yield is equal to the
ion current produced. Of particular interest is the yield of NO at
Lyman-alpha (1215.7 Å), which has been measured by Watanabe
et al. (1953) and Watanabe (Samson, 1967, P. 250, Table 7.4) to
be 81%. Samson (1967) has a complete review of recent measure-
ments of photoionization efficiencies. The value for the yield of
NO has been used to determine the intensity of hydrogen Lyman-
alpha emitted from the sun by using NO ionization chambers in

rockets and satellites. The photoionization yield technique is used for measuring detector response by comparing the response of an unknown detector to an ionization chamber output for the same input radiation from a discharge lamp. This method, however, cannot be used directly to determine monochromator response. Thus, it is not an adequate means of calibrating a complete optical instrument. Moreover, it is limited to short wavelengths above the ionization potential--for nitric oxide the useful range is up to only 1343 Å.

It was necessary to do the calibration, piecemeal, by calibrating the detector, the monochromator and lithium fluoride window in separate calibrations. Finally, by multiplying the resulting calibration factors together, it was possible to get the overall response of the instrument. The lithium fluoride window and the monochromator were calibrated by measuring both the input radiation to each from a discharge lamp at many wavelengths. The detector, a 541 G EMR photomultiplier, was calibrated absolutely at Lyman-alpha using a hydrogen d.c. discharge lamp with a nitric oxide cell and relative to Lyman-alpha at all other wavelengths of interest (1200 Å - 2000 Å) by a sodium salicylate calibration. Sodium salicylate is a fluorescent material. The fluorescent efficiency of a freshly prepared layer is a constant between 1400 Å and 2000 Å and slightly less from 1200 Å to 1400 Å (Knapp and

Smith, 1964). By comparing the response of the unknown detector to a detector with a sodium salicylate layer for the same incident radiation, it was possible to obtain a relative wavelength calibration for the photomultiplier.

All calibrations were made on the McPherson 225 monochromator. It was an f/10 by f/20 system. Using this instrument had many advantages. The 225 had butterfly slits on both the entrance and exit slits with its own roughing pump. This set-up enabled one to isolate the exit slit from the main chamber for a quick change of detectors in the photomultiplier calibration. The 225 also had a faster pump-down time than the 218, since it had a 4 inch diffusion pump and a higher ultimate vacuum of about 5×10^{-7} torr. The source in the relative calibration measurements was a Hinteregger d.c. discharge lamp operated at 400 microns pressure with nitrogen as the gas source. The Hinteregger source needed about a one hour warm-up for stability in reproducing spectral lines. Thus, calibration points were obtained at the same wavelengths as measured in the experiment. The discharge lamp formed a rich spectrum between 1200 Å and 2000 Å--filled with the Lyman-Birge-Hopfield and Birge-Hopfield band systems and with many atomic nitrogen lines. The discharge lamp was separated from the spectrometer by a lithium fluoride window.

3.2   Transmission of the Lithium Fluoride Window.

The transmission of the lithium fluoride window is shown

in Figure 3.1. This was the transmission characteristic of the

lithium fluoride window used in the electron beam experiment.

The window was 2 mm thick and 1 inch in diameter. The detector

in the calibration was a 541 F EMR photomultiplier, since it had

a very good long wavelength response. The window was mounted

on a filter wheel with one blank opening and one opening for the

lithium window. The filter wheel was placed between the photo-

multiplier and the exit slit. By rotating the window in and out of

the monochromatic radiation supplied by the spectrometer, the

transmission was obtained at about 50 wavelengths between 1200 Å

and 2000 Å. Due to the low intensity of the ultraviolet radiation in

the electron beam chamber, there was no indicated change in the

transmission of the window such as caused by color centers. Both

sides of the window were always maintained at high vacuum, pre-

venting any contamination.

3.3   Relative Calibration of the Photomultiplier.

The 541 G-08-18 EMR photomultiplier was calibrated be-

tween 1200 Å and 2000 Å by direct comparison with a 541 A EMR

tube, which had a sodium salicylate fluorescent filter in front.

The relative quantum efficiency of the 541 G photomultiplier used

47

TRANSMISSION OF LITHIUM FLUORIDE WINDOW
OF ELECTRON BEAM EXCITATION EXPERIMENT

ESTIMATED ERROR LESS
THAN 2%

WAVELENGTH (Å)
FIGURE 3.1
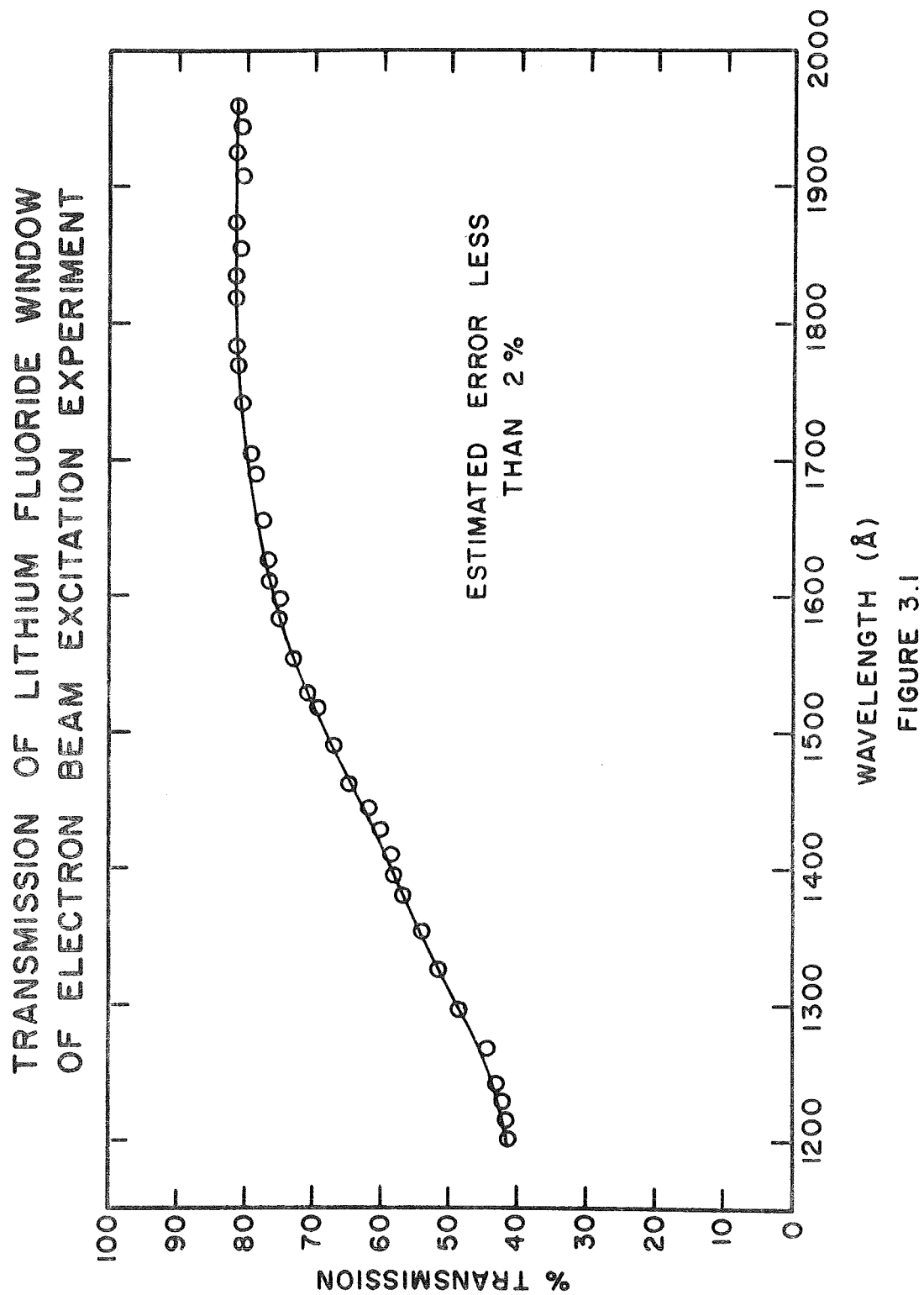
in the experiment is shown in Figure 3.2. The results were normalized to 1216 Å, since it was at this wavelength the absolute calibration of the photomultiplier was made.

Sodium salicylate had the important property of having a high fluorescent efficiency between 850 Å and 2000 Å. It has been shown (Knapp and Smith, 1964) that the quantum efficiency of sodium salicylate was a constant from 1420 Å to 1700 Å to within 3%. These authors gave relative quantum efficiencies from 1200 Å to 1700 Å. This data was used in the calibration to normalize the data to 1216 Å, thus putting the relative calibration on the same scale.

Sodium salicylate is a very fine crystalline power. It readily dissolved in ethyl alcohol. After obtaining a saturated solution, it was sprayed onto a quartz slide using an atomizer. The surface densities used were 2, 3 and 4 mg/cm^2, in three separate calibrations. The response of sodium salicylate peaks at a surface density of 1 mg/cm^2 and falls off slowly with increasing thickness. The results of the separate calibrations were the same to within 3%. The averaged results are displayed in Figure 3.2. The sodium salicylate filters were used within an hour after preparation. The fluorescence occurred in a wavelength region centered about 4400 Å and matched the wavelength sensitivity of the 541 A tube. The filter was placed in front of the 541 A

RELATIVE QUANTUM EFFICIENCY OF 541G-08-18 PHOTOMULTIPLIER OF ELECTRON BEAM EXCITATION EXPERIMENT VS WAVELENGTH-NORMALIZED TO 1216 A

ESTIMATED ERROR LESS THAN 5%
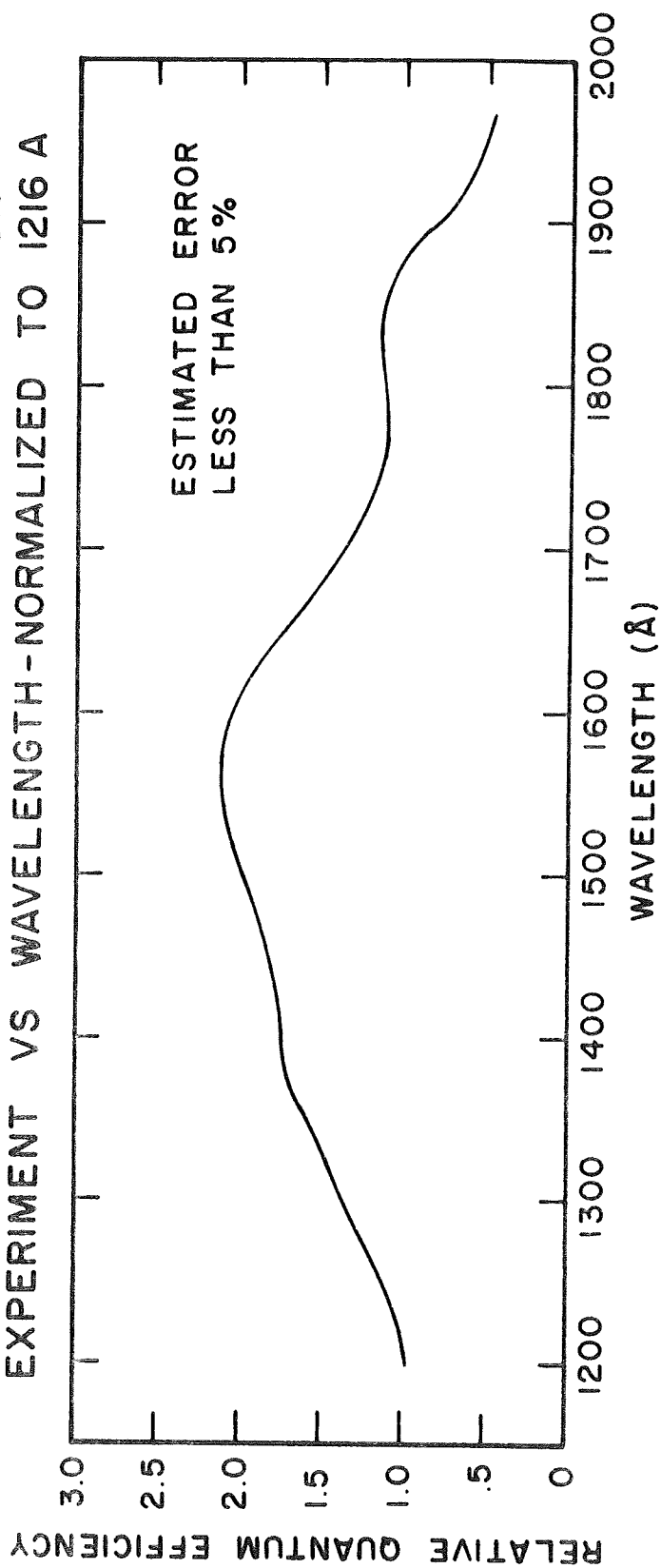
FIGURE 3.2

photomultiplier and a spectral scan was made from 1200 Å to 2000

Å. Then a sequential scan was made with the 541 G tube. This

procedure was repeated. A ratio was made of the intensity of a

spectral line with the G tube to the intensity of a line with the A

tube. This procedure was repeated with about 50 lines. The re-

sults were normalized to the 1216 Å line calculation and included

the quantum efficiency corrections for sodium salicylate of Knapp

and Smith (1964). The peak response of the photomultiplier was

at 1550 Å. The response fell to 1/2 of the peak at about 1220 Å

and 1875 Å. Care was taken to illuminate the same portion of the

photocathode as used in the experiment. This precaution was nec-

essary, since the quantum efficiency of photomultipliers varies

across the surface of the photocathode, especially at long wave-

lengths.

3.4   Absolute Calibration of the Photomultiplier at 1216 Å.

The absolute calibration of the 541 G EMR photomultiplier

was made at 1216 Å with a NO ion chamber. The basic principle

involved was that the number of ions produced in an ionization

chamber depends on the number of photons absorbed by the gas

and on the photoionization yield of the gas. The number of pho-

tons absorbed by a gas is given by the Lambert-Beer law as

$$\text{Number of photons absorbed} = I(1-e^{-\sigma nL}) \qquad (3.1)$$

where:

I   is the intensity of the radiation in photons per

second entering the chamber,

L   is the length of the chamber,

n   is the number of molecules per cm^3,

σ is the total absorption cross-section of the gas

at 1216 $\overset{\circ}{A}$,

T   is the transmittance of the window material--

lithium fluoride in this case,

I_o is the intensity of the incident radiation, thus,

$$I = T \ I_o \ , \qquad\qquad (3.2)$$

and the number of primary ions produced per second is given by

$$\frac{i}{e} = T \ I_o \ \gamma \ (1-e^{-\sigma nL}) \ , \qquad\qquad (3.3)$$

where γ is the photoionization yield and i is the ion current.

If the optical depth, τ, is much greater than 1, that is, if

$$\tau = \sigma nL \gg 1 \qquad\qquad (3.4)$$

then,

$$\frac{i}{e} = T \ I_o \ \gamma \ . \qquad\qquad (3.5)$$

By quickly replacing the NO chamber on the exit slit with

the 541 G photomultiplier and measuring the current generated in

the tube, a relationship for the response of the tube at 1216 Å was

obtained using

$$I_o = \frac{\ell_{pmt}}{e \, q'_{\lambda=1216} \, g} ,$$ (3.6)

where:

ℓ_{pmt} is the output current of the photomultiplier,

$q'_{\lambda=1216}$ is the quantum of efficiency of the photo-

mutiplier, at 1216 Å,

g is the gain of the photomultiplier.

Thus,

$$q'_{\lambda=1216} \, g = \frac{T\gamma \, \ell_{pmt}}{i} .$$ (3.7)

When all the ions are collected, Eqn. (3.5) represents

the total current in the ion chamber. The ion current saturates at

a few volts and then stays constant for nearly 150 volts until ion

multiplication begins. Ion multiplication sets in when an electron

acquires enough energy to cause secondary multiplication. The

voltage used in the calibration was 23 volts and the pressure was

about 100 microns, leaving the chamber in the linear range with

respect to intensity versus ion current and with $\tau \gg 1$. Fifteen

separate measurements with hydrogen as the source gas in the

lamp gave an average value of 7.54×10^3 electrons/photon with

a deviation of 3% for the quantum efficiency times gain with -3000

volts on the photocathode. The transmission of the window was measured both before and after the calibration and usually indicated about a 1.5% change after irradiation by Lyman-alpha. The quantum efficiency times gain, $q'_\lambda \times g$, at any other wavelength equals 7.54 $\times 10^3 \times$ response of photomultiplier relative to 1216 Å (See Figure 3.2).

3.5 Efficiency of the McPherson 218 Monochromator.

The efficiency of the monochromator at a given wavelength can be defined as the percentage of the incident radiation returned by the monochromator (grating and two mirrors) into a given order. It would have been very difficult to illuminate the grating in the same manner as in the excitation experiment. In the cross-section measurements of the Lyman-Birge-Hopfield system, the horizontal center line of the grating received most of the light. The effect of non-uniform lighting arises from the fact that LBH radiation is an extended source with an emission rate that varies as the distance from the electron beam. (See Chapter IV for the derivation of the relationship between integrated intensity at the slit as a function of minimum distance from the electron beam). The change in intensity from the center of the grating to the top or bottom of the grating was only about a factor of 2 with a slit height of 4 mm. The atomic nitrogen line radiation was caused by a line source that illuminated about 7 mm of the grating or about 20% of the grating.

The efficiency of the monochromator was measured by putting the 218 in series with the McPherson 225 spectrometer. The 225 served as a monochromatic light source for the 218. The two spectrometers were physically separated by 4 inches. The exit slit of the 218 was used as the entrance slit and the entrance slit was used as an exit slit. This set-up was necessary to permit a physical coupling of the two monochromators. Since the grating equation was invariant to interchanging the entrance and exit angles with respect to the normal of the grating, the first order spectrum was imaged on the entrance slit. When the grating is illuminated in this direction, a fraction of the diffracted beam strikes the steep edge of the grooves, producing scattered light. Because of the large light output of the Hinteregger lamp, the signal to noise ratio was still very high. For example, the noise current on the photomultiplier measuring the exit beam increased from 0.2×10^{-12} amps in normal operation to 0.6×10^{-12} amps with the grating reversed. The monochromatic radiation exiting the 225 was made diffuse by a lithium fluoride diffusing plate, supplied by Harshaw Chemical Company of Cleveland, Ohio. The diffusing plate was placed 1 3/4 inches from the entrance slit of the McPherson 218. The diffusing plate had a 2 mm x 4 mm slit aperture stop in back of it with the long dimension horizontal. The entrance slit of the 218 was set to an opening of 400 microns with a slit

height of 2 mm. This geometrical configuration uniformly illum-
inated about 70% of the grating. The incoming monochromatic
radiation was monitored by a 541 G-08-18 EMR side window photo-
multiplier suspended from a vacuum mechanical feed-through. The
side window photomultiplier was placed 1 3/4 inches from the
entrance slit and could be moved vertically in and out of the en-
trance beam. The exit beam was monitored by a 541 G-08-18 EMR
end on photomultiplier. Another top was purchased for the 218 in
order to mechanically mount and vacuum seal the side window photo-
multiplier. The side window photomultiplier was aligned vertically,
horizontally, and angularly by electrical means before pump down
by observing the zero order spectrum. Calibration points were ob-
tained at 21 wavelengths between 1200 and 2000 Å. A ratio, R_λ,
was determined for each of these wavelengths of the exit beam in-
tensity to the entrance beam intensity.

The two photomultipliers were compared as to sensitivity,
S_λ, on the McPherson 225. The efficiency, ϵ_λ, of the spectrometer
at each wavelength was then calculated by

$$\epsilon_\lambda = R_\lambda S_\lambda . \tag{3.8}$$

The efficiency of the monochromator is displayed in Figure 3.3. The
peak transmission of the spectrometer was 13.4% at 1383 Å. The
result was surprising in that the grating was blazed at 1500 Å.

EFFICIENCY OF 218 MONOCHROMATOR
OF ELECTRON BEAM EXCITATION EXPERIMENT
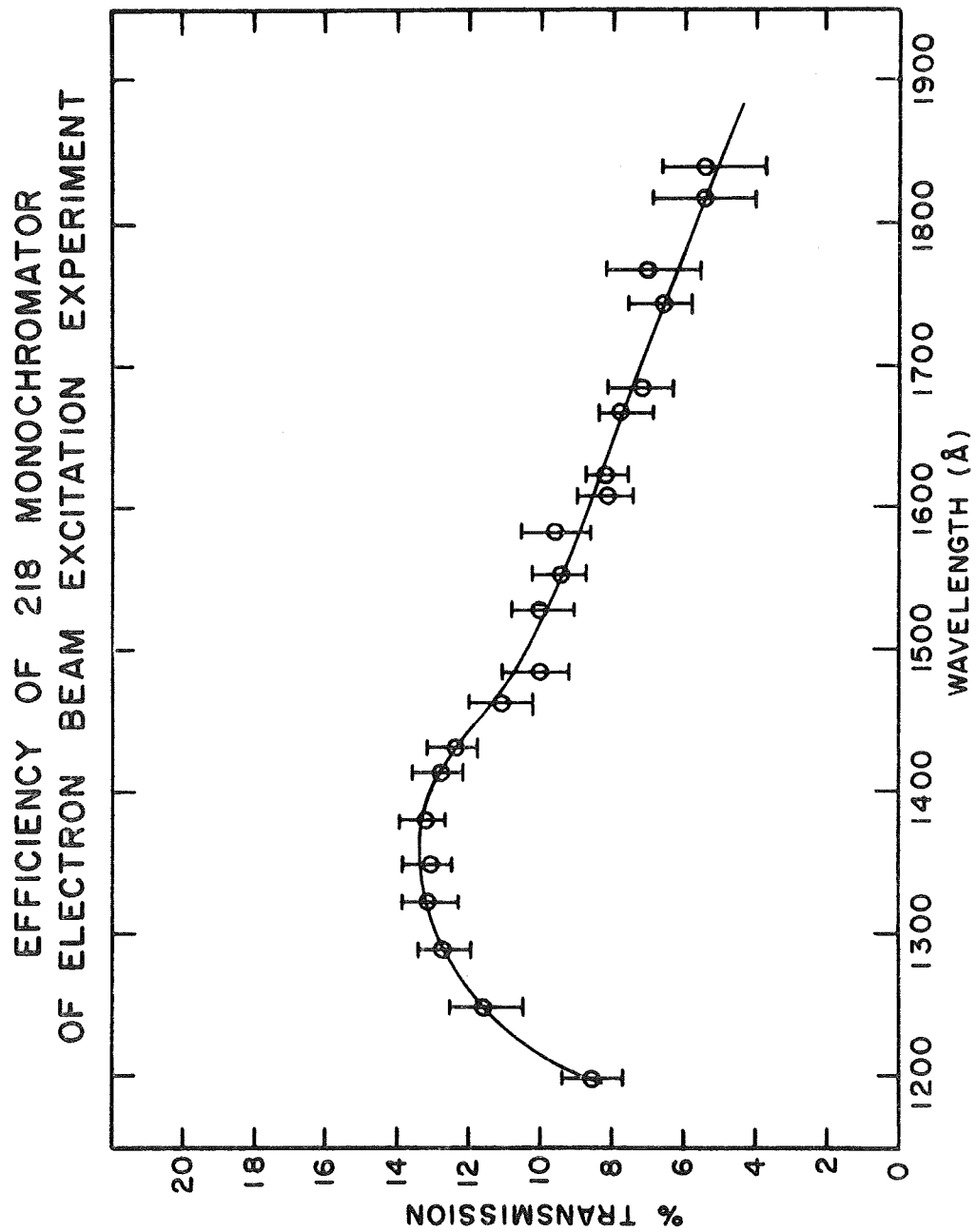
FIGURE 3.3

This effect was probably due to the reflectivity of the two mirrors having higher reflectivities at shorter wavelengths. The transmission of the monochromator was also measured without the diffusing plate and was 10% lower. In this case, only the center of the grating was illuminated. The change could be interpreted as either a variation in efficiency across the grating and mirror surfaces or as a polarization characteristic of the monochromator. The latter effect implies that the light from the first monochromator is polarized. The state of polarization would be different when the diffusing plate is inserted in front of the beam. The diffusing plate would tend to unpolarize the light beam. Thus, there was a 10% uncertainty introduced by the different geometrical configuration of the incident radiation of the experiment and the calibration.

CHAPTER IV

THEORY

4.1   Introduction

The theory of cross-section measurements can be divided into

two parts. First, the theory of excitation of a particular energy

level in an atom or molecule can be considered from the standpoint

of the interaction of an electron with an atom or molecule. Depend-

ing on the energy of the impinging electron, there are probabilities

or cross-sections for the type of reaction that can occur during

the collision: for example, excitation, ionization, elastic scatter-

ing and dissociation for a molecule. In this thesis, the main

theoretical and experimental interest lies in electron excitation and

electron dissociative excitation. Secondly, after the collision the

loss of the excitation energy by spontaneous emission of radiation

by the atomic or molecular system must be looked at in detail to

formulate a theory that balances the steady-state emission and

excitation of each energy level being studied. For a permitted

transition, the production and loss of excited atoms or molecules

per unit volume may be considered equal since the radiation is

emitted practically instantaneously (of the order of 10^{-8} seconds).

However, for a forbidden transition, such as the Lyman-Birge-

Hopfield transition, the product of velocity and the lifetime of the vibrational levels are of such order that molecular flow must be included in the balance of production and loss per unit volume.

The basic physical processes and the geometrical problems involved for determining the apparent excitation cross-section of molecular nitrogen for the forbidden Lyman-Birge-Hopfield transition in an electron beam experiment are considered. The primary reaction is

$$N_2 \ (X^1\Sigma_g^+) \ + \ e \ \xrightarrow{Q'_{ov'}} \ N_2 \ (a^1\Pi_g) \ + \ e \ , \qquad (4.1)$$

followed by

$$N_2 \ (a^1\Pi_g) \ \rightarrow \ N_2 \ (X^1\Sigma_g^+) \ + \ h\nu_{LBH} \ , \qquad (4.2)$$
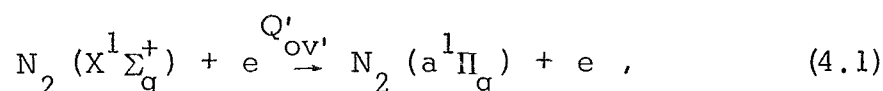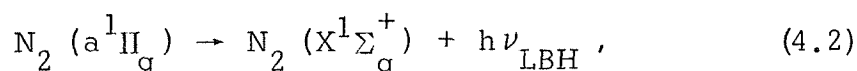
where $Q'_{ov'}$ is the apparent excitation cross-section for excitation to the v' vibrational level of the $a^1\Pi_g$ state of molecular nitrogen. For the dissociative transitions considered in this thesis, the primary reactions are:

a)
$$N_2 \ (X^1\Sigma_g^+) \ + \ e \ \xrightarrow{Q'_{D_1} \ (^4P)} \ N(^4P) \ + \ N \ + \ e \ , \qquad (4.3)$$

b)
$$N_2 \ (X^1\Sigma_g^+) \ + \ e \ \xrightarrow{Q'_{D_1} \ (^2P)} \ N(^2P) \ + \ N \ + \ e \ ,$$

a) $$N_2(X^1\Sigma_g^+) + e \xrightarrow{\quad Q'_{D_2}(^4P) \quad} N(^4P) + N^+ + 2e \,, \qquad (4.4)$$

b) $$N_2(X^1\Sigma_g^+) + e \xrightarrow{\quad Q'_{D_2}(^2P) \quad} N(^2P) + N^+ + 2e \,,$$

$$N(^4P) \to N + h\nu_{1200\text{Å}} \,, \qquad (4.5)$$

$$N(^2P) \to N + h\nu_{1493\text{Å or }1743\text{Å}} \,, \qquad (4.6)$$
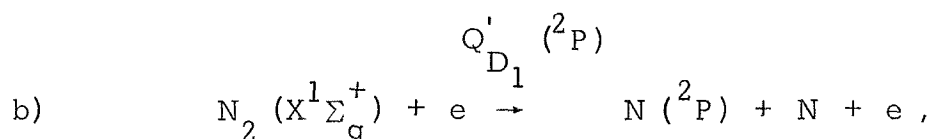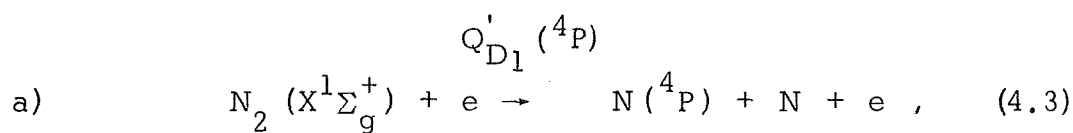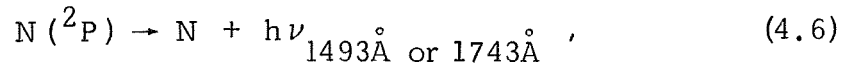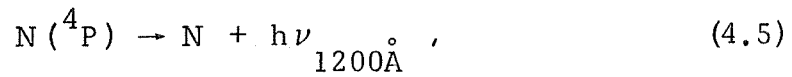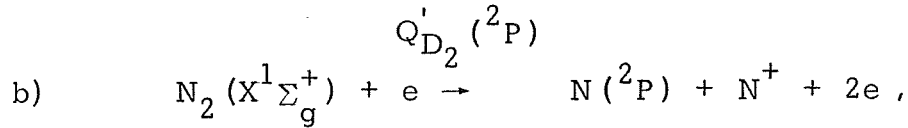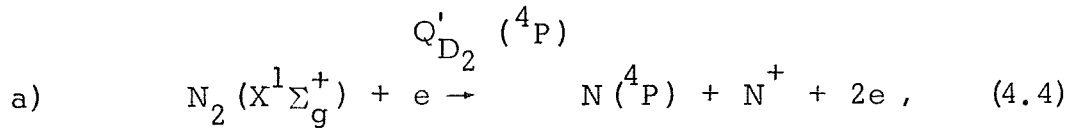
where:

$Q'_{D_1}(^4P)$ is the apparent dissociative excitation cross-section leading to a photon at $\lambda = 1200$ Å,

$Q'_{D_1}(^2P)$ is the apparent dissociative excitation cross-section leading to photons at 1493 Å and 1743 Å,

$Q'_{D_2}(^4P)$ is the apparent dissociative ionization excitation cross-section leading to a photon at $\lambda = 1200$ Å,

$Q'_{D_2}(^2P)$ is the apparent dissociative ionization excitation cross-section leading to photons at $\lambda = 1493$ Å and 1743 Å.

Since it is impossible to distinguish 4.3 and 4.4 above the threshold for 4.4, the sum of the apparent cross-sections for

both processes are measured. Thus,

$$Q'_D (^4P) = Q'_{D_1} (^4P) + Q'_{D_2} (^4P) ,$$

$$Q'_D (^2P) = Q'_{D_1} (^2P) + Q'_{D_2} (^2P) ,$$

where it must be remembered that $Q'_D (^2P)$ is actually the sum of

two partial cross-sections due to the branching of the ^2P level

leading to the 1493 Å multiplet and 1743 Å multiplet. In the

thesis, both the terms emission cross-section and apparent cross-

section are used. The term emission cross-section signifies a

measurement of apparent cross-section (cross-section uncorrected

for cascading) by optical means.

4.2   Energy Level Diagram of Molecular Nitrogen.

The energy level diagram of molecular nitrogen and once

ionized molecular nitrogen is shown in Figure 4.1. The $a^1\Pi_g$

state lies 8.55 eV above the zero vibrational level of the ground

$X^1\Sigma_g^+$ electronic state. The spacing of the LBH vibrational levels

is ω_e = 1692 cm^{-1}, or about 0.2 eV (Herzberg, 1950). The

$a^1\Pi_g \rightarrow X^1\Sigma_g^+$ transition is forbidden as an electric dipole tran-

sition. It is permitted as a magnetic dipole transition. The two

types of transitions are not distinguished experimentally unless

quadrupole lines are present. The high resolution spectra of

Wilkinson and Mulliken (1957) showed the presence of S and

PARTIAL ENERGY LEVEL DIAGRAM FOR N_2 and N_2^+

FIGURE 4.1

62
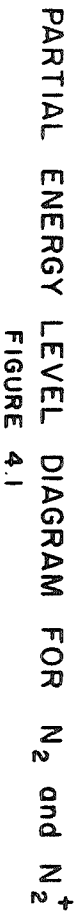
O branches (quadrupole lines). The maximum quadrupole contribution to the transition is about 13% of the total. The bands are single headed and degraded to the red, and consist of P, Q, R, S and O branches.

In Table 4.1 are shown some important selection rules for electronic transitions in diatomic molecules. Since $a^1\Pi_g \rightarrow X^1\Sigma_g^+$ is a $g \rightarrow g$ transition, it is forbidden by electric dipole selection rules.

From a study of the energy levels and electron configurations of molecular nitrogen such ad Mulliken (1957) and a list of observed transitions in nitrogen (Wallace, 1962) it appears there are about ten possible cascading transitions to the $a^1\Pi_g$ state, some permitted and some forbidden. Furthermore, some are permitted and some forbidden to the $X^1\Sigma_g^+$ ground state, making an estimate of cascading very difficult. The most important cascading transitions, since they are observed in discharge lamps, are of the form $^1\Sigma_u^+ \rightarrow a^1\Pi_g$ and $^1\Pi_u \rightarrow a^1\Pi_g$. Transitions of this form are permitted to the $a^1\Pi_g$ state and also to the $X^1\Sigma_g^+$ ground state by electric dipole selection rules if the transitions involve a one electron jump. Thus, there is the possibility of both slow and fast cascade to the $a^1\Pi_g$ state. These upper states lie between 12 and 14 eV. The spectra due to cascading lie between 2000 Å and 3000 Å. No attempt was made to observe the spectra in this region. It is

TABLE 4.1

Important Selection Rules for Molecular Transitions

Electric Dipole	Magnetic Dipole	Electric Quadrupole
$\Delta J = 0, \pm 1$	$\Delta J = 0, \pm 1$	$\Delta J = 0, \pm 1, \pm 2$
$0 \leftarrow/\rightarrow 0$	$0 \leftarrow/\rightarrow 0$	$1 \leftarrow/\rightarrow 0$
		$1/2 \leftarrow/\rightarrow 1/2$
$+ \leftarrow \rightarrow -$	$+ \leftarrow/\rightarrow -$	$+ \leftarrow/\rightarrow -$

Identical Nuclei

Electric Dipole	Magnetic Dipole	Electric Quadrupole
$s \leftarrow/\rightarrow a$	$s \leftarrow/\rightarrow a$	$s \leftarrow/\rightarrow a$

Equal Nuclear Charge

Electric Dipole	Magnetic Dipole	Electric Quadrupole
$g \leftarrow \rightarrow u$	$g \leftarrow/\rightarrow u$	$g \leftarrow/\rightarrow u$
$\Delta\Sigma = 0$	$\Delta\Sigma = 0$	$\Delta\Sigma = 0$
$\Delta S = 0$	$\Delta S = 0$	$\Delta S = 0$
$\Sigma^+ \leftarrow/\rightarrow \Sigma^-$	$\Sigma^+ \leftarrow/\rightarrow \Sigma^-$	$\Sigma^+ \leftarrow/\rightarrow \Sigma^-$
$\Delta\Lambda = 0, \pm 1$	$\Delta\Lambda = 0, \pm 1$	$\Delta\Lambda = 0, \pm 1, \pm 2$

P
a
r
i
t
y

TABLE 4.1 (continued)

where:

J is the total angular momentum of the molecule, (disregarding nuclear spin),

S is total electronic spin quantum number,

Σ is total electronic spin quantum number projected along the internuclear axis,

Λ is magnitude of orbital angular momentum of electrons projected on the internuclear axis,

a, s, g, u, +, − refer to symmetry properties of a molecule (See Herzberg, 1950).

determined in this experiment that the cascading contribution is less than 29%. (See Experimental Results, Chapter V). Furthermore, both this experimental measurement of emission cross-section and that of Holland (1969) find excellent agreement between measurement and prediction on the basis of Franck-Condon factors for direct electron excitation of the $a\,^1\Pi_g$ state as to the fraction of the total cross-section from each vibrational level. This relationship implies that cascading is a small effect, probably much less than 29%. There is also evidence that cascading is a small effect in auroral measurement of the LBH system (Miller, Fastie and Isler, 1968).

A transition that enabled one to "see" the beam was the first negative band system of N_2^+ ($B\,^2\Sigma_u^+ \rightarrow X\,^2\Sigma_g^+$). Its most prominent feature is the (0,0) band at 3914 Å. It made the beam appear blue.

The first dissociation limit of nitrogen is at 9.8 eV. The dissociation products consist of two ground state $^4S^o$ nitrogen atoms. The corresponding dissociative ionization limit of N_2^+ is at 24.3 eV and gives rise to dissociation products--atomic nitrogen in the $^4S^o$ electronic state and a once ionized nitrogen atom in the ^3P electronic state. Dissociative excitation is observed in the experiment. The multiplets observed at 1200 Å, 1493 Å, and 1743 Å,

are from $^4P \rightarrow$ $^4S^o$, $^2P \rightarrow$ $^2P^o$ electronic transitions of atomic

nitrogen, respectively, and are caused by dissociative excitation.

The total transition probability of the multiplet at 1493 Å, is

5.5×10^8 sec^{-1}, and at 1743 Å is 2.0×10^8 sec^{-1} (see Table 4.2).

The transition probabilities are taken from a compilation of atomic

transition probabilities by Wiese, Smith and Glennon (1966). The

branching ratios for multiplets for the transition from the ^2P term

would be 0.74 and 0.26, respectively. These lines originate from

simultaneous dissociation and excitation of molecular nitrogen into

one excited nitrogen atom (excited to one of the aforementioned

electronic states) and a nitrogen atom or nitrogen ion. From experi-

mental measurements at threshold, the ground state nitrogen atom

or ion may be one of the products. Since there are other dissoci-

ation limits for N_2 and N_2^+, it is also possible the nitrogen atom

or ion may be in other than a ground state configuration. There is

also the possibility of a cascade contribution to the ^2P and ^4P

states since there are many permitted transitions to these levels.

(See the energy level diagram of NI, Figure 4.2). The minimum

energy needed to produce one of these lines is the sum of the min-

imum dissociation energy for creating two nitrogen atoms (one in the

ground state configuration), plus the electronic excitation energy

(10.33 eV for the 1200 Å multiplet and 10.69 eV for the 1743 Å and

1493 Å multiplet) above the $^4S^o$ ground state of NI. The minimum

PARTIAL ENERGY LEVEL DIAGRAM OF NI

FIGURE 4.2

TABLE 4.2

Transition Probabilities of the Atomic Nitrogen Multiplets (Wiese, Smith and Glennon, 1966)

Transition Array	Multiplet	λ (A)	Ax $(10^8 sec^{-1})$
$2p^3$-$2p^2$ (^{3}P) 3s	$^4S^o$ – ^4P	1199.9*	5.4*
		1199.58	5.5
		1200.22	5.3
		1200.71	5.8
$2p^3$-$2p^2$ (^{3}P) 3s	$^2D^o$ – ^2P	1493.3*	5.5*
		1492.62	5.3
		1494.67	5.0
		1492.67	0.58
$2p^3$-$2p^2$ (^{3}P) 3s	$^2P^o$ – ^2P	1743.6*	2.0*
		1742.73	1.8
		1745.25	1.3
		1745.26	0.65
		1742.72	0.35

* indicates values for the multiplet,

no asterisk indicates values for the lines.

energies are 20.1 eV for the 1200 $\overset{\circ}{A}$ multiplet and 20.5 eV for the 1493 $\overset{\circ}{A}$ and 1743 $\overset{\circ}{A}$ multiplets.

The minimum energies for dissociative ionization excitation is 34.6 eV for the ^4P term and 35.0 eV for the ^2P term. Thus, these atomic nitrogen lines are produced by excitation, either to a repulsive potential curve or to a stable potential curve with an equilibrium distance very different from the ground state potential curve of N_2, such that by Franck-Condon factor consideration, the excitation is to the continuum of nuclear levels. The dissociation products can have relative kinetic energy as well as internal electronic excitation energy.

4.3 Band Volume Emission Rates.

The factors determining the volume emission rate of a molecular band (v', v") will be briefly reviewed and applied to the LBH band system. The development of the theory of volume emission rates is analogous to the approach of Nicholls (1963), Chamberlain (1961), and McEwen (1965) for band intensities.

The Einstein A coefficient, the transition probability, can be expressed in a way similar to atomic transitions. Thus for electric dipole, magnetic dipole and electric quadrupole transitions, respectively, the following equations hold:

a)
$$A^E_{v'v''} = \frac{64\pi^4}{3h} \frac{S^E_{v'v''}}{g_{v'}\lambda^3_{v'v''}} \ sec^{-1} , \qquad (4.7)$$

b)
$$A^M_{v'v''} = \frac{64\pi^4}{3h} \frac{S^M_{v'v''}}{g_{v'}\lambda^3_{v'v''}} \ sec^{-1} ,$$

c)
$$A^Q_{v'v''} = \frac{32\pi^6}{5h} \frac{S^Q_{v'v''}}{g_{v'}\lambda^5_{v'v''}} \ sec^{-1} ,$$

where:

$S_{v'v''}$ is the band strength, the superscript denoting electric

dipole, magnetic dipole and electric quadrupole tran-

sitions, respectively,

$g_{v'}$ is the statistical weight of the upper level,

$\lambda_{v'v''}$ is the wavelength of the emitted photon.

The band strength in the general case is defined as,

$$S_{v'v''} = \left| \int \Psi_{v'} \ R_e(r) \ \Psi_{v''} \ dr \right|^2 \qquad (4.8)$$

where:

$\Psi_{v'}$ and $\Psi_{v''}$ are the vibrational wave functions of the

v' and v'' levels,

r   is the internuclear separation,

$R_e(r)$ is the electronic transition moment of the band system, defined as follows for the three types of transitions:

a)
$$R_e^E(r) = \int \Psi_{ev'}^* \, P_e \, \Psi_{ev''} \, d\tau \ ,$$
(4.9)

b)
$$R_e^M(r) = \int \Psi_{ev'}^* \, M \, \Psi_{ev''} \, d\tau \ ,$$

c)
$$R_e^Q(r) = \int \Psi_{ev'}^* \, R \, \Psi_{ev''} \, d\tau \ ,$$

where:

$\Psi_{ev'}$ and $\Psi_{ev''}$ are the molecular electronic wave functions,

$d\tau$ is an element of configuration space,

P_e, M and R are the electric dipole, magnetic dipole and electric quadrupole moments, respectively.

The electronic transition moment is most often a slowly varying function of internuclear separation. If it has the same functional dependence on r for all bands being analyzed, it may be expressed (Fraser, 1954) as $R_e(\bar{r}_{v'v''})$ where $\bar{r}_{v'v''}$, the r centroid, is the mean internuclear separation in the transition.

The r centroid,

$$\bar{r}_{v'v''} = \frac{\int \Psi_{v'} \, \Psi_{v''} \, r \, dr}{\int \Psi_{v'} \, \Psi_{v''} \, dr} \ ,$$

is, thus, a characteristic internuclear separation associated

with the band.

The band strength may be written as

$$S_{v'v''} = R_e^2 \, (\bar{r}_{v'v''}) \; q_{v'v''} \quad ,$$

where

$$q_{v'v''} = \left| \int \Psi_{v'} \; \Psi_{v''} \; dr \right|^2$$

the vibrational overlap integral is called the Franck-Condon

factor of the band.

The volume emission rate, $I_{v'v''}$, of a molecular band, in

units of photons $sec^{-1} \; cm^{-3}$ is

$$I_{v'v''} = N_{v'} \; A_{v'v''} \quad , \tag{4.10}$$

where $N_{v'}$ is the number of excited molecules in the v' vibrational

level per cubic centimeter.

Thus, the equation for volume emission rate may be written

for each type of transition as follows:

a)
$$I_{v'v''}^E = C_1 \; N_{v'} \; \nu^3 \left(R_e^E\right)^2 q_{v'v''} \quad , \tag{4.11}$$

b)
$$I_{v'v''}^M = C_2 \; N_{v'} \; \nu^3 \left(R_e^M\right)^2 q_{v'v''} \quad ,$$

c) $\qquad I^Q_{v'v''} = C_3 \ N_{v'} \ \nu^5 \ R^Q_e{}^2 \ q_{v'v''}$,

where the C's are constants, incorporating constants of Eqn. 4.7.

For the LBH band system, the volume emission rate may be written as

$$I_{v'v''} = I^M_{v'v''} + I^Q_{v'v''}$$

$$= K'N_{v'} \ \nu^3 \left[\left(R^M_e\right)^2 + \alpha \nu^2 \left(R^Q_e\right)^2 \right] q_{v'v''} \ ,$$

where K' and α are constants.

If it is assumed that the dependence of R^M_e and R^Q_e on $\bar{r}_{v'v''}$ are of the same form, the contribution of the quadrupole transition varies from 14% at 1300 Å to 6% at 2000 Å from the effect of the ν^2 term (McEwen, 1965).

Thus with this assumption and the fact the wavelength dependence is small, it can be written that

$$I_{v'v''} = K'N_{v'} \ \nu^3 \ R^2_e \ q_{v'v''} \ , \qquad\qquad (4.12)$$

where $R^2_e \ (\bar{r}_{v'v''})$ now contains the two transition moment terms and is an effective transition moment.

The greatest influence over the intensity distribution is the Franck-Condon factor, $q_{v'v''}$, which varies over several orders of

magnitude across the band system. Franck-Condon factors for the

LBH system are displayed in Table 4.3 (Benesch et al., 1966).

McEwen plotted $(I/q\nu^3)^{1/2}_{v'v''}$ versus $\bar{r}_{v'v''}$ for each of the

upper bands $v' = 0$ to $v' = 3$, inclusive, to investigate the vari-

ation of the electronic transition moment as a function of inter-

nuclear separation. He found $(I/q\nu^3)^{1/2}_{v'v''}$ for the band system

(which is proportional to R_e $(\bar{r}_{v'v''})$ to be a constant as a function

of $\bar{r}_{v'v''}$ within 5%. The population factors $N_{v'}$ were divided out.

The band oscillator strength, $f_{v'v''}$, which is a measure

of the fraction of the optical electron associated with the transi-

tion is defined as

$$g_{v'v''} f_{v'v''} = \frac{8\pi^2 m c S_{v'v''}}{3h e^2 \lambda^2_{v'v''}} ,$$

where:

m   is the mass of the electron,

c   is the speed of light,

e   is the charge of the electron.

Thus,

$$f_{v'v''} = 1.5 \times 10^{-8} \lambda^2_{v'v''} A_{v'v''} , \qquad (4.13)$$

where λ is in microns, A is in sec^{-1}.

TABLE 4.3

Franck–Condon Factors for the Lyman–Birge–Hopfield Transition
(Benesch, Vanderslice, Tilford and Wilkinson, 1966)

$$a^1\Pi_g \ - \ X^1\Sigma_g \ + \ (N^{14} \ - \ N^{15})$$

v'' \ v'	0	1	2	3	4	5	6
0	.4087-1	.1117-0	.1671-0	.1825-0	.1606-0	.1240-0	.8439-1
1	.1472-0	.1929-0	.1014-0	.1499-1	.4511-2	.4288-1	.8075-1
2	.2449-0	.8534-1	.1949-2	.7135-1	.9670-1	.5037-1	.6173-2
3	.2505-0	.6836-4	.1037-0	.7327-1	1384-2	.3025-1	.7033-1
4	.1767-0	.8264-1	.8959-1	.2220-2	.7414-1	.5983-1	.4201-2
5	.9085-1	.1834-0	.1614-2	.9236-1	.4041-1	.6314-2	.6003-1
6	.3550-1	.1776-0	.6081-1	.6922-1	.1440-1	.7866-1	.1673-1
7	.1069-1	.1059-0	.1628-0	.7797-5	.9610-1	.9653-2	.3757-1
8	.2519-2	.4424-1	.1639-0	.7585-1	.3908-1	.4429-1	.5694-1
9	.4643-3	.1341-1	.9612-1	.1626-0	.7894-2	.8661-1	.1415-2

TABLE 4.3 (continued)

Franck-Condon Factors for the Lyman-Birge-Hopfield Transition
(Benesch, Vanderslice, Tilford and Wilkinson, 1966)

$$a^1\Pi_g - X^1\Sigma_g^+ (N^{14} - N^{15})$$

v'' \ v'	0	1	2	3	4	5	6
10	.6749-4	.3102-2	.3807-1	.1441-0	.1068-0	.9022-2	.7771-1
11	.8843-5	.5428-3	.1096-1	.7629-1	.1640-0	.3779-1	.5354-1
12	.9387-6	.7274-4	.2333-2	.2721-1	.1194-0	.1399-0	.1348-2
13	.1422-8	.9297-5	.3658-3	.6979-2	.5404-1	.1509-0	.8817-1
14	δ2962-8	.8884-6	.4328-4	.1293-2	.1653-1	.8734-1	.1595-0
15	.1165-7	.1371-6	.3946-5	.1747-3	.3635-2	.3255-1	.1234-0
16	.1514-7	.8131-8	.3724-6	.1951-4	.5686-3	.8411-2	.5661-1
17	.1275-7	.9154-8	.7331-8	.1909-5	.6443-4	.1519-2	.1718-1
18	.1101-6	.3279-7	.1417-7	.2476-6	.5484-5	.1919-3	.3625-2

TABLE 4.3 (continued)

Franck-Condon Factors for the Lyman-Birge-Hopfield Transition
(Benesch, Vanderslice, Tilford and Wilkinson, 1966)

$$a\,^1\Pi_g - X\,^1\Sigma_g{}^+ \; (N^{14} - N^{15})$$

$v''\,^{v'}$	0	1	2	3	4	5	6
19	.1557-7	.8061-8	.4198-8	.9400-8	.4915-6	.2018-4	.5185-3
20	.3210-7	.1190-8	.1193-7	.8834-9	.4305-9	.1726-5	.5238-4

Ching et al. (1967) measured the band oscillator strengths

for the $a^1\Pi_g \leftarrow X^1\Sigma_g^+$ transition in an absorption experiment for a v'

progression, v" = 0. The absorption oscillator strength, the

measured quantity, is related to the band oscillator strength by

$$g_{v"} \, f_{v"v'} = g_{v'} \, f_{v'v"} \qquad (4.14)$$

($f_{v"v'}$ is given in Table 4.4).

Thus, the lifetime of the LBH state can be calculated using Eqn.

4.13 and 4.14, and the equation

$$A_{v'v"} = \frac{2.026 \times 10^6 \; R_e^2 \; q_{v'v"}}{g_{v'} \; \lambda^3_{v'v"}} , \qquad (4.15)$$

where $g_{v'} = 2$, due to λ doubling of the LBH state, and R_e^2 is

determined from the absorption measurements of Ching et al.

and McEwen's measurements showing R_e is a constant for the

band system.

The result is a lifetime of approximately 37 microseconds

for the LBH state where t, the lifetime, $= 1/\Sigma_{v"}A_{v'v"}$. This life-

time is to be contrasted with the 80 microsecond lifetime as mea-

sured by Holland in an electron beam experiment similar to this

one. He measured the integrated intensity of the band system as

a function of distance from an electron beam to obtain this value.

One reason for this discrepancy would be a slow cascade

TABLE 4.4

Absorption Band Oscillator Strengths

for the $a^1\Pi_g$ - $X^1\Sigma_g^+$ Transition

(Ching, Cook, and Becker, 1967)

| $v'-v''$	$f_{v''v'}$
0-0	1.3×10^{-6}
1-0	3.0×10^{-6}
2-0	4.1×10^{-6}
3-0	4.6×10^{-6}
4-0	5.1×10^{-6}
5-0	3.9×10^{-6}
6-0	3.5×10^{-6}
7-0	2.0×10^{-6}
8-0	1.5×10^{-6}
9-0	9.2×10^{-7}

contribution to the LBH lifetime. Holland's measurement of life-time is the one used in the experimental calculations.

The reason for using Holland's data is that the cascade contribution to the LBH state appears to be small and Holland's measurement is a direct measurement of lifetime. If there is a slow cascade contribution to the LBH state, then Holland's measurements represent an upper limit to lifetime. To justify using the lifetime obtained from the absorption measurements, there would have to be evidence for a cascade contribution of 25% to 35%. From cross-section measurements near threshold, there is no evidence for a large cascade contribution.

4.4   Electron-Molecule Interactions.

The primary excitation reaction considered in this experiment is the interaction of low energy electrons (10 eV to 208 eV) with nitrogen molecules. The threshold for excitation of the $a^1\Pi_g$ state by electrons corresponds to 8.55 eV. The reaction is

$$N_2 + e \xrightarrow{Q'_{ov'}(\epsilon)} N_2^* + e \ ,$$
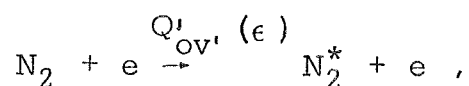
where $Q'_{ov'}(\epsilon)$ is the apparent cross-section, or emission cross-section, for excitation of the v' vibrational level of the $a^1\Pi_g$ state from the zero vibrational level of the $X^1\Sigma_g^+$ state, uncorrected for cascading, by an electron of energy ϵ.

Thus, the interaction is an inelastic collision between electrons and nitrogen molecules in which some kinetic energy is lost by the electron in exciting internal motion in the molecule. The molecules dispose of their surplus energy by radiation and it is possible to determine the cross-section for excitation of the $a^1\Pi_g$ state by measurement of the absolute intensities of the emitted spectral bands.

If a molecule is excited by electron collision from vibrational levels (v") of the ground state to levels (v') of the upper state, the excitation probability, P_{XB}, per collision is proporational to the matrix element (Nicholls, 1962),

$$| \Psi_{v"} \Psi_{v'}^* G_{XB,v"v'} \, dr |^2 .$$

$G_{XB,v"v'}$ is the perturbation integral for the interaction between the electron and the molecule for a transition between the ground electronic state X and the excited electronic state B.

If $G_{XB,v"v'}$ is a slowly varying function of internuclear separation, then

$$P_{XB} = \text{constant } G_{XB}^2 (\bar{r}_{v'v"}) | \int \Psi_{v"} \Psi_{v'} \, dr |^2 ,$$

or

$$P_{XB} = \text{constant } G_{XB}^2 \, (\bar{r}_{v'v''}) \, q_{v'v''} \; .$$

That is,

$$Q_{ov'} = \text{constant } G_{XB, \, o \, v'}^2 \, q_{v'o} \; .$$

The similarity between emission and excitation is pointed out in this approximation. In emission,

$$A_{v'v''} = \text{constant } R_e^2 \, (\bar{r}_{v'v''}) \, q_{v'v''}/\lambda_{v'v''}^3 \; .$$

Before showing how to calculate the cross-section for excitation experimentally, it is worthwhile to look at some of the other interactions between electrons and nitrogen molecules, such as elastic scattering, dissociation and ionization.

4.4.1 Elastic Scattering.

In addition to excitation, the primary electron may be elastically scattered. In an elastic collision, no energy interchange takes place between the internal motion of the molecule and the electron. The electron loses some energy in these encounters, but this is from the finite ratio of the mass, m, of the electron to that M of the molecule. As a result, a fraction of about 2 m/M of the initial kinetic energy of the electron is lost in an elastic collision. This fraction is less than 10^{-3} and may

be neglected. It is desirable to have very few of the primary elec-
trons undergo elastic scattering, since the electron path through
the chamber of elastic scattered electrons would be helical; thus,
increasing the path length of electrons across the chamber. To
keep this effect small, it is necessary to have the mean free path
for elastic scattering much greater than the 6 inch length of the
beam. Elastic scattering cross-sections are about 8.8×10^{-16} cm^2
(Massey and Burhop, 1952) at energies of 10 to 40 eV. The mean
free path for elastic scattering, λ_s, is

$$\lambda_s = \frac{1}{N_o \times Q_s} , \qquad (4.16)$$

where:

$Q_s \simeq 8.8 \times 10^{-16}$ cm^2 is the elastic scattering cross-section, N_o
is the molecular nitrogen number density, and for the 0.2 microns
pressure of this experiment, $N_o = 6.6 \times 10^{-12}$ cm^{-3}. Thus,
$\lambda_s = 172$ cm, which is much greater than the 15 cm path length
of the electrons. It is expected that at higher pressures, elastic
scattering of the primary electrons will be one cause leading to a
nonlinear pressure dependence between intensity and pressure.

4.4.2 Dissociation.

The LBH transition represents an electronic transition from
one potential curve that has an equilibrium separation or potential

energy minimum to another potential energy curve with a potential

energy minimum. Thus this is a transition that involves a stable

molecule before and after the electron jump. In dissociation such

as that exciting the atomic nitrogen lines, the final state of an

electronic transition resulting from an electron impact lies within

the continuum of nuclear motion. In this case, dissociation of the

molecule accompanies all transitions from the lower to the upper

electronic state. The dissociation products will have relative

kinetic energy. In the transition, the final state is either a repul-

sive molecular state or a stable state with an equilibrium distance

which is different from the equilibrium distance of the ground state

potential energy curve such that by Franck-Condon considerations,

dissociation always results. Figure 4.3 shows a hypothetical

transition from a stable ground state to a repulsive molecular

state. The minimum energy to produce the transition is (Massey

and Burhop, 1952)

$$\epsilon_{min} = U'_A + U''_B + D_{AB} + T_{min} \, ,$$

where:

D_{AB} is the dissociation energy of AB,

T_{min} is the minimum energy of relative motion of the re-

       sulting atoms after the transition, and lies between
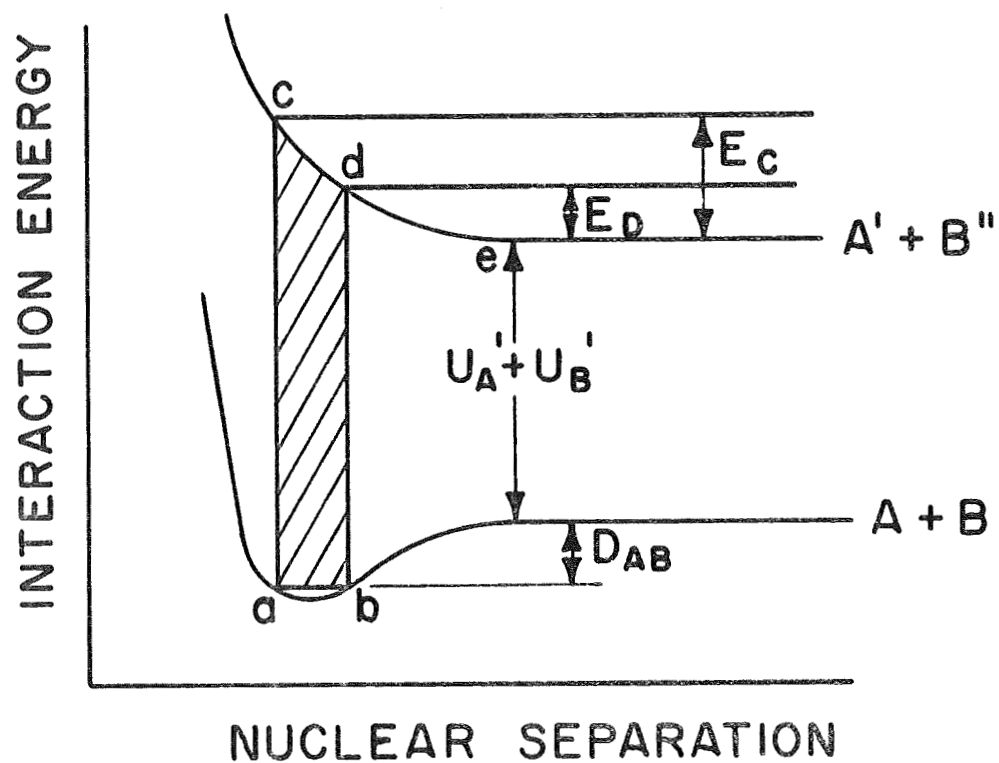
DISSOCIATIVE ELECTRONIC TRANSITION
OF A MOLECULE FROM A STABLE STATE
TO A REPULSIVE STATE.

FIGURE 4.3

ϵ_c and ϵ_d (see Figure 4.3),

$U'_A + U''_B$ is the total excitation energy of the atoms.

This relation can be easily understood from the Franck-

Condon factor which can be summarized; in an electronic transi-

tion, the nuclear separation and velocity of relative motion alter

to a negligible extent--the transition takes place so quickly that

due to the great ratio of nuclear to electronic mass, the nuclei

have no time to move an appreciable distance. Thus, on the dia-

gram, the transition is vertical, and takes place at a value of r

such that the velocity of the nuclei is unchanged during the tran-

sition. Originally, the nuclear separation in the ground vibrational

level will effectively lie between the limits a and b. Hence, final-

ly, according to the Franck-Condon factor, it must also lie within

these limits after the transition. For the case of a transition to a

stable state whose potential energy minimum lies at a different

equilibrium distance than the potential energy minimum of the

ground state, a similar diagram can be drawn. In this instance,

points c and d will be in the continuum of nuclear levels of the

final state. Thus, the stable state (if any) of the final state lies

outside the region determined by points c and d and are, thus, un-

reachable by the Franck-Condon principle. In this experiment the

stable state is the ground vibrational state of N_2. The unstable

state is one of the dissociative transitions leading to the formation

of the 1200, 1493 or 1743 Å line.

There is no theoretical curve available of the shape of the

unstable state to estimate T_{min}. The actual shape of the curve is

unimportant since it does not affect the cross-section measurement

and since all that can be determined is an estimate of T_{min} from

threshold measurements. Thus, although the dissociation energy

is defined as $U'_A + U''_B + D_{AB}$, this energy may bear no simple re-

lation to the energy required to produce the dissociated molecule.

Mulliken (Massey and Burhop, 1952) has, therefore, defined the

vertical dissociation or ionization energy as a more useful quan-

tity. From the experimental measurements around threshold T_{min}

is about 1 eV for both dissociative transitions considered. These

numbers were obtained by linearly extrapolating cross-section

measurements to zero cross-section on a linear plot as a function

of energy. One reason for the inability to determine T_{min} more

accurately is that this treatment is only approximate since there

is a small, but finite chance of dissociation of the molecule if it

receives less than the vertical energy, that is, the transition from

b to e (see Figure 4.3) is theoretically of small but finite probabil-

ity.

4.4.3 Ionization.

For electron beam energies greater than 15.5 eV, it is possible to ionize N_2 into N_2^+. These cross-sections rise steeply from zero at the threshold, peak at an electron energy several times the threshold and then decrease slowly at higher energy. For ionization of N_2 the peak is at about 100 eV. Thus, in an electron beam experiment, the maximum number of secondary electrons produced per cm^3 would be at 100 eV. These secondaries would be expected to produce a non-linearity of intensity versus pressure if the number of secondaries became large enough. It is desirable to have the mean free path of ionization to be much greater than the 6 inch length of the electron beam. At 100 eV the cross-section for ionization is 3×10^{-16} cm^{-2} (Tate and Smith, 1932). Thus

$$\lambda_I = \frac{1}{N_o Q_I} = 505 \text{ cm} \quad ,$$

where:

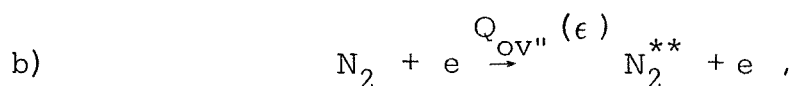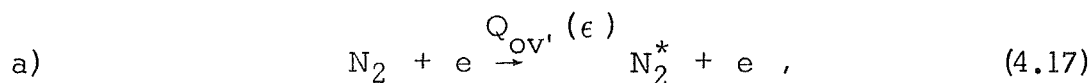λ_I is the mean free path for ionization,

Q_I is the total ionization cross-section of N_2,

N_o is the number density of molecular nitrogen at

         0.2 microns pressure.

It is thus expected that at 0.2 microns pressure, excitation by secondary electrons is negligible although it will contribute to a nonlinearity in intensity versus pressure measurements at higher pressures. This expectation is borne out in the experimental measurements of intensity versus pressure (see Chapter V).
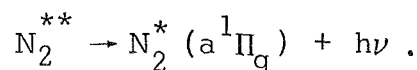
4.5 Steady State Emission and Excitation--The Lyman-Birge-Hopfield Transition.

The primary reactions affecting the population of the $a^1\Pi_g$ state when an electron beam is incident on a neutral nitrogen gas of low pressure are:
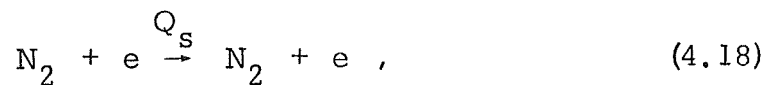
a)
$$N_2 + e \xrightarrow{Q_{ov'}(\epsilon)} N_2^* + e \, , \qquad (4.17)$$

b)
$$N_2 + e \xrightarrow{Q_{ov''}(\epsilon)} N_2^{**} + e \, ,$$

c)
$$N_2^* \xrightarrow{A} N_2 + h\nu$$

d) Diffusion or molecular flow of excited LBH molecules,
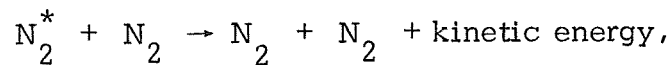
e) Cascading,

$$N_2^{**} \rightarrow N_2^* \, (a^1\Pi_g) + h\nu \, .$$

Some other processes that may affect the LBH state at higher pressures are:

a) Elastic scattering of electrons,

$$N_2 + e \xrightarrow{Q_s} N_2 + e \; , \tag{4.18}$$
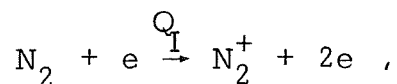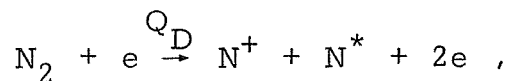
b) Collisional deactivation,

$$N_2^* + N_2 \rightarrow N_2 + N_2 + \text{kinetic energy},$$

c) Excitation by secondaries,

$$N_2 + e \text{ (secondaries)} \rightarrow N_2^* + e \; ,$$

d) Ionization,

$$N_2 + e \xrightarrow{Q_I} N_2^+ + 2e \; ,$$

e) Dissociative ionization,

$$N_2 + e \xrightarrow{Q_D} N^+ + N^* + 2e \; ,$$

f) Dissociation,

$$N_2 + e \rightarrow N + N^* + e \; ,$$
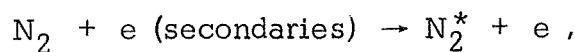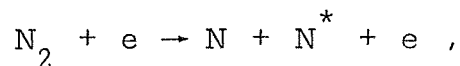
where:

$Q_{ov'}$ is the cross-section for excitation to a v' a $^1\Pi_g$ vibrational level from the ground vibrational state of N_2 by an electron of energy ϵ,

$Q_{ov''}$ is the cross-section for excitation to a vibrational level of an electronic state other than the a $^1\Pi_g$ state from the ground vibrational state of N_2 by an electron of energy ϵ,

A   is the radiative transition probability of the $a\,^1\Pi_g$ state,

N_2^* is a nitrogen molecule excited to the $a\,^1\Pi_g$ state,

N_2^{**} is a nitrogen molecule excited to an electronic state

other than the $a\,^1\Pi_g$ state.

Thus, there are many reactions going on simultaneously when an electron beam impinges on a neutral gas. The primary interest in any atmosphere calculation would be the number of photons coming out of an $a\,^1\Pi_g$ vibrational level per electron of energy, ϵ, impinging onto the gas. This number is proportional to the emission cross-section which is related to the absolute cross-section. The emission cross-section is defined from the equation

$$Q_{ov'}(\epsilon) = Q'_{ov'}(\epsilon) - \Sigma_{v'''} Q'_{ov'''}(\epsilon) \frac{A_{v'''v'}}{\Sigma_v A_{v'''v}} ,$$

$$(4.19)$$

where:

$Q'_{ov'}(\epsilon)$ is the emission cross-section,

$Q'_{ov'''}(\epsilon)$ is the emission cross-section of any v''' state

higher on the energy level diagram than the $a\,^1\Pi_g$

states (v'), but connected to it by a possible

transition,

$A_{v'''v'}$ is the transition probability from the higher state

to the $a\,^1\Pi_g$ state,

$\Sigma_v A_{v'''v}$ is the total transition probability from the v'''

state to all lower states.

The reactions described are completely general. In this specific application, with pressures below 0.2 microns, only reactions 4.17 a, b, c, d and e are of significance in determining the steady state LBH emission. Mean free paths for nitrogen-nitrogen collisions are greater than 50 cm, and mean free paths for elastic scattering of electrons are greater than 100 cm. The mean free path for excitation or ionization is greater than 300 cm. Thus, the steady state emission is determined by the balancing of 4.17 a, b, c, d and e for the LBH transition.

The theoretical problem of determining the emission cross-section of nitrogen for the forbidden Lyman-Birge-Hopfield transition from absolute intensity measurements of radiation emitted by molecules excited to the $a\,^1\Pi_g$ state by an electron beam can be divided into four separate problems:

(1)   Calculation of the volume emission rate from the excited $a\,^1\Pi_g$ molecules as a function of r, the distance from the electron beam.

(2)   Calculation of the integrated intensity at the entrance slit, (photons/sec cm^2 steradian).

(3)   Calculation of total light input to the slit (in photon/cm^2 sec) by integrating over the solid angle of the field of view.

(4)   Determination of cross-section by measuring the integrated

band intensities with a photomultiplier and strip chart

recorder.

These four calculations represent the geometrical and

physical factors encountered in this particular problem. The most

important physical process, other than the excitation and emission

processes, is the radial molecular flow of the excited molecules

away from the beam region due to the long lifetime (80 microseconds)

of the $a^1\Pi_g$ state. The effect of cascading has been combined with

the direct excitation cross-section to the $a^1\Pi_g$ state and contributes

to the apparent excitation cross-section. The state can be populated

by cascading ($^1\Sigma_u^+$ and $^1\Pi_u \rightarrow a^1\Pi_g$). The first calculation solves

the physical problem of electron excitation followed by spontaneous

radiation. The basic reactions are:

a) $N_2 + e \rightarrow N_2^* + e$,   (4.20)

and

b) $N_2^* \rightarrow N_2 + h\nu$.
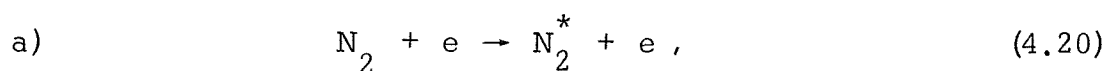
It assumes that the emission per unit length, and the excitation per

unit length, are equal. The final two integrals, or calculations,

account for the finite field of view ($9°40'$) of the spectrometer and

make the geometrical calculation of the fraction of the spontaneous

radiation seen by the spectrometer.

In the pressure range below 0.2 microns, there are no deactivations and no secondary processes. The flux of radiation, $F_{v'}$, seen at the entrance slit of the spectrometer from any v" progression, is proportional to pressure, cross-section, and electron beam current.

Thus,

$$F_{v'} \propto Q'_{ov'} (\epsilon) \, P_o J \qquad (4.21)$$

where:

$F_{v'}$ is the flux of radiation from a v' vibrational level of the $a\,^1\Pi_g$ state, incident on the entrance slit of the monochromator in units of photons/cm^2 sec,

P_o is the molecular nitrogen pressure,

J is the electron beam current.

The first three calculations give the constant of proportionality.

4.5.1   <u>The Volume Emission Rate from the Excited a $^1\Pi_g$ Molecules</u> <u>as a Function of the Distance from the Electron Beam</u>.

For the calculation of the volume emission rate from the $a\,^1\Pi_g$ molecules as a function of distance from the electron beam, let,

N_o be the number density of N_2 molecules in the collision chamber,

$Q'_{ov'}$ (ϵ)   be the apparent cross-section for excitation of a

neutral N_2 molecule to any vibrational level, v',

of the $a^1\Pi_g$ state by electrons of energy, ϵ,

e   be the charge of the electron,

T   be the temperature of the N_2 molecules,

A   be the transitional probability from an $a^1\Pi_g$ v'

vibrational level to the ground state,

S   be the cross-sectional area of the beam,

m   be the mass of the nitrogen molecule,

K   be the Boltzman constant.

The basic assumption is that the excitation per unit

length of the beam equals the emission per unit length. Further-

more, the geometry is one of cylindrical symmetry.

The production of $a^1\Pi_g$ molecules in the v' vibrational level

by an electron beam is

$$\text{Production} = \frac{N_o \, Q'_{ov'} \, J}{eS} = \#/cm^3 \, sec. \tag{4.22}$$

$$\text{Define } P = \frac{N_o \, Q'_{ov'} \, J}{e} = \#/cm \, sec = $$

excitation per unit length. $\tag{4.23}$

Let F (v_r) dv_r be the velocity distribution function of N_2 molecules

in cylindrical coordinates. Then, P F (v_r) dv_r is the number of

excited molecules produced in the velocity range, $\overline{v_r}$ to $\overline{v_r} + \overline{dv_r}$.

It can be shown that,

$$F(v_r) \; dv_r \; = \; 2\pi \left(\frac{m}{2\pi \; KT}\right) \exp \left[-\frac{m \; v_r^2}{2KT}\right] v_r \; dv_r \; . \qquad (4.24)$$

The r subscript from v_r and the prime superscript from Q'_{ov} will be omitted for convenience.

The probability of an excited molecule having a lifetime longer than a time, t, is e^{-At}. And, the probability of reaching a distance, r, is $\exp(-Ar/v)$.

The probability of decaying in t to t + dt is $Ae^{-At}dt$, or in r to r + dr is $A \exp(-Ar/v) \; dr/v$. Let $N_{v'}(r)$ be the number density of excited molecules in level v', then the emission in photons/sec in any volume element, $2\pi r \; drdz$ is

$$2\pi r \; A \; N_{v'}(r) \; drdz \; =$$

$$\int_{v=0}^{v=\infty} Pdz \; F(v) \; dv \; A \; \exp\left(\frac{-Ar}{v}\right) \frac{dr}{v} \; . \qquad (4.25)$$

Therefore,

a) $\qquad I_{v'}(r) \; = \; \frac{N_o \; Q_{ov'} \; J}{e} \; \frac{m}{2\pi KT} \; .$

$$A\left[\frac{1}{r} \; \int_0^\infty \exp\left[-\frac{mv^2}{2KT}\right] \exp\left[-\frac{Ar}{v}\right] \; dv \right], \qquad (4.26)$$

where:

$\left(\dfrac{2KT}{m}\right)^{1/2}$ is the mean velocity, v_m ,

$I_{v'}(r)$ is the volume emission rate in photons/sec cm^3 from

the v' vibrational level.

b) $I_{v'}(r) = \dfrac{N_o \, Q_{ov'} \, J}{\pi e \, v_m^2} \, A \, .$

$$\int_0^\infty \dfrac{1}{r} \exp\left[-\dfrac{v^2}{v_m^2}\right] \exp\left[-\dfrac{Ar}{v}\right] dv \, ,$$

define

$$x = \dfrac{v}{v_m} \, .$$

Then

$$v_m dx = dv \, .$$

Making this substitution into equation 4.26b, the following

equation is obtained

$I_{v'}(r) = \dfrac{N_o \, Q_{ov'} \, J}{\pi e} \dfrac{A}{v_m}$.

$$\int_0^\infty \dfrac{1}{r} e^{-x^2} \exp\left[-\dfrac{Ar}{v_m x}\right] dx \, . \tag{4.27}$$

By using the perfect gas law, $P_o = N_o KT$, and a temperature of

$294°K$, it is determined that,

$$N_O \, (cm^{-3}) \; = \; 3.28 \times 10^{13} \; P_O \; (microns) \qquad (4.28)$$

and using a molecular weight of 28 for N_2, it is found that,

$$v_m \; = \; 4.163 \times 10^4 \quad cm/sec \; ,$$

then,

$$\frac{I_{v'}(r)}{P_O \, (microns) \; J \, (microamps) \; Q_{ov'} \; (cm^2)} \; =$$

$$7.824 \times 10^{20} \; \times \; \frac{A}{r} \; \int_{-\infty}^{\infty} \; e^{-x^2} \; exp \left[- \frac{Ar}{v_m \, |x|} \right] \, dx \; . \qquad (4.29)$$

Equation 4.29 is in the Hermite form for a numerical integration by computer program. A plot of

$$M_{v'} \, (r) \; = \; \frac{I_{v'}}{P_O \, J \, Q_{ov'}} \quad versus \; r$$

is shown in Figure 4.4 for various values of A.

The fraction of the volume emission rate, $I_{v'}$, from any particular $(v'v'')$ transition is $\beta_{v'v''} I_{v'}$, where $\beta_{v'v''}$, the branching ratio for emission, is determined by the transition probabilities of the vibrational bands. Thus,

$$\beta_{v'v''} \; = \; \frac{A_{v'v''}}{\sum_{v''} A_{v'v''}} \; . \qquad (4.30)$$

It is seen that the intensity or volume emission rate is a glow of cylindrical symmetry about the beam, the intensity falling off a

$$M_V'(r) = 7.824 \times 10^{20} \times A/r \int_{-\infty}^{\infty} EXP(-X^2)$$

$$EXP(-Ar/V_m |X|)\, dX \text{ FOR } 3$$
DIFFERENT LBH LIFETIMES –
$$A = 1/\tau$$
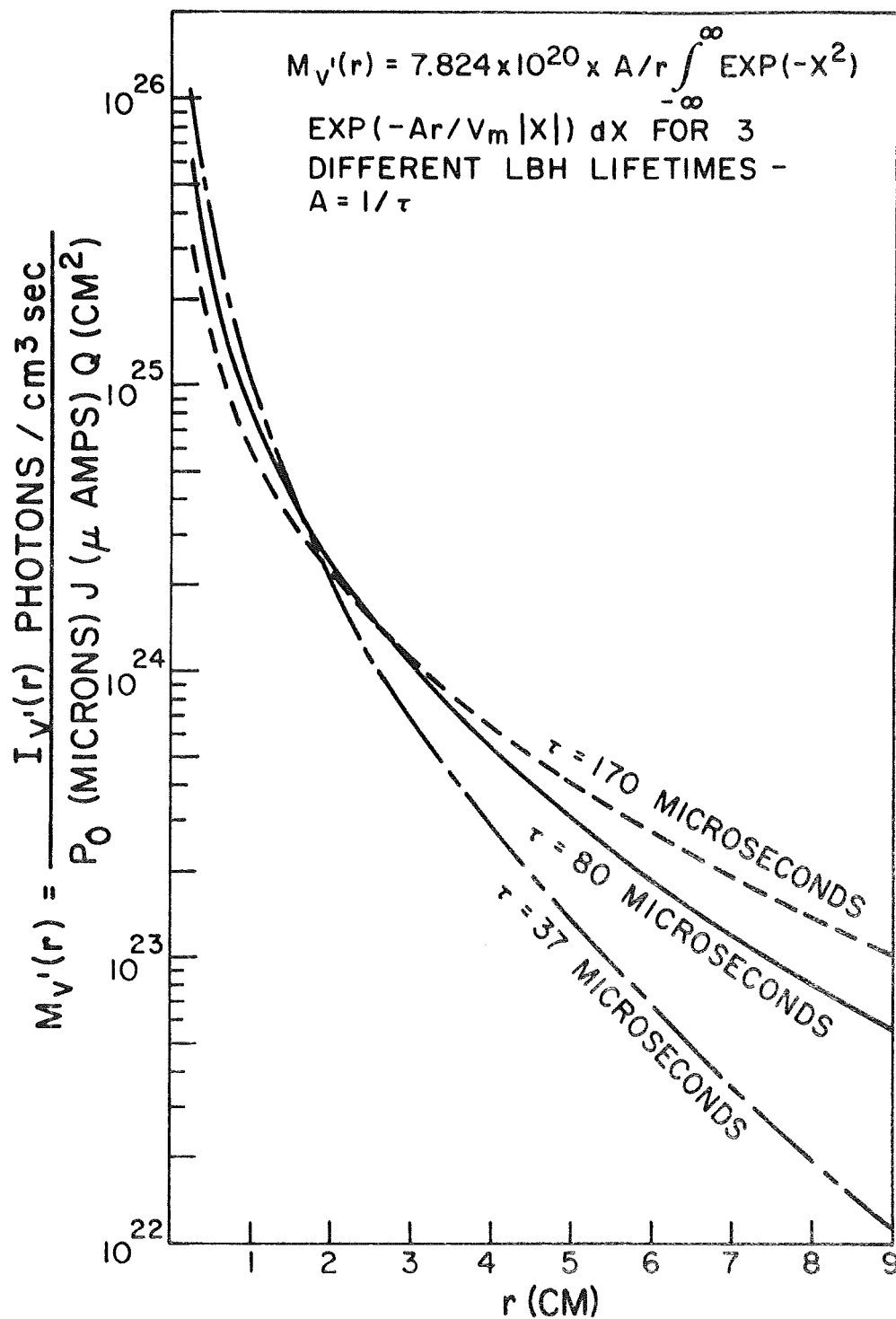
Figure   THE SHAPE OF THE LBH GLOW REGION AS A
4.4   FUNCTION OF DISTANCE FROM THE ELECTRON
          BEAM FOR 3 LIFETIMES

little faster than $1/r$ due to the term, $\exp\left(-Ar/v_m \,|x\,|\right)$ in the integral. Since the assumption of an 80 microsecond lifetime for each vibrational level of the $a^1\Pi_g$ state is made, each vibrational level has a glow of the same relative shape. The absolute intensity or volume emission rate for each vibrational level of the $a^1\Pi_g$ state is proportional to $Q_{ov'}$, all other factors being equal.

By multiplying both side of Eqn. 4.27 by $2\pi r \, dr$ and integrating from 0 to ∞, it can be shown that the total emission per cm equals the total excitation per cm - $N_o \, Q_{ov'} \, (\epsilon\,)\, J/e$.

4.5.2 Calculation of the Integrated Intensity at the Entrance Slit of the Monochromator.

Define "a" as the minimum distance to the beam from a line of sight, and p as the distance measured along the line of sight perpendicular to "a", then $\vartheta_{v'}$ the integrated intensity at the slit in photons/cm^2 sec steradian is

$$\vartheta_{v'}\,(a\,) = \frac{1}{4\pi} \int_{-\infty}^{\infty} I_{v'}'\,(p\,)\, dp. \qquad (4.31)$$

(See Figure 4.5)

The justification for this equation can be seen from the following considerations: The slit has an area A_s, and subtends an angle A_s/R^2, as seen from the source. The number of photons
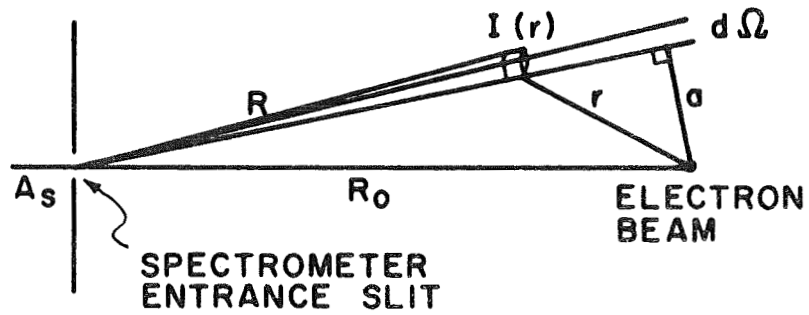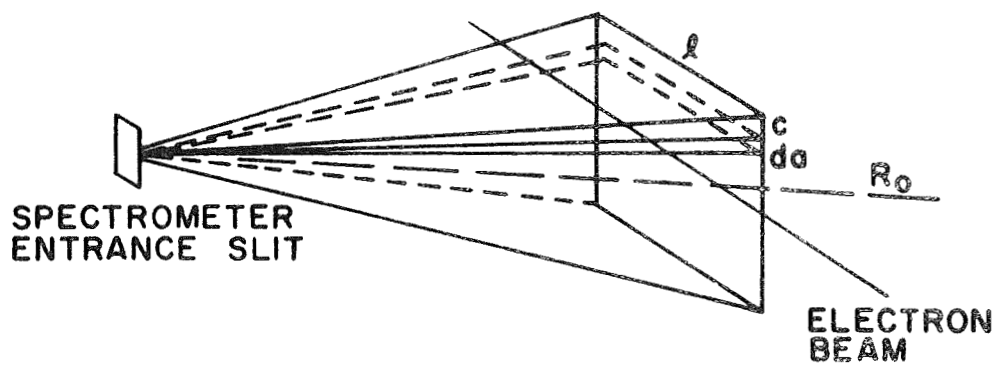
FIGURE 4.5 Geometry for line of sight calculation.

FIGURE 4.6 Geometry for the integration over the field.

reaching the entrance slit from an element of length $dR = dp$,

and an area $R^2 d\Omega$, perpendicular to the line of sight, is

$$\frac{A_s R^2}{4\pi R^2} I'_{v'} (p) \, dp \, d\Omega \ .$$

Thus, the total number of photons per cm^2 per steradian per second

at the slit from a v'' progression is

$$\vartheta_{v'} = \frac{1}{4\pi} \int_{-\infty}^{\infty} I'_{v'} (p) \, dp, \qquad (4.32)$$

where

$$r = (p^2 + a^2)^{1/2}$$

and

$$I'_{v'} (p) = I_{v'} (p^2 + a^2)^{1/2} \ . \qquad (4.33)$$

Then,

$$\frac{\vartheta_{v'} (a)}{P_0 \, (\text{microns}) \, Q_{ov'} \, (cm^2) \, J \, (\text{microamps})} =$$

$$L_{v'} (a) = 1.2452 \times 10^{20} \, A \int_{-\infty}^{\infty} e^{-x^2} .$$

$$dx \int_0^{\infty} \frac{1}{(p^2 + a^2)^{1/2}} e^{-p} .$$

$$\exp\left\{-p\left[\frac{A}{v_m |x|} (1 + \frac{a^2}{p^2})^{1/2} -1\right]\right\} dp \ . \qquad (4.34)$$

Unity in the form, $e^{-p} e^{+p}$, is multiplied into the line of sight integral, Eqn. 4.34, to put it in the Laguerre form for a numerical integration. A plot of $\vartheta_{v'}$ versus a is shown in Figure 4.7.

4.5.3 The Total Light Input to the Slit from a v" Progression.

The total light input to the slit from a v" progression (in units of photon/cm^2 sec) is obtained by integrating $\vartheta_{v'}$ (a) over the solid angle of the field of view. The result is

$$F_{v'} = \int_{\Omega} \vartheta_{v'}(a) \, d\Omega(a) \qquad (4.35)$$

where:

Ω (a)   is the solid angle determined by the field of view of the spectrometer, $d\Omega(a) = \ell \, da/R_0^2$,

R_0 is the distance from the slit to the beam,

ℓ is the width of field of view at the beam, its actual size depends on the width of grating projected onto the beam. (See Figure 4.6).

Thus,

$$\frac{F_{v'}}{P_0 \text{ (microns) } J \text{ (microamps) } Q_{ov'} \text{ (cm}^2)} =$$

$$2 \frac{\ell}{R_0} \int_0^C L(a) \, da \, . \qquad (4.36)$$

$$L_{v'}(a) = 1.2452 \times 10^{20} A \int_{-\infty}^{\infty} e^{-X^2} dX \int_{0}^{\infty} e^{-p}/\sqrt{p^2 + a^2} \; EXP \left\{ -p \left[A/V_m |X| \right] \left[\sqrt{1 + a^2/p^2} - 1 \right] \right\} dp \; \text{FOR 3 DIFFERENT LIFETIMES} \; A = 1/\tau$$

$\tau = 170$ MICROSECONDS

$\tau = 80$ MICROSECONDS

$\tau = 37$ MICROSECONDS

$$L_{v'}(a) = \frac{\ell_{v'}(a) \; \text{PHOTONS/sec. ster. cm}^2}{P_0 \; (\text{MICRONS}) \; J \; (\mu \; \text{AMPS}) \; Q \; (\text{CM}^2)}$$

a (CM)
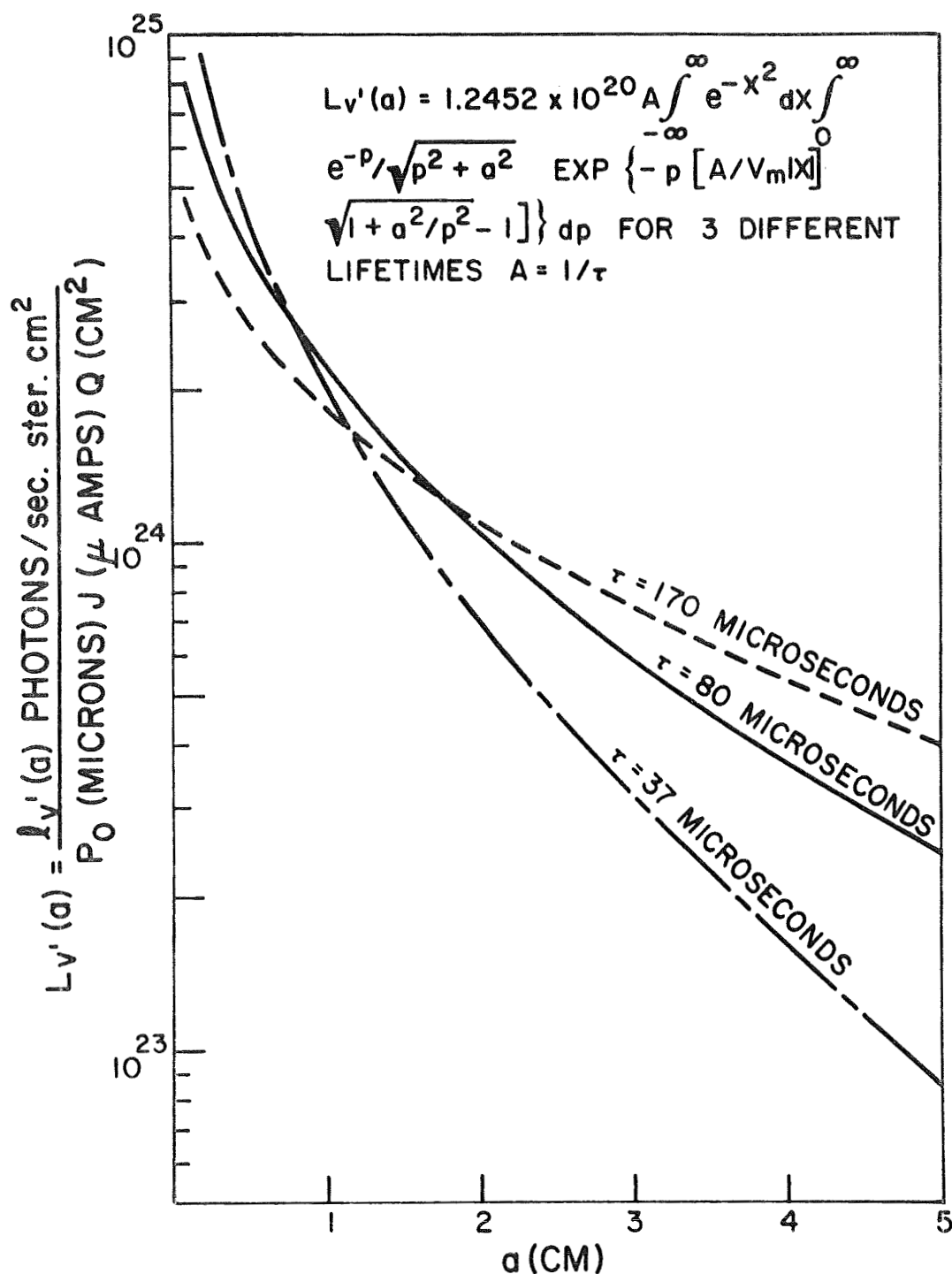
Figure 4.7   THE INTEGRATED INTENSITY OF A v" PROGRESSION OF THE LBH SYSTEM AT THE ENTRANCE SLIT AS A FUNCTION OF MINIMUM DISTANCE FROM THE ELECTRON BEAM TO THE LINE OF SIGHT

where c is the height of the field of view at the beam.

Eqn. 4.36 is essentially a triple integral in the variables a, r, v, and can be determined by a suitable computer program once all the geometrical and physical constants have been determined. The result is a constant for a particular geometry. Thus

$$F_{v'} = k \ P_O \ (\text{microns}) \ J \ (\text{microamps}) \ Q_{ov'} \ (\text{cm}^{+2}) \ . \quad (4.37)$$

k represents the triple integral of Eqn. 4.36, if the area of the slit is A_s, then

$$Z_{v'} = F A_s = k \ P_O \ J \ Q_{ov'} \ A_s \ . \quad (4.38)$$

is the experimentally measured quantity in photons/sec from a v" progression for a calibrated system.

In this experiment, ℓ = 4.22 cm. It is determined by projecting the width of the grating onto the beam. c is equal to 2.05 cm. It is determined by projecting the height of the grating onto the beam. The vignetting effect, caused by the finite height of the slit for the LBH bands, must be included in the calculation. Using these values for ℓ and c, and the fact R_O is 24.924 cm, the value of k determined is

a) $$k = 8.258 \times 10^{22}, \quad (4.39)$$

for t = 80 microseconds,

b) $k = 9.800 \times 10^{22}$,

for t = 37 microseconds,

c) $k = 6.12 \times 10^{22}$,

for t = 170 microseconds.

The value of k used is determined from the 80 microsecond life-time measured by Holland. If it turns out that one of the other values is more accurate, all cross-sections will have to be divided by the ratio of the proper k to 8.258×10^{22}.

Although this calculation is purely geometrical, it is important to note the effect of the variance of the three measured of calculated lifetimes. It is this lifetime which determined how much of the spontaneous radiation is seen by the spectrometer and photomultiplier tube. If t is very small, i.e., molecular flow is negligible, as in the case of the atomic nitrogen lines, then $k = 1.1607 \times 10^{23}$. Thus, the fraction of spontaneous radiation seen by the detection system is as follows for the various lifetimes:

Lifetime	Fraction of radiation detected
t = 37 microseconds	.84
t = 80 microseconds	.71
t = 170 microseconds	.53

4.5.4 Determination of Cross-Section by Using a Photomultiplier

and Strip Chart Recorder.

By measuring the integrated band intensities with a calibrated

photomultiplier, monochromator, and strip chart recorder, it is

possible to determine $Z_{v'}$, the light input per second from a v' vi-

brational level at the entrance slit of the monochromator. Consider

the following quantities:

S_{spec} is the scan speed of the monochromator,

S_{rec} is the speed of the recorder chart paper,

w is the slit width in mm,

D is the dispersion of the instrument in $\overset{\circ}{A}/mm$,

ϵ_{λ} is the efficiency of the monochromator (grating

and two mirrors),

g is the gain of the PMT tube,

q_{λ}' is the quantum efficiency of the PMT tube,

τ_{λ} is the transmission of the LiF window.

Figure 4.8a represents the output current versus time, or

chart paper distance, for a particular band. Figure 4.8b represents

the desired current caused by a linear transformation of Figure 4.8a

to yield the total band intensity. If Y_{λ} is the current output from the

photomultiplier, then,

$$Z_{\lambda}' = \frac{Y_{\lambda}}{wD}$$

Y$_\lambda$ (amps)

O -

Recorder paper distance - S (mm)
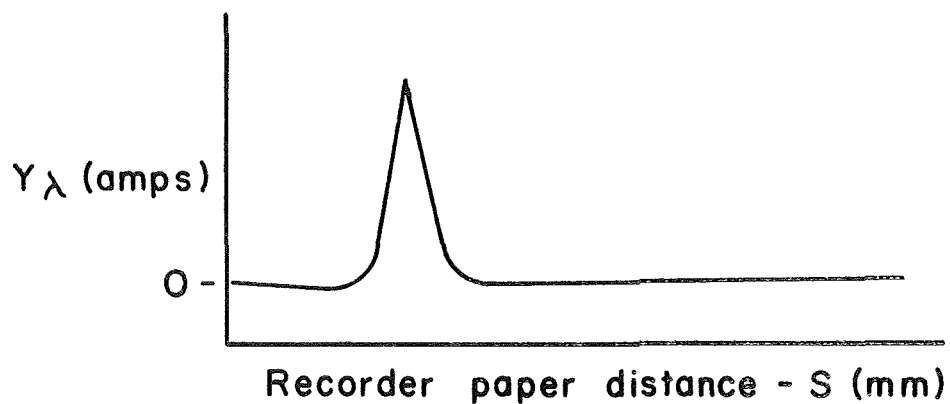
FIGURE 4.8 a

LINEAR TRANSFORMATION OF OUTPUT FROM
RECORDER V S CHART PAPER DISTANCE $\longrightarrow$
BAND INTENSITY V S WAVELENGTH.

$Z'_\lambda = \dfrac{Y\lambda}{wD}$

(amps / Å)

O -

Wavelength (Angstroms) $\lambda = \dfrac{S\,spec}{S\,rec} \times S$
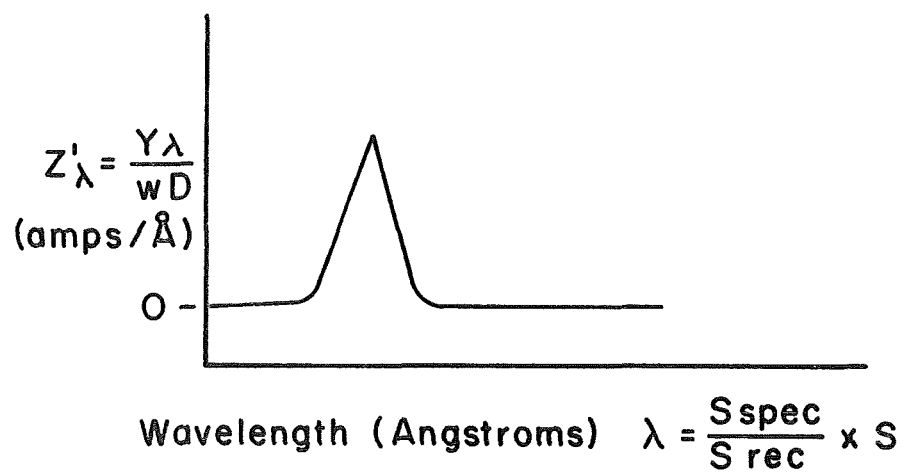
FIGURE 4.8 b

is the current output in amps per Angstrom. If s is the distance in mm along the chart paper, then,

$$d\lambda = \frac{S_{spec}}{S_{rec}} \times ds$$

and the output current of the photomultiplier, from any band $-[v'v'']$ is

$$Z'_{v'v''} = \int_{band} Z'_\lambda \, d\lambda = \frac{S_{spec}}{S_{rec}} \times \frac{1}{wD} \int_{band} Y_\lambda \, ds \quad . \qquad (4.40)$$

$\int Y_\lambda \, ds$ is the area under 4.8a in amp x mm.

To convert $Z'_{v'v''}$, the current, or coulombs/sec, to photons/sec, it is noted that

$$\frac{Z'_{v'v''}}{e} = Z_{v'v''} \, \epsilon_\lambda \, q'_\lambda \, g \, \tau_\lambda \quad .$$

Thus,

$$Z_{v'v''} = \frac{Z'_{v'v''}}{\epsilon_\lambda \, eq'_\lambda \, \tau_\lambda \, g} \, , \qquad (4.41)$$

and

$$Z_{v'} = \Sigma_{v''} \, Z_{v'v''} = \Sigma_{v''} \, Z'_{v'v''} / \epsilon_\lambda \, eq'_\lambda \, \tau_\lambda \, g. \qquad (4.42)$$

Thus, from 4.38 and 4.42, where ϵ_λ and q'_λ vary slowly over a band, and λ corresponds to the wavelength of the center of a $(v'v'')$ band, it follows that,

$$Z_{v'} = \frac{S_{spec}}{S_{rec}} \times \frac{1}{wD} \times \frac{1}{e} \times \Sigma_{v''} \left\{ \frac{\int Y_\lambda \, ds}{v'v'' \text{ band}} \frac{}{\epsilon_\lambda \, q_\lambda^r \, g \, \tau_\lambda} \right\} \quad (4.43)$$

and

$$\frac{S_{spec}}{S_{rec}} \times \frac{1}{wD} \times \frac{1}{e} \times$$

$$\Sigma_{v''} \quad \left\{ \frac{\int Y_\lambda \, ds}{v'v'' \text{ band}} \frac{}{\epsilon_\lambda \, q_\lambda^r \, g \, \tau_\lambda} \right\} =$$

all bands
from a common
v'

$$k \ P_o \ J \ Q_{ov'} \ A_s \ . \quad (4.44)$$

$$Q_{ov'} = \frac{1}{k \ P_o \ J \ A} \times \frac{S_{spec}}{S_{rec}} \times$$

$$\frac{1}{wD} \times \frac{1}{e} \times \Sigma_{v''} \left\{ \frac{\int Y_\lambda \, ds}{v'v'' \text{ band}} \frac{}{\epsilon_\lambda \, q_\lambda^r \, g \, \tau_\lambda} \right\}$$

$$(4.45)$$

Thus, the total electronic Lyman-Birge-Hopfield cross-section is

$$Q_{LBH} = \Sigma_{v'} \ Q_{ov'} \ . \quad (4.46)$$

In the experiment the various parameters had the following

values:

a) $\qquad S_{spec} = 50 \ \text{Å/mm} \qquad (4.47)$

b) $\quad S_{rec} \quad = 1 \text{ mm/sec}$

c) $\quad\quad D \quad = 13.9 \text{ Å/mm}$

d) $\quad\quad A_s \quad = w \times 3.92 \text{ mm}$

e) $\quad\quad k \quad = 8.258 \times 10^{22}$

where w, the slit width, was usually 0.200 mm, and 3.92 mm

was the effective slit height. Thus, inserting these values into

Eqn. 4.45, the following result is obtained,

$$Q_{ov'} = \frac{5.780 \times 10^{-18}}{P_o \, J \, w^2} \times$$

$$\frac{\Sigma_{v''} \, W_{v'v''} \times H_{v'v''} \times \text{Scale}_{v'v''}}{\epsilon_\lambda \, q_\lambda \, g \, \tau_\lambda}$$

$$(4.48)$$

where $\int Y_\lambda \, ds$ is approximated by a triangular band shape. The

following experimental parameters are defined:

$W_{v'v''}$ $\quad$ is the width of the band in mm,

$H_{v'v''}$ $\quad$ is the height of the band in mm,

$\text{Scale}_{v'v''}$ $\quad$ refers to the scale on the picoammeter used to

$\quad\quad\quad\quad\quad$ record the data. It is the sensitivity of the pico-

$\quad\quad\quad\quad\quad$ ammeter-recorder combination. It has units of 0.1

$\quad\quad\quad\quad\quad$ picoamperes/mm.

$\quad$ The monochromator can be viewed as a black box with a

certain transfer function. Its output is a convolution of the incident

radiation with the slit function. In the ideal case the slit function is triangular and the incident radiation a series of delta functions of various amplitudes. The resultant convolved output of the instrument is a series of triangles.

This is a very good approximation since at the $200\,\mu$ slit widths used, all band shapes were recorded as triangular, i.e., the instrumental width is much greater than the width of the band. It should be noted that the total cross-section for any vibrational level is the sum of partial cross-sections, due to the branching of the emission electron to various v" vibrational levels of the ground state. That is,

$$\beta_{v'v''}\ Q_{ov'} = Q_{v'v''} = $$

$$\frac{5.780 \times 10^{-18}}{P_o\, J\, w^2} \quad \times \quad \frac{W_{v'v''}\ H_{v'v''} \times Scale_{v'v''}}{\epsilon_\lambda\ q_\lambda\ g\ \tau_\lambda} ,$$

$$(4.49)$$

where we have defined $Q_{v'v''}$ as the emission cross-section for the [v'v"] band. This is the equation used for determining emission cross-sections for each [v'v"] vibrational band from the experimental data.

4.6 Steady State Emission and Excitation--The Atomic Nitrogen Lines.

Excitation of atomic nitrogen from the ground state of molecular nitrogen by dissociative excitation processes has been observed, and emission cross-sections determined.

The steady state equation relating population gain and loss of the j-th state of an atomic-molecular system in an electron beam dissociation process is

$$Q_D(j) \frac{J N_o}{eS} + \Sigma_i N_i A_{ij} +$$

$$\text{transfer gain} = N_j A_j + \text{transfer loss}, \qquad (4.50)$$

where:

$Q_D(j)$ is the absolute cross-section for dissociative excitation (either ionization or pure dissociation) by electron impact from the ground state of molecular nitrogen to the j-th state of atomic nitrogen,

N_j is the number density of atomic nitrogen atoms in the j-th state,

N_i is the number density of atomic nitrogen atoms in the i-th state,

A_{ij} is the probability of transition from the i-th state to the j-th state,

A_j is the probability of transition from the j-th state to all lower states.

The transfer of excitation is negligible for pressures of 1 micron or less. The current strength in the beam is so small that

collisions between excited atoms and beam electrons may be neglected. Thus, it is found,

$$\frac{Q_D(j) \, J \, N_o}{e \, S} + \Sigma_i \, N_i \, A_{ij} = N_j \, A_j \ . \tag{4.51}$$

It follows that if absolute intensity measurements are made of radiation, both to and from the j-th state, then the absolute cross-section $Q_D(j)$ can be derived. What is usually measured in optical experiments of this kind is the absolute intensity variation with energy of radiation from the j-th state.

An apparent cross-section $Q'_D(j)$ is defined from the equation

$$Q'_D(j) \, \frac{J}{e} \, \frac{N_o}{S} = N_j \, A_j \ . \tag{4.52}$$

It is seen that the emission cross-section is related to the absolute cross-section by Eqn. 4.53 since the right hand sides of 4.51 and 4.52 are equal.

$$Q'_D(j) \, \frac{J}{eS} \, N_o = \frac{Q_D(j) \, J}{eS} \, N_o + \Sigma_i \, N_i \, A_{ij} \tag{4.53}$$

or

$$Q_D(j) = Q'_D(j) - \Sigma_i \, N_i \, A_{ij} \, x \, \frac{eS}{J \, N_o} \ , \tag{4.54}$$

but

$$Q'_D(i) = \frac{N_i \, A_{ij} \, A_i}{A_{ij}} \times \frac{eS}{J \, N_o} \quad . \tag{4.55}$$

Making this substitution into Eqn. 4.54, it follows that

$$Q_D(j) = Q'_D(j) - \sum_i Q'_D(i) \frac{A_{ij}}{A_i} \quad . \tag{4.56}$$

This is the relation between emission of apparent cross-section and absolute excitation cross-section. The two cross-sections are equal if cascading is negligible.

If experimentally, all that is observed is a particular transition from the j-th state to the k-th state, then

$$Q'_D(j) \frac{J}{e} \frac{N_o}{S} = N_j \, A_j = N_j \, A_{jk} \frac{A_j}{A_{jk}} \tag{4.57}$$

or

$$\beta_{jk} \, Q'_D(j) \frac{J}{e} \frac{N_o}{S} = N_j \, A_{jk} \quad , \tag{4.58}$$

where β_{jk} is the emission branching ratio from the j-th state to the k-th state.

We will drop the prime superscript and assume all cross-sections are apparent or emission cross-sections. In particular, we are interested in the following dissociative reactions:

a)
$$N_2(X^1\Sigma_g^+) + e \xrightarrow{\ Q_{D_1}(^4P)\ } N(^4P) + N + e \ , \qquad (4.59)$$

b)
$$N(^4P) \rightarrow N(^4S^\circ) + h\nu_{1200} \ ,$$

c)
$$N_2(X^1\Sigma_g^+) + e \xrightarrow{\ Q_{D_2}(^4P)\ } N(^4P) + N^+ + 2e \ ,$$

d)
$$N(^4P) \rightarrow N(^4S^\circ) + h\nu_{1200} \ ,$$

e)
$$N_2(X^1\Sigma_g^+) + e \xrightarrow{\ Q_{D_1}(^2P)\ } N(^2P) + N + e \ ,$$

f)
$$N(^2P) \rightarrow N(^2D^\circ) + h\nu_{1493} \ ,$$

g)
$$N(^2P) \rightarrow N(^2P^\circ) + h\nu_{1743} \ ,$$

h)
$$N_2(X^1\Sigma_g^+) + e \xrightarrow{\ Q_{D_2}(^2P)\ } N(^2P) + N^+ + 2e \ ,$$

i)
$$N(^2P) \rightarrow N(^2D^\circ) + h\nu_{1493} \ ,$$

j)
$$N(^2P) \rightarrow N(^2P^\circ) + h\nu_{1743} \ ,$$
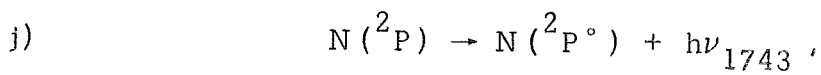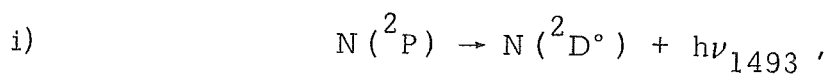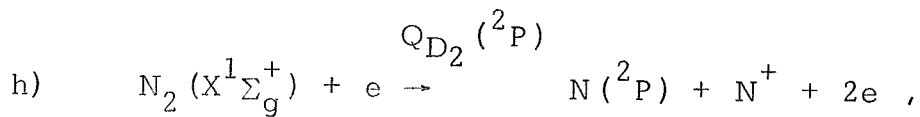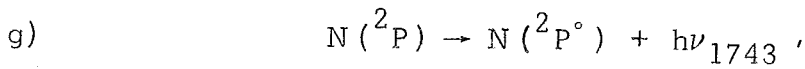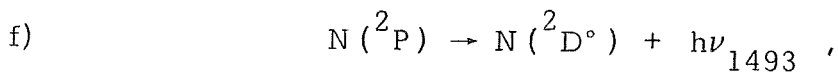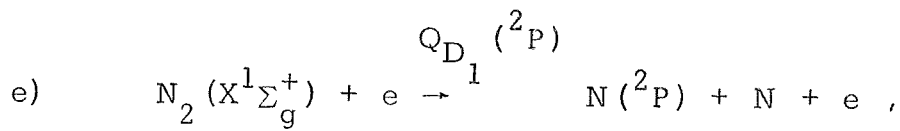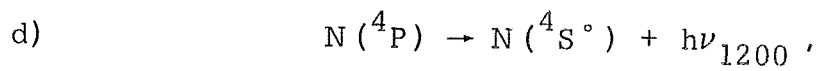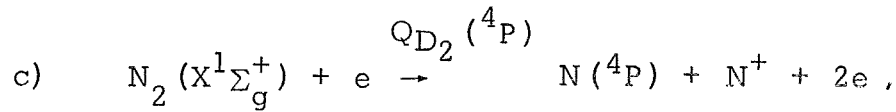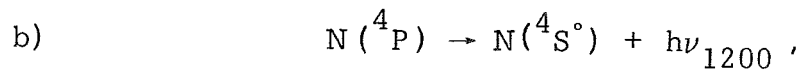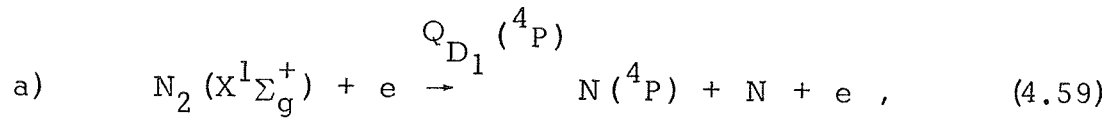
where:

$Q_{D_i}(j)$ is a dissociative excitation reaction if i = 1

where $j = {}^4P, {}^2P,$

$Q_{D_i}(j)$ is a dissociative ionization excitation reaction if

i = 2 where $j = {}^4P, {}^2P.$

$Q_{D_i}({}^2P)$ can be further broken up into partial cross-sections, since a branching is involved:

$$Q_{D_i}({}^2P) = Q_{D_i}(1493 \text{ Å}) + Q_{D_i}(1743 \text{ Å}). \qquad (4.60)$$

It is not possible to distinguish the radiation from each type of dissociation above the threshold for dissociative ionization. Therefore, what is determined is the sum of cross-sections of the two types of dissociative transitions. That is,

$$Q_D = Q_{D_1}(j) + Q_{D_2}(j) . \qquad (4.61)$$

This is the important quantity in any atmospheric calculation. There is the possibility of a cascade contribution to these cross-sections, since there are many permitted transitions to the ^2P and ^4P levels. See the energy level diagram of NI (Figure 4.2).

4.7   Photometry for the Atomic Nitrogen Lines.

The geometrical calculation of the radiation detected is very similar to the determination of the Lyman-Birge-Hopfield

radiation detected, except, there are no molecular flow effects.

From Eqn. 4.52,

$$I_j = N_j A_j = Q'_o (j) \frac{J N_o}{eS}$$ (4.62)

is the volume emission rate from the j-th state to all lower states.
The emission per unit length of the beam is

$$\frac{Q_D (j) J N_o}{e} \quad .$$

The total emission from a small increment of length of the
beam, $d\ell$, is

$$\frac{Q_D (j) J N_o d\ell}{e} \quad .$$

The fraction of the radiation detected is equal to the solid

angle subtended by the entrance slit, divided by 4π. This quantity

is

$$\frac{Q_D (j) J N_o A_s d\ell}{e \ 4\pi \ R_o^2} \quad .$$

Thus the total radiation, in units of photons/sec, at the

entrance of the spectrometer from the length, ℓ , of the beam in

the field of view is

$$Z(j) = \frac{Q_D (j) J N_o A_s \ell}{e \ 4\pi \ R_o^2}$$ (4.63)

or

$$Z(j) = K_D \, Q_D(j) \, P_o \, J \, A_s \, , \qquad (4.64)$$

where K_D is a constant of proportionality containing the geometrical factors.

Using the perfect gas law to determine N_o in terms of P_o, in microns, and where:

J   is in microamps,

ℓ   is 4.22 cm,

R_o is 24.924 cm,

A_s is 4 mm x w,

the following value of K_D is obtained,

$$K_D = 1.1607 \times 10^{23} \, . \qquad (4.65)$$

Thus,

$$Q_D(j) = \frac{Z(j)}{K_D \, J \, P_o \, A_s} \, . \qquad (4.66)$$

Incorporating the monochromator and photomultiplier calibration factors into this equation in a similar way as in the LBH calculation, the following result is obtained for the total emission cross-section of the j-th electronic term of an atom in this experiment

$$Q_o'(j) = \frac{4.2269 \times 10^{-18}}{P_o \, J \, w^2} \cdot$$

$$\sum_{\substack{k \\ \text{all final} \\ \text{states}}} \frac{W_{jk} \, H_{jk} \, \text{Scale}_{jk}}{\epsilon_\lambda \, q_\lambda' \, g \, \tau_\lambda} \, , \qquad (4.67)$$

where:

W_{jk} is the width of the line in mm from a $j \rightarrow k$ transition,

H_{jk} is the height of the line in mm,

Scale_{jk} is the sensitivity of the recorder-picoammeter com-

bination in units of 0.1 picoamperes/mm,

w is the slit width in mm.

In particular, for the 1200 Å, 1493 Å and 1743 Å multiplets

of atomic nitrogen, respectively, the individual emission cross-

sections are:

a) $Q_D(1200) = Q_D(^4P) =$

$$\frac{4.2269 \times 10^{-18}}{P_o \, J \, w^2} \quad \frac{W_{1200} \, H_{1200} \, \text{Scale}_{1200}}{\epsilon_{1200} \, q'_{1200} \, g \, \tau_{1200}}, \qquad (4.68)$$

b) $Q_D(1493) =$

$$\frac{4.2269 \times 10^{-18}}{P_o \, J \, w^2} \quad \frac{W_{1493} \, H_{1493} \, \text{Scale}_{1493}}{\epsilon_{1493} \, q'_{1493} \, g \, \tau_{1493}},$$

c) $Q_D(1743) =$

$$\frac{4.2269 \times 10^{-18}}{P_o \ J \ w^2} \ \frac{W_{1743} \ H_{1743} \ Scale_{1743}}{\epsilon_{1743} \ q'_{1743} \ g \ \tau_{1743}} \ .$$

$$Q_D(^2P) = Q_D(1493) + Q_D(1743) \ . \tag{4.69}$$

Equations 4.68 and 4.69 were the equations used to determine the dissociative excitation cross-sections of molecular nitrogen from the experimental data.

CHAPTER V

EXPERIMENTAL RESULTS

5.1   Introduction

The experimental results can be divided into two parts.

First, there were the linearity tests on the LBH band system and

nitrogen lines. These were preliminary measurements to determine

the range of electron beam currents and molecular nitrogen pres-

sures in which the measured flux of radiation was linear in these

two parameters. The basic equation for experimentally determining

emission cross-sections is

$$F_{v'} = k \ P_O \ Q_{Ov'} \ (\epsilon) \ J \ . \qquad (Eqn. \ 4.37)$$

This equation assumes the measured flux of radiation $F_{v'}$ is linearly

proportional to the molecular nitrogen pressure in the chamber and

the electron beam current. By varying P_O and J over a range of

pressures and electron beam currents, respectively, it can be

determined over what range $F_{v'}$ is linear in these parameters. For

low enough pressures and electron beam currents, this equation is

valid in determining cross-sections. For high pressures and/or

electron beam currents, secondary processes become important.

Using the results of the linearity measurements, the electron beam chamber was maintained in the linear pressure and electron beam current regime for the cross-section measurement and the entire spectrum recorded between 1200 Å and 2000 Å. The emission cross-section for each LBH band and each nitrogen line was then determined using Eqn. 4.49 or Eqn. 4.68 of Chapter IV. The emission cross-sections of the LBH band system were summed to obtain a total cross-section for the entire electronic transition and total cross-sections for each vibrational level.

5.2   Pressure Dependence.

The pressure dependence of the flux of radiation from various bands of the LBH system was investigated for energies between 25 eV and 100 eV and for pressures from .03 microns to 1 micron. The results indicated that secondary processes became important at pressures greater than 0.2 microns, since non-linearity of flux versus pressure began at this pressure. The linearity tests were performed by focusing a particular band on the exit slit of the monochromator at a particular energy and changing the pressure in small increments, noting the current in the pico-ammeter, the pressure and the electron beam current. The three bands tested were the (1,1), (2,0) and (3,0). The results are displayed in Figures 5.1, 5.2 and 5.3. Consider for a moment
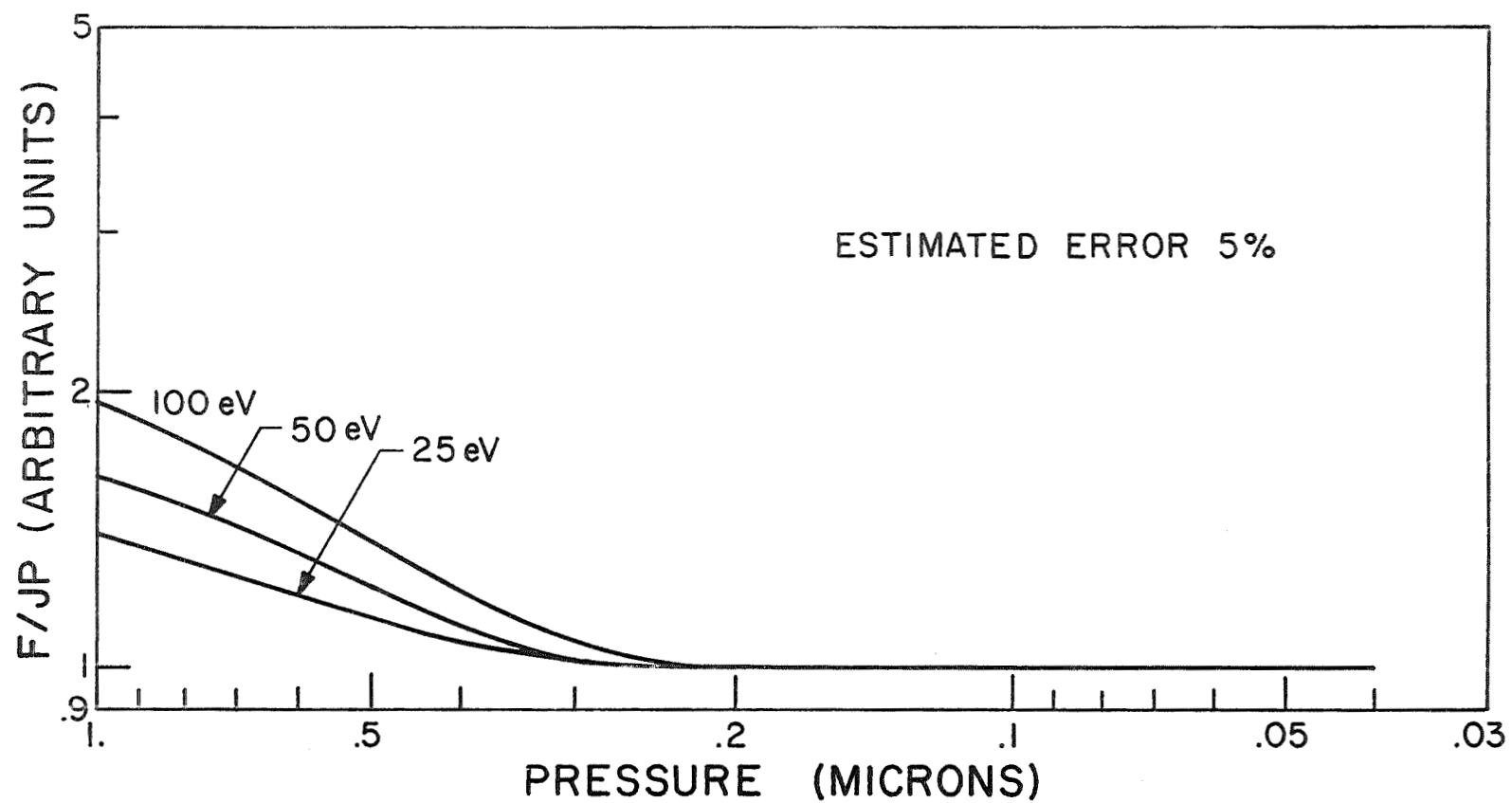
Figure 5.1   FLUX/ELECTRON BEAM CURRENT x PRESSURE
vs. PRESSURE FOR (I,I) LBH BAND

126
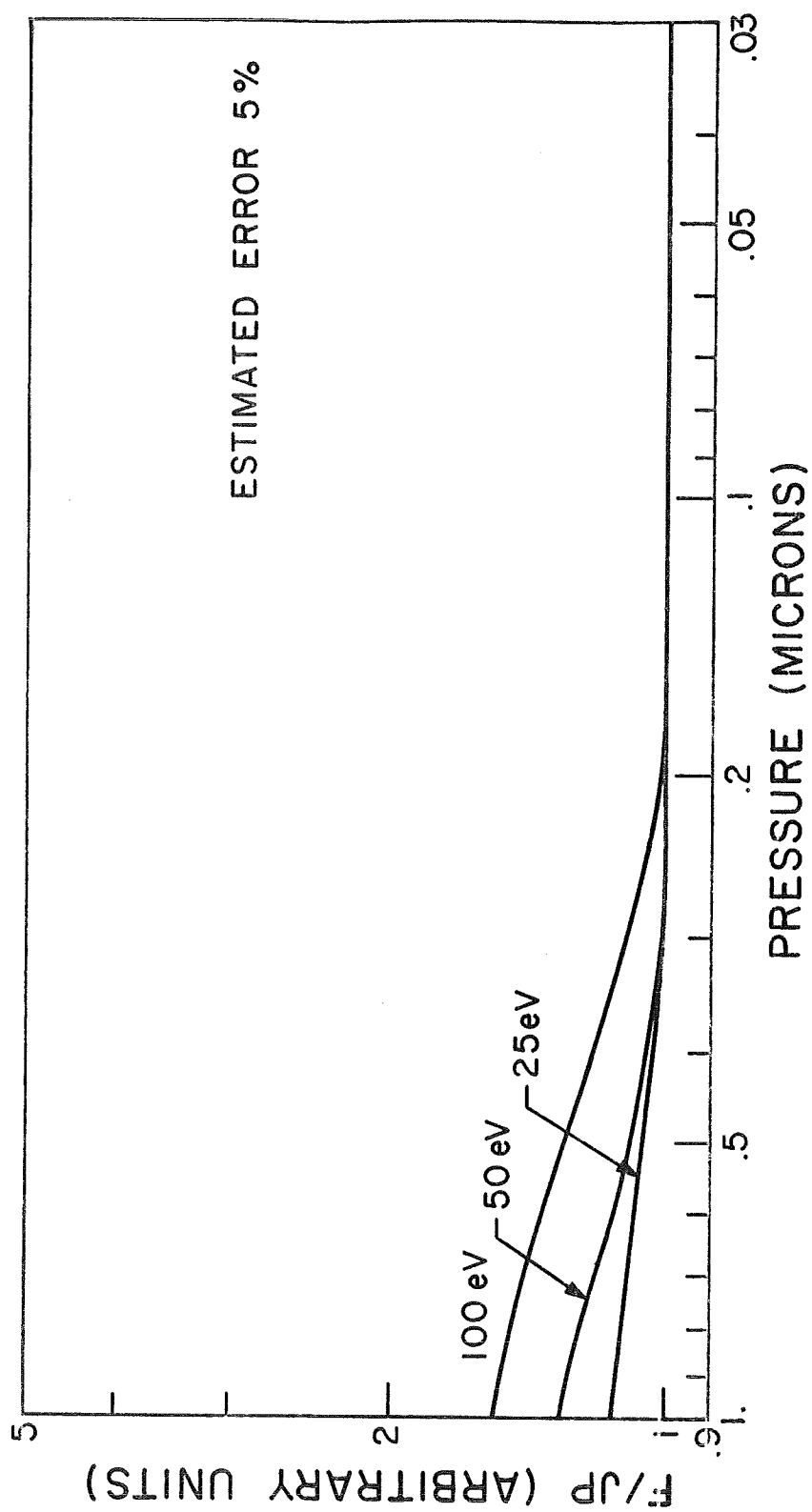
Figure 5.2   FLUX/ELECTRON BEAM CURRENT x PRESSURE
vs. PRESSURE FOR (2,0) LBH BAND
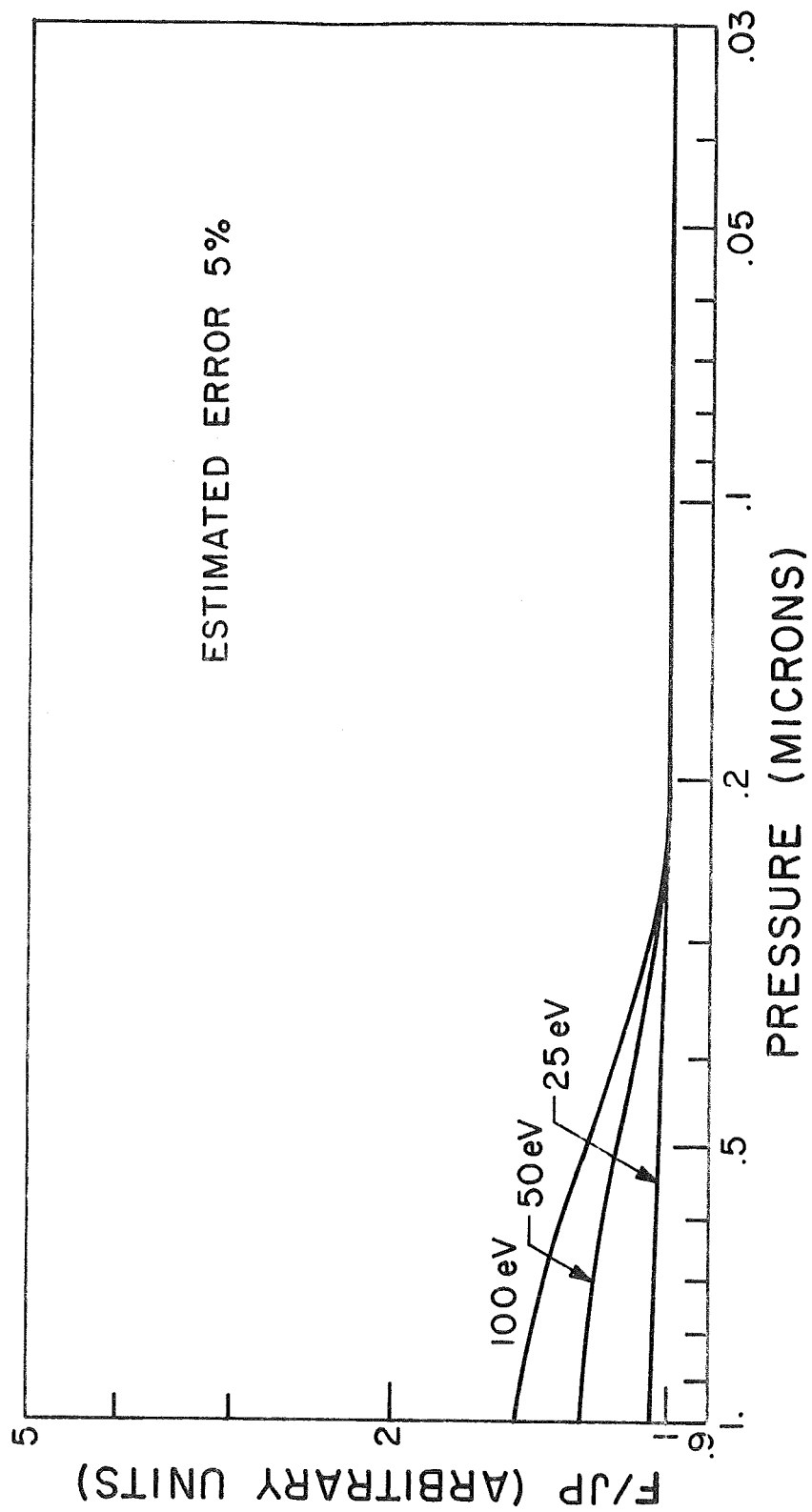
Figure 5.3 FLUX/ELECTRON BEAM CURRENT x PRESSURE
vs. PRESSURE FOR (3,0) LBH BAND

one band, say the (1,1) band in Figure 5.1. In this figure is plotted

the flux of radiation in arbitrary units, divided by pressure and beam

current versus pressure at three different energies, 25 eV, 50 eV

and 100 eV. It can be seen that the ratio of flux divided by pres-

sure was a constant for all these energies up to pressures of 0.18

microns. The non-linearity was greatest at 100 eV, and least at

25 eV for pressures greater than 0.18 microns. Similar results

held true for the (3,0) and (2,0) bands. In other words, for

pressures greater than 0.18 microns, the measured flux varied as

a power of the pressure greater than one. This power depends on

the energy and probably to a certain extent, on the currents used.

For pressures between .8 microns and 1 micron, and for energies

of 75 eV and 100 eV, there appeared to be a slight decrease in the

slope of F/J P versus P, indicating that deactivation or vibrational

energy exchange was beginning, due to the increased number of

molecule-molecule collisions. The non-linearity is most strongly

influenced by secondary electrons which can contribute to the

excitation. The non-linearity is also determined by elastic colli-

sions which can increase the effective path length of the primary

electrons across the chamber. Since the peak cross-section of N_2

for ionization by electron bombardment is at 100 eV, it would be

expected that the non-linearity would be greatest at this energy.

At 25 eV, the secondary electrons still have enough energy to excite

the LBH band system. In these measurements, the electron beam

current is divided out. It is of the order of 150 microamps at energies greater than 50 eV, and 50 microamps at 25 eV. Since the number of secondaries produced is proportional to the electron beam current, a larger electron beam current would produce a greater non-linearity. The non-linearity also depends on the length of the electron beam, since a longer beam increases the number of collisions.

One more phenomena is of interest. A plot of the $(1,1)$, $(2,0)$ and $(3,0)$ bands on the same relative scale at 100 eV (see Figure 5.4) indicated that the higher the v' vibrational level the smaller the pressure dependence. Thus, by collisions, there is a transfer of vibrational energy from higher vibrational levels to lower vibrational levels. Vibrational relaxation becomes more important as the pressure increases. Thus, vibrational levels are tending to a Boltzmann distribution, due to collisions.

The atomic nitrogen lines, on the other hand, have such a short lifetime that they will radiate before being perturbed by collisions. This idea was borne out in the F/J P versus P measurements. The nitrogen lines were linear with pressure from 50 eV to 100 eV over all pressures measured, .03 microns to 1 micron. However, the measurement at 25 eV indicated a non-linear effect above 0.2 microns for both the 1200 Å multiplet and 1493 Å multiplet. The cause of this effect would not be from secondary electrons, since
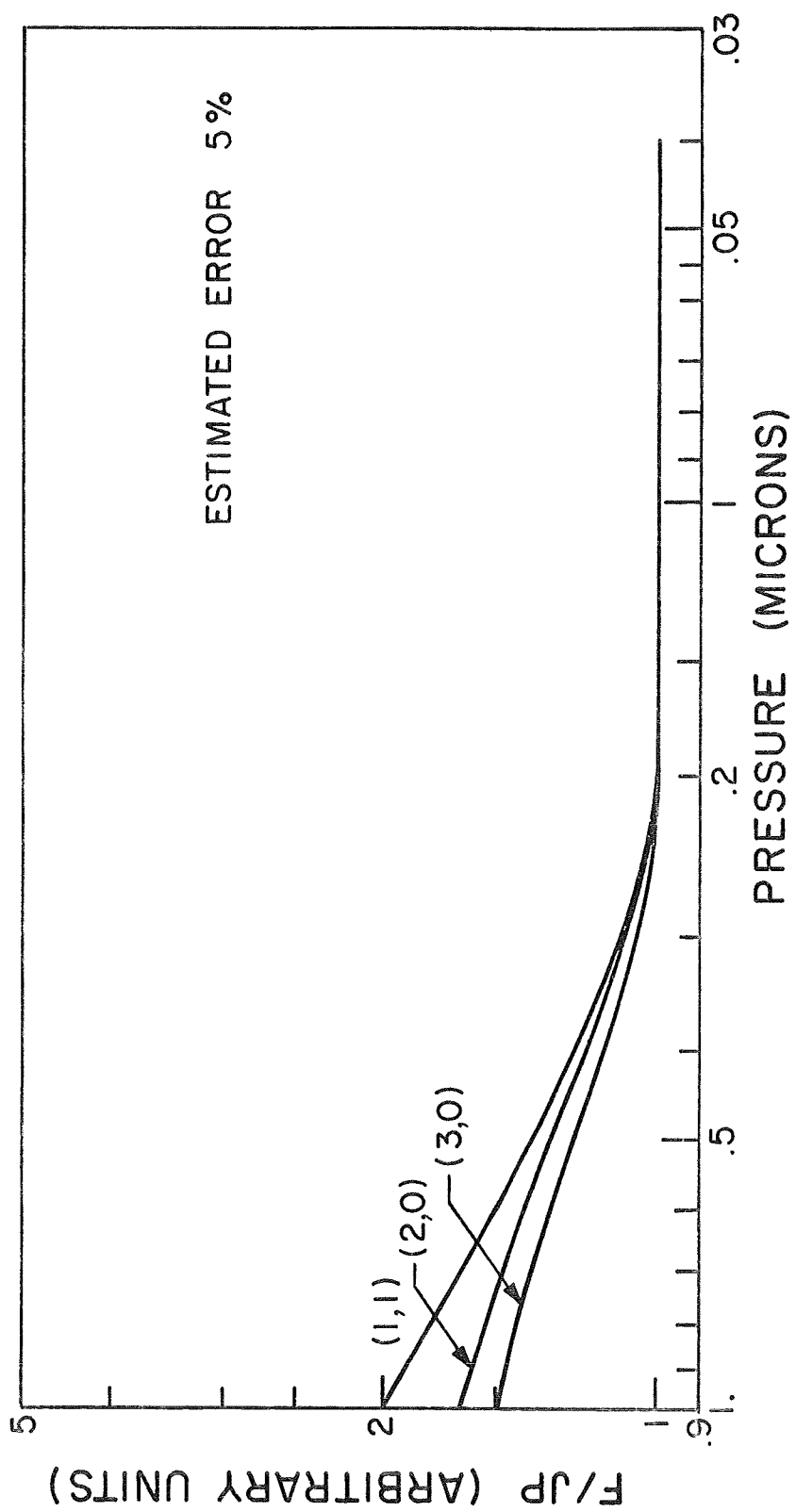
Figure 5.4   FLUX / ELECTRON BEAM CURRENT x PRESSURE vs.
PRESSURE AT 100 eV

secondary electrons do not have enough energy to produce ex-
citation. The cause in this case may be elastic scattering of
primary electrons.

The results of the pressure measurements for the 1200 Å
multiplet and 1493 Å multiplet are displayed in Figures 5.5 and
5.6 respectively.

5.3   Electron Beam Current Dependence.

In an analogous manner to the pressure dependence deter-
minations, measurements were made of the ratio of the flux of
radiation to electron beam current versus electron beam current
for the (3,0), (2,0) and (1,1) LBH bands at 0.18 microns pressure,
and for the nitrogen lines at 0.15 microns pressure, with several
energies as parameters. These pressures were chosen to insure
adequate intensity readings over the range of electron beam currents
employed. The results indicated that the LBH bands were linear in
beam current versus flux for electron energies from 15 eV to 100 eV.
The range of currents measured was from 20 microamps to 300 micro-
amps. The results for the (1,1) band are shown in Figure 5.7. The
nitrogen lines were linear with current for energies of 50 eV and
greater, and for currents less than 220 microamps. The 1493 Å
line revealed a slight non-linearity for current greater than 220
microamps, and the 1200 Å line did not. At 25 eV, both the 1200 Å
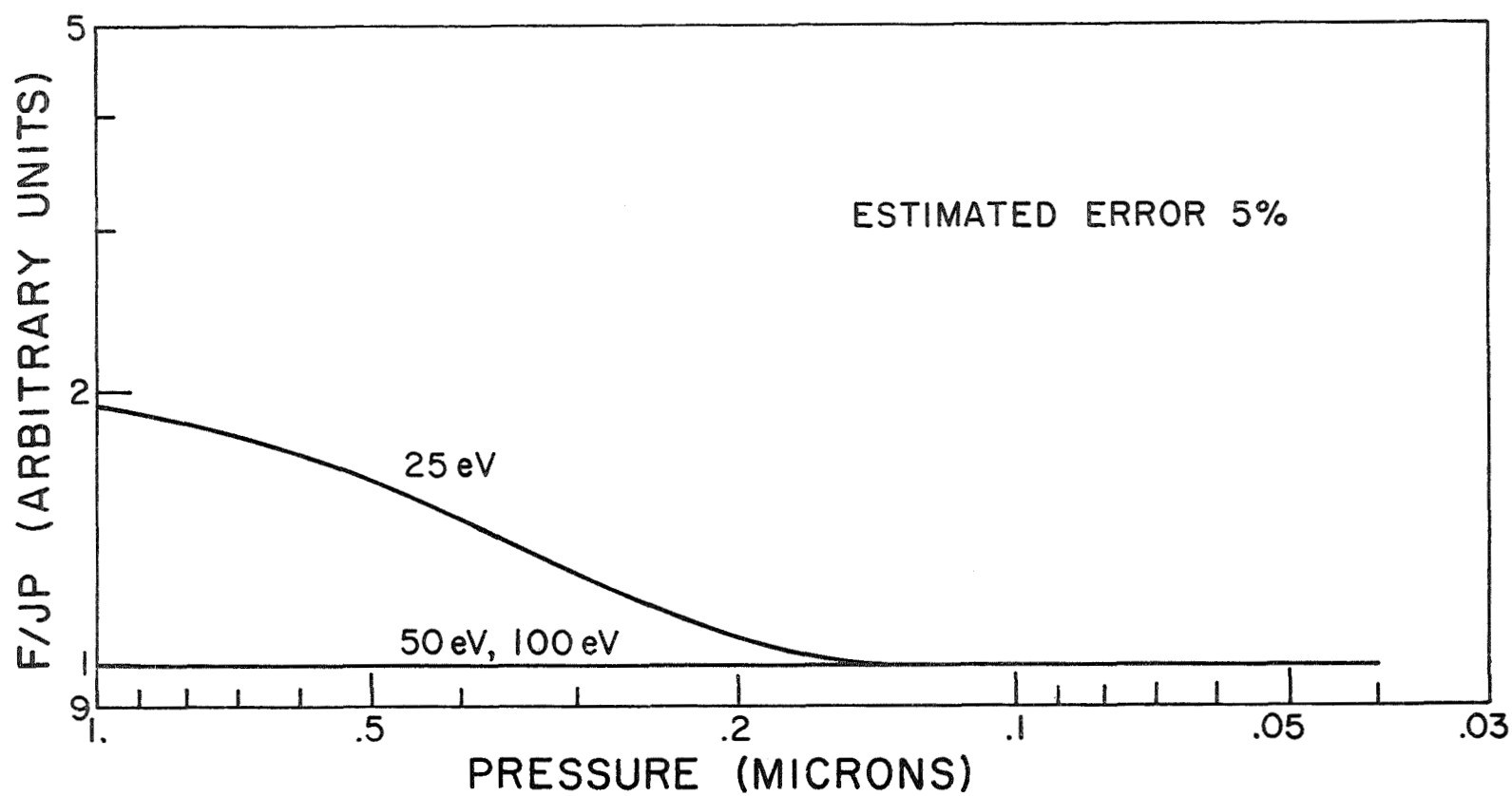
Figure 5.5   FLUX/ELECTRON BEAM CURRENT x PRESSURE vs. PRESSURE FOR 1200Å TRANSITION
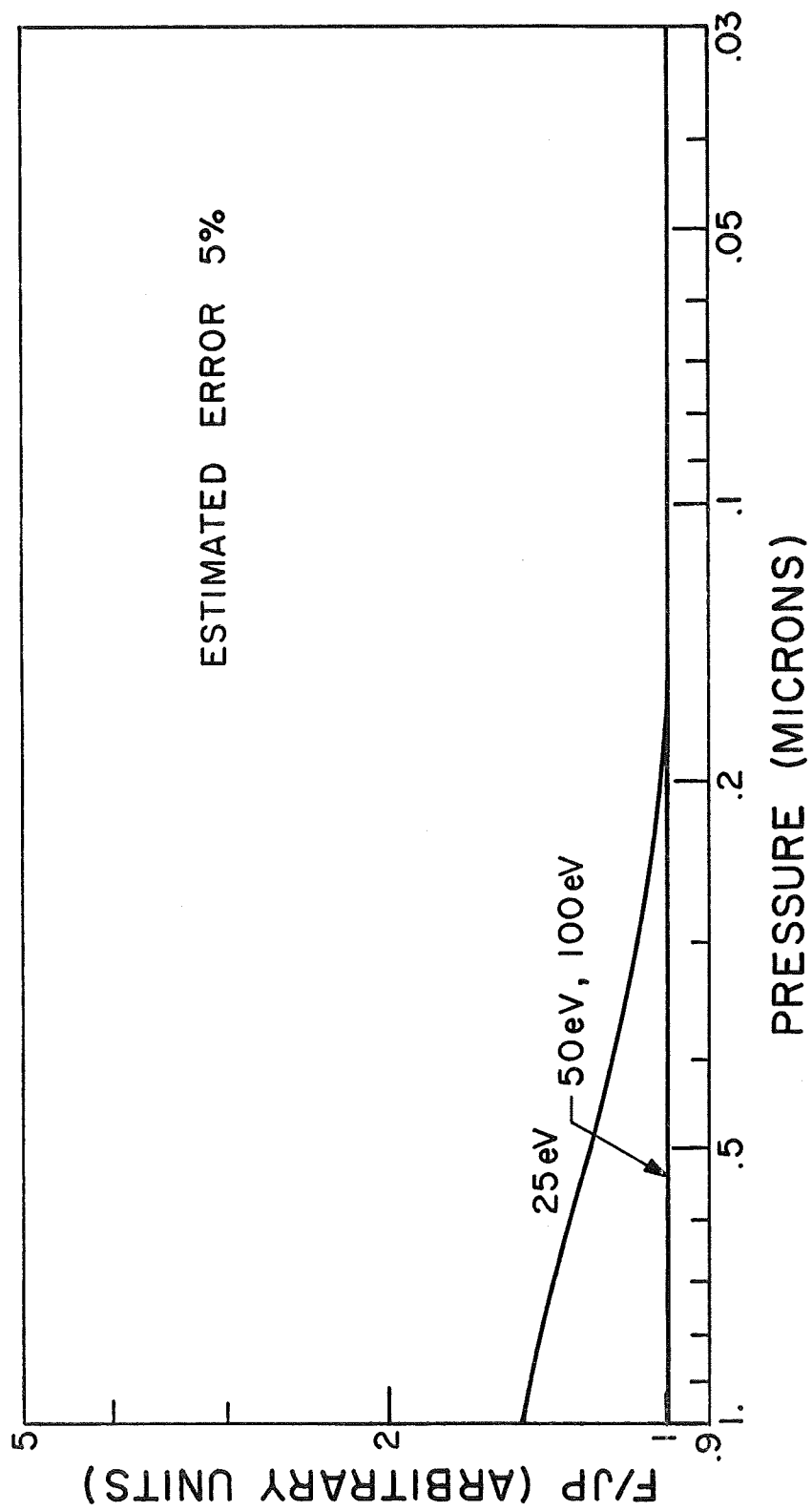
Figure 5.6   FLUX/ELECTRON BEAM CURRENT x PRESSURE
vs. PRESSURE FOR 1493Å TRANSITION
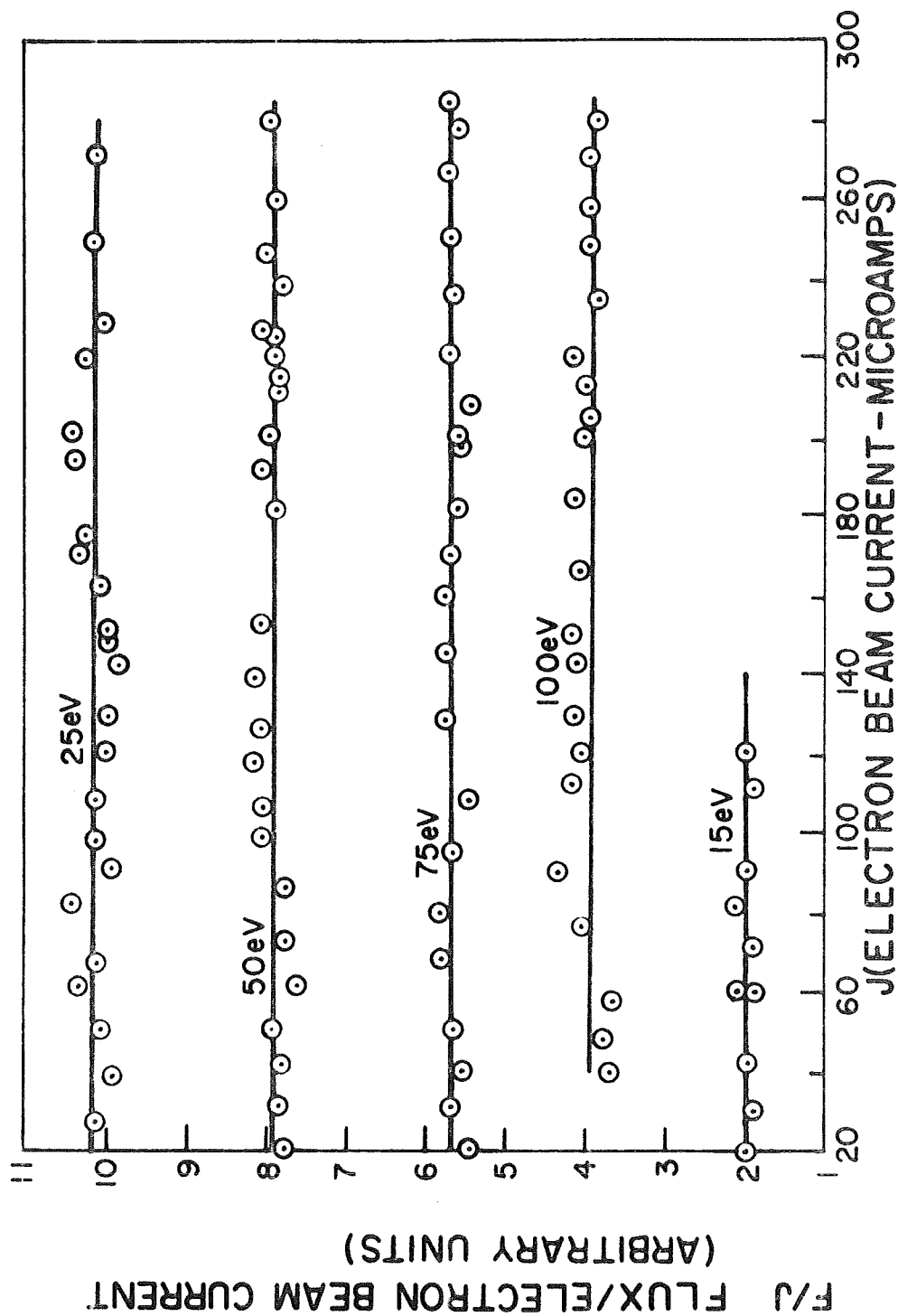
Figure 5.7   CURRENT LINEARITY TEST FOR (1,1) BAND OF LBH BAND SYSTEM
AT 0.18 MICRONS

line and 1493 Å line were non-linear for currents greater than 100

microamps. The results of the current linearity test for the nitrogen

lines at energies of 100 eV and 25 eV are displayed in Figures 5.8

and 5.9, respectively. It should be remembered that the (3,3) LBH

band overlaps the 1493 Å atomic nitrogen line. Similar linearity

tests were performed on the 1743 Å transition of atomic nitrogen.

The same conclusions held for this multiplet as for the 1493 Å

multiplet.

5.4   Spectral Observations.

Spectral scans were made of the electron beam excitation

spectrum of molecular nitrogen from 1200 Å to 1962 Å. During the

spectral scans, at a particular electron beam energy, the electron

beam current and molecular nitrogen pressure were monitored and

recorded. The electron beam current remained constant to within

1 microamp. Currents used varied from 50 microamps at low ener-

gies to 200 microamps at high energies. Typical pressures were in

the range, 0.12 microns to 0.18 microns. This range of pressure

was chosen in order to obtain adequate intensity determinations

for the LBH bands. The pressure remained constant to within 3%

over any spectral scan. Any change in either current or pressure

was recorded. A typical low pressure scan at 75 eV is shown in

Figure 5.10. Three or four complete spectra were obtained at each
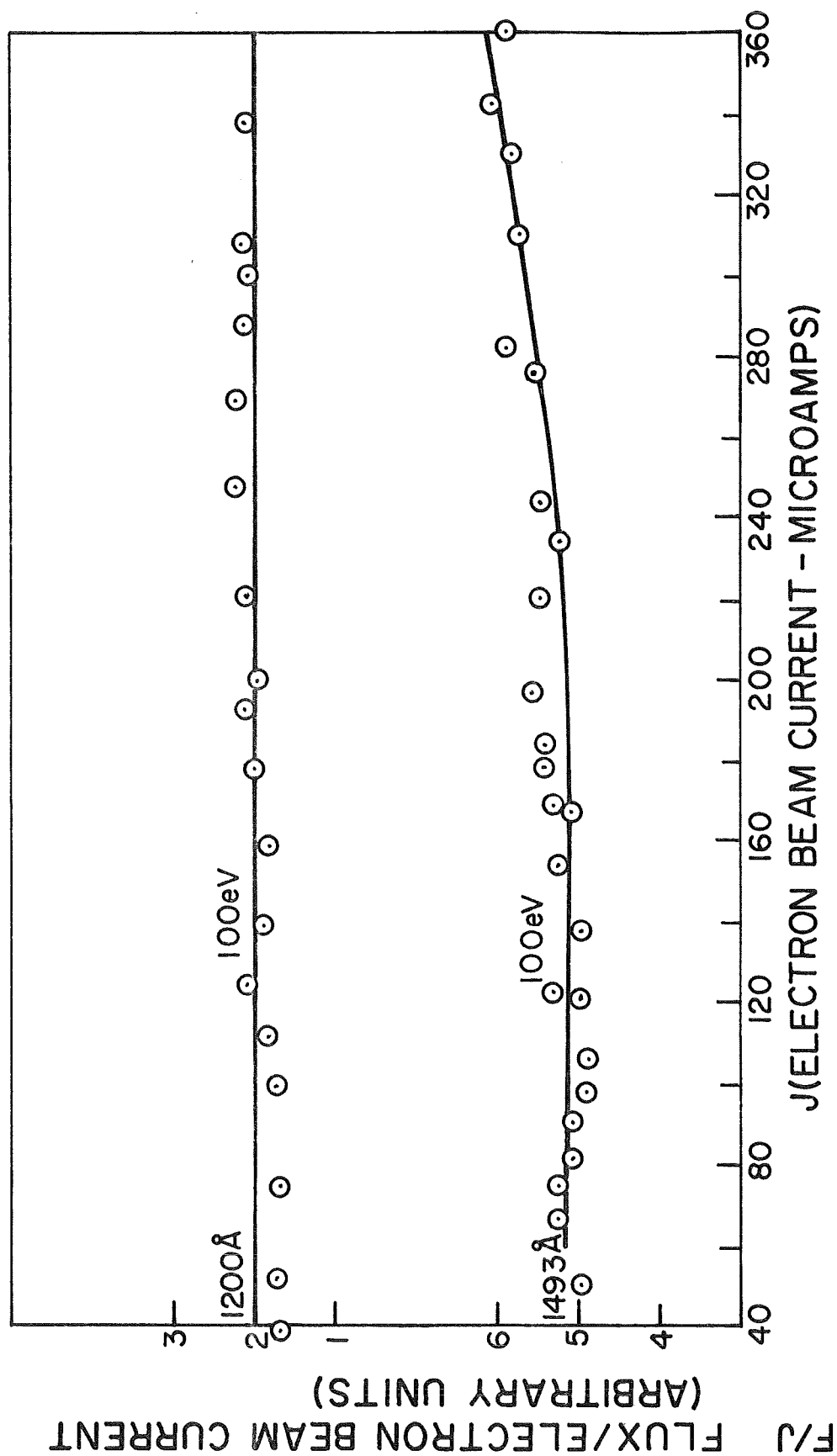
Figure 5.8 CURRENT LINEARITY TEST FOR 1200Å & 1493Å TRANSITIONS OF NI AT A PRESSURE OF 0.15μ
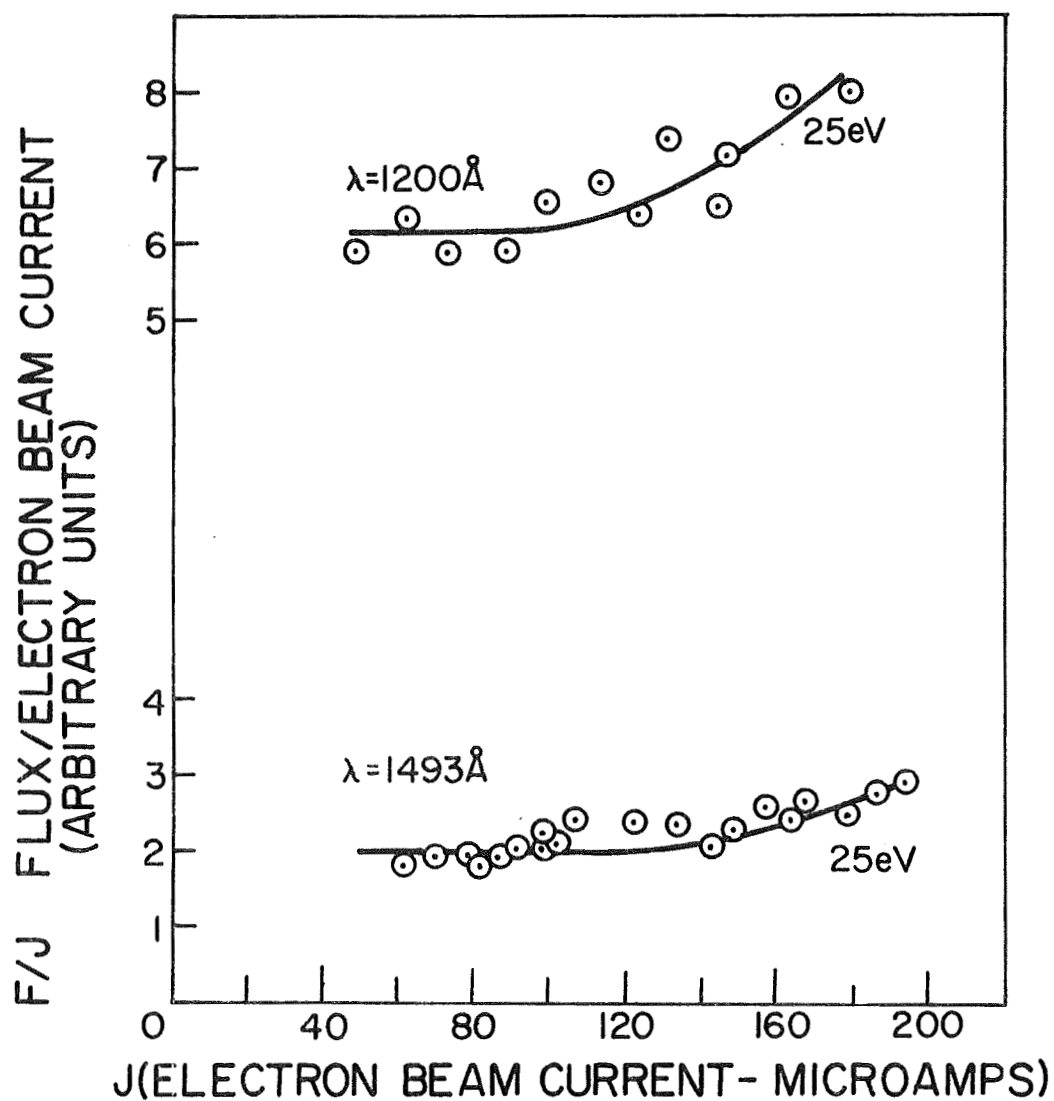
Figure 5.9 CURRENT LINEARITY TEST FOR 1200Å & 1493Å TRANSITIONS OF NI AT A PRESSURE OF 0.15 μ
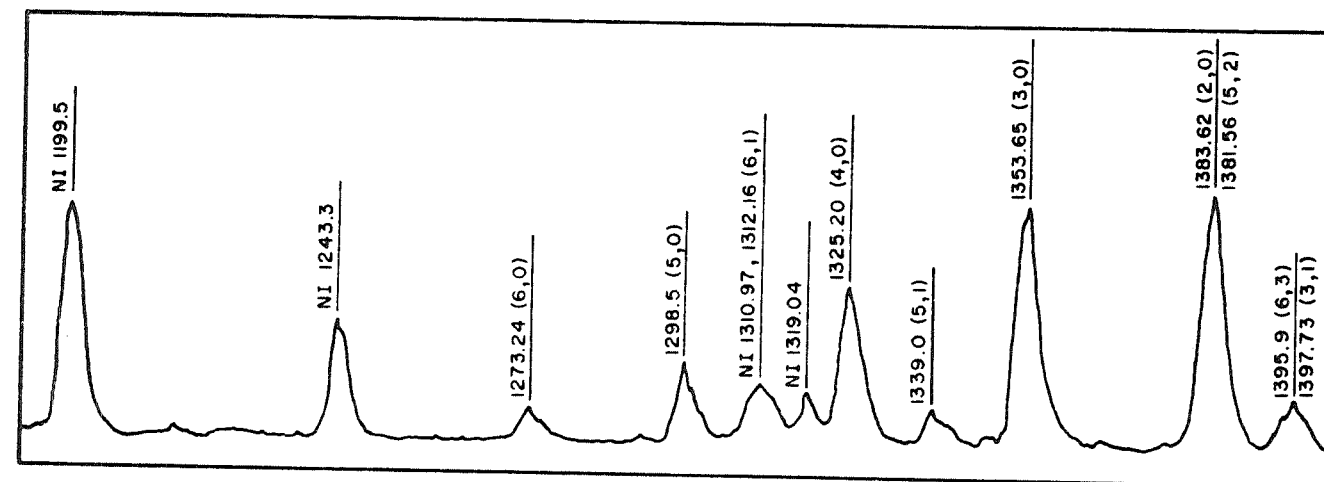
FIGURE 5.10 ELECTRON BEAM EXCITATION SPECTRUM OF N_2 AT 75 eV
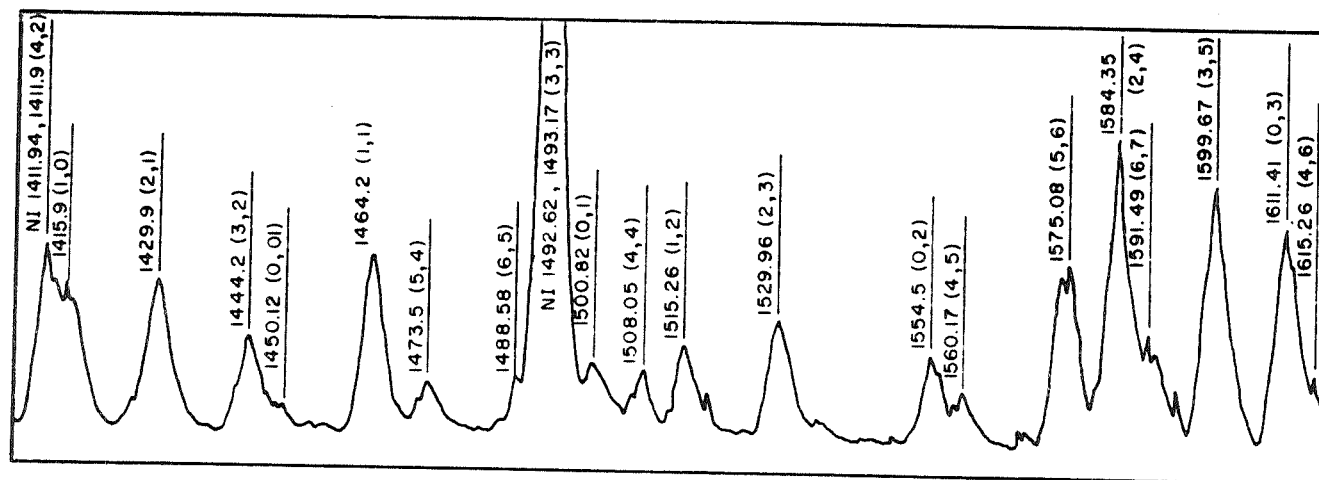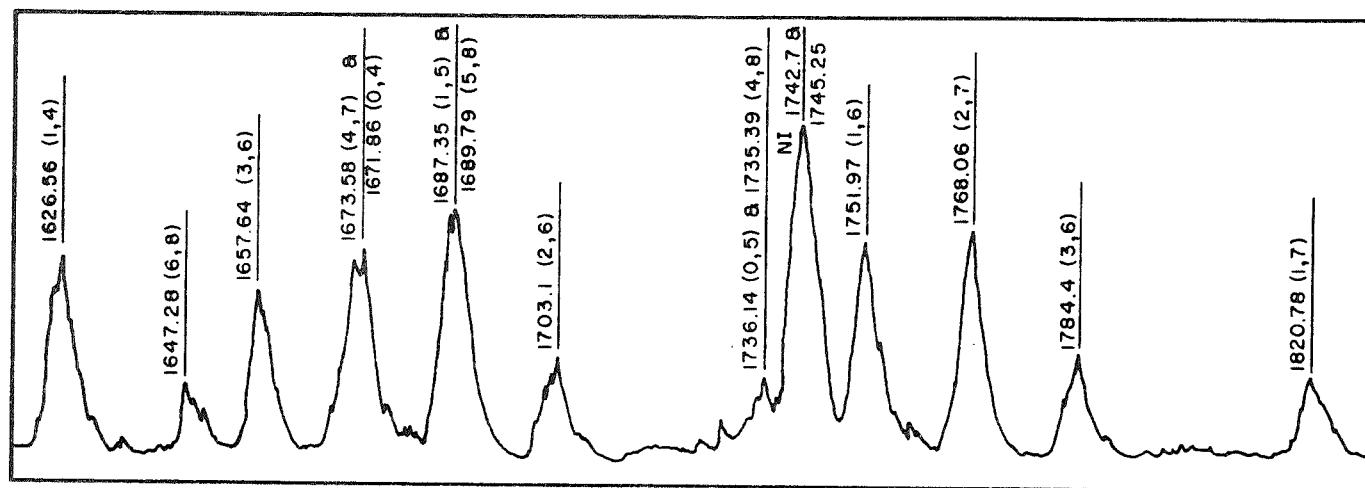
FIGURE 5.10 Con't. ELECTRON BEAM EXCITATION SPECTRUM OF N_2 AT 75 eV
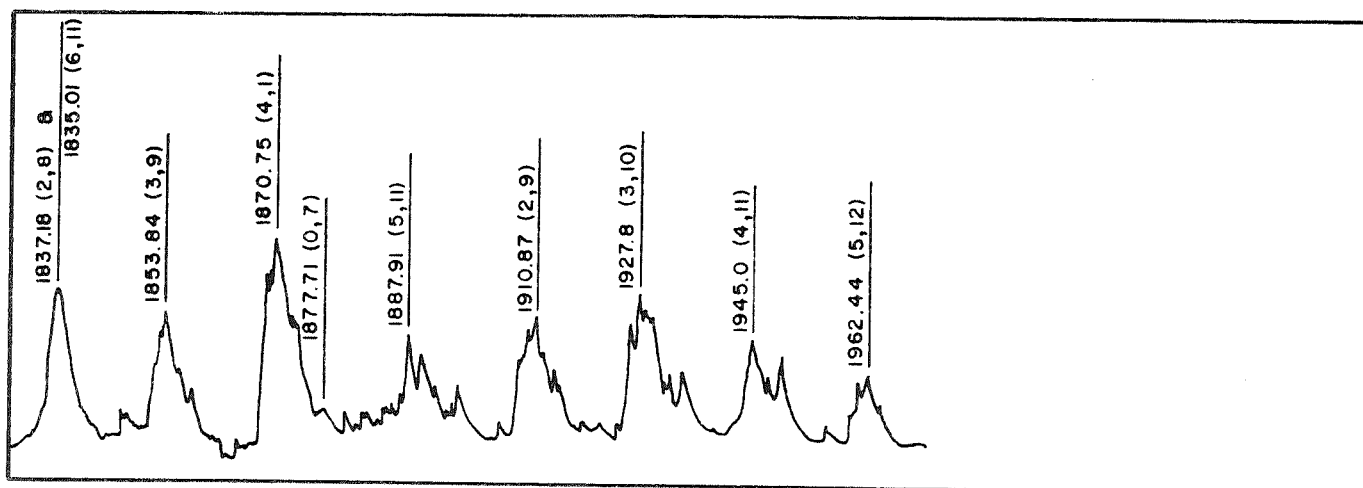
energy. A total of 25 energies from 100 eV to 208 eV was investigated for the LBH bands, and approximately the same number of energies were investigated for the nitrogen lines from 20 eV to 208 eV. The important quantity was the area under each band. This quantity, with the instrumental factors and calibration factors included was the number of photons/second entering the entrance slit of the monochromator. By dividing this number by the electron beam current, the area of the slit, the nitrogen pressure and the geometrical factor, k, the emission cross-sections were determined (Refer to theory, Chapter IV). Slits were normally 200 microns wide by 4mm high. The cross-section of the field of view at the beam was rectangular, 4, 10 cm, vertically by 4.22 cm horizontally.

The LBH bands observed in the experiment are listed by wavelength in Table 5.1. Listed with the bands is the quantity $f'_{v'v''}$ which is the fraction of the total electronic cross-section contributed by each band, or partial cross-section, as calculated by using Franck-Condon factors for direct electron of the $a^1\Pi_g$ state (Holland, 1969). The quantity $f'_{v'v''}$ is

$$f'_{v'v''} = \frac{Q_{v'v''}}{\Sigma_{v'} Q_{ov'}} = \frac{\beta_{v'v''} \; Q_{ov'}}{\Sigma_{v'} Q_{ov'}}$$

$$= \frac{q_{v'v''} \lambda_{v'v''}^{-3}}{(\Sigma_{v''} q_{v'v''} \lambda_{v'v''}^{-3})} \quad x \quad \frac{q_{v'o}}{\Sigma_{v'} q_{v'o}} \qquad (5.1)$$

TABLE 5.1

Observed Emission Features, Between 1200 Å and 1962 Å,
of Molecular Nitrogen by Electron Bombardment

Wavelength Å	Band (v', v")	$f'_{v'v''}$ (%)
1226.6	(8,0)	
1262.9	(8,1)	
1273.2	(6,0)	1.76
1298.5	(5,0)	3.50
1312.2 '	(6,1)	1.54
1325.3	(4,0)	5.46
1339.0	(5,1)	1.10
1353.7	(3,0)	6.50
1381.6 +	(5,2)	1.18
1383.8 +	(2,0)	5.04
1395.9 +	(6,3)	1.12
1397.7 +	(3,1)	0.49
1411.9 '	(4,2)	2.72
1415.9	(1,0)	1.97
1426.3 +	(5,3)	0.65
1429.9 +	(2,1)	2.78

TABLE 5.1 (continued)

Observed Emission Features, Between 1200 Å and 1962 Å,
of Molecular Nitrogen by Electron Bombardment

Wavelength Å	Band (v', v")	$f'_{v'v''}$
1444.2	(3,2)	1.96
1450.1	(0,0)	0.26
1464.2	(1,1)	3.09
1473.5	(5,4)	1.16
1488.6	(6,5)	0.79
1493.2	(3,3)	1.96
1500.8	(0,1)	0.83
1508.1	(4,4)	1.72
1515.3	(1,2)	1.23
1530.0	(2,3)	2.32
1554.5	(0,2)	1.25
1560.2	(4,5)	0.84
1575.7	(5,6)	1.25
1584.4 °	(2,4)	1.81
1591.5 °	(6,7)	0.40
1599.7	(3,5)	2.01

TABLE 5.1 (continued)

Observed Emission Features, Between 1200 Å and 1962 Å,
of Molecular Nitrogen by Electron Bombardment

Wavelength Å	Band (v', v")	$f'_{v'v''}$
1611.4	(0,3)	1.15
1615.3	(4,6)	0.27
1626.6 +	(1,4)	0.97
1631.1 +	(5,7)	0.14
1647.3	(6,8)	0.55
1657.6	(3,6)	1.36
1671.9 +	(0,4)	0.73
1673.6 +	(4,7)	1.64
1687.4 +	(1,5)	1.93
1689.8 +	(5,8)	0.57
1703.1	(2,6)	0.99
1735.4 +	(4,8)	0.60
1736.1 +	(0,5)	0.33
1751.9 +	(5,9)	1.01
1752.0 +	(1,6)	1.67
1768.1 +	(2,7)	2.38

TABLE 5.1 (continued)

Observed Emission Features, Between 1200 Å and 1962 Å,
of Molecular Nitrogen by Electron Bombardment

Wavelength Å	Band (v', v")	$f'_{v'v''}$
1768.8	(6,10)	0.61
1784.4	(3,8)	1.20
1801.0 +	(4,9)	0.11
1804.6 +	(0,6)	0.12
1820.8	(1,7)	0.89
1835.0 +	(6,11)	0.38
1837.2 +	(2,8)	2.14
1853.8	(3,9)	2.29
1870.8	(4,10)	1.31
1887.9	(5,11)	0.35
1894.2	(1,8)	0.33
1910.9	(2,9)	1.12
1927.8	(3,10)	1.81
1945.0	(4,11)	1.79
1962.4	(5,12)	1.16
1980.1 *	(6,13)	0.50

TABLE 5.1 (continued)

Observed Emission Features, Between 1200 Å and 1962 Å,
of Molecular Nitrogen by Electron Bombardment

Wavelength Å	Band (v', v")	$f'_{v'v''}$
1989.6 *	(2,10)	0.39
2006.8 *	(3,11)	0.85
2024.2 *	(4,12)	1.16
2041.9 *	(5,13)	1.12
2059.8 *	(6,14)	0.80
2091.2 *	(3,12)	0.27
2108.8 *	(4,13)	0.47
2126.7 *	(5,14)	0.58
2144.8 *	(6,15)	0.55
2216.6 *	(5,15)	0.19
2234.8 *	(6,16)	0.22
		95.6%

TABLE 5.1 (continued)

Observed Emission Features, Between 1200 $\overset{o}{A}$ and 1962 $\overset{o}{A}$,
of Molecular Nitrogen by Electron Bombardment

---

* These bands were not observed since they were beyond the

wavelength cut-off of the instrument, but their partial cross-

sections were calculated, using Eqn. 5.1, and their strength

relative to the (3,0) band.

+ These bands were overlapping LBH bands and the individual

partial cross-sections were determined, using Eqn. 5.1 and

5.2.

' These bands overlapped with atomic nitrogen lines. Their

cross-sections were measured from 10 eV to 18 eV and extra-

polated to higher energy, using a normalized LBH cross-

section curve.

o These two bands overlapped at energies greater than about

50 eV with the intense N_2^{++} ($d' \, \Sigma_g^+ \rightarrow d' \, \Sigma_g^+$) transition of

Carroll and Hurley (Holland, 1969).

This approximation is valid since McEwen (1965) has

shown the electronic transition moment is a constant over the band

system to within 5%. Also, in inelastic scattering experiments,

Lassettre et al. (1968) found the relative probabilities of directly

exciting the $a^1\Pi_g$ vibrational levels were proportional to the (v', o)

Franck-Condon factors. Holland (1969) found excellent agreement

by comparing his observations to this formulation. This agreement

suggests that most of the LBH emission is from direct electron ex-

citation. The Franck-Condon factors used in determining $f'_{v'v''}$ were

those of Benesch et al. (1966). Only $v' = 0$ to $v' = 6$ were in-

cluded, since only two bands for $v' > 6$ were observed and these

were weak, owing to the importance of predissociation for $v' > 6$.

The resolution of the monochromator was about 3 $\overset{\circ}{A}$. Thus,

if the bands were less than 3 $\overset{\circ}{A}$ apart, they could not be resolved.

The numbers $f'_{v'v''}$ were used to separate about 20 overlapping bands.

The contribution of each particular overlapping band to the cross-

section was calculated from Eqn. 5.1. Consider two overlapped

bands. The contribution to the emission cross-section of this

spectral feature by the first band is

a) $$\frac{f'_{v'_1 v''_2}}{f'_{v'_1 v''_2} + f'_{v'_3 v''_4}}$$ (5.2)

and for the second is

b)
$$\frac{f'_{v'_3 v''_4}}{f'_{v'_1 v''_2} + f'_{v'_3 v''_4}} ,$$

where:

$f'_{v'_1 v''_2}$ refers to the contribution to the total cross-section

by the first band,

$f'_{v'_3 v''_4}$ refers to the contribution to the total cross-section by

the second band.

The numbers $f'_{v' v''}$ were also used to calculate the partial cross-

sections of bands between 1962 Å and 2300 Å if their contribution

to the total cross-section was greater than 0.2%. The intense (3,0)

band, at 1353 Å, was used as a reference for these calculations.

It is seen from Table 5.1 that about 65 bands are observed,

and the effects of about 10 more to the cross-section, are estimated.

These bands represent about 96% of the electronic transition. The

remaining 4% is distributed over about 30 weak bands. Three bands

could only be observed up to the onset of dissociative excitation of

molecular nitrogen. These bands were the (6,1), (4,2) and (3,3).

The threshold for dissociative excitation is about 20 eV. Therefore,

these bands were observed from 10 eV to 18 eV. This procedure

gave enough points to extrapolate the cross-section to higher energy,

once the relative shape of the LBH cross-section curve was determined. Finally, the 1584 $\overset{\circ}{A}$ and 1591 $\overset{\circ}{A}$ bands were overlapped by an N_2^{++} transition for energies greater than about 50 eV. The cross-sections of these bands were also extrapolated to higher energy after the relative shape of the LBH cross-section curve was determined.

Table 5.2 gives a list of the observed atomic nitrogen multiplets. The only multiplets that were evaluated as to cross-section were the multiplets at 1200 $\overset{\circ}{A}$, 1493 $\overset{\circ}{A}$ and 1743 $\overset{\circ}{A}$, although the data is available to determine the cross-sections for the other transitions.

Both the bands and the lines were evaluated identically. The shapes of the bands and lines were triangular since the instrumental width was greater than the natural width. Triangles were drawn over the bands and lines. The width and height of the triangle was measured and put on data cards. Each band was evaluated several times at 25 different energies, from 10 eV to 208 eV. The results for each band at each energy were averaged. The formula used for the determination of partial cross-section for the LBH bands was Eqn. 4.49, and for the nitrogen multiplets, Eqn. 4.68.

The absolute energy for the electrons as determined from the voltmeters was found to be in error by 2 $\pm$ 0.5 volts since the LBH bands and the nitrogen lines were observed at 2 $\pm$ 0.5 volts

TABLE 5.2

List of Observed Atomic Nitrogen Transitions

Wavelength	Multiplet
1200	$^4S^o - {}^4P$
1243	$^2D^o - {}^2D$
1311	$^2P^o - {}^2D$
1316	$^2P^o - {}^2F$
1319	$^2P^o - {}^2P$
1412	$^2P^o - {}^2D$
1493	$^2D^o - {}^2P$
1743	$^2P^o - {}^2P$

below the threshold as indicated by the voltmeters. The volt-
meters were calibrated and could not be in error by this amount.
Furthermore, by assuming a linear relationship between cross-
section and energy near threshold, and extrapolating six bands to
zero cross-section on a linear by linear plot, the intersection with
the energy axis was determined to be at 2.5 ± 0.5 eV below the
threshold. Two volts were added to all recorded accelerating volt-
ages to determine the absolute energy scale. The absolute determin-
ation of energy is important at low energies where the cross-section
is changing rapidly.

The effects that contribute spurious potentials to the in-
dicated energy, in an electron beam experiment, are contact poten-
tials between the electrodes in the electron gun and the space
charge potential of the electron beam. The latter effect also causes
a spread in energies of the beam. The effective energy resolution
of the electron gun can be determined by considering this problem.
Pierce (1954) has considered the effect of space charge in magneti-
cally focused (Brillouin flow) and magnetically confined beams of
axial symmetry. Due to space charge, the space potential inside
the chamber is not uniform but assumes a distribution that decreases
from the edge of the beam to the center of the beam. The potential
gradient tends to move the electrons to the outside of the beam. A
strong magnetic field constrains the motion. Using Pierce's

results for a magnetically confined beam 1 mm in diameter, an

electron beam current of 150 microamps, an electron energy of 40

eV and a magnetic field of 160 gauss, a potential difference of

approximately 0.9 eV from the center of the beam to the edge of the

beam is obtained. Thus, in progressing from the center of the beam

to the edge of the beam, there is a potential difference caused by

the collective space charge of the electrons. Since the total energy

of the electron, kinetic energy plus potential energy, is a constant

equal to the accelerating energy, there is an effective spreading of

the kinetic energy of the electrons across the beam of about 0.9

eV. The absolute energy scale is estimated to be accurate to $\pm$ 1 eV.

5.5   Energy Dependence of the Emission Cross-Section of the

         Nitrogen Lines.

The emission cross-section, Q_D (^{4}P), of the ^{4}P state of

NI due to dissociation of N_2 by electron impact is plotted in Figure

5.11. This cross-section was measured by experimentally deter-

mining the excitation function of the 1200 Å transition from the ^{4}P

state. The region between 20 eV and 35 eV corresponds to dissoci-

ative excitation of N_2, and the region between 35 eV and 208 eV is

the total cross-section of dissociative excitation plus dissociative

ionization excitation. Both the dissociative excitation cross-section

and the dissociative ionization excitation cross-section rise very

steeply from the threshold. The total cross-section reaches a peak
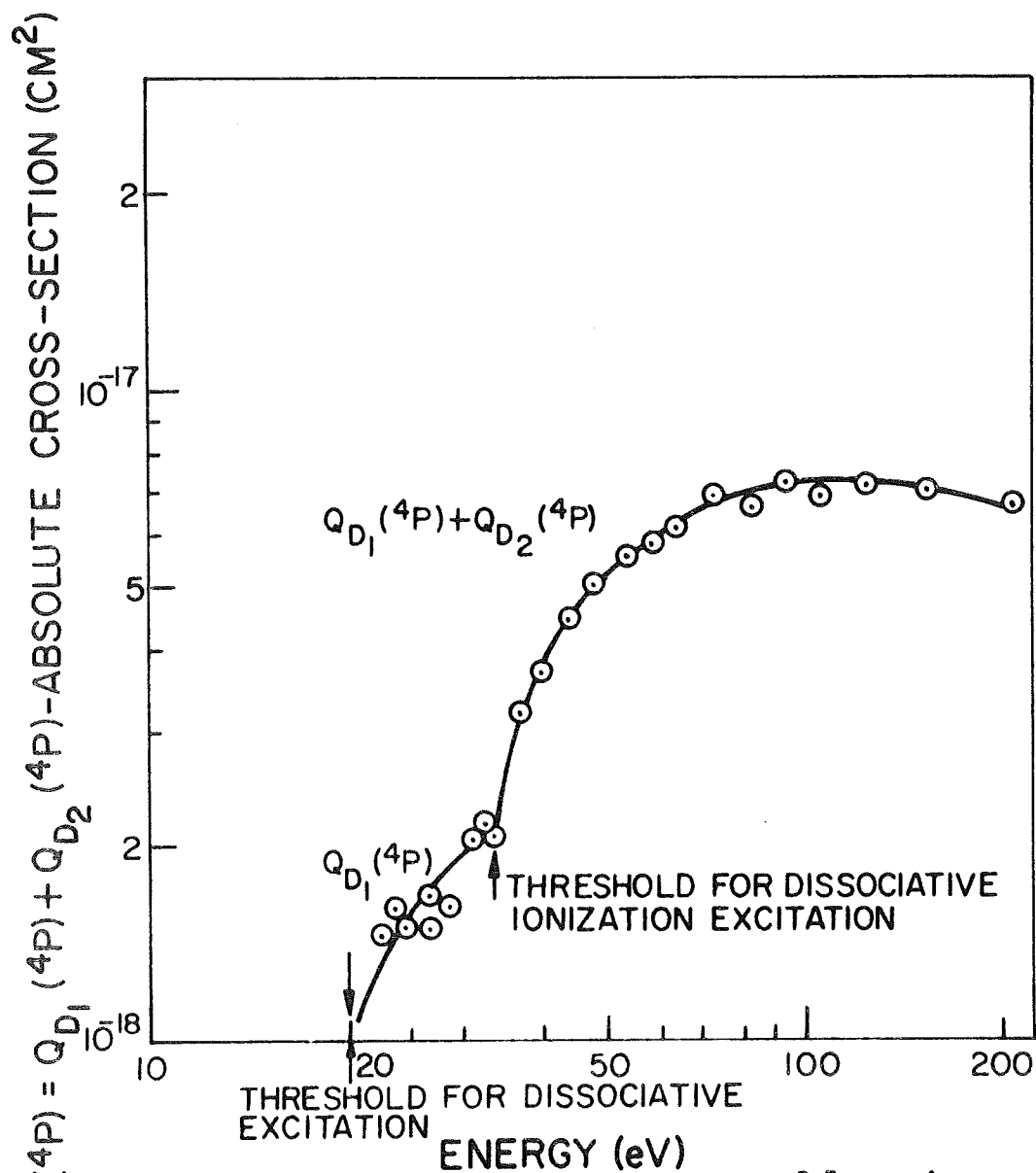
Figure 5.11 EMISSION CROSS-SECTION OF THE $2p^2(^3P)\ 3s\ (^4P)$ STATE OF NI, $\lambda = 1200\text{\AA}$, DUE TO DISSOCIATION OF N_2 BY ELECTRON IMPACT

at about 110 eV and decreases very slowly to 200 eV. The 1200 Å line is thus the most intense individual feature in the electron excitation spectrum of N_2 in the wavelength region from 1200 Å to 2000 Å and for electron impact energies greater than 40 eV. It is observed from the shape of the cross-section curve that dissociative ionization excitation is the more important of the two processes above 50 eV.

The emission cross-section of the λ = 1743 Å transition, Q_D (1743), is displayed in Figure 5.12. Its shape is almost identical to that of the 1200 Å excitation function except it has a much lower cross-section. It, too, peaks at about 110 eV. Above 50 eV, dissociative ionization excitation is the dominant process. It represents a partial emission cross-section of the ^2P state of atomic nitrogen and should make a contribution to the total cross-section of 26%. The ^2P state decays by emitting the 1493 Å multiplet and 1743 Å multiplet in the ratio, .74 to .26. The energy level of the ^2P state is about 0.4 eV higher than that of the ^4P state.

The emission cross-section of the λ = 1493 Å transition, from excitation of molecular nitrogen by low energy electrons, is shown in Figure 5.13. This spectral feature is actually caused by two emissions at the same wavelength--one emission from the (3,3) LBH band and the other emission, at 1493 Å, from the $^2P \rightarrow {}^2D^o$
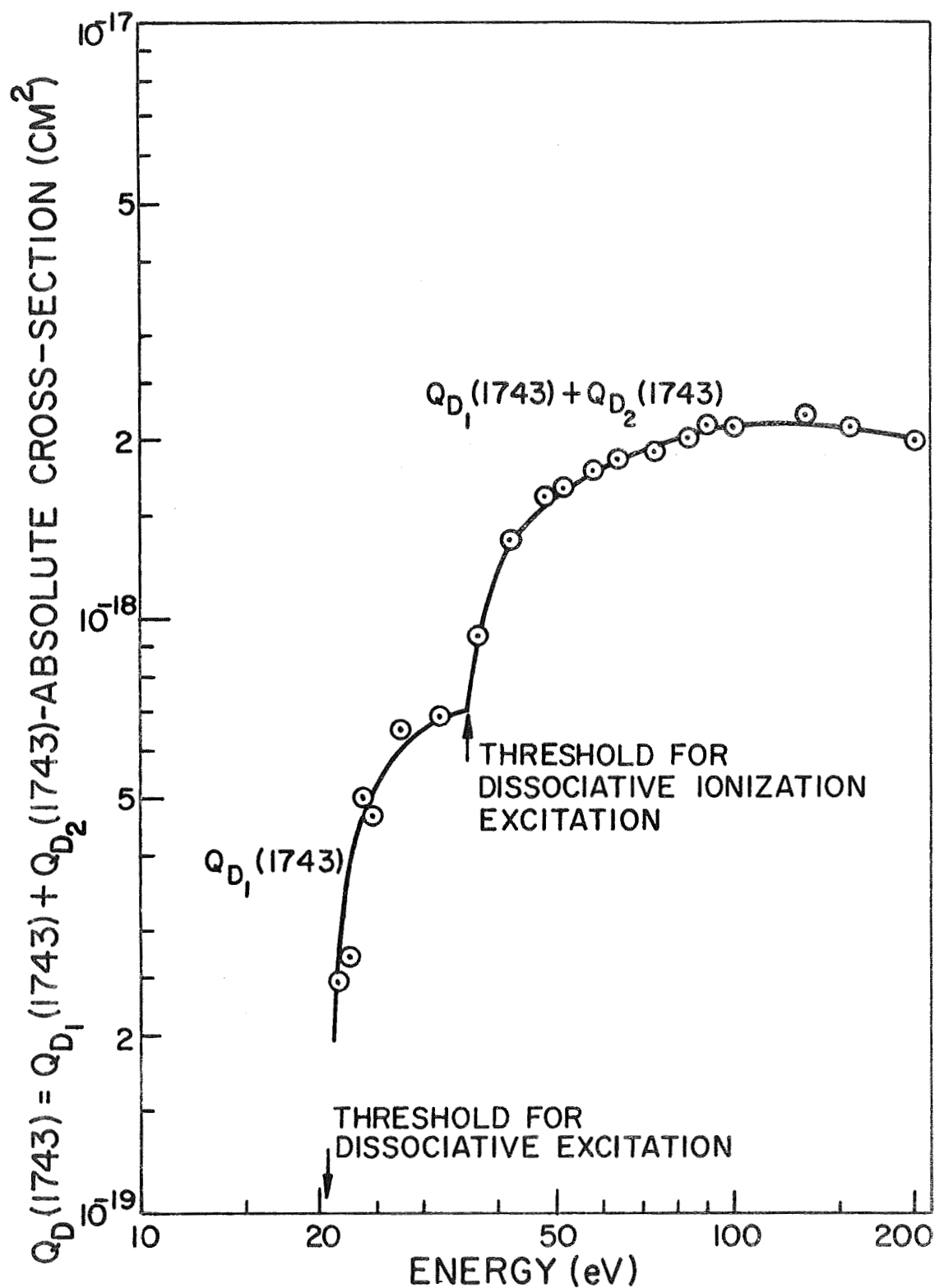
Figure 5.12   EMISSION CROSS-SECTION OF THE 1743Å TRANSITION OF NI DUE TO DISSOCIATION OF N$_2$ BY ELECTRON IMPACT
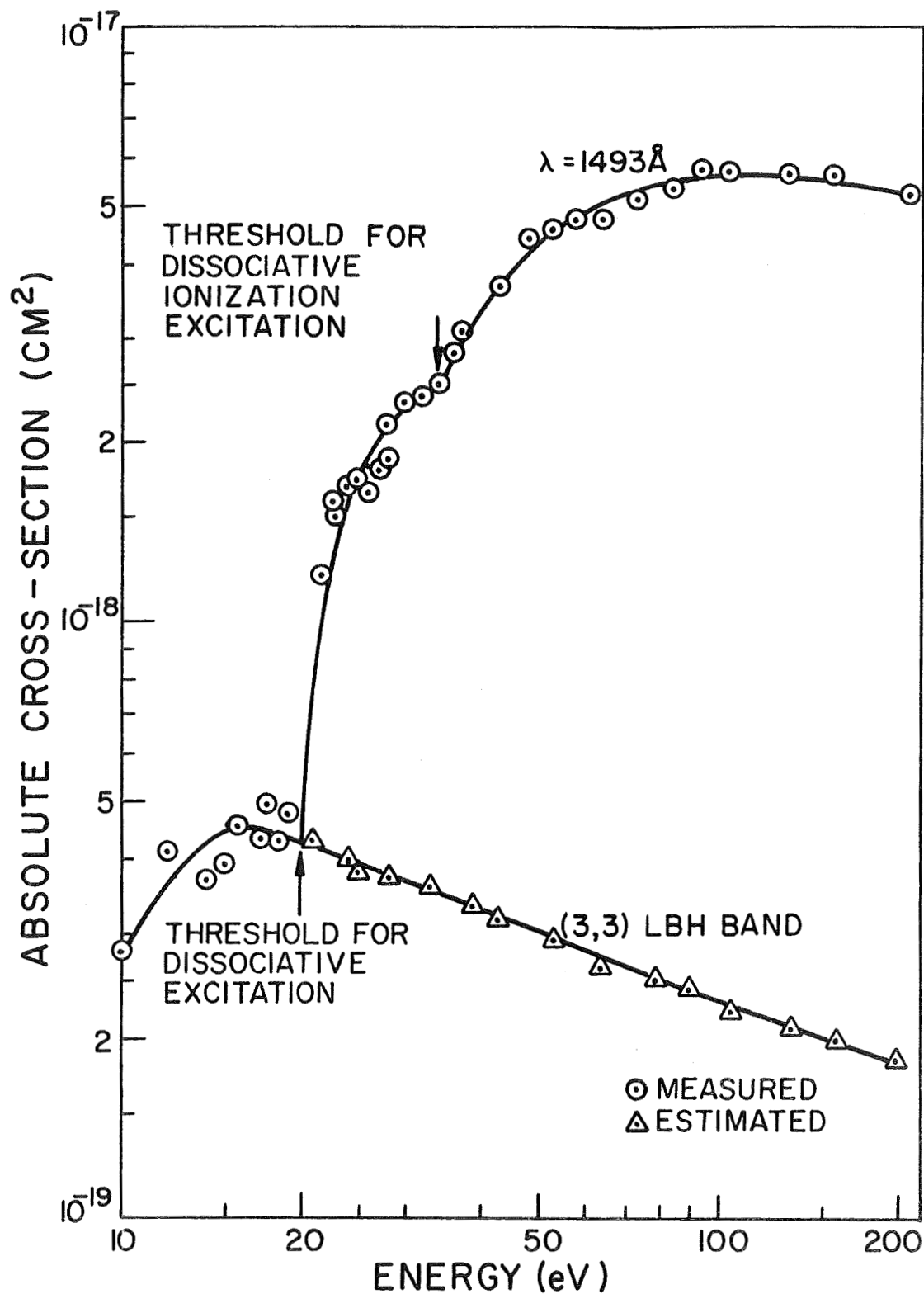
Figure 5.13 EMISSION CROSS-SECTION OF THE 1493Å TRANSITION OF NI DUE TO DISSOCIATION OF N_2 + EMISSION CROSS-SECTION (3,3) LBH BAND BY ELECTRON IMPACT

transition of atomic nitrogen. Both transitions are excited from the ground state of molecular nitrogen. The 1493 Å line is the second most intense feature of the vacuum ultraviolet excitation spectra of N_2, for electron impact energies greater than 40 eV. Thus the excitation function of this transition shows three thresholds. The first at about 9.1 eV, the threshold for the v' = 3 level of the $a^1\Pi_g$ state. The next threshold is at about 20.5 eV, due to dissociative excitation of molecular nitrogen--one of the dissociation products being atomic nitrogen excited to the ^2P term. The final threshold is at 35.0 eV, from dissociative ionization excitation of molecular nitrogen.

The solid line of Figure 5.13 marked with triangles represents the estimated cross-section of the (3,3) band above 20 eV. The numbers were determined by taking the relative shape of the LBH cross-section of the next section and extrapolating the cross-section obtained below 20 eV to higher energies. For energies greater than 40 eV, the contribution of the (3,3) band to the total excitation cross-section becomes less than 10%. By subtracting the cross-section of the (3,3) band from the total cross-section, the emission cross-section, Q_D (1493), of the λ = 1493 Å multiplet of NI is determined. This cross-section is shown in Figure 5.14. It represents a partial emission cross-section of the ^2P
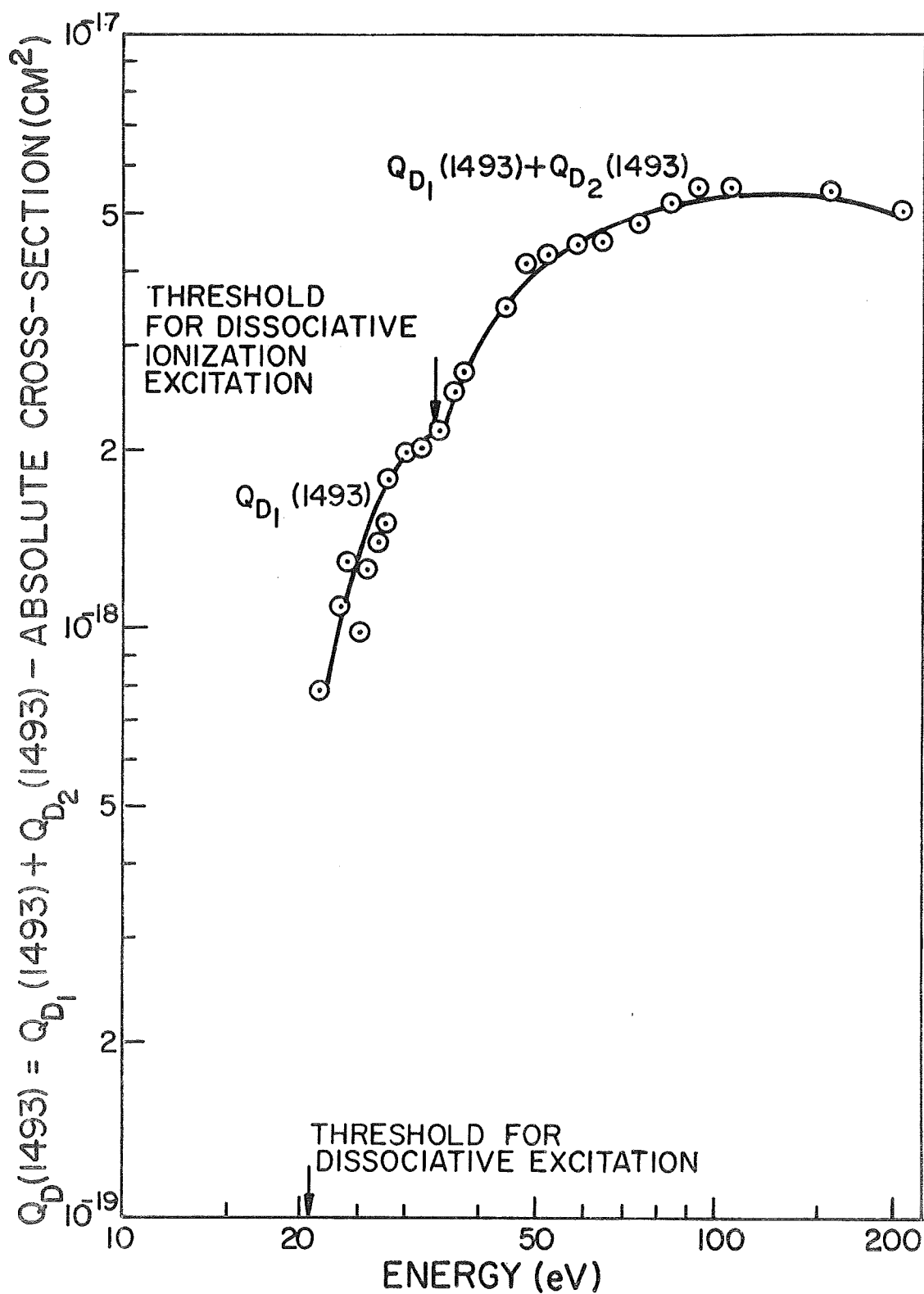
Figure 5.14 EMISSION CROSS-SECTION OF THE 1493Å TRANSITION OF NI DUE TO DISSOCIATION OF N_2 BY ELECTRON IMPACT

state of NI. The cross-section peaks at 110 eV, with a broad maximum from 70 eV to 200 eV. Both types of dissociative excitation cross-sections rise steeply from the threshold. Above 50 eV, dissociative ionization excitation is the predominant excitation process.

The total excitation cross-section, $Q_D(^2P)$, of the ^2P state of NI, by dissociation of molecular nitrogen, is shown in Figure 5.15. The total cross-section of the ^2P state, at 100 eV, is 7.78×10^{-18} cm^2. The contribution at 100 eV from the 1493 Å transition is 5.68×10^{-18} cm^2 and from the 1743 Å transition is 2.10×10^{-18} cm^2. Thus the 1493 Å transition contributes 73% of the radiation, and the 1743 Å transition, 27%. So it is seen there is excellent agreement between the branching ratio calculation and the experiment as to the contribution of each transition to the total cross-section.

It is expected that the other nitrogen lines observed, as listed in Table 5.2, all have identical shapes as the three transitions measured. That is, the other nitrogen lines are almost certainly caused by dissociative excitation of N_2.

As was mentioned in Chapter IV, there are other dissociation limits of molecular nitrogen that lie within a few eV of the first dissociation level of molecular nitrogen. In addition to the dissociation reaction that yields two $^4S^o$ ground state nitrogen
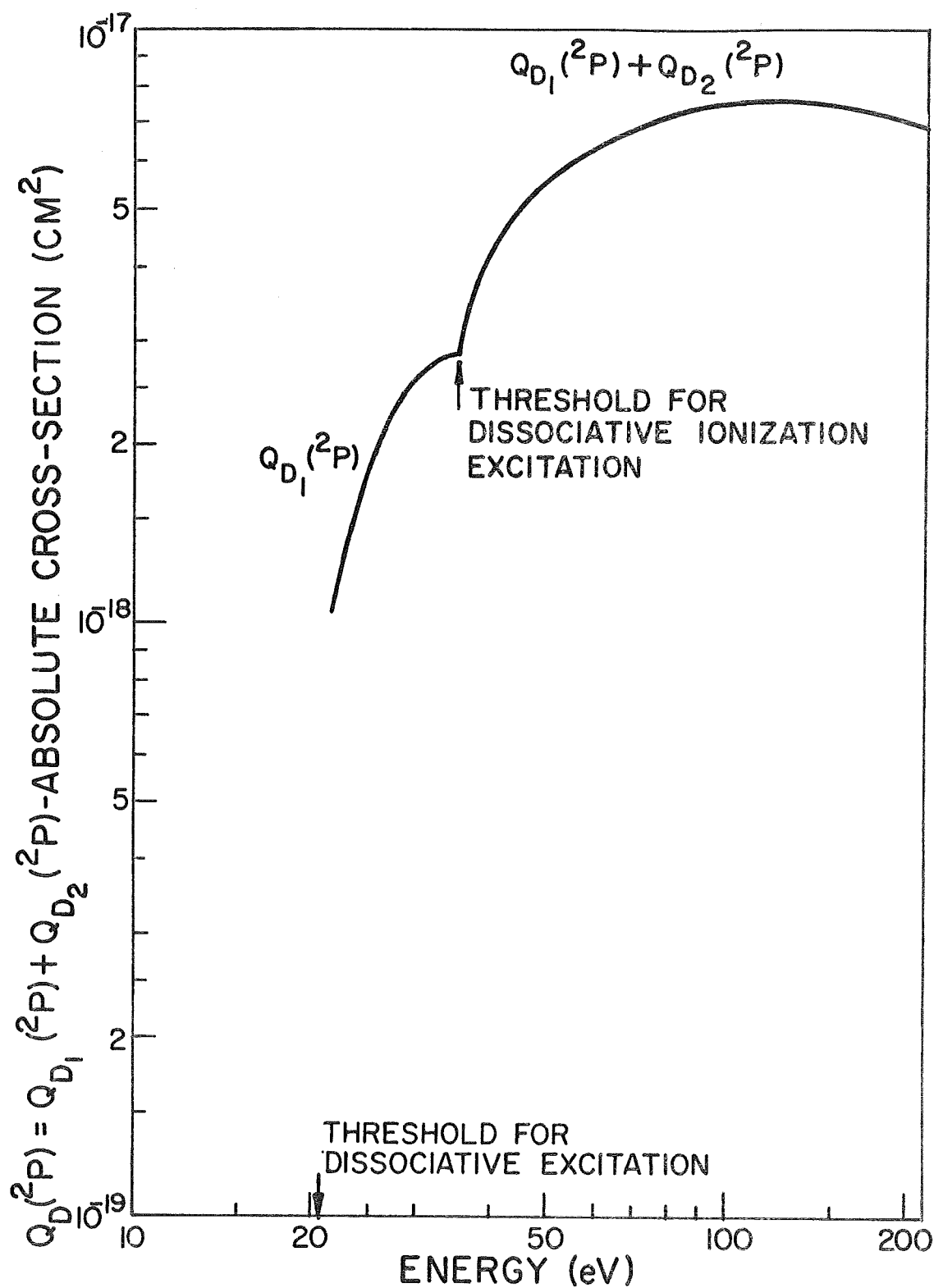
Figure 5.15   EMISSION CROSS - SECTION OF THE $2p^2(^3P)3s$ (^2P) STATE OF NI DUE TO DISSOCIATION OF N_2 BY ELECTRON IMPACT

atoms, there are reactions that yield $^4S^O$ and $^2D^O$ nitrogen atoms,
and also $^4S^O$ and $^2P^O$ nitrogen atoms. By analogy, it would be
expected that dissociative excitation, in addition to yielding $^4S^O$
and ^2P nitrogen atoms and $^4S^O$ and ^4P nitrogen atoms, would yield
$^2D^O$ or $^2P^O$ and ^2P nitrogen atoms and $^2D^O$ or $^2P^O$ and ^4P nitrogen
atoms. Thus there would be other dissociative excitation thres-
holds that would be denoted by an increase in cross-section, when
the threshold is reached. It is not possible from this data to assess
the importance of these additional possibilities. It would be nec-
essary to have an electron gun with much finer energy resolution
than that used here, and also to take measurement on a much
finer energy scale of the order of tenths of eV apart in the threshold
region. Furthermore, cross-sections are increasing so rapidly
near threshold, it is difficult from these measurements to deter-
mine the importance of crossing these excitation thresholds. A
similar argument applies to the dissociative ionization excitation
process and also to the effects of cascading.

The total cross-section for dissociative ionization of
molecular nitrogen by electron impact was measured by Englander-
Golden and Rapp (1964). The peak cross-section was measured
to be 6.4×10^{-17} cm^2 at an energy of 120 eV. The product ions
were detected, if their kinetic energy was greater than 0.25 eV.
In this experiment, both the effects of dissociative ionization and

dissociative excitation were summed. It appears that dissociative ionization excitation is the predominant process. If, as a lower limit, it is assumed at a 110 eV that half the cross-section of the nitrogen emission lines is from dissociative ionization, then the total cross-section in the vacuum ultraviolet, due to dissociative ionization is about 7×10^{-18} cm^2 for the three lines measured, and about 3×10^{-18} cm^2 for the other nitrogen lines of Table 5.2. Thus, in the dissociative ionization process measured by Englander-Golden and Rapp (1964), at least 15% of the nitrogen atoms produced are in highly excited states.

Furthermore, the total dissociative ionization cross-section falls by a factor of 0.36 from peak to 1 keV. One would expect the dissociative ionization excitation process to fall in about the same proportion. Thus the dissociative ionization cross-section falls slowly with increasing energy.

5.6   Energy Dependence of the Emission Cross-Section of the $a^1\Pi_g$ State.

The total measured emission cross-section of the LBH transition by electron impact is shown in Figure 5.16. It is defined as

$$Q_{LBH} = {}^6\Sigma_{v'=o} Q_{ov'} .$$

(Eqn. 4.46)

Each of the individual $Q_{ov'}$ are in turn illustrated in Figures 5.17
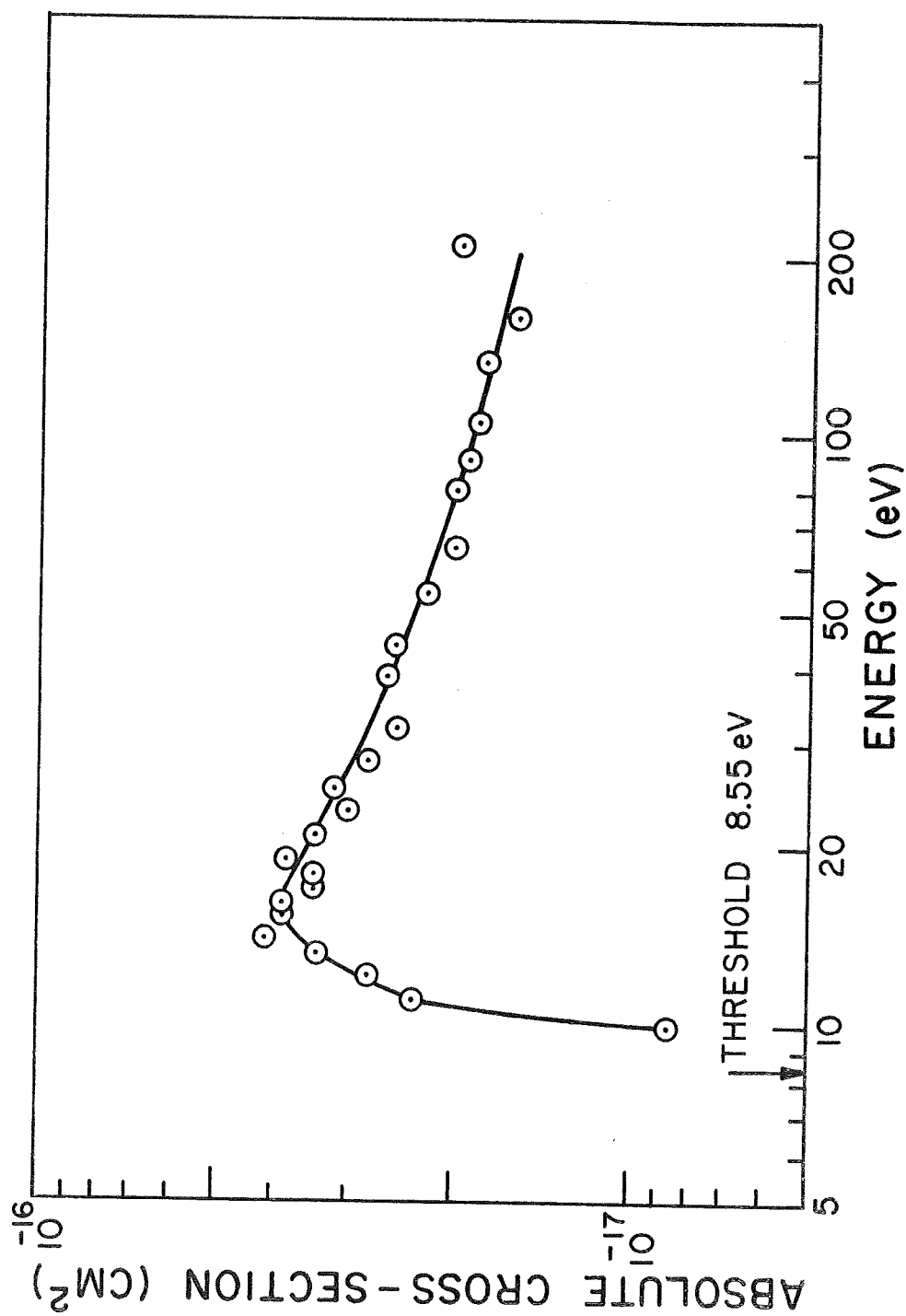
Figure
5.16

EMISSION CROSS-SECTION OF THE $a^1\Pi_g$
ELECTRONIC STATE OF N_2 BY ELECTRON IMPACT

EMISSION CROSS SECTION OF THE V=0
VIBRATIONAL LEVEL OF THE LBH STATE
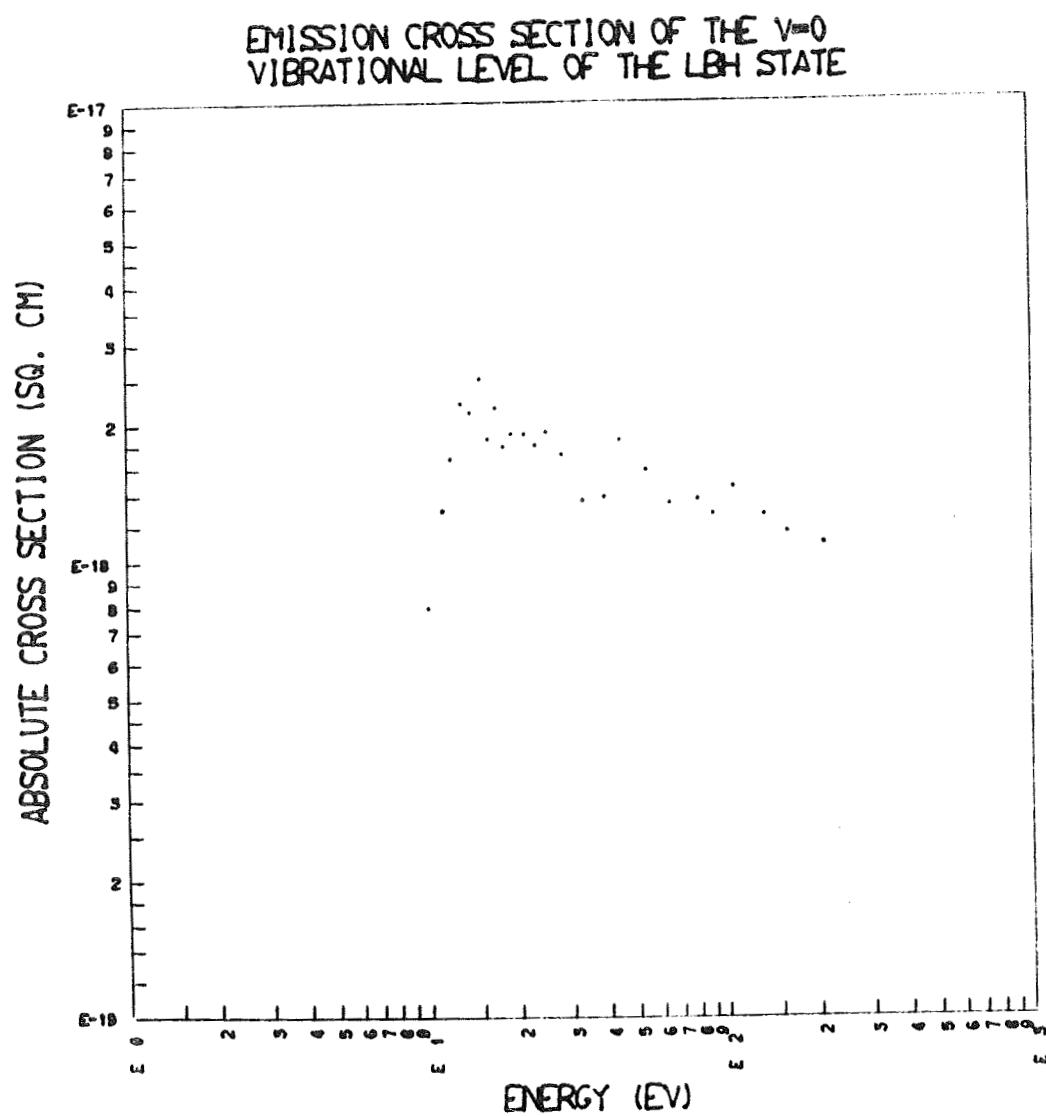
Figure 5.17

Figure 5.18

166

Figure 5.19

Figure 5.20

EMISSION CROSS SECTION OF THE V=4
VIBRATIONAL LEVEL OF THE LBH STATE

Figure 5.21

EMISSION CROSS SECTION OF THE V=5
VIBRATIONAL LEVEL OF THE LBH STATE
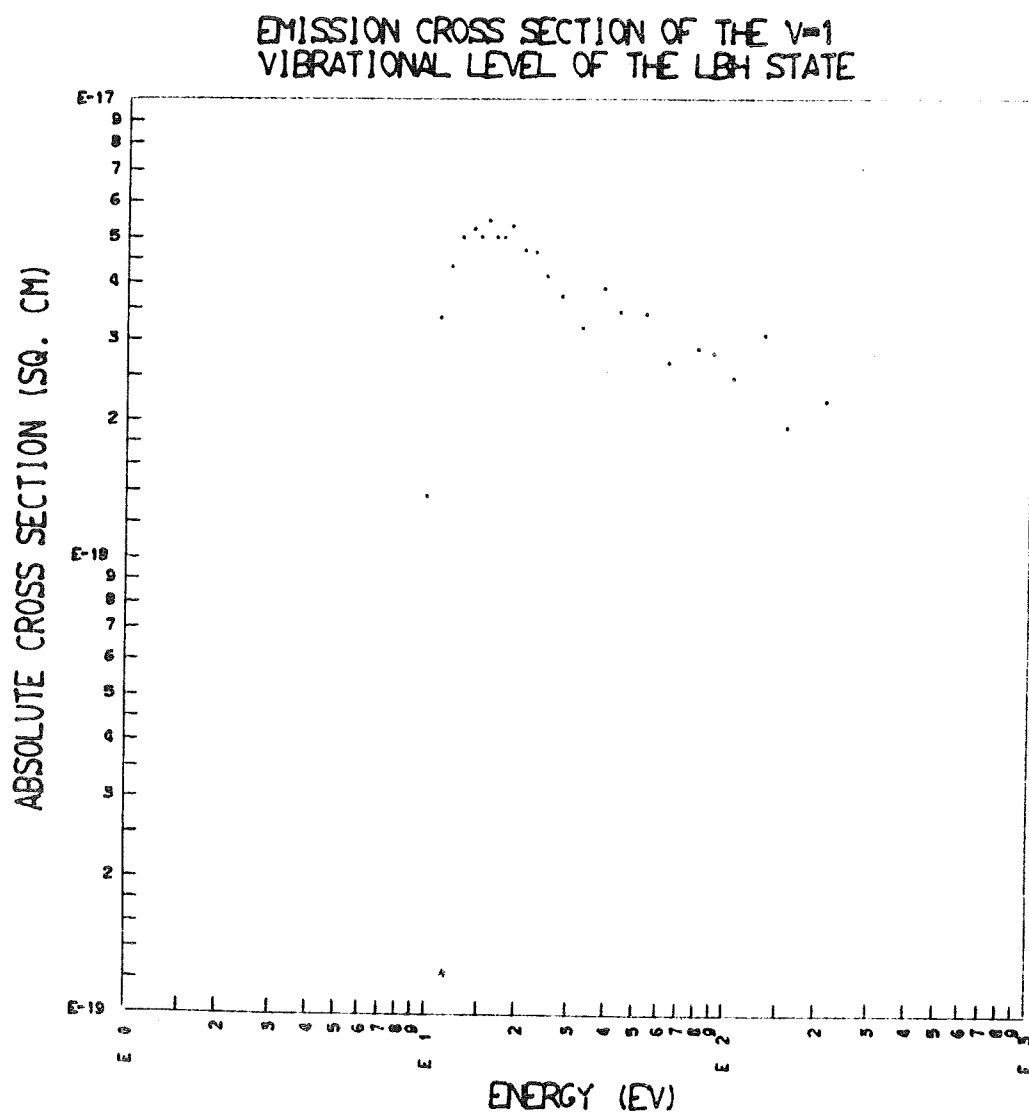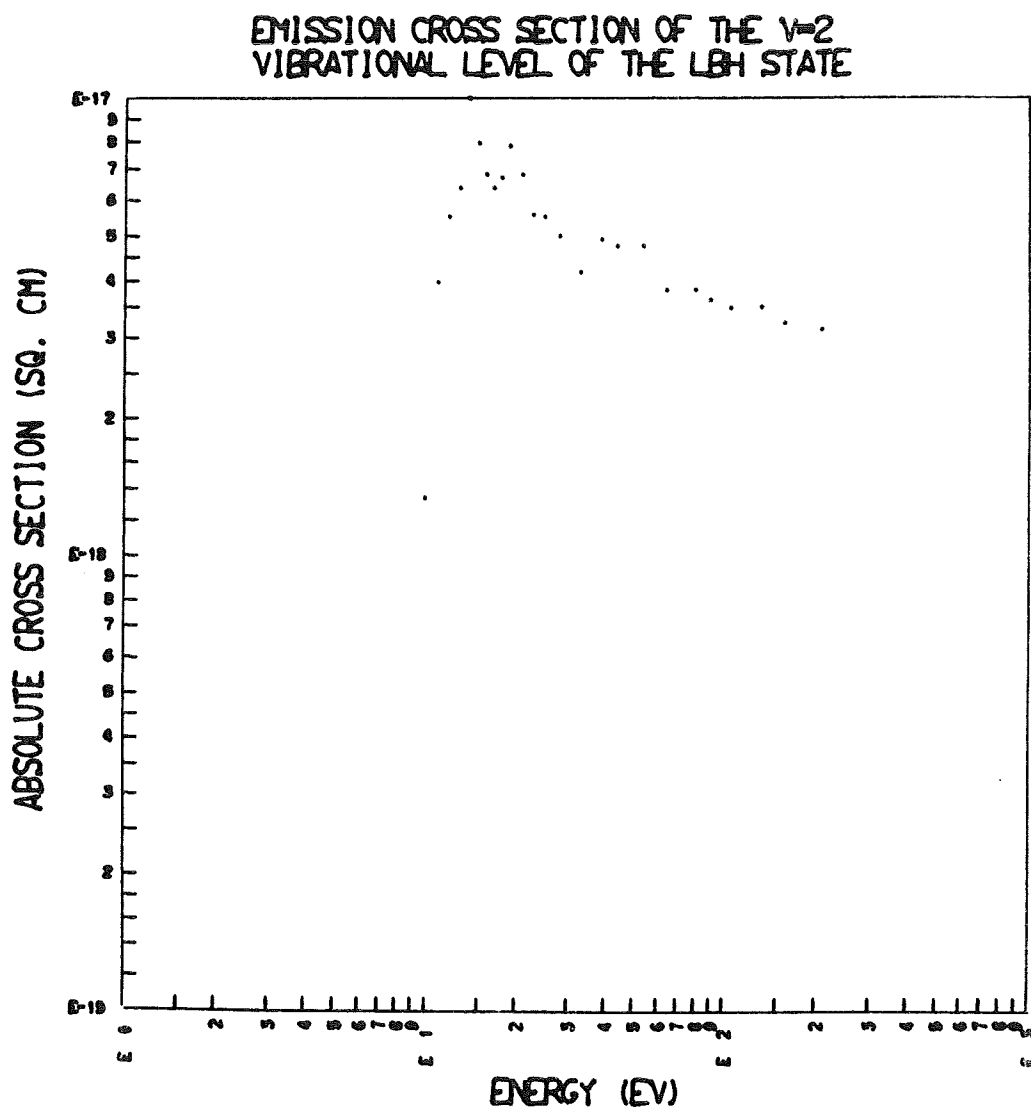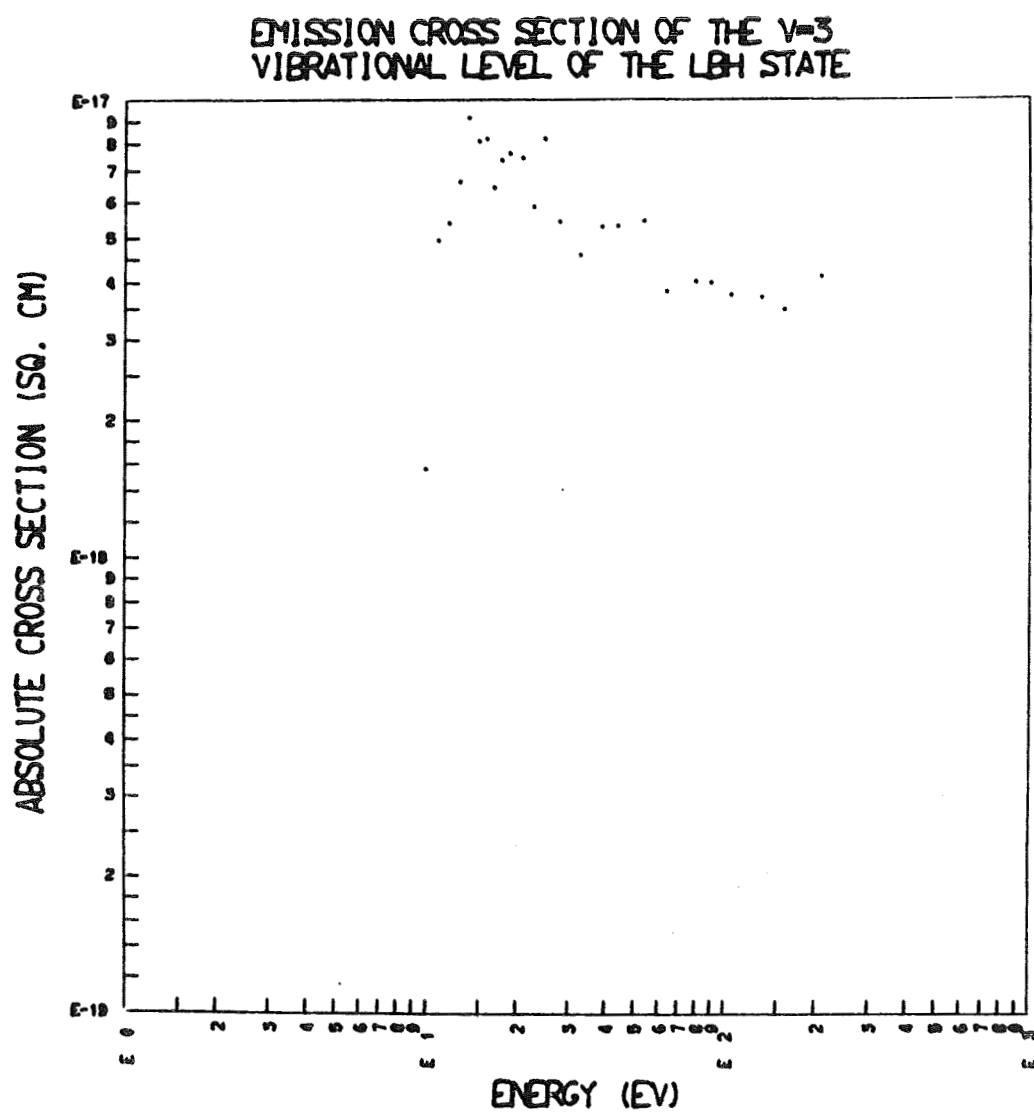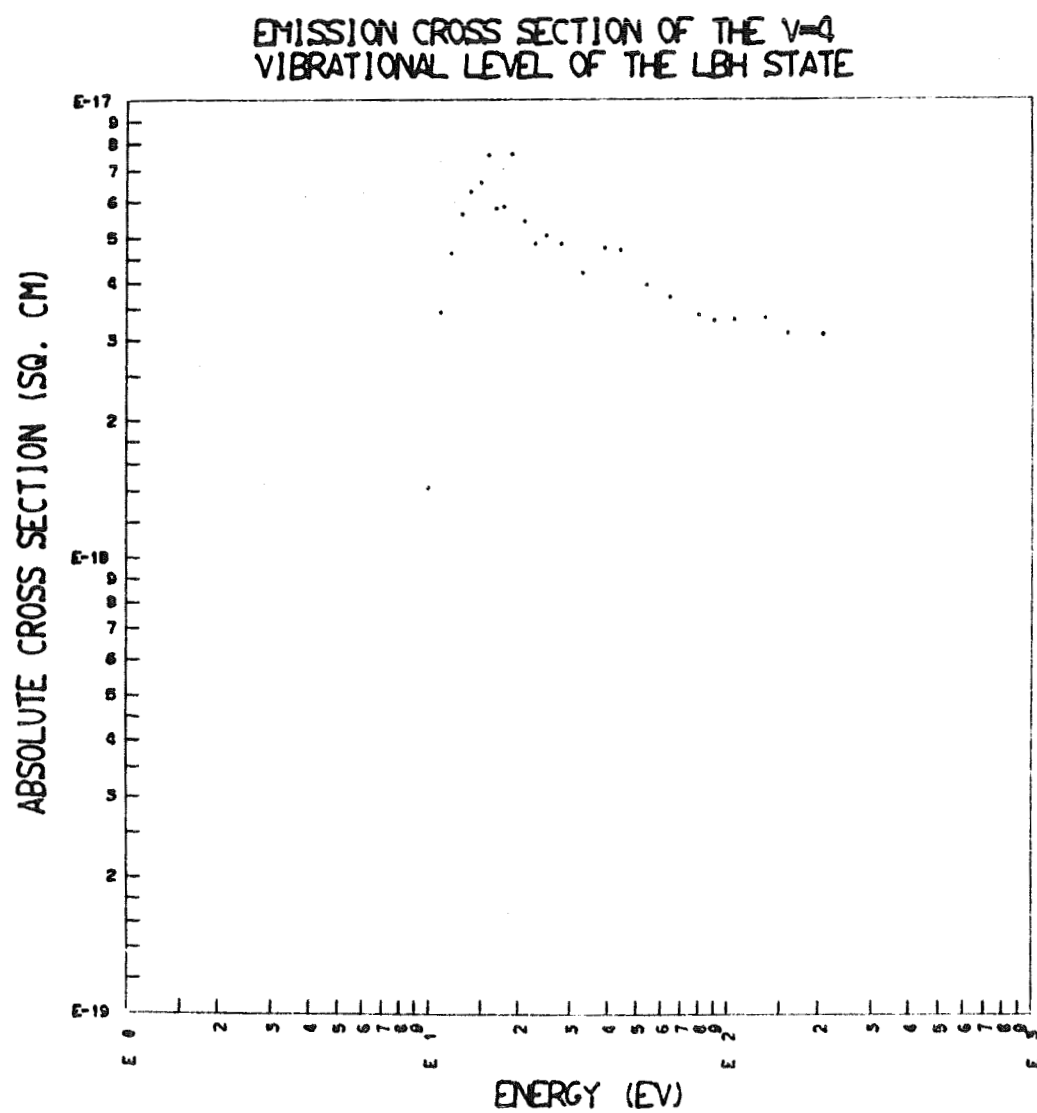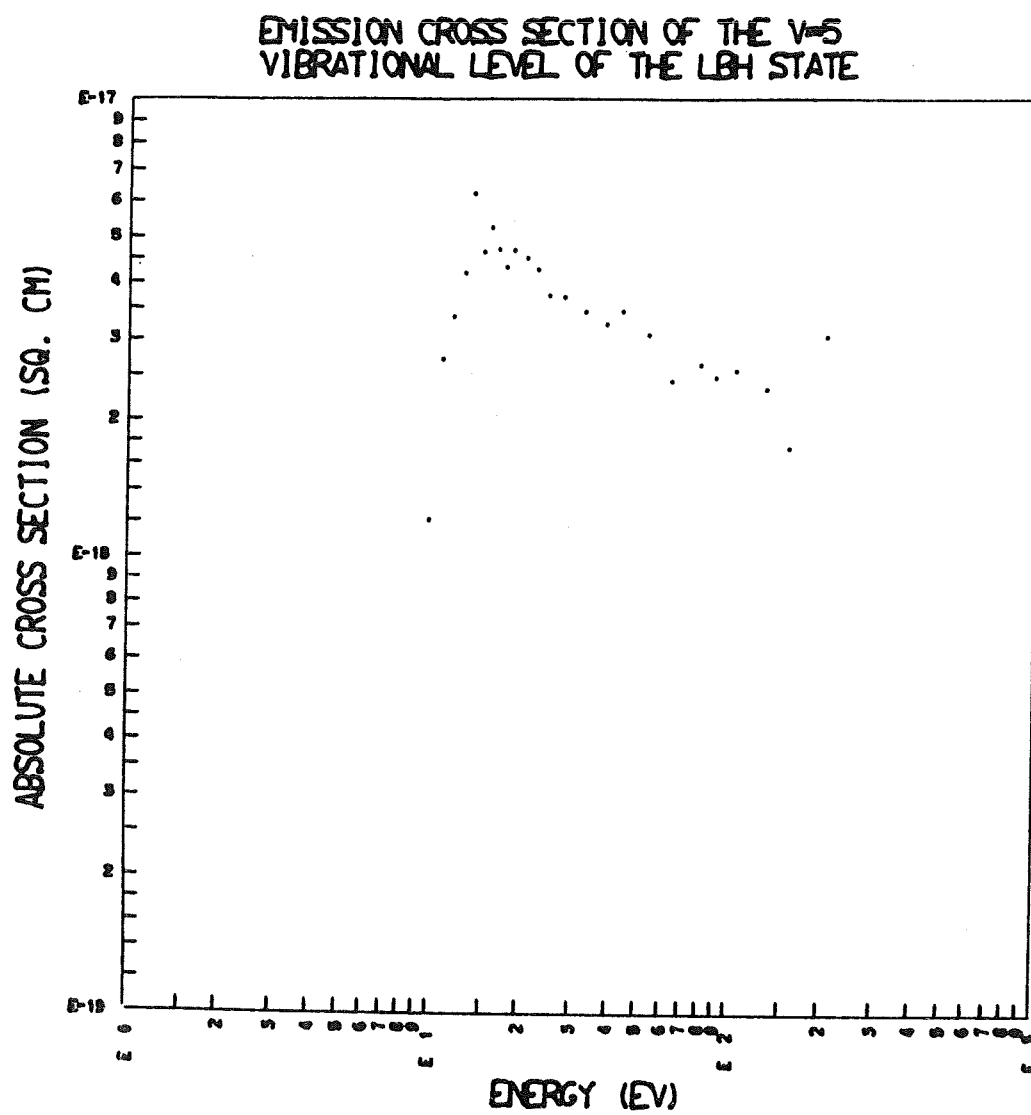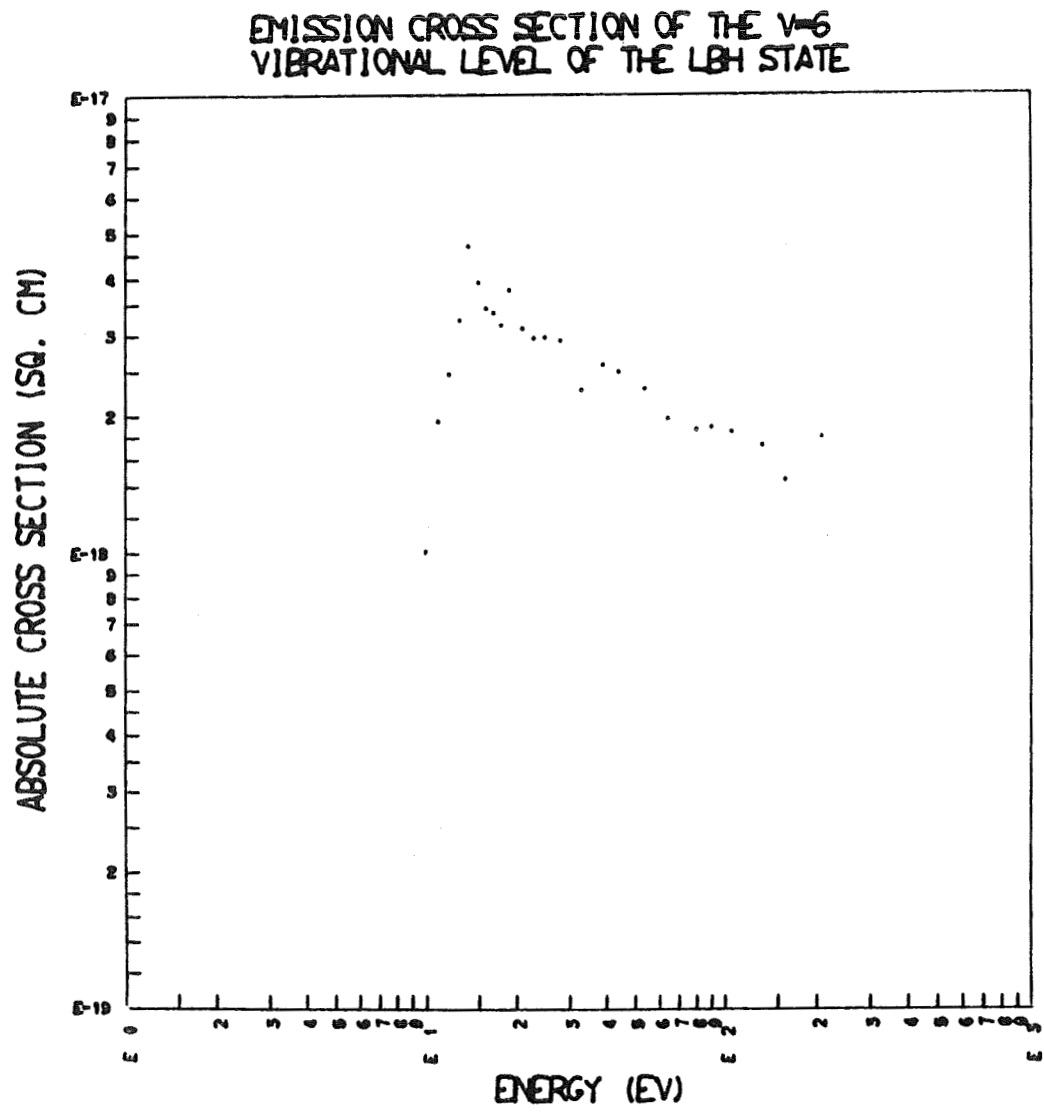
Figure 5.22

Figure 5.23

to 5.23. Each of the $Q_{ov'}$ are defined from the equation

$$Q_{ov'} = \Sigma_{v''} \ Q_{v'v''} \ ,$$

that is, as a sum of band emission cross-sections. These band

emission cross-sections, which represent the actual experimental

data points, are depicted in Appendix B.

The peak total cross-section is at 15.5 $\pm$ 1.5 eV with a

broad maximum between 14 eV and 19 eV. The total cross-section,

at peak, is 3.85 x 10^{-17} cm^2 and at 105 eV is 1.90 x 10^{-17} cm^2.

The shape of the cross-section curve agrees very well with the

shape predicted by Green and Barth (1965), although the peak

cross-section occurs at about 3 eV lower energy. The absolute

values predicted by Green and Barth agree to within 15% to the

experimentally measured cross-section.

The results for the total LBH cross-section agree very

well with the inelastic cross-section measurement for electrons

in nitrogen by Engelhardt, Phelps and Risk (1964). The cross-

section for excitation to the a $^1\Pi_g$ state was measured in an electron

swarm experiment by solving the Boltzman equation for the distri-

bution function of electron energies in a neutral gas. The peak

cross-section at 9.1 eV was 4.1 x 10^{-17} cm^2.

The results also compare reasonably well with the theo-

retical predictions of Rozsnyai (1967). Rozsnyai calculated a

peak value for the absolute cross-section of 2.6 x 10^{-17} cm^2 at

about 18 eV for excitation to the a$^1\Pi_g$ state, using the first Born

approximation for homonuclear diatomic molecules. The results

presented here show a peak emission cross-section of 3.85 x 10^{-17}

cm^2. Thus there is about a 33% difference. Part of the difference

could be from a cascade contribution, although the cascade contri-

bution to the emission cross-section is felt to be small.

However, the results differ significantly from the experi-

mental results of Holland (1969). At 105 eV, for example, the

total measured cross-section is a factor 2.8 larger than that mea-

sured by Holland. In this experiment, as well as in Holland's,

there is excellent agreement between theory and experiment as to

the fraction of the total cross-section contributed by each vibra-

tional level. For the LBH transition, it is expected that

$$\frac{Q_{ov'}}{\sum\limits_{v'} Q_{ov'}} = \frac{q_{ov'}}{\sum\limits_{v'} q_{ov'}} .$$

At 105 eV the ratio of $Q_{ov'}$ to Q_{LBH} was calculated and compared to

the ratios predicted by the Franck-Condon factors for direct electron

excitation of the various vibrational levels. The results are pre-

sented in Table 5.3. The agreement is very good and implies most

of the excitation is due to direct electron impact. It is observed

that the v' = 3 vibrational level has the largest cross-section in

agreement with the Franck-Condon factors.

TABLE 5.3

Fractional of Total Cross-Section Contributed by
Each Vibrational Level at 105 eV

v'	$Q_{ov'}$ (cm^2)	$\dfrac{Q_{ov'}}{Q_{LBH}}$	$q_{v'o}$	$\dfrac{q_{v'o}}{\Sigma\, q_{v'o}}$
0	1.40×10^{-18}	.074	.041	.047
1	2.47×10^{-18}	.130	.112	.128
2	3.51×10^{-18}	.185	.167	.192
3	3.76×10^{-18}	.198	.183	.210
4	3.31×10^{-18}	.173	.161	.184
5	2.56×10^{-18}	.134	.124	.142
6	1.89×10^{-18}	.099	.084	.096

$$Q_{LBH} = 1.90 \times 10^{-17} \qquad \sum_{v'=0}^{6} q_{v'o} = .871$$

Since the electron resolution of the electron gun is of the order of 1 eV and the intensity of the individual bands very small, it was not possible to determine with accuracy if there was a cascade contribution onset. Furthermore, the cross-section curve is rising very steeply from threshold. If it is assumed that the total change in cross-section from 12 eV to 15.5 eV is from cascading, then the maximum cascade contribution (slow cascade plus fast cascade) is 29%, since the total cross-section is 2.73 x 10^{-17} cm^2 at 12 eV and 3.85 x 10^{-17} cm^2 at 15.5 eV. The actual cascade contribution should be much less since most of the increase in cross-section from 12 eV to 15.5 eV is probably by direct electron excitation of the a$^1\Pi_g$ state. To determine with accuracy the contribution of cascade, a very careful study of the cross-section as a function of energy near threshold would have to be made. It would require an electron gun with higher energy resolution then the one used in the experiment. Either this approach or the approach of looking for the cascade radiation in the region of 2000-3000 Å region would have to be adopted to determine the amount of cascading and, further, if there is a cascade which is slow, to determine its effect on the 80 microsecond lifetime, as measured by Holland. In Appendix B are shown the experimentally measured cross-sections for the most prominent LBH bands. In these data any bands that were overlapped were separated out, assuming the validity of

using the Franck-Condon factors for direct electron excitation. The bands separated out are listed in Table 5.1. Thus the actual data for these bands is a sum of the two overlapped bands. The most prominent LBH band features are the (4,0) band at 1325 Å, the (3,0) band at 1353 Å, the (5,2) band and (2,0) band at 1383 Å, the (2,1) band at 1429 Å and the (1,1) band at 1464 Å. Of these individual bands, the (3,0) band at 1353 Å has the largest excitation cross-section. Within the experimental error, each band has the same relative shape. This result is consistent with the exper- mental results of McEwen (1965), Lassettre, et al. (1968), and Holland (1969).

Two bands that were extremely weak were the (8,0) and (8,1) band. It is of interest to mention these bands since they have not been observed previously in electron beam excitation experiments. In fact, the v' = 8 vibrational level is in the predissociation region of the $a^1\Pi_g$ state, which accounts for its small excitation cross- section. The results on these bands were uncertain. The measured points are shown in Appendix B.

There is some indication that the (7,0) band at 1249 Å may be present in the wing of the 1243 NI line. If it is present it has an extremely small cross-section. less than that of the (8,0) and (8,1) band. The v' = 7 and v' = 8 vibrational levels were not

included in the total cross-section calculation due to the large un-
certainity of their individual cross-sections. The total cross-section
of the $v' = 7$ and $v' = 8$ vibrational levels is less than 3% of the
total LBH cross-section.

5.7   Polarization.

Two types of transitions have been studied, one is the exci-
tation of the $a\,^1\Pi_g$ state of molecular nitrogen and the other is the
dissociative excitation of molecular nitrogen. In this section it is
intended to show the polarization effects on the cross-section are
small. No measurements of polarization were made.

First, consider the dissociative excitation of N_2 in an
electron beam experiment. The target molecule is subjected to
impact by electrons having a preferred direction of incidence. Van
Brunt and Zare (1968) have shown that two necessary conditions for
polarization are: (a) an anisotropic spatial distribution of dissoci-
ation products, and (b) a preferential population of the magnetic
sublevels of the excited fragments. These conditions are satisfied
when dissociation proceeds via a single, well defined potential
curve. In this case, the atoms depart from one another in well
defined M states, with respect to the internuclear axis. Further,
the distribution of the quantization axis is nearly the same as the
angular distribution of the products. In a recent experiment, Kieffer
and Van Brunt (1967) report a nearly isotropic angular distribution of

N^+ ions in studying the dissociative ionization of N_2. This is presumably due to the fact that many repulsive states of N_2 contribute to the dissociation. In the previous discussion of dissociation in section 4.4.2, it was only necessary to develop the concept of dissociation by considering one potential curve. When two atoms are placed near each other, an inhomogeneous electric field is produced along the direction joining the nuclei. Thus, two atoms brought together form a manifold of electronic molecular states having well defined projections of their angular momenta on the internuclear axis. Conversely, when these same two atoms separate via a repulsive state, they leave each other in well defined M states with respect to the internuclear axis. When two nitrogen atoms, or a nitrogen ion and nitrogen atom, in definite electronic states, are brought together, a whole series of states result, depending on the orientation of L_i the orbital angular momentum, with respect to the internuclear axis. Molecular dissociation is an efficient M state selector only if one or a limited number of states, contribute to the dissociative process. Undoubtedly in the case of N_2, many states contribute to the dissociation, washing out the polarization effect.

For the LBH bands, it is expected the conditions for polarization are greatest near the threshold region where the direction of the electron beam, the direction of the magnetic field and the direction

of the momentum transfer vector are all very close to one another. Thus there is a space quantization of the total angular momentum of the molecule. The rotational levels of the molecule characterized by J, splits into 2J + 1 sublevels. The polarization of radiation emitted in a transition from a state of definite orbital angular momentum can be expressed in terms of the cross-sections for exciting the various magnetic substates. As an approximation, assume the cross-section for exciting the various sublevels are proportional to the transition probability for exciting the sublevel. This is a very crude approximation in the threshold region, but a detailed analysis of polarization by electron impact is beyond the scope of this thesis. Then the polarization formulas are the same as for molecular fluorescence, when a beam of linearly polarized light is incident upon a collection of randomly oriented molecules in the gas phase. This problem has been solved by Zare (1966). Formulae are given for polarization for the P, Q and R branches. Polarization calculations, using Zare's results, indicate a 'worst case' degree of polarization of about 30%. This percentage introduces an uncertainty of about 10% in the cross-section measurement near the threshold. For dipole radiation and observations at 90° to the beam, it can be shown (Moiseiwitch and Smith, 1968)

$$\bar{I}' = I'(90^{\circ}) \left[1 - \frac{P}{300}\right],$$

where:

I'   is the average intensity of radiation resulting from averaging

the intensity over a sphere,

P   is the percentage of polarization,

$I'(90°)$ is the intensity at $90°$ to the beam.

The percent of polarization varies from 10% to 30%, depending on the sequence involved in exciting a rotational line. For example, an orbital electron can go to an excited state via a Q branch and emit radiation in a P branch. In all, there are nine possibilities affecting the angular distribution of the spontaneous radiation. In this experiment, rotational structure was not resolved. The net effect of resolving just vibrational structure was to sum over the rotational transitions and remove most of the anistropy.

It is expected that the degree of polarization decreases rapidly as the electron beam energy increases above threshold. This arises from the fact the momentum transfer vector is no longer oriented along the beam axis, but will be at an angle to it. In this case, the resultant angular momentum vector precesses about the magnetic field and results in a disorientation of the radiators.

5.8   Error Analysis.

The major uncertainties in the measurements arise from the uncertainties in the following parameters: absolute calibration, relative calibration, pressure, transition probability of the LBH state,

relative cross-section, and photomultiplier current measurements with the picoammeter-Brush recorder combination. The uncertainties discussed in the section are: estimated root mean square deviations, as determined from either repeatability measurements, manufacturer's specifications, or from experimental work of other authors. The uncertainties for these parameters were determined as follows:

1)   Absolute Calibration: The absolute calibration uncertainty was determined by taking each of the quantities of Eqn. 3.7 and assigning experimental uncertainties to each parameter. These uncertainties included the uncertainty in the NO quantum efficiency, 5% (Samson, 1967); the uncertainty in the transmission of the lithium fluoride window, 1%; the uncertainty of the two current measurements, 3% each; the drift of the lamp, 3%; and the noise in the NO cell, 3%.

2)   Relative Calibration: There is a 10% uncertainty in the efficiency of the monochromator because of the different experimental conditions present during the calibration and experiment. There is a 5% uncertainty in the repeatability of the efficiency measurement during calibration. This number was obtained by taking an average of the experimental points at each wavelength and then determining a root mean

square deviation from the average. The uncertainty

in the relative calibration of the 541G photomultiplier

is due to a 3% uncertainty in the experimentally averaged

points and a 3% uncertainty in the relative response of

sodium salicylate.

3) <u>Pressure Calibration</u>: There is a 5% uncertainty in the

absolute calibration method.

4) <u>The Transition Probability of the LBH State</u>: There is

an uncertainty of a factor of 2 in the transition probabil-

ity which leads to an approximate 10% uncertainty in the

fraction of the LBH radiation collected.

5) <u>Relative Cross-Section</u>: The uncertainty in the shape of

the relative cross-section curve for the LBH bands is

primarily from the scatter of experimentally measured

points (Appendix B). By fitting many of the experi-

mentally measured emission cross-section points of

each individual band with the shape of the LBH curve,

as determined for the total LBH electronic transition,

an approximate uncertainty for the root mean square de-

viation of the individual experimental points from the

true value was determined. The value was 8% for the

stronger bands, $1273 < \lambda < 1600$ Å, and 16% for the

weaker bands, $1600 < \lambda < 1962$ Å. The average

value used for the uncertainty was 12%. For the

atomic nitrogen lines, by a similar procedure, the

value was 3%.

6)   The Current in the Photomultiplier with a Picoammeter-

Brush Recorder Combination: There is a 3% uncer-

tainty in the repeatability of the current measuring

combination, according to the manufacturer specifi-

cations.

The resultant root mean square deviation or uncertainty in

the absolute emission cross-section because of each of these in-

dependent, ramdom effects is 22% for the LBH bands and 16% for

the nitrogen lines.

The large scatter of points in the case of the LBH bands

was caused by the low intensity of radiation emitted by each in-

dividual band. The signal to noise ratio was much less than in

the case of the atomic nitrogen lines. Therefore it was more

difficult to accurately determine the area under each band, the weaker

the band.

For the more intense LBH bands, that is, for the bands with

the largest emission cross-section, there was very little scatter of

the individual points. These bands include the (5,0), (4,0), (3,0),

(2,0) and (1,1). In order not to rely totally on Franck-Condon fac-

tors for the determination of cross-section, all transitions from the

LBH state were measured experimentally except for about 5% of the transition from 1962 Å to 2300 Å. For the region from 1600 Å to 1900 Å, which contained the weaker bands and also the minimum response of the optics, the scatter was appreciable. The best results for the LBH system was the region 1273 Å to 1600 Å, which contained the strongest bands and also maximum response of the system. Because of the laws of statistics which states the distribution of experimental points are Gaussian about the true mean value, the effect of adding all the emission corss-sections at a particular energy to form the total cross-section filtered out most of the uncertainty in the shape of the total cross-section curve. Furthermore, since the most intense bands had a larger partial cross-section and smaller uncertainty in its absolute value, these cross-sections had a larger weight of the total cross-section.

CHAPTER VI

ATMOSPHERIC APPLICATIONS

6.1   Introduction

Two of the most important atmospheric applications of these measurements are the calculations of emission rate factors in the dayglow and aurora by electron impact. Both the Lyman-Birge-Hopfield band system and the atomic nitrogen lines have been observed in the aurora (Fastie, 1967) and in the dayglow in the recent Bushmaster rocket flights (Barth, 1969) conducted by the Laboratory for Atmospheric and Space Physics. In the aurora, the main excitation mechanism for the LBH bands is the low energy secondary electrons. The secondary electrons are produced by ionization of the atmospheric constituents by a primary electron flux in the energy range 500 eV to 10 keV. The excitation of the nitrogen lines, being primarily an ionization process, is caused both by the primary and the secondary fluxes. This stems from the fact the ionization cross-sections for the nitrogen lines are still relatively large in the primary energy range, while the production of the LBH bands is mainly determined by the secondary electron flux.

The dayglow consists of spectral features that occur in the upper atmosphere when it is directly illuminated by solar

radiation. The phenomena that produce these emission features are resonant and fluorescent scattering of solar radiation, chemical and ionic reaction and photoelectron excitation of atoms and molecules. It is the last of these phenomena for which the emission cross-section measurements have application. The photoelectrons are produced in the process of ionization of atoms and molecules by extreme ultraviolet solar radiation. The effects of secondary electrons, which are produced by further ionization of the atmospheric species by the primary photoelectrons, are negligible in the dayglow for the N_2 ultraviolet features, since the mean secondary electron energy is about 5 eV (Green and Barth, 1967). The main excitation mechanism in the dayglow for the LBH bands is the photoelectron mechanism. For the atomic nitrogen lines, photodissociation and photoionization of N_2 may be important. Because of the unavailability of photodissociative excitation cross-sections and photoionization excitation cross-sections, it is not possible to predict the amount of dayglow radiation produced by the effect. The calculation of the intensities of the atomic nitrogen lines by assuming only photoelectron mechanism represents a lower limit. By a comparison with a measurement of intensity by rocket measurements, it would be possible to determine if the other excitation mechanism needs to be considered.

In this chapter the emission rate factor is calculated for the LBH band system and the atomic nitrogen lines in the dayglow as a function of slant column density of the atmosphere. The slant

column density is the integeral of the number density between the

observer and the Sun. The computation uses the results of Dalgarno,

McElroy and Stewart (1969) who have calculated steady state pri-

mary photoelectron electron fluxes for a zenith angle of 72°. The

calculation of emission rate factors presented here provides a method

of determining volume emission rates for these emission features in

the dayglow for any model atmosphere or zenith angle.

A calculation of the emission rate factor in an auroral oval

is made using the computation of secondary electron fluxes of Rees

(1969).

6.2   The Dayglow.

Photoelectrons are produced by the ionizing solar radiation

between $31 \overset{\circ}{A}$ and $1027 \overset{\circ}{A}$. The solar spectrum in this region has

been measured by Hinteregger, Hall and Schmidtke (1964). They

have tabulated the flux in the region, $\lambda < 1775 \overset{\circ}{A}$, at wavelengths

fo 24 major spectral lines and in 67 zones of the continuum.

For photons of wavelength λ, the rate of production of

primary photoelectrons in the i-th ionization state of the k-th atmo-

spheric species, having particle density $n_k (z)$ is

$$C_{ik} (\epsilon , z , \chi) = {}_I Q_{ik} (\lambda) \, n_k (z) \, F (\lambda, z, \chi) , \qquad (6.1)$$

where:

${}_I Q_{ik} (\lambda)$ is the i-th ionization cross-section of the k-th species
   by photons of wavelength λ,

$n_k(z)$ is the number density of the k-th atmospheric

constituent at altitude z,

$F(\lambda, z, \chi)$ is the solar flux at altitutde z, zenith angle χ

and wavelength λ. The solar XUV flux also

depends on the solar cycle.

The energy of the photoelectron produced in this par-

ticular reaction is given by

$$\epsilon_{ik} = \frac{hc}{\lambda} - I_{ik} .$$ (6.2)

I_{ik} is the ionization potential of the i-th state of species k.

There are several ionization limits for each species.

Thus, incident photons of a single energy generates photoelectrons

with a set of energies determined by the ionization thresholds of

each atmospheric species. Alternatively, a set of wavelengths,

defined by $hc/\lambda - I_{ik}$ = constant, generates photoelectrons of a

single energy. The solar flux at any altitutde and for zenith angle

χ ($\chi < 80^\circ$) is given by

$$F(\lambda, z, \chi) = F_o(\lambda) .$$

$$\exp \left[-\sec \chi \sum_m {_A}Q_m(\lambda) \int_z^\infty n_m(y) \, dy \right] ,$$ (6.3)

where $\sec \chi$ is an approximation to the Chapman function.

$$\int_z^\infty n_m(y) \, dy = \eta_m(z) ,$$ (6.4)

where:

$_A Q_m (\lambda)$ is the total absorption cross-section of the m-th

species at wavelength λ, and

$\eta_m (z)$ is the column density of the m-th species.

Combining equations 6.1, 6.3 and 6.4, the production rate of

photoelectrons of energy ϵ_{ik} by the i-th ionization state of the k-th

species is

$$C_{ik} (\lambda, y, \chi) = F_o (\lambda) \; _I Q_{ik} (\lambda) \; n_k (z) .$$

$$\exp \left[-\sec \chi \sum_m {}_A Q_m (\lambda) \; \eta_m (z) \right] . \qquad (6.5)$$

The total production rate of primary photoelectrons of energy ϵ,

created by photoionization, is a sum over i and k such that

$$\epsilon = \frac{hc}{\lambda} - I_{ik} .$$

Thus,

$$C (\epsilon, z, \chi) = \sum_i \sum_k .$$

$$F_o \left(\frac{hc}{\epsilon + I_{ik}} \right) \; _I Q_{ik} \left(\frac{hc}{\epsilon + I_{ik}} \right) .$$

$$n_k (z) \; \exp \left(-\sec \chi \sum_m {}_A Q_m \left(\frac{hc}{\epsilon + I_{ik}} \right) \eta_m (z) \right) .$$

$$\qquad (6.6)$$

Define $S_{ik} (\epsilon, z, \chi)$ as

$$S_{ik} (\epsilon, z, \chi) = F_o \left(\frac{hc}{\epsilon + I_{ik}} \right) \; _I Q_{ik} \left(\frac{hc}{\epsilon + I_{ik}} \right) .$$

$$\exp\left(-\sec\chi \sum_m {}_A Q_m \left(\frac{hc}{\epsilon + I_{ik}}\right) \eta_m(z)\right) \,. \qquad (6.7)$$

This quantity is the number of photoelectrons produced per second of energy ϵ at altitude z per molecule with solar illumination at zenith angle χ in the i-th ionization state of the k-th constituent.

The total photoelectron production rate at energy ϵ is

$$C(\epsilon,z,\chi) = \sum_{ik} n_k(z) S_{ik}(\epsilon,z,\chi) \frac{electrons}{cm^3 \ sec} \,. \qquad (6.8)$$

The steady-state photoelectron flux is (Dalgarno et al., 1969)

$$\Phi(\epsilon,z,\chi) = \frac{\sum_{\epsilon_j > \epsilon} C(\epsilon_j,z,\chi)}{\sum_\ell n_\ell \ L_\ell(\epsilon)} \frac{electrons}{cm^2 \ sec \ eV} \,, \qquad (6.9)$$

where $L_\ell(\epsilon)$ is the total loss function for the ℓ-th constituent in units of $eV \ cm^2$. It describes the total energy loss of the photo-electrons to all processes. The assumption of continuous energy loss is made. This is an approximation which is adequate for $\epsilon > 8$ eV. The assumption is also made that the photoelectrons interact locally. This is satisfactory at altitudes less than 250 km, where most of the dayglow emission occurs.

Dalgarno, McElroy and Stewart (1969) have used the solar fluxes of Hinteregger, Hall and Schmidtke (1964) to calculate the equilibrium photoelectrons fluxes at various altitudes for a solar zenith angle of 72° and for a model atmosphere with an exospheric

temperature of 750 °K. Their calculations assumed a continuous energy loss for the photoelectrons. The photoelectron flux as a function of energy is, on the average, a decreasing function as energy increases. The emission cross-section of the LBH bands is a decreasing function of energy past 15.5 eV. Thus, the excitation of the LBH bands is caused for the greater part by electrons in the 8.55 eV to 30 eV range. With a knowledge of the photoelectron fluxes it is straightforward to write an expression for the volume emission rate for the j-th excitation level of the k-th species. Deactivation is negligible for the N_2 transitions being considered above an altitude of 120 km, so that the volume excitation rate is equal to the volume emission rate. Thus, the volume emission rate is

$$I_{jk}(z, \chi) = n_k(z) \cdot$$

$$\int_{\epsilon_T}^{\infty} \Phi(\epsilon, z, \chi) \, Q_{jk}(\epsilon) \, d\epsilon \left(\frac{\text{photons}}{\text{cm}^3 \text{ sec}} \right), \qquad (6.10)$$

where:

ϵ is the energy of the photoelectron,

ϵ_T is the threshold energy for process j,

Q_{jk} is the emission cross-section of the j-th state of the k-th species.

The emission rate factor, g_{jk}, for the photoelectron excitation

of the j-th transition of the k-th species is defined as

$$g_{jk} (z, \chi) = \int_{\epsilon_T}^{\infty} \Phi(\epsilon, z, \chi) \ Q_{jk} (\epsilon) \ d\epsilon \left(\frac{\text{photons}}{\text{sec molecule}} \right) \ . \qquad (6.11)$$

A plot of the results of Dalgarno, McElroy and Stewart is shown

in Figure 6.1. It is obvious from these curves that $\Phi(\epsilon, z, \chi = 72^{\circ})$

can be written with sufficient accuracy (within 15%) as

$$\Phi(\epsilon, z, \chi = 72^{\circ}) = \Phi_O (\epsilon) \ f(z, \chi = 72^{\circ}) \ \text{for} \ \epsilon > 8 \ \text{eV} \qquad (6.12)$$

and over the altitude range 120 to 300 km, where Φ_O is the photo-

electron flux at 300 km.

Thus,

$$g_{jk} (z, \chi = 72^{\circ}) = g_{O_{jk}} \ f(z, \chi = 72^{\circ}) \ , \qquad (6.13)$$

where

$$g_{O_{jk}} = \int_{\epsilon_T}^{\infty} \Phi_O (\epsilon) \ Q_{jk} (\epsilon) \ d\epsilon \ .$$

$f(z, \chi)$ is a function of both altitude and solar zenith angle. It is

equal to 1 at 300 km.

$$f(z, \chi) \equiv e^{-\alpha (z) \eta_\chi (z)} \ , \qquad (6.14)$$

where

$$\eta_\chi (z) = \sec \chi \int_z^{\infty} \sum_k n_k (y) \ dy. \qquad (6.15)$$
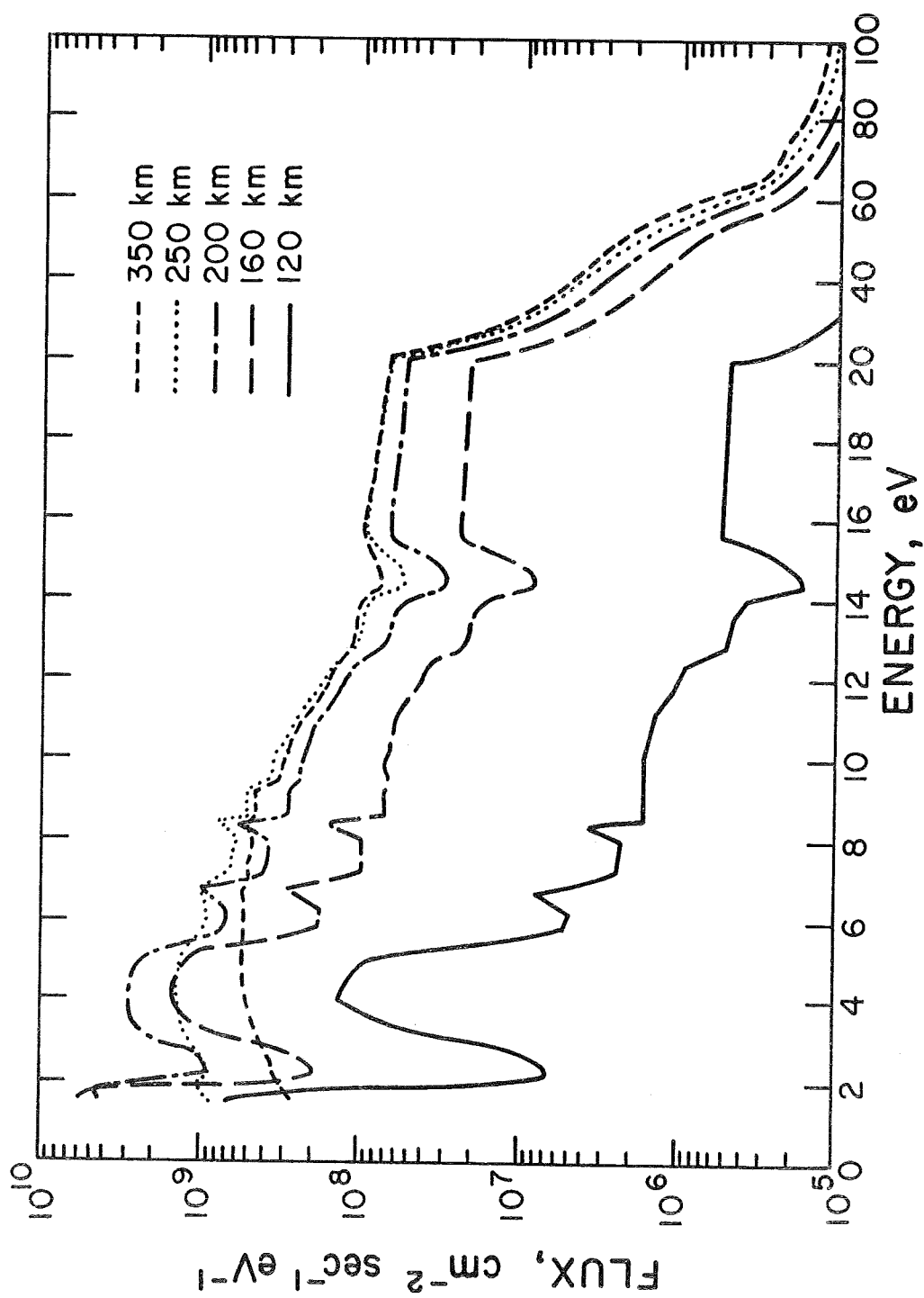
Figure 6.1 EQUILIBRIUM PHOTOELECTRON FLUXES $\phi(E)$ AS A FUNCTION OF ENERGY AT VARIOUS ALTITUDES. NOTE THE CHANGE IN THE HORIZONTAL SCALE AT 20 eV

Thus, η_χ (z) is the total slant column density of the atmosphere between level z and the Sun. f(z,χ) is defined this way, since the change with altitude of photoelectron flux is primarily due to absorption of the solar XUV radiation by the atmospheric constituents. α is a function of altitude, since the relative composition of the atmosphere is changing with height, thus absorbing the solar radiation in a manner that depends on altitude. This definition of f(z,χ) is equivalent to the following approximation in Eqn. 6.6:

$$\sum_m A^Q_m \left(\frac{hc}{\epsilon + I_{ik}} \right) \eta_m(z) = \alpha(z) \sum_m \eta_m(z) \qquad (6.16)$$

where α is an effective absorption. With this approximation it is now possible to separate S_{ik} into a product of functions, one dependent on energy, the other on slant column density. α is the effective cross-section for the solar flux at altitude z. It is an average with respect to wavelength over the XUV spectral region weighted by the column density of each species between the observer and the top of the atmosphere. It is determined empirically and is justified by the fact the quantity α reproduces the effect of the atmospheric absorption on the solar XUV radiation as far as it determines the photoelectron flux. Separating S_{ik} into two functions, one dependent on energy, $B_{ik}(\epsilon)$, and the other an exponential function of slant column density, it is found that

$$S_{ik}(\epsilon, z, \chi) = B_{ik}(\epsilon) \exp \left[-\alpha \sec \chi \sum_m \eta_m(z) \right]$$

$$(6.17)$$

where

$$B_{ik} = F_o \left(\frac{hc}{\epsilon + I_{ik}} \right) I^Q_{ik} \left(\frac{hc}{\epsilon + I_{ik}} \right).$$

B_{ik} is the number of photoelectrons produced per second at the top of the atmosphere by ionization process (i, k). The total photo-electron production rate at energy ϵ is

$$C(\epsilon, z, \chi) = \exp \left(-\alpha \sec \chi \sum_m \eta_m(z) \right) \sum_{ik} n_k B_{ik}(\epsilon) \qquad (6.18)$$

or

$$C(\epsilon, z, \chi) = \exp \left[-\alpha \sec \chi \sum_m \eta_m \right] \sum_k n_k B_k(\epsilon) \qquad (6.19)$$

where

$$B_k(\epsilon) = \sum_i B_{ik}(\epsilon). \qquad (6.20)$$

Define

$$\bar{B}(\epsilon) = \frac{\sum_k n_k B_k(\epsilon)}{\sum_k n_k}, \qquad (6.21)$$

where

$$\sum_k n_k = N.$$

N is the total number density.

Then,

$$C(\epsilon, z, \chi) = N \bar{B}(\epsilon) \exp\left(-\alpha \sec \chi \sum_m \eta_m(z)\right) . \qquad (6.22)$$

An energy loss function for the atmosphere at any given altitude can be defined by

$$L(\epsilon) = \frac{\sum_k n_k L_k(\epsilon)}{\sum_k n_k} . \qquad (6.23)$$

Thus,

$$\Phi(\epsilon, z, \chi) = \frac{N \exp\left[-\alpha \sec \chi \sum_m \eta_m(z)\right] \sum_{\epsilon_j > \epsilon} \bar{B}(\epsilon_j)}{N L(\epsilon)} \qquad (6.24)$$

or dividing the numerator and denominator of Eqn. 6.24 by N, it is seen that

$$\Phi(\epsilon, z, \chi) = \exp\left[-\alpha \sec \chi \sum_m \eta_m(z)\right] \frac{\sum_{\epsilon_j > \epsilon} B(\epsilon_j)}{L(\epsilon)} . \qquad (6.25)$$

Thus, Φ in this approximation is a product of two functions, where:

$$\Phi_o(\epsilon) = \frac{\sum_{\epsilon_j > \epsilon} B(\epsilon_j)}{L(\epsilon)} \qquad (6.26)$$

and

$$\eta_\chi = \sec \chi \sum_m \eta_m . \qquad (6.27)$$

Substituting these two equations into Eqn. 6.25, it is found that

$$\Phi(\epsilon, z, \chi) = \Phi_0(\epsilon) \exp[-\alpha \, \eta_\chi] \, , \qquad (6.28)$$

and hence

$$g_{jk}(z, \chi) = \exp[-\alpha \, \eta_\chi] \int_{\epsilon_T}^{\infty} \Phi_0(\epsilon) \, Q_{jk}(\epsilon) \, d\epsilon \qquad (6.29)$$

or,

$$g_{jk}(z, \chi) = g_{0_{jk}} \exp[-\alpha \, \eta_\chi] \, ,$$

where

$$g_{0_{jk}} = \int_{\epsilon_T}^{\infty} \Phi_0(\epsilon) \, Q_{jk}(\epsilon) \, d\epsilon \, .$$

A semi-log plot of g versus η_χ for the LBH bands and nitrogen lines is shown in Figure 6.2. It is a straight line for slant column densities less than 7×10^{17} particles/cm^2. The altitudes corresponding to

$$\eta_\chi = \sec 72° \int_z^{\infty} n(z) \, dz$$

are shown for the particular model atmospheres of the Dalgarno, et al., calculation. If it is assumed that the emission rate factor depends only on the slant column density, then the plot of g versus η_χ is a good approximation to the emission rate factor for other model atmospheres with the same boundary conditions for the major atmospheric constituents as used in the calculation of Dalgarno, McElroy and Stewart, and for all zenith angles ($\sec \chi$ becomes the Chapman function for $\chi > 80°$), although g is calculated for a solar zenith angle of $72°$ and a model atmosphere of $750°$K exospheric temperature. Thus, if η_χ is calculated for the conditions of a particular observation, the emission rate factor can be read from Figure 6.2.
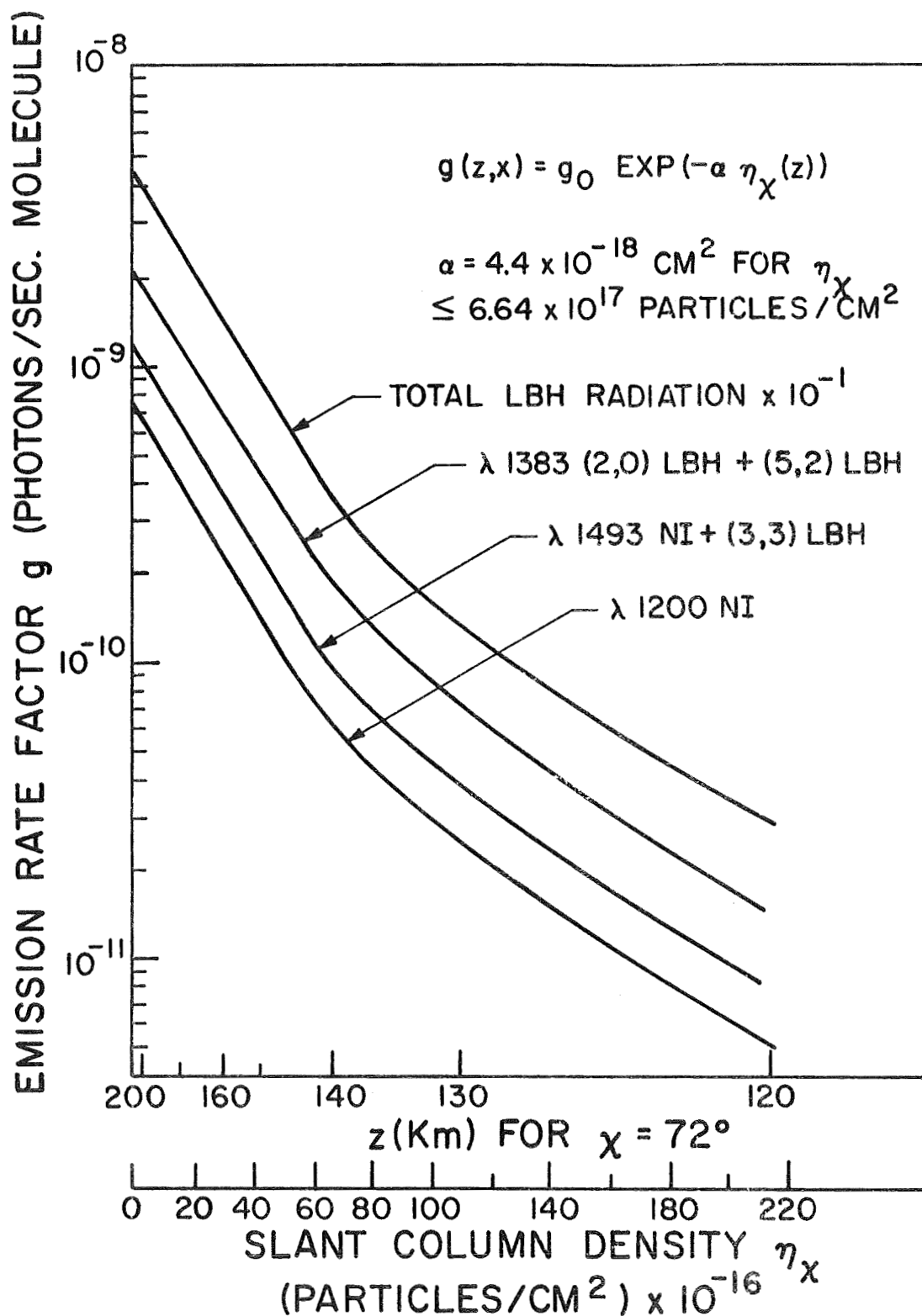
Figure 6.2 EMISSION RATE FACTOR, g, AS A FUNCTION OF SLANT COLUMN DENSITY (TOTAL ATMOSPHERIC COLUMN DENSITY BETWEEN OBSERVER AND SUN) FOR EXCITATION OF N_2 BY PHOTOELECTRONS

If α is regarded as an effective absorption coefficient of solar XUV radiation, then α is determined by

$$\alpha = \frac{1}{\eta_\chi} \ln \frac{g_o}{g}$$

$$= \text{constant for } \eta < 7 \times 10^{17} \frac{\text{particles}}{\text{cm}^2} \, . \tag{6.30}$$

From the semi-log plot of g vs. η_χ, $\alpha = 4.4 \times 10^{-18} \text{ cm}^2$ in the linear region. For altitudes greater than 130 km, atomic oxygen is the dominant species so that the depth of penetration of the solar ionizing radiation depends mainly on the absorption coefficient of oxygen and its concentration. In the region 120 to 130 km, conditions in the atmosphere are changing as N_2 and O_2 become more predominant. Approaching 130 km, the production of O_2^+ increases as a fraction of the total production of photoions because the more abundant O and N_2 have absorbed out those wavelengths, causing high production of O^+ and N_2^+ at higher altitudes. In the range, 120 to 130 km, α depends on z. From the shape of the curve, the effective absorption coefficient has decreased. In the region where α is changing, it may not be possible to read the emission rate factors off Figure 6.2 for other zenith angles and model atmospheres with great accuracy. This is because α is a function of altitude and not just dependent on the slant column density. Thus, the emission rate factors can be determined from this chart for $\eta_\chi < 7 \times 10^{17}$ particles/cm^2.

In Table 6.1 the values of g_o at an altitude of 300 km are given for the transitions, whose emission cross-sections were determined in this experiment.

TABLE 6.1

Emission Rate Factors at 300 km

λ $(\overset{\circ}{A})$	Band or Feature	g_o $\left(\dfrac{photons}{sec\ molecule}\right)$
1200	NI	8.19×10^{-10}
1298	(5,0)	1.30×10^{-9}
1325	(4,0)	2.54×10^{-9}
1353	(3,0)	2.62×10^{-9}
1383	(2,0) + (5,2)	2.44×10^{-9}
1464	(1,1) LBH	1.43×10^{-9}
1493	(3,3) LBH + NI	1.32×10^{-9}
LBH TOTAL		4.94×10^{-8}

In Table 6.2 the model atmosphere of Dalgarno, McElroy and Stewart is given, where the column densities for the individual species are the vertical column densities.

6.3   The Aurora.

In a recent paper Rees (1969) has calculated differential electron fluxes for the auroral oval using the data of Hoffman (1969). The principal initial energy loss process of the primary electrons is ionization of the neutral species. Excitation of electronic levels in the un-ionized atmospheric gas are produced principally by secondary electrons. Spectral features such as the 1200 Å, 1493 Å and 1743 Å multiplets of NI, which are partly caused by ionization processes, are probably excited by both the secondary and primary electrons. The production of excited atmospheric species is given by Eqn. 6.10, where Φ now represents the auroral energy flux. The emission rate factor is

$$g_{jk} = \int_{\epsilon_T}^{\infty} \Phi(\epsilon) \, Q_{jk}(\epsilon) \, d\epsilon \; . \qquad (6.31)$$

For illustrative purposes, emission rate factors are calculated for the LBH band system and the nitrogen lines using Eqn. 6.11 and are presented in Table 6.3. The calculation uses the auroral differential energy flux for the auroral oval, as determined by Rees at an altitude of 150 km.

TABLE 6.2

The Model Atmosphere (Dalgarno, McElroy and Stewart, 1969)

z	n_{N_2} particles cm^3	n_{O_2} particles cm^3	n_O particles cm^3	η_{N_2} particles cm^2	η_{O_2} particles cm^2	η_O particles cm^2
120	4.0 (11)	7.25 (10)	7.6 (10)	4.42 (17)	7.25 (16)	1.48 (17)
130	1.3 (11)	2.19 (10)	3.41 (10)	2.10 (17)	3.09 (16)	9.67 (16)
140	6.19 (10)	9.62 (9)	2.08 (10)	1.19 (17)	1.61 (16)	6.99 (16)
150	1.42 (10)	4.95 (9)	1.42 (10)	7.21 (16)	9.12 (15)	5.27 (16)
160	2.04 (10)	2.77 (9)	1.04 (10)	4.54 (16)	5.38 (15)	4.06 (16)
170	1.27 (10)	1.61 (9)	7.78 (9)	2.92 (16)	3.25 (15)	3.16 (16)
180	8.08 (9)	9.66 (8)	5.97 (9)	2.47 (16)	1.99 (15)	2.47 (16)
190	5.23 (9)	5.89 (8)	4.64 (9)	1.25 (16)	1.23 (15)	1.95 (16)

TABLE 6.2 (continued)

The Model Atmosphere (Dalgarno, McElroy and Stewart, 1969)

z	n_{N_2} $\frac{particles}{cm^3}$	n_{O_2} $\frac{particles}{cm^3}$	n_O $\frac{particles}{cm^3}$	η_{N_2} $\frac{particles}{cm^2}$	η_{O_2} $\frac{particles}{cm^2}$	η_O $\frac{particles}{cm^2}$
200	3.41 (9)	3.62 (8)	3.62 (9)	8.21 (15)	7.61 (14)	1.53 (16)
225	1.20 (9)	1.10 (8)	1.99 (9)	2.93 (15)	2.34 (14)	8.54 (15)
250	4.29 (8)	3.39 (7)	1.10 (9)	1.06 (15)	7.32 (13)	4.79 (15)
300	5.66 (7)	3.36 (6)	3.47 (8)	1.42 (14)	7.36 (12)	1.53 (15)

Where the number in paranthesis is the power of ten, $T_{120km} = 350\ °K$ $T_\infty = 750\ °K.$

TABLE 6.3

Auroral Oval Emission Rate Factors

Wavelength (Å)	Band or Feature	Emission Rate Factor $\frac{\text{photons}}{\text{sec molecule}}$
1200	NI	5.69×10^{-11}
1298	(5,0) LBH	1.53×10^{-10}
1325	(4,0) LBH	2.96×10^{-10}
1353	(3,0) LBH	3.06×10^{-10}
1383	(2,0) (5,2) LBH	2.86×10^{-10}
1464	(1,1) LBH	1.67×10^{-10}
1493	(3,3) LBH, NI	1.14×10^{-10}
LBH TOTAL		5.77×10^{-9}

The emission rate factors are true for only this particular auroral oval observation, since the primary auroral flux will, in general, be different for another aurora. The shape of the secondary electron flux spectrum will be approximately the same although its magnitude depends on the intensity of the primary flux.

The computations use only the low energy, or secondary electron flux (less than 100 eV), since the emission cross-sections were measured in the secondary electron region. The calculations are expected to be a good approximation to the LBH production rate and hence, emission rate, since most of the excitation is produced by secondary electrons. However, the emission rate factors for the nitrogen lines probably underestimates the actual emission rate by a factor of 2 or 3, since a substantial part of the emission is caused by dissociative excitation ionization of N_2 by the high energy primary electrons. Cross-sections are not available for this energy region.

CHAPTER VII

SUMMARY

7.1 The Electron Beam Excitation Chamber.

An electron beam excitation chamber has been designed
and constructed for measuring emission cross-sections of gases by
electron impact for both electric dipole and magnetic dipole transi-
tions. The radiation detection system consisted of a McPherson
218 monochromator and 541 G-08-18 photomultiplier. This system
is capable of measuring radiation in the vacuum ultraviolet and
other spectral regions with a change of the grating and the photo-
multiplier. The instrument was calibrated absolutely for radiation
in the region, 1200 Å to 2000 Å, by measuring the quantum effi-
ciency times gain of the photomultiplier at 1216 Å with an NO ion-
ization cell, and relative to 1216 Å at other wavelengths by a so-
dium salicylate comparison. The monochromator was calibrated
with a double monochromator arrangement. The steady-state elec-
tron beam excitation spectrum of N_2 in the vacuum ultraviolet has
been studied for monoenergetic electrons from 10 eV to 208 eV. The
LBH transition of N_2, and several dissociative transitions, were
excited. The geometrical problem of determining the fraction of the
LBH spontaneous radiation detected was solved. The problem stems

from the forbidden nature of the LBH transition (a magnetic dipole transition). Thus, an N_2 molecule, excited to the $a^1\Pi_g$ state by electron impact, can travel several centimeters before radiating. The profile of the LBH radiation as a function of distance from the electron beam in a molecular flow regime is a glow of cylindrical symmetry, most intense at the beam. This phenomenon of molecular flow of an excited LBH molecule dictated that the excitation chamber had to be large so as to preclude wall effects. The dissociatively excited transitions of atomic nitrogen studied were permitted electric dipole transitions and did not have a molecular flow problem, but could be studied with this design.

7.2   The Observations.

The emission cross-section of the $a^1\Pi_g$ electronic state of molecular nitrogen was determined from 10 eV to 208 eV for mono-energetic electrons. The primary measured data was the emission cross-section of each of the vibrational bands of the LBH band system (approximately 65). The emission cross-section of each vibrational transition was summed to give the emission cross-section for each vibrational level and for the total electronic transition. The maximum cascade contribution to the apparent cross-section is 29%. The actual cascade contribution is probably much less since the measured fraction of the total cross-section contributed by each vibrational level agrees with the fraction calculated by assuming

direct electron excitation of the $a^1\Pi_g$ state. The peak measured cross-section is at 15.5 eV $\pm$ 1.5 eV and has a value of 3.85×10^{-17} cm^2 for the total electronic transition. Each of the bands has the same relative cross-section shape with energy.

The emission cross-section of the multiplets of atomic nitrogen at 1200 Å, 1493 Å and 1743 Å, by dissociative excitation of N_2, was measured. These cross-sections typically had two thresholds, one at about 20 eV due to dissociative excitation of N_2, and the other at about 35 eV due to dissociative ionization excitation of N_2. The 1493 Å multiplet and the 1743 Å multiplet originated from the same electronic level. Their measured cross-sections were in the ratio as predicted by a branching ratio calculation. The peak cross-section for the dissociative excitation transitions is at about 110 eV, with dissociative ionization excitation being the more important process for electron energies greater than 50 eV. The emission cross-section of the $\lambda = 1200$ Å multiplet was the emission cross-section for the ^4P state of atomic nitrogen due to dissociative excitation of molecular nitrogen. The emission cross-section of the $\lambda = 1743$ Å multiplet and the 1493 Å multiplet were summed to give the emission cross-section of the ^2P state of atomic nitrogen due to dissociative excitation of molecular nitrogen.

7.3   Atmospheric Calculations.

The measured emission cross-sections of N_2 were applied to the photoelectron excited dayglow and the auroral oval. The emission rate factor was calculated for the LBH band system and the nitrogen lines in the dayglow as a function of slant abundance. The emission rate factor was calculated for the auroral oval at 150 km altitude.

BIBLIOGRAPHY

Barth, C. A., "Spectrum of the Ultraviolet Aurora." Ann. Geophys., 24, 1, 1968.

Barth, C. A., Private Communication, 1969.

Benesch, W., T. Vanderslice, S. G. Tilford, and P. G. Wilkinson, "Franck-Condon Factors for Observed Transitions in N_2 above 6 eV." Ap. J., 143, 236, 1966.

Birge, R. T. and J. J. Hopfield, "The Ultraviolet Band Spectrum of Nitrogen." Ap. J., 68, 257, 1928.

Chamberlain, J. W., "Physics of the Aurora and Airglow." Academic Press, New York, New York, chap. I, 1961.

Ching, B. K., G. R. Cook, and R. A. Becker, "Oscillator Strengths of the a, w, and c Bands of N_2." J. Quant. Spectrosc. Radiat. Transfer, 1, 323, 1967.

Dalgarno, A., M. B. McElroy and A. I. Stewart, "Electron Impact Excitation of the Dayglow." J. Atmos Sciences, 26, 753, 1969.

Englehardt, A. G., A. V. Phelps, and C. G. Risk, "Atomic Collision Processes Occurring in Atmospheric Gases." Phys. Rev., 135, A 1566, 1964.

Englander-Golden, P. and D. Rapp, "Total Cross-Sections for Ionization of Atoms and Molecules by Electron Impact." Lockheed Missiles and Space Company, Palo Alto, California, Report No. LMSC-6-74-64-72, 1964.

Fastie, W. G., "Ultraviolet Measurements in Planetary Atmospheres." Applied Optics, 6, 397, 1967.

Fraser, P. A., "A Method of Determining the Electronic Transition Moment for Diatomic Molecules." Can. J. Phys., 32, 575, 1954.

Green, A. E. S. and C. A. Barth, "Calculations of Ultraviolet Molecular Nitrogen Emissions from the Aurora." J. Geophys. Res., 70, 1083, 1965.

Green, A. E. S. and C. A. Barth, "Calculation of the Photoelectron Excitation of the Dayglow." J. Geophys. Res., 72, 3975, 1967.

Harris, L. and J. K. Beasley, "Infrared Properties of Gold Smoke Deposits." J. Opt. Soc. Am., 42, 134, 1952.

Herman, R. and L. Herman, "Extension du Systeme de Bandes de Lyman-Birge-Hopfield de la Molecule d'Azote." Ann. d'Astrophys., 5, 71, 1942.

Herzberg, G., "On the Electronic Structure of the Nitrogen Molecule." Phys. Rev., 69, 362, 1946.

Herzberg, G., "Spectra of Diatomic Molecules." D. Van Nostrand Company, Inc., Princeton, New Jersey, chap. V, p. 552, 1950.

Hinteregger, H. E., L. H. Hall, and G. Schmidtke, "Solar XUV Radiation and Neutral Particle Distribution in the Thermosphere." Space Science V, North Holland Publishing Co., Amsterdam, p. 1175, 1964.

Hoffman, R., "Low Energy Electron Precipitation at High Latitudes." J. Geophys. Res., 74, 2425, 1969.

Holland, R. F., "Excitation of Nitrogen by Electrons: The Lyman-Birge-Hopfield System of N_2." Los Alamos Scientific Laboratory, Los Alamos, New Mexico, Report No. 9468, 1969.

Kieffer, L. J. and R. J. Van Brunt, "Energetic Ions from N_2 Produced by Electron Impact." J. Chem. Phys., 46, 2728, 1967.

Knapp, R. A. and A. M. Smith, "Fatigue Effects in the Luminescent Yield of Sodium Salicylate." Applied Optics, 3, 637, 1964.

Lassettre, E. N. and M. E. Krasnow, "Collision Cross-Section Study of Two Transitions in Nitrogen." J. Chem. Phys., 40, 1248, 1964.

Lassettre, E. N., A. Skerbele, and V. D. Meyer, "Quadrupole Allowed Transitions in the Electron Impact Spectrum of N_2." J. Chem. Phys., 45, 214, 1966.

Lassettre, E. N., A. Skerbele, M. A. Dillion, and K. J. Ross, "High Resolution Study of Electron Impact Phenomena at Kinetic Energies Between 33 and 100 eV and Scattering Angles to 16." J. Chem. Phys., 48, 5066, 1968.

Lichten, W., "Lifetime Measurements of Metastable States in Molecular Nitrogen." J. Chem. Phys., 26, 306, 1957.

Loftus, A., "Nitrogen Emission Band Spectra." Can. J. Phys., 34, 780, 1956.

Lyman, T., "Spectroscopy of the Extreme Ultraviolet." Ap. J., 38 98, 1911.

Massey, H. S. W. and E. H. S. Burhop, "Electronic and Ionic Impact Phenomena." Oxford at the Clarendon Press, London, England, chap. IV, 1952.

McDaniel, E. W., "Collision Phenomena in Ionized Gases." John Wiley and Sons, New York, New York, p. 668, 1964.

McEwen, D. J., "Intensity Measurements of the Lyman-Birge-Hopfield System of Nitrogen." Thesis: University of Western Ontario, London, Ontario, Canada, 1965.

Miller, R. E., W. G. Fastie, and R. C. Isler, "Rocket Studies of Far-Ultraviolet Radiation in an Aurora." J. Geophys. Res., 73, 3353, 1968.

Moisewitsch, B. L. and S. J. Smith, "Electron Impact Excitation of Atoms." Rev. Mod. Phys., 40, 1968.

Mulliken, R. S., "The Energy Levels of the Nitrogen Molecule." The Threshold of Space, edited by M. Zelikoff, Pergamon Press, New York, New York, p. 169, 1957.

Nicholls, R. W., "Laboratory Astrophysics." J. Quant. Spectrosc. Radiat. Transfer, 2, 433, 1962.

Nicholls, R. W., "Transition Probabilities of Aeronomically Important Spectra." Symposium d'Aeronomie, presented at International Union of Geodesy and Geophysics, Berkeley, California, p. 99, 1963.

Olmstead, J., A. S. Newton and K. Street, "Determination of the Excitation Functions for Formation of Metastable States of Some Rare Gases and Diatomic Molecules by Electron Impact." J. Chem. Phys., 42, 2321, 1965.

Pierce, J. R., "Theory and Design of Electron Guns." D. Van Nostrand Company, Inc., Princeton, New Jersey, chap. 9, 1954.

Rees, M. H., "Effects of Low Energy Electron Precipitation on the Upper Atmosphere." To be published in Production and Maintenance of the Polar Ionosphere, G. Scovli, Editor, 1969.

Rozsnyai, G. F., "Theory of Electron Collisions with Homonuclear Diatomic Molecules." J. Chem. Phys., 47, 4102, 1967.

Samson, J. A. R., "Techniques of Vacuum Ultraviolet Spectroscopy." John Wiley and Sons, New York, New York, chap. 7, 8, 1967.

Stolarski, R. S., V. A. Dulock, C. E. Watson, and A. E. S. Green, "Electron Impact Cross-Sections for Atmospheric Species-- Molecular Nitrogen." J. Geophys. Res., 72, 3953, 1967.

Tate, J. T. and P. T. Smith, "The Efficiencies of Ionization and Ionization Potentials of Various Gases Under Electron Impact." Phys. Rev., 39, 270, 1932.

Van Brunt, R. J. and R. N. Zare, "Fluorescence Excited by Molecular Dissociation." J. Chem. Phys., 48, 4304, 1968.

Wallace, L., "A Collection of the Band Head Wavelengths of N_2 and N_2^+." Ap. J., Supplement 62, Volume VI, 445, 1962.

Watanabe, K., F. F. Marmo, E. C. Y. Inn, "Photoionization Cross-Section of Nitric Oxide." Phys. Rev., 91, 1156, 1953.

Westerlund, L. H., "The Auroral Electron Energy Spectrum Extended to 45 eV." Report: Rice University, 1968.

Wiese, W. L., M. W. Smith, and B. M. Glennon, "Atomic Transition Probabilities-- Hydrogen through Helium." National Bureau of Standards, Washington, D. C., Volume I, p. 50, 1966.

Wilkinson, P. G. and R. S. Mulliken, "An Electric Quadrupole Electronic Band System in Molecular Nitrogen." Ap. J., 126, 10, 1957.

Zare, R. N., "Molecular Level Crossing Spectroscopy." J. Chem. Phys., 45, 4510, 1966.

Zare, R. N., E. O. Larsson, and R. A. Berg, "Franck-Condon Factors for Electronic Band Systems of Molecular Nitrogen." J. Molec. Spectrosc., 15, 117, 1965.

APPENDIX A

A Description of the Electron Beam Excitation Chamber.

The excitation chamber is 10 3/8 inches long and 8 inches in outside diameter. The walls were 1/4 inch thick. The end flanges for the chamber were Varian 954-5064 stainless steel blank conflat flanges, 10 inches in diameter and 0.96 inches thick. The flanges were drilled on center for a 1 1/4 inch hole. A specially designed electrical feed-through was welded to the flange in the hole. On the feed-through were eight nickel pins to provide electrical continuity between the electron gun and collector and the appropriate outside electronics. The feed-through was ceramic (aluminum oxide) to which kovar expansion sleeves were inserted around the nickel pins and around the outside diammeter of the feed-through. All seals for the feed-through were made by a copper braze.

The chamber and vacuum system was specially constructed by Granville Phillips Company of Boulder, Colorado, for this experiment. The various ports on the chamber were as follows:

(1)   Gas Inlet: The gas inlet port was connected to the chamber by a 1/4 inch outside diameter and 1/8 inch inside diameter stainless steel tubing, which was

welded to the chamber. A 2 inch baffle was placed at the inlet port to provide a well diffused flow of nitrogen into the chamber. Matheson pre-purified nitrogen was used as the gas source. Between the gas and the chamber was a Granville Phillips automatic pressure controlling leak valve, used to control the pressure in the chamber.

(2)   Spectrometer port: The spectrometer port was placed on the chamber so as to view the center of the interaction region of the chamber. The port was a 2 inch outside diameter pipe of 0.65 inches wall thickness welded to the chamber. It was 2 1/2 inches long and had a 4 1/2 inch conflat rotatable flang set in it. Various size nipples were made to bolt onto this flange to control the distance from the spectrometer entrance slit to the chamber. A special two-faced flange provided adaptation between the Granville Phillips flange and the McPherson flange. The distance between the center of the excitation chamber and the entrance slit on the spectrometer, decided upon for this experiment, was 9 13/16 inches.

(3)   Gas outlet port: The gas outlet port was 2 inches in outside diameter. It let to the pumps, gate valve and pressure measuring gauges.

(4)   High pressure measuring port: This port was

        open only during initial pump-down and led to

        a Wallace-Tiernan gauge, capable of measuring

        pressure from 1 to 20 torr. A C-valve (Granville

        Phillips trademark) was used to seal the gauge

        from the chamber when low pressure (less than 1

        torr) was reached.

(5)   Viewing port: A 2 1/2 inch wide angle quartz

        window was placed on top of the chamber in the

        center of the interaction region so as to "view" the

        beam. This port could be used for photographic pur-

        poses in the visible and infrared. It also provided

        information about the collimation of the beam.

(6)   Auxiliary port: An auxiliary port, sealed by a

        2 1/2 inch conflat flange, was provided as an

        accessory. It could be used for pressure cali-

        bration or to admit a buffer gas.

        On the side of the chamber directly opposite the spectro-

meter port, an aluminum sheet, .020 inch and 5 inches square, was

placed and shaped to the wall. It had a gold black deposit of about

50×10^{-6} gm/cm^2. It was prepared by evaporating gold into the

aluminum plate in a nitrogen atmosphere. It is a very porous

structure of colloidal gold particles about 100 Å in diameter

(Harris and Beasley, 1952). These particles adhere together to form chains and aggregates. This structure was used to absorb the ultraviolet radiation, preventing detection of reflected ultraviolet radiation.

The entire chamber was submitted to a 24-hour, 500 $^{\circ}$C bakeout before operation. Four mounting tapped holes were placed on each 10-inch flange to facilitate mounting of the electron gun and collector.

APPENDIX B

The Emission Cross-Sections of the Vibrational

Transitions of the a $^1\Pi_g$ State of N$_2$

EMISSION CROSS SECTION OF
THE 1226A (8, 0) LBH BAND

ABSOLUTE CROSS SECTION (SQ. CM)

ENERGY (EV)
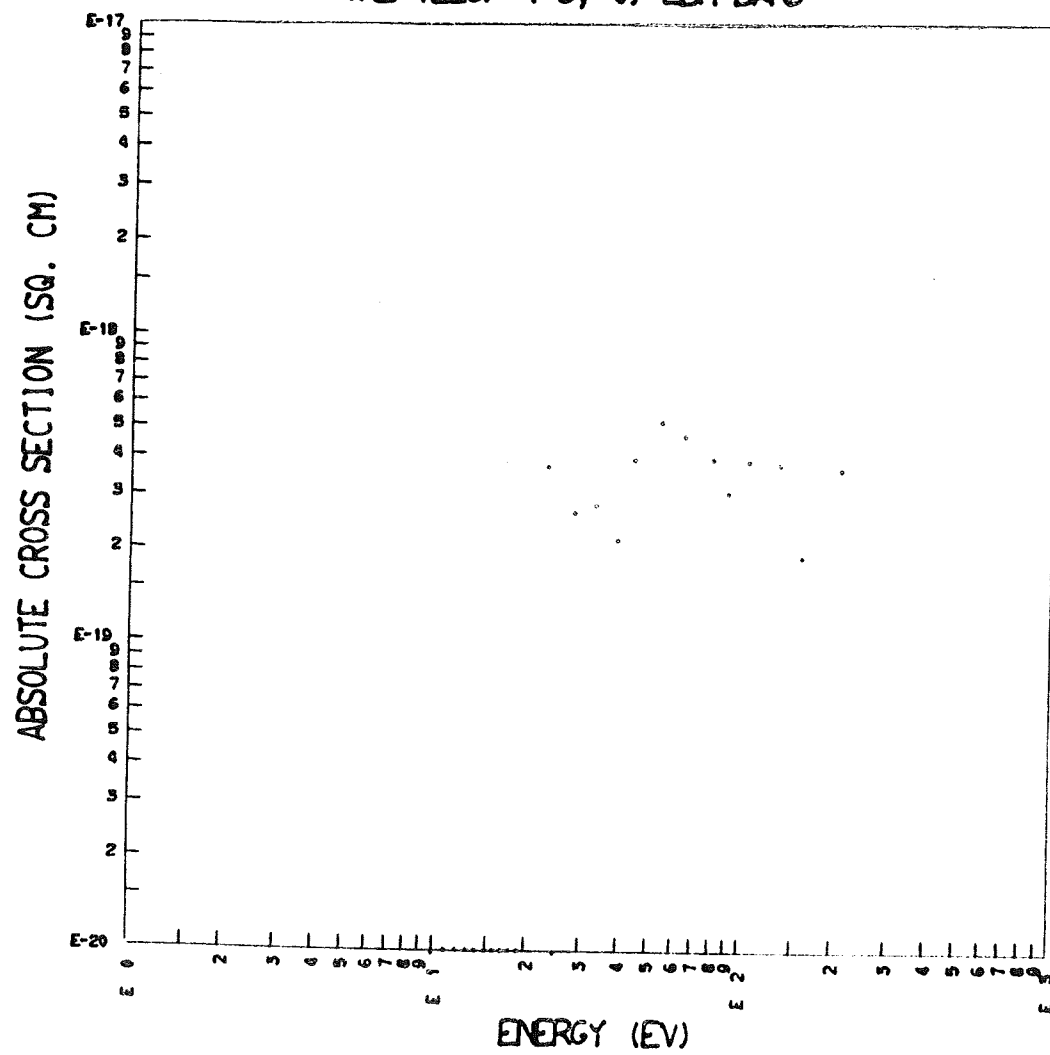
EMISSION CROSS SECTION OF
THE 1262A (8, 1) LBH BAND
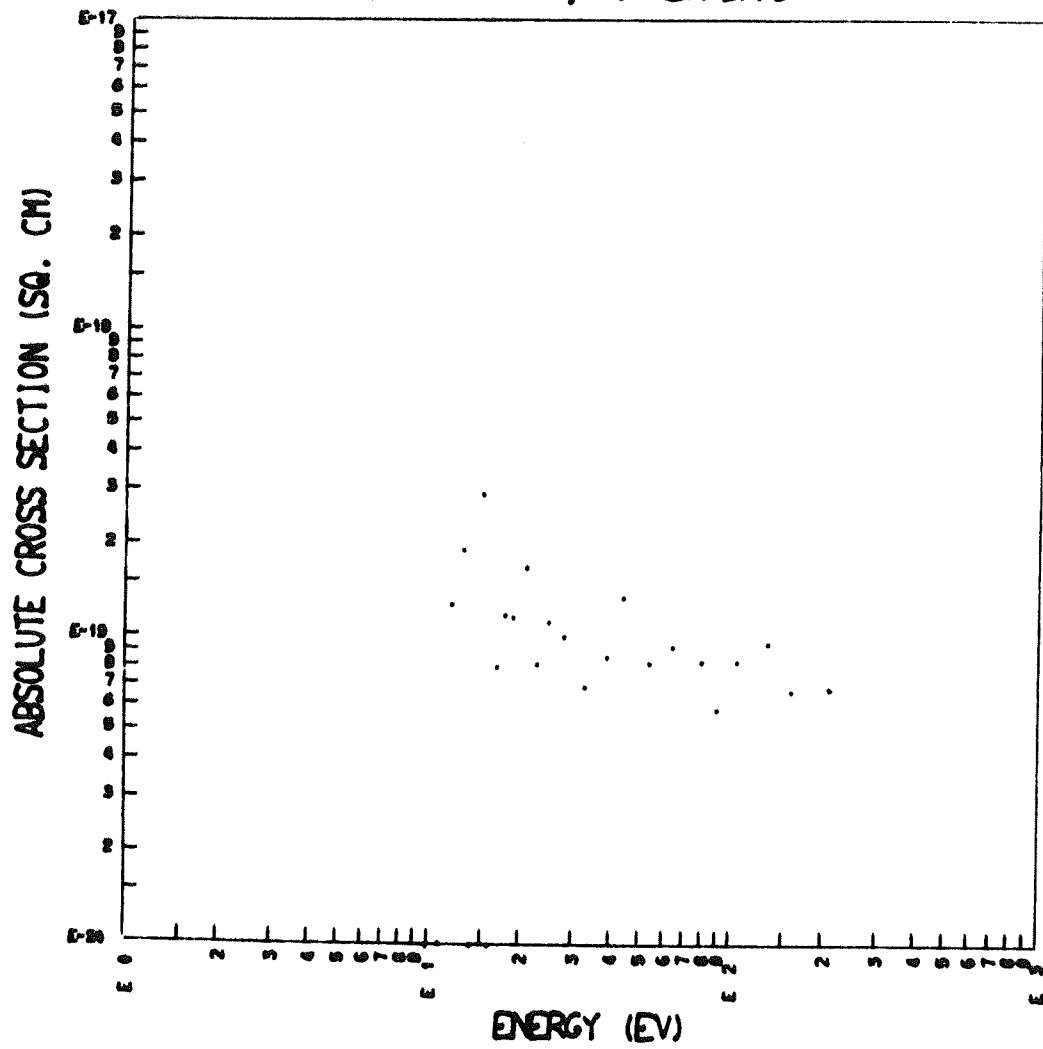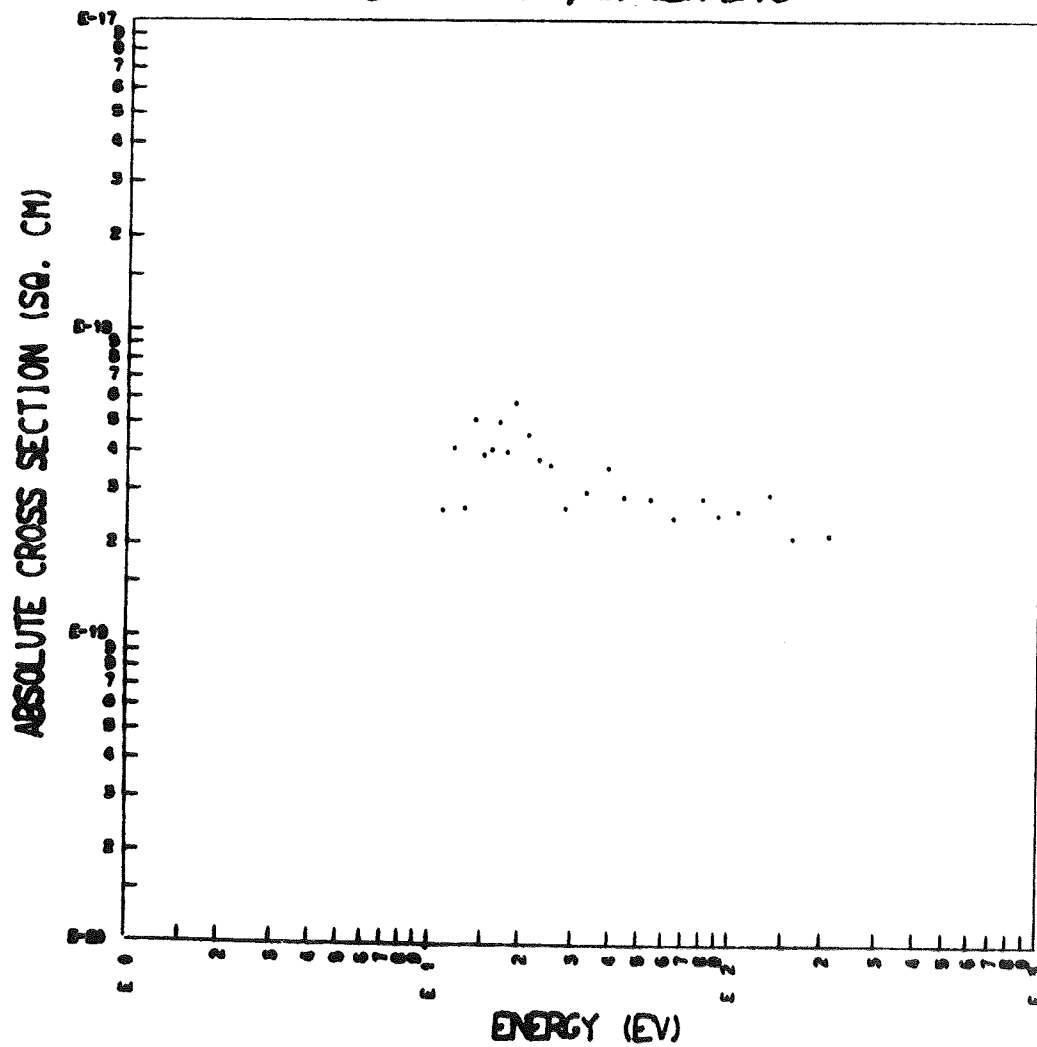

ABSOLUTE CROSS SECTION (SQ. CM)

ENERGY (EV)
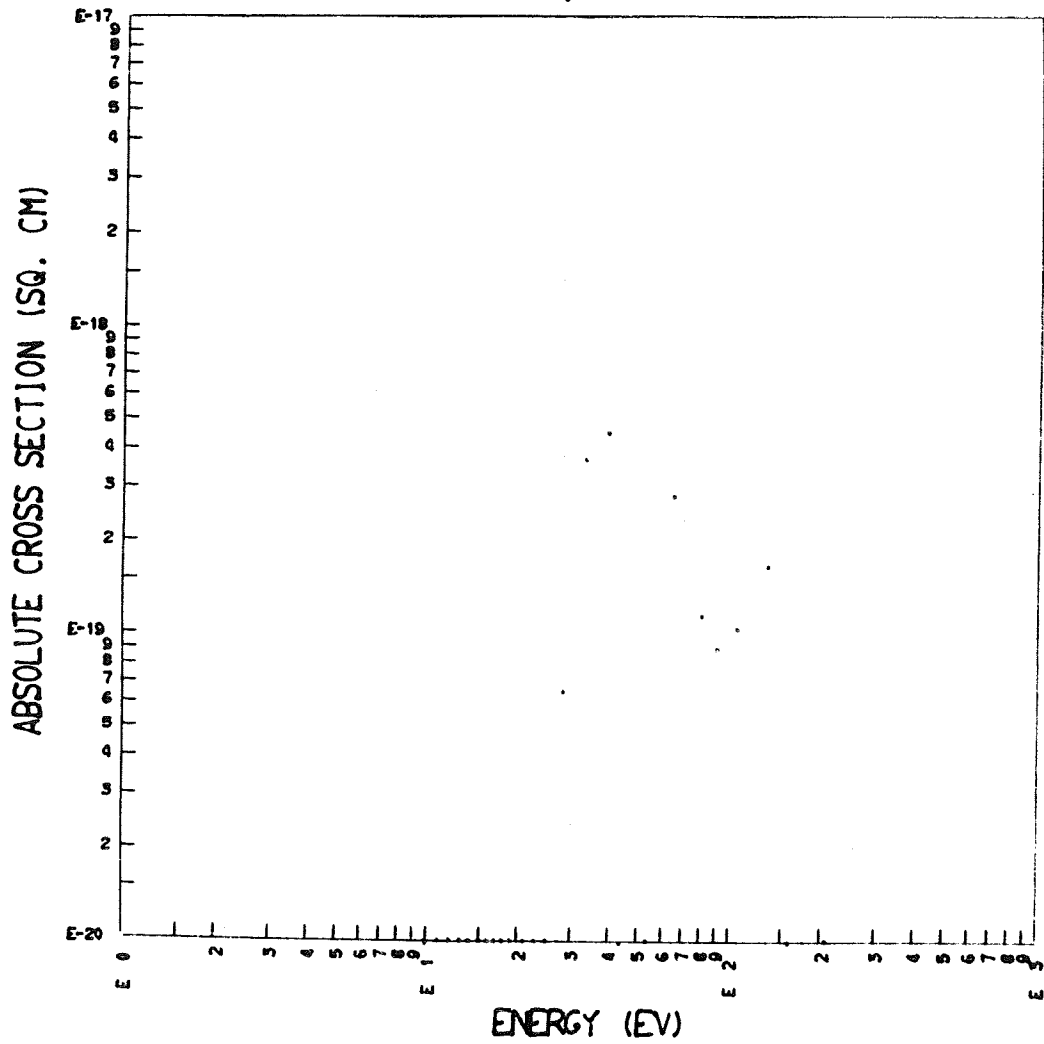
EMISSION CROSS SECTION OF
THE 1273A (6, 0) LBH BAND
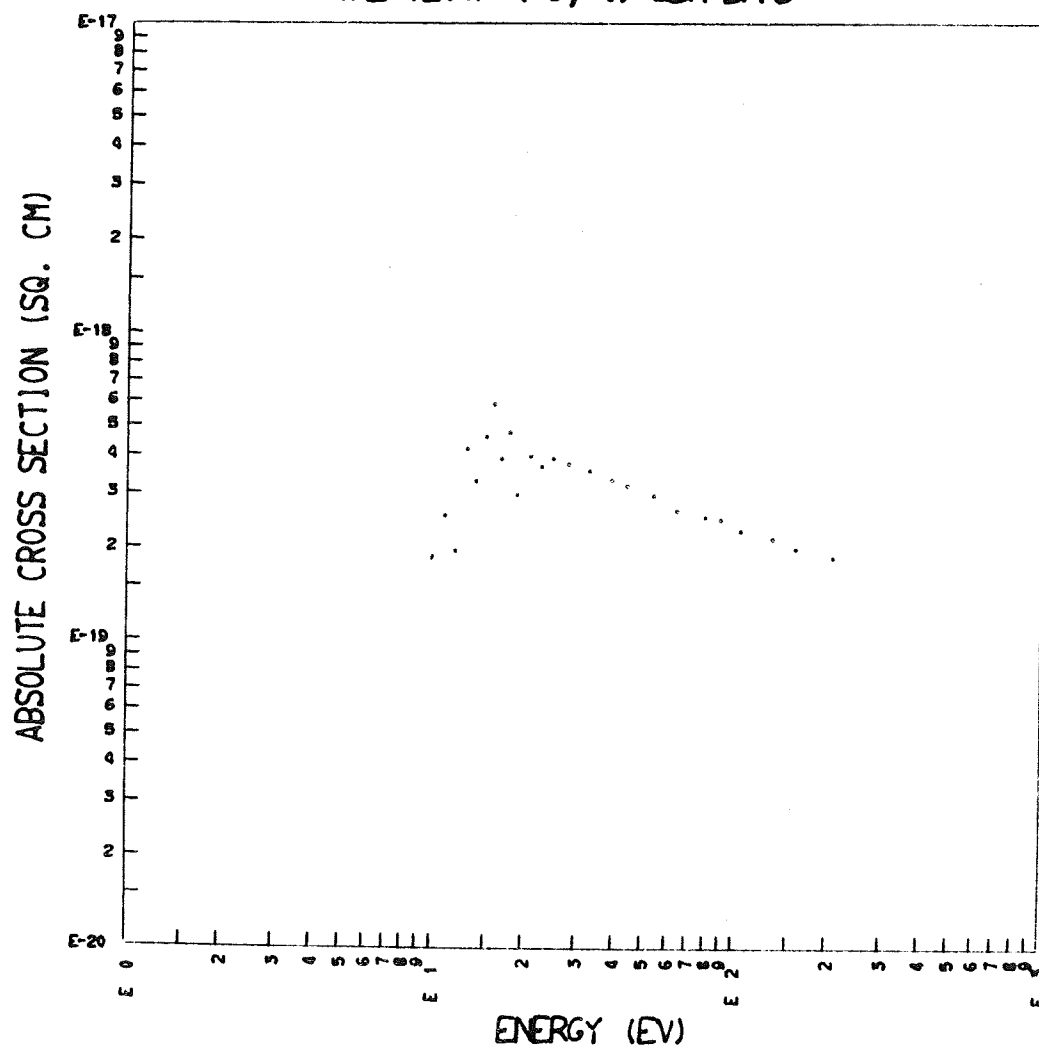
EMISSION CROSS SECTION OF
THE 1298A (5, 0) LBH BAND
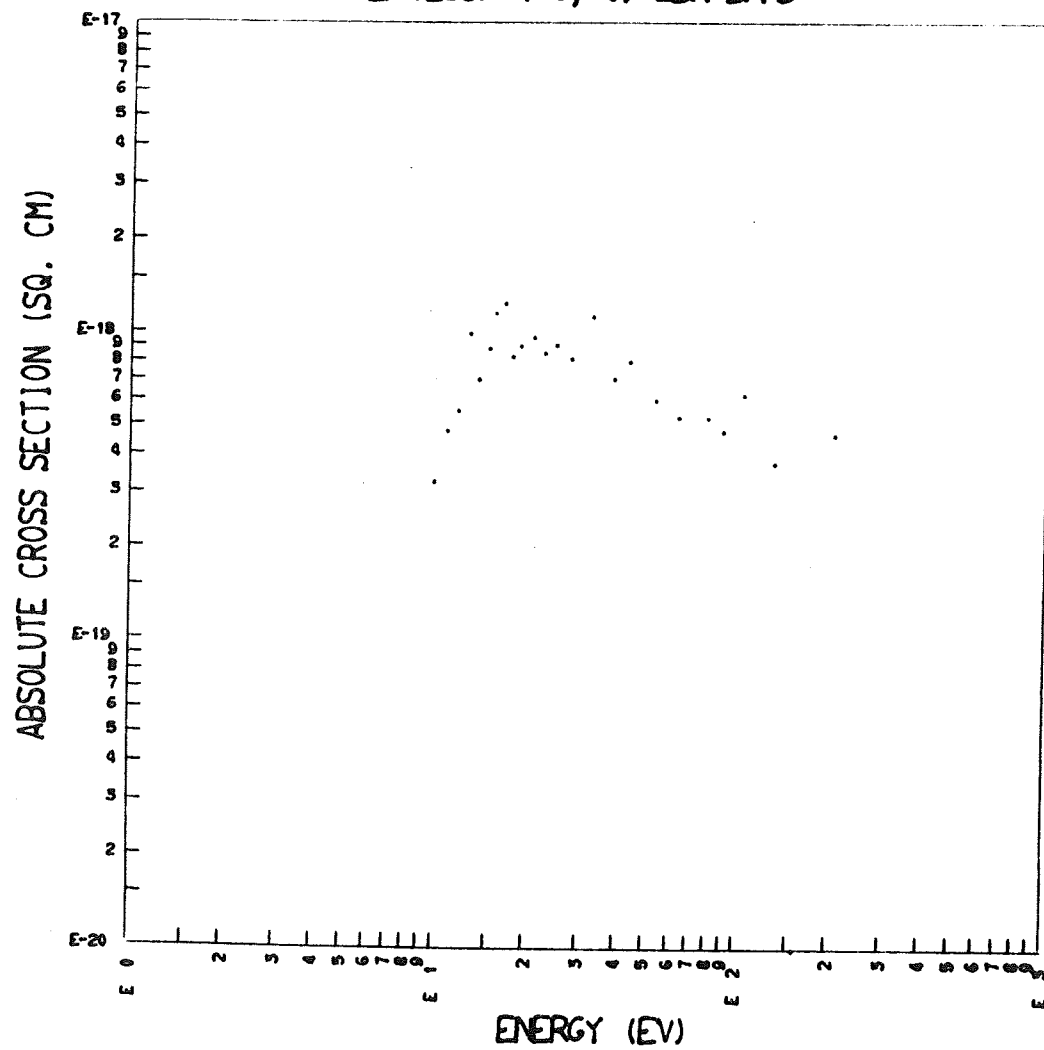
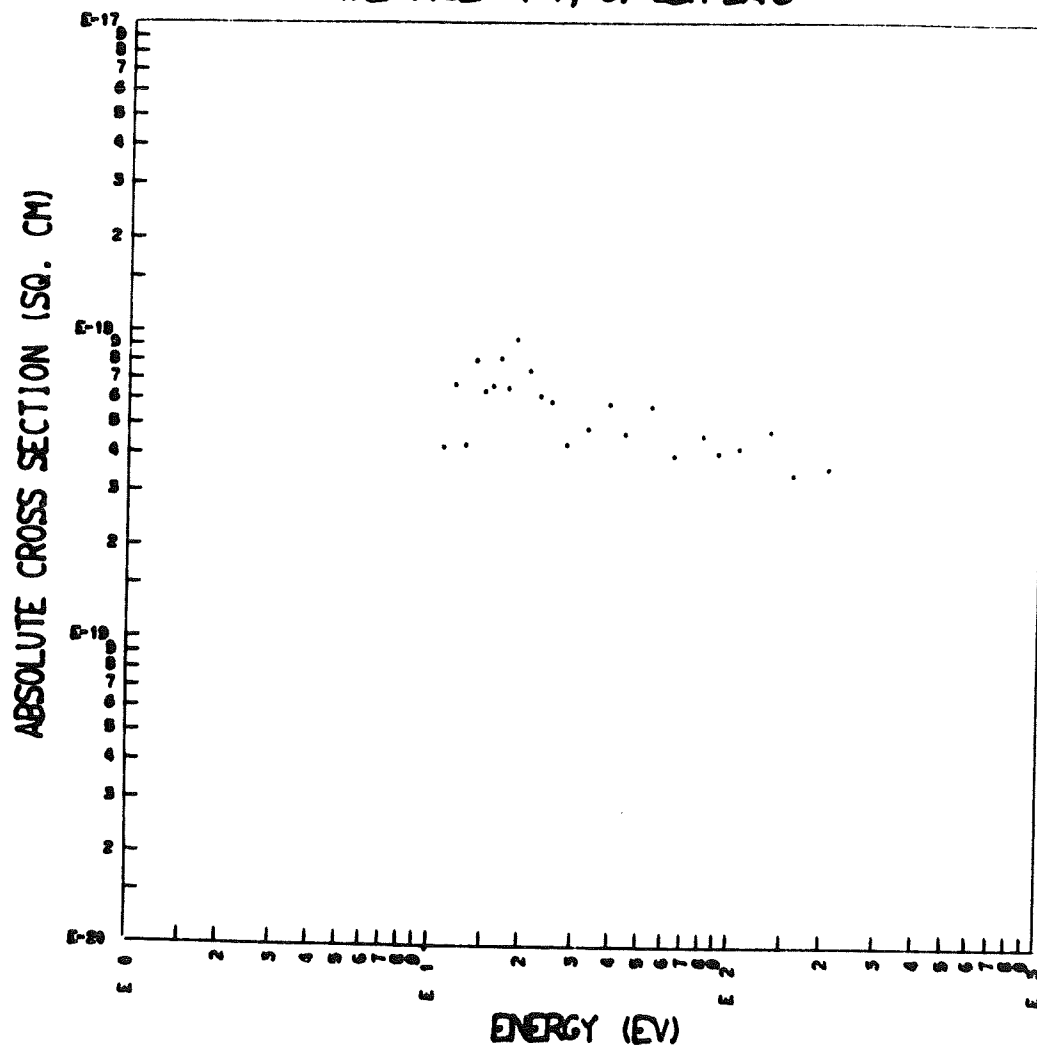# EMISSION CROSS SECTION OF THE 1312A (6, 1) LBH BAND

ABSOLUTE CROSS SECTION (SQ. CM)

ENERGY (EV)

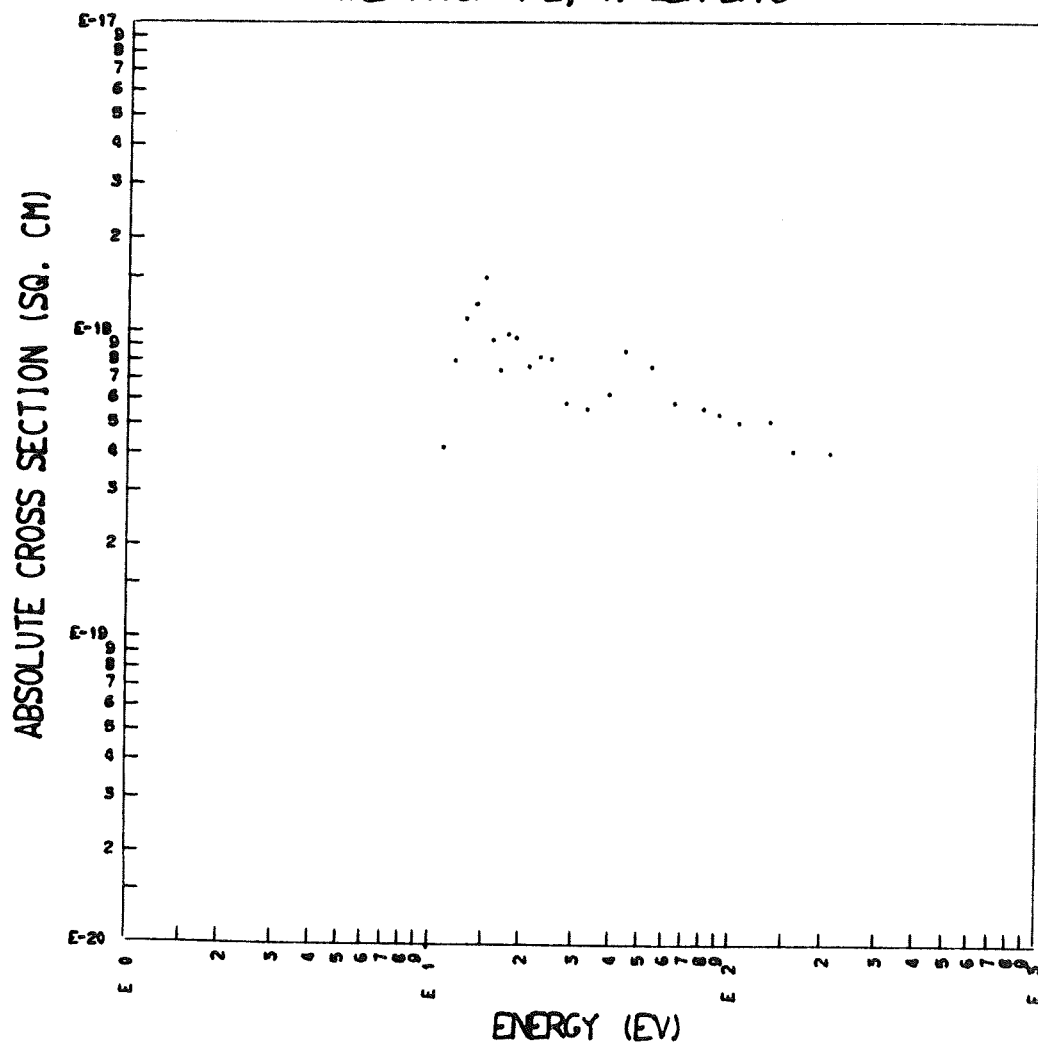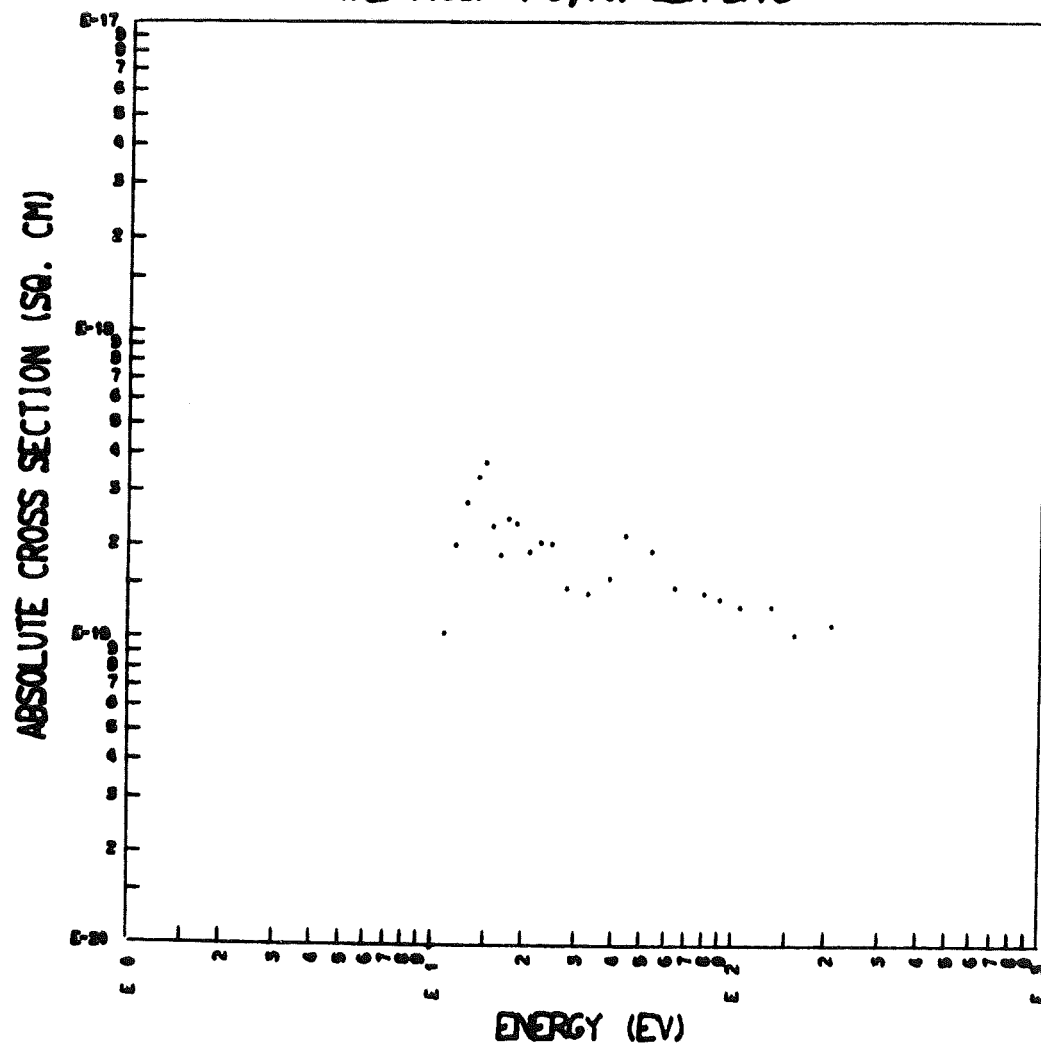# EMISSION CROSS SECTION OF
THE 1325A (4, 0) LBH BAND
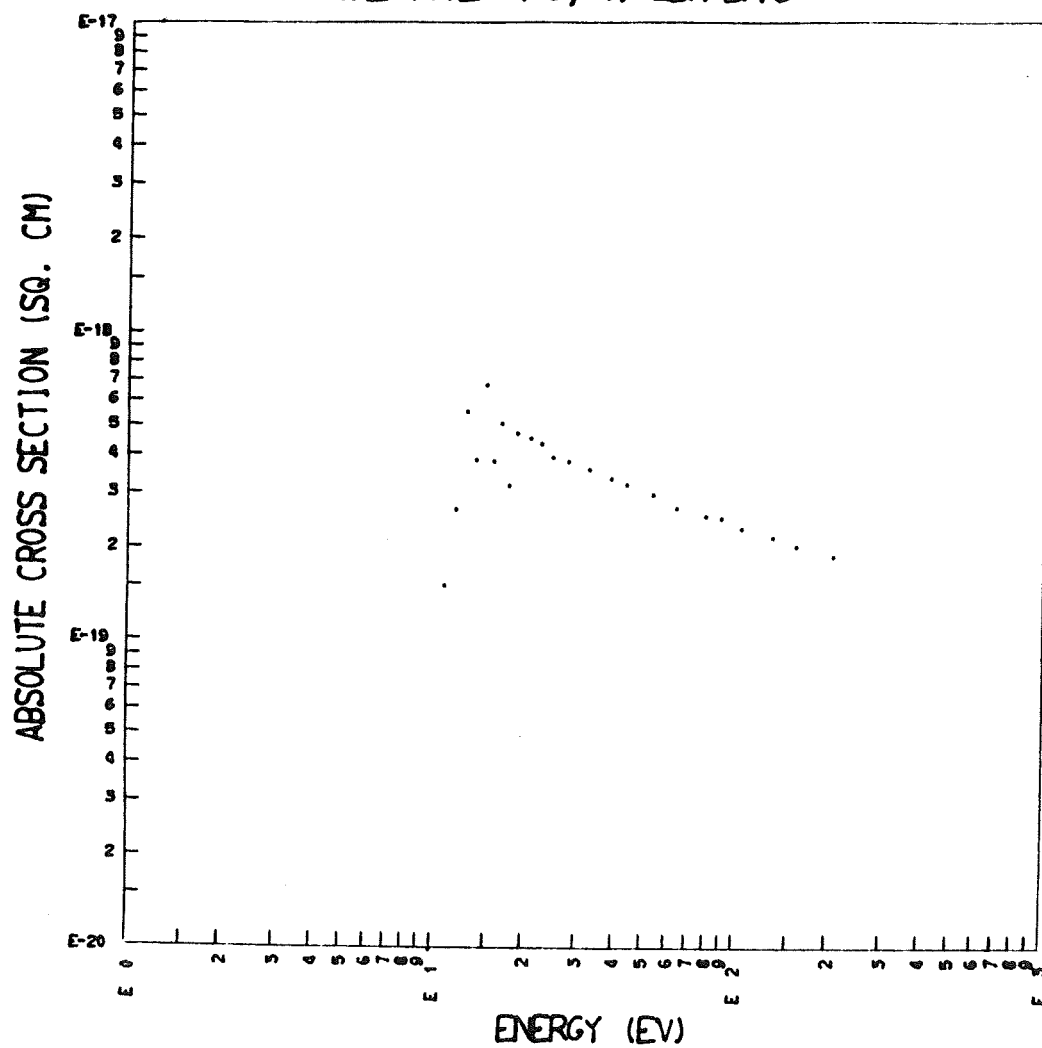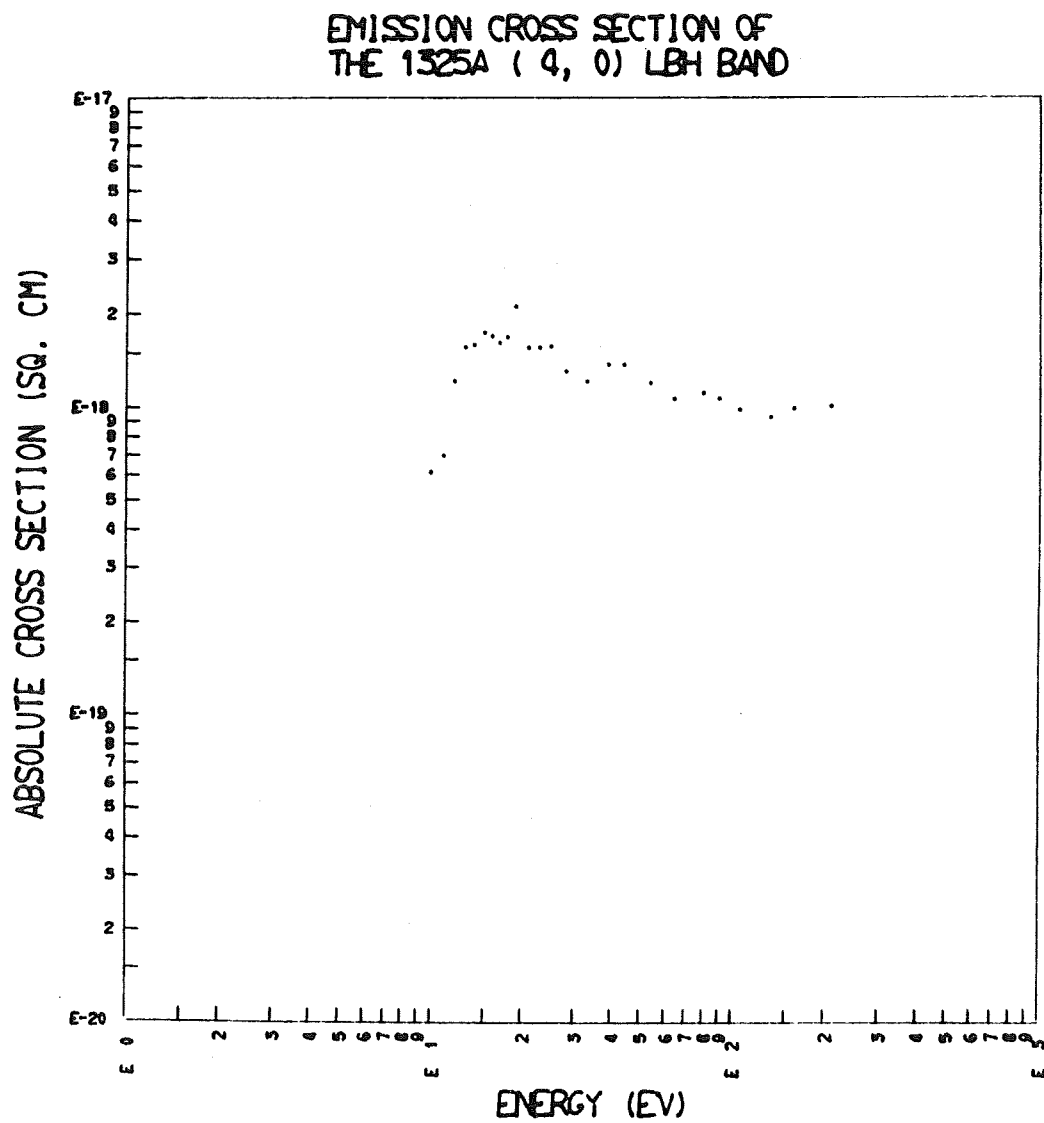
EMISSION CROSS SECTION OF
THE 1359A (5, 1) LBH BAND
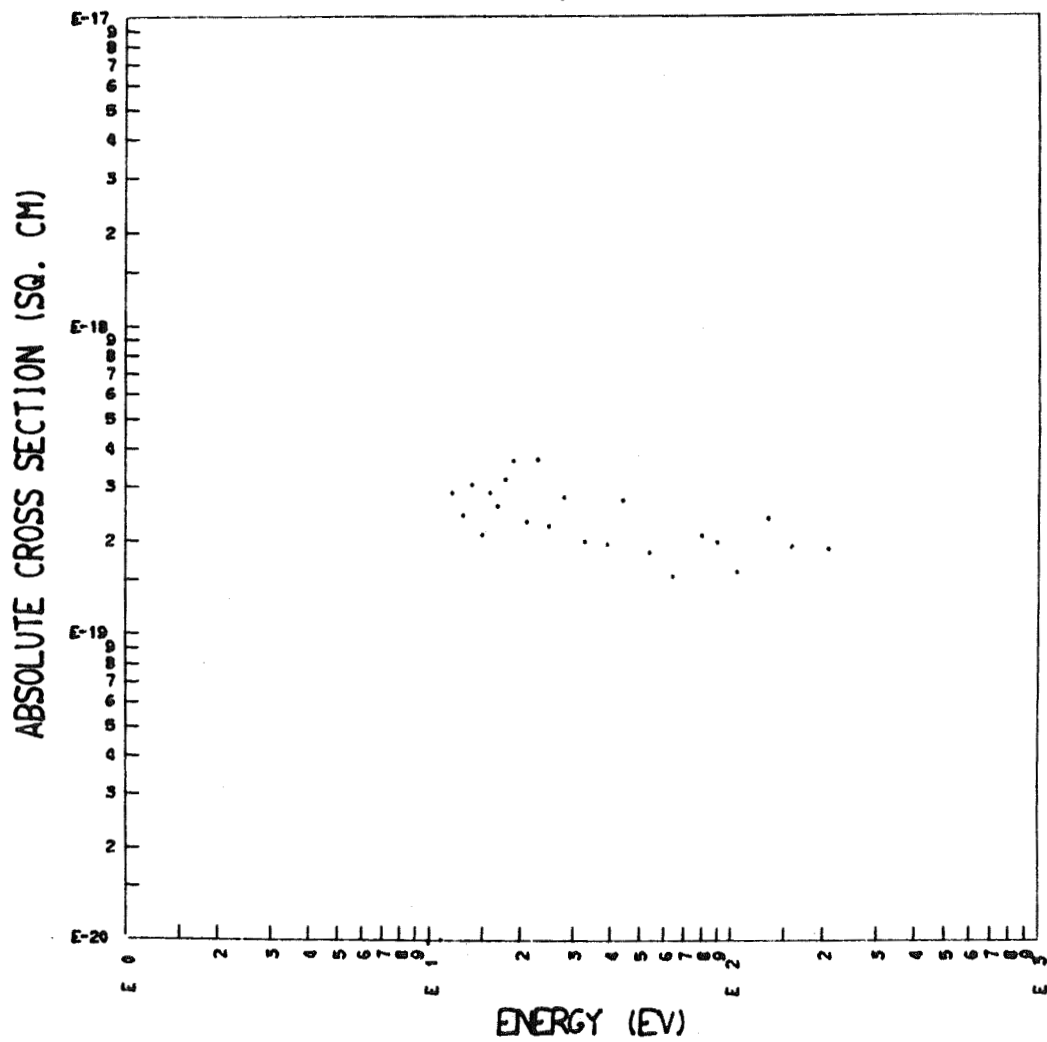
EMISSION CROSS SECTION OF
THE 1354A (3, 0) LBH BAND
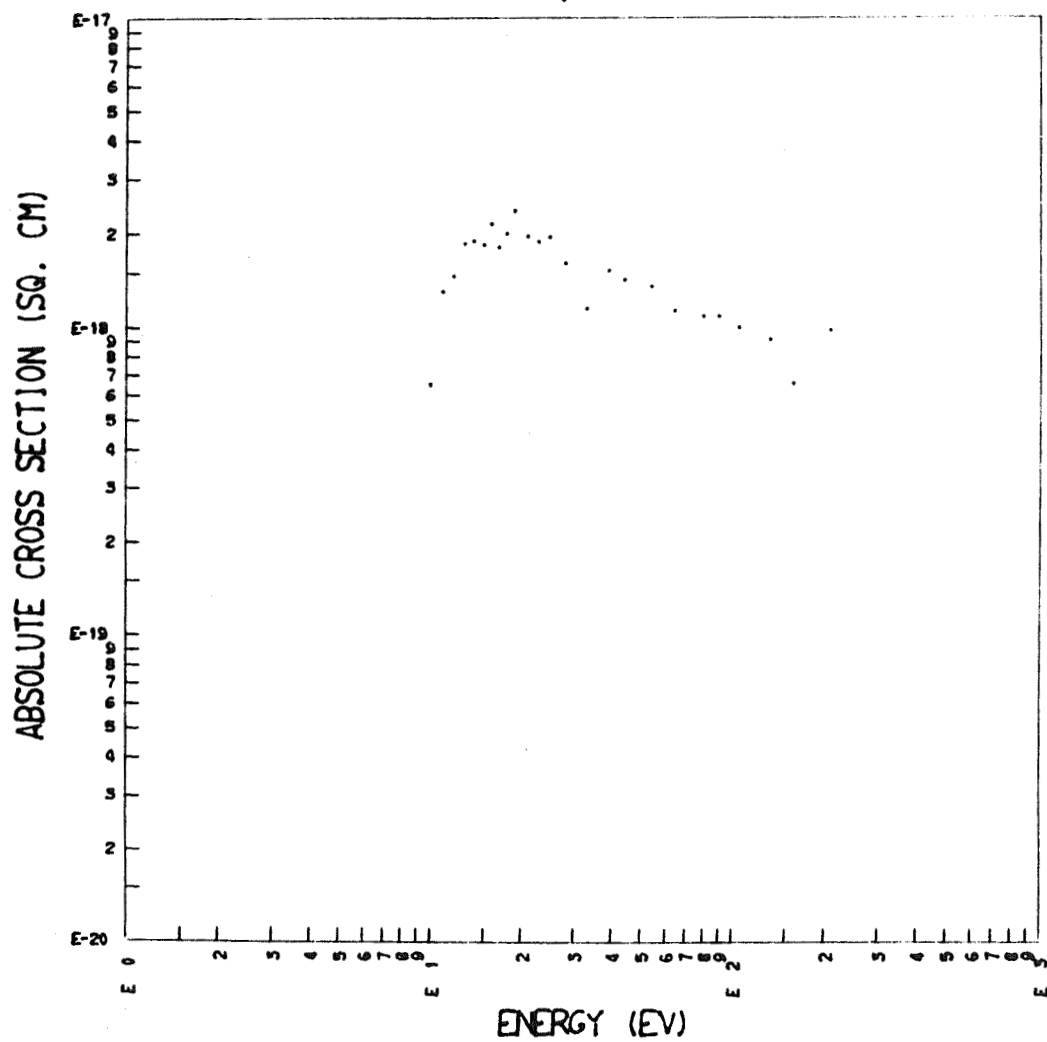
EMISSION CROSS SECTION OF
THE 1381A (5, 2) LBH BAND

ABSOLUTE CROSS SECTION (SQ. CM)
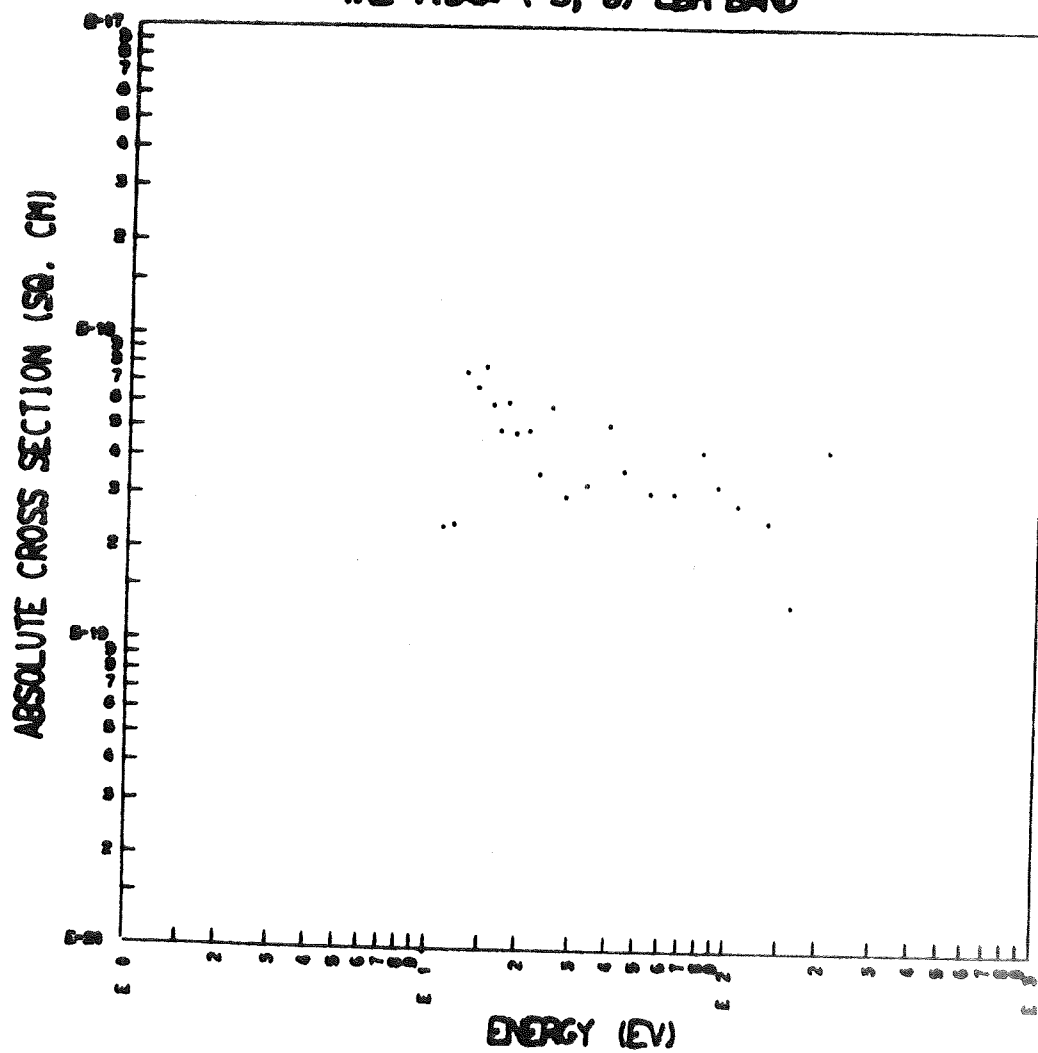
ENERGY (EV)
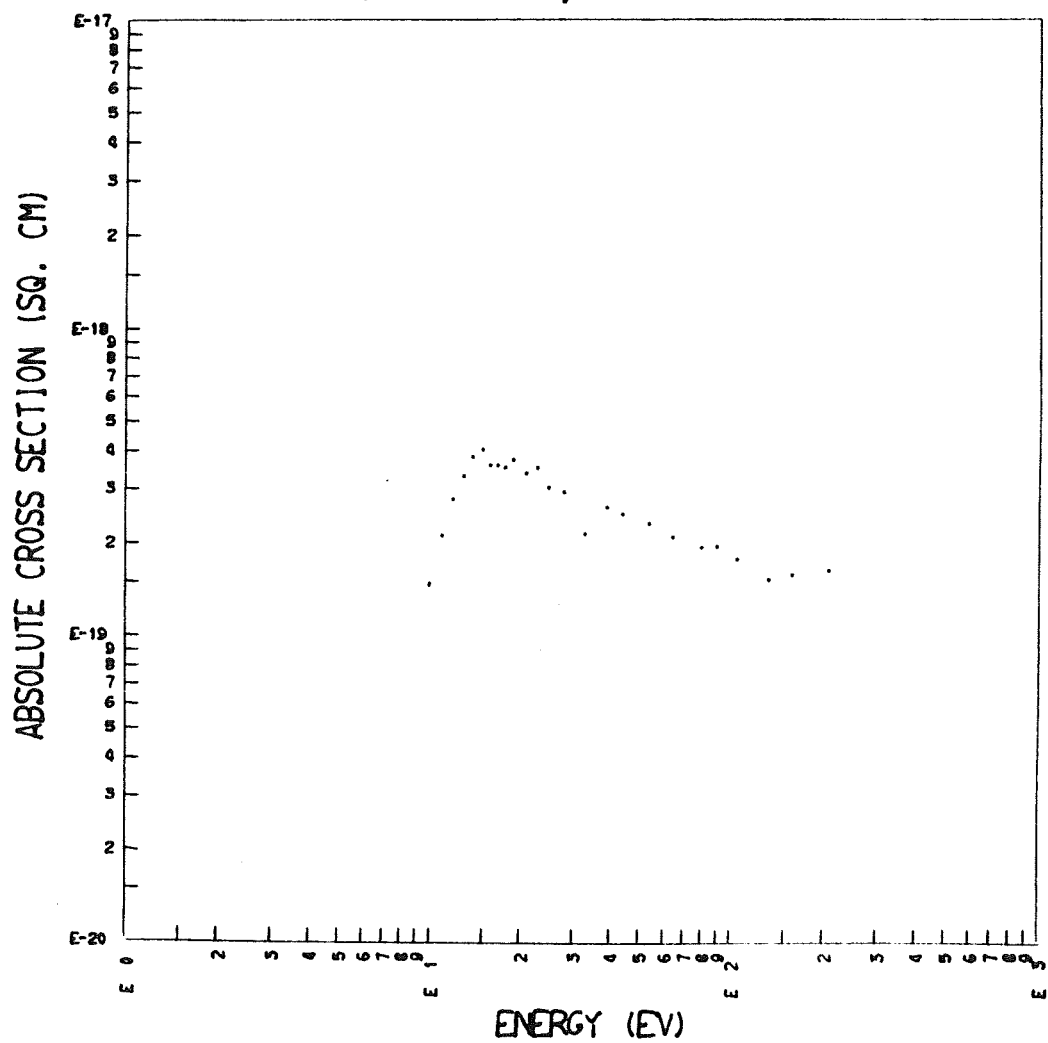
EMISSION CROSS SECTION OF
THE 1383A (2, 0) LBH BAND
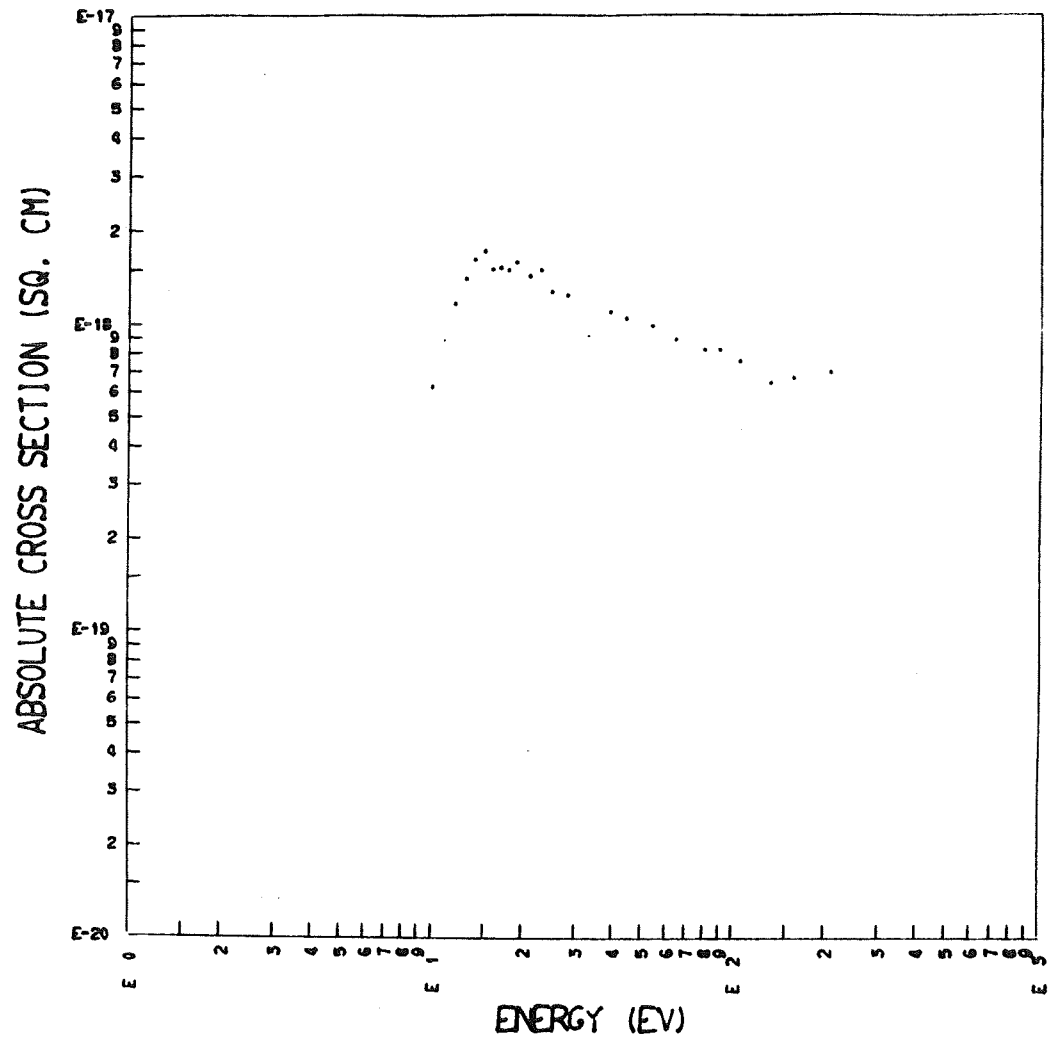
EMISSION CROSS SECTION OF
THE 1395A (6, 3) LBH BAND
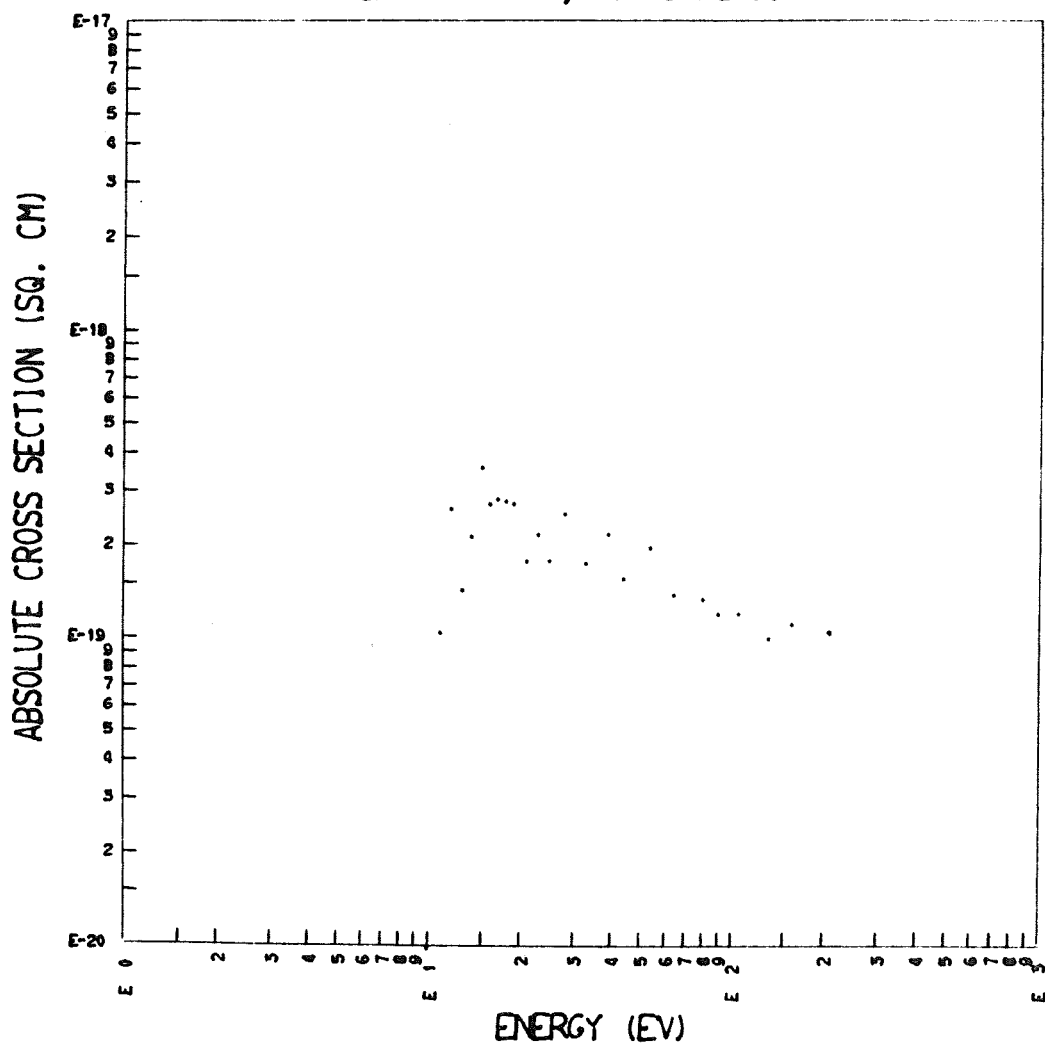
EMISSION CROSS SECTION OF THE 1397A (3, 1) LBH BAND

ABSOLUTE CROSS SECTION (SQ. CM)

ENERGY (EV)
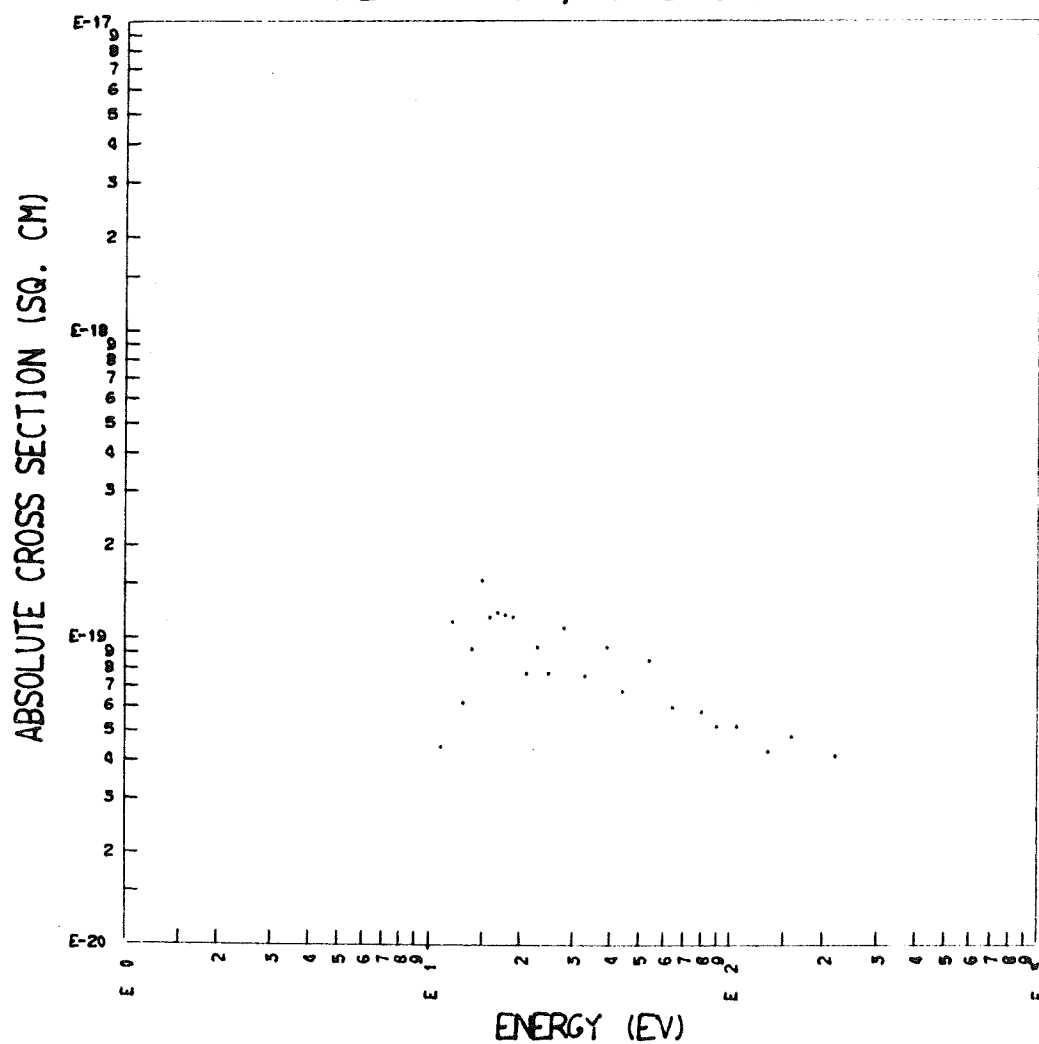
EMISSION CROSS SECTION OF
THE 1411A (4, 2) LBH BAND
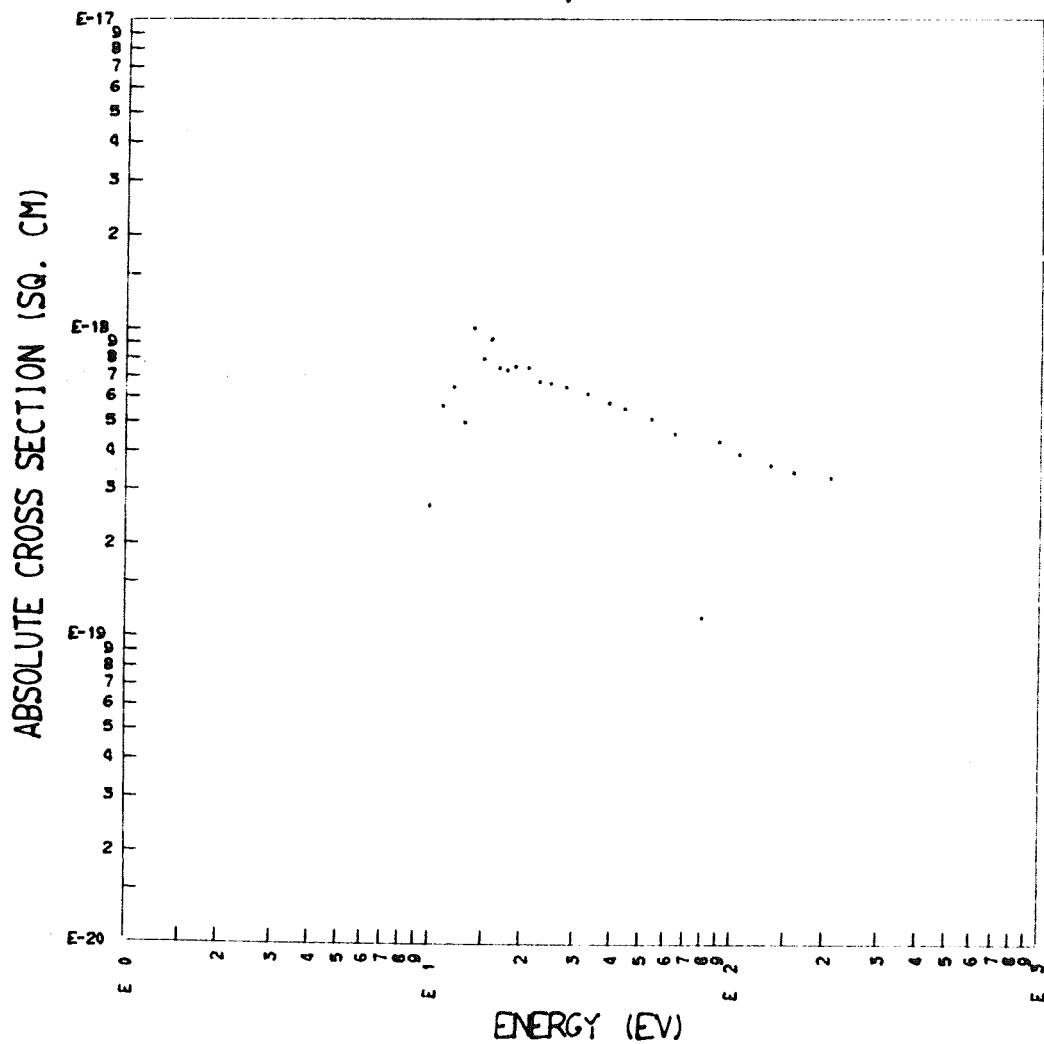
EMISSION CROSS SECTION OF
THE 1415A (1, 0) LBH BAND
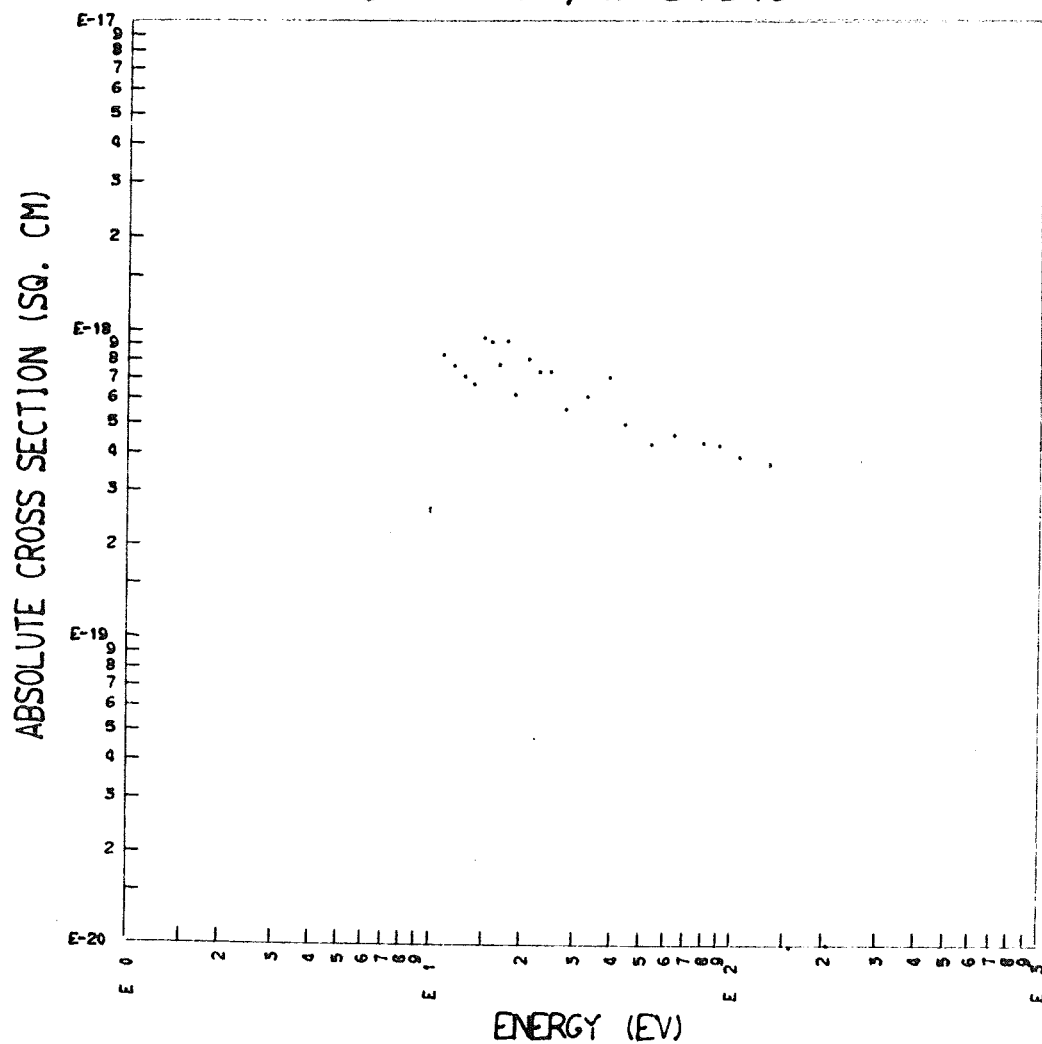
EMISSION CROSS SECTION OF
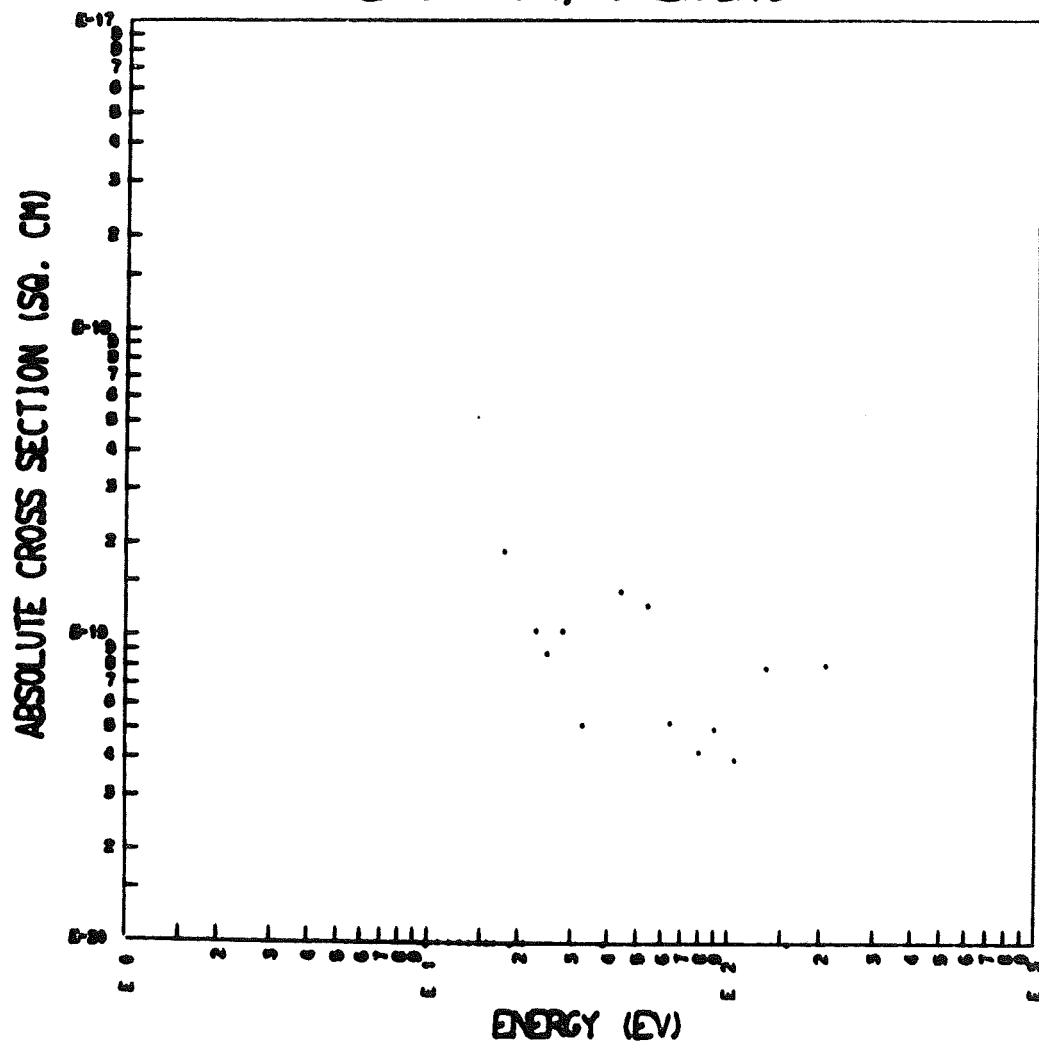THE 1426A (5, 3) LBH BAND
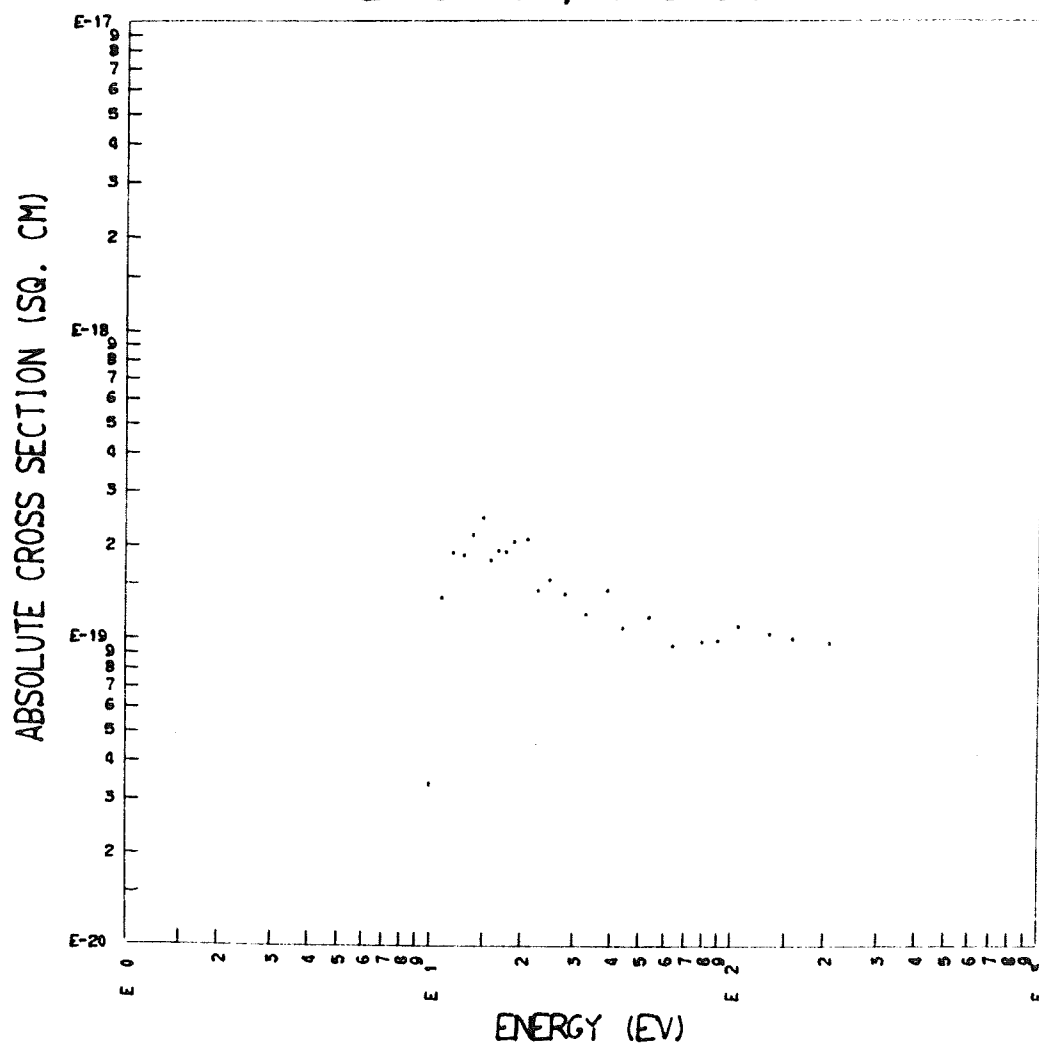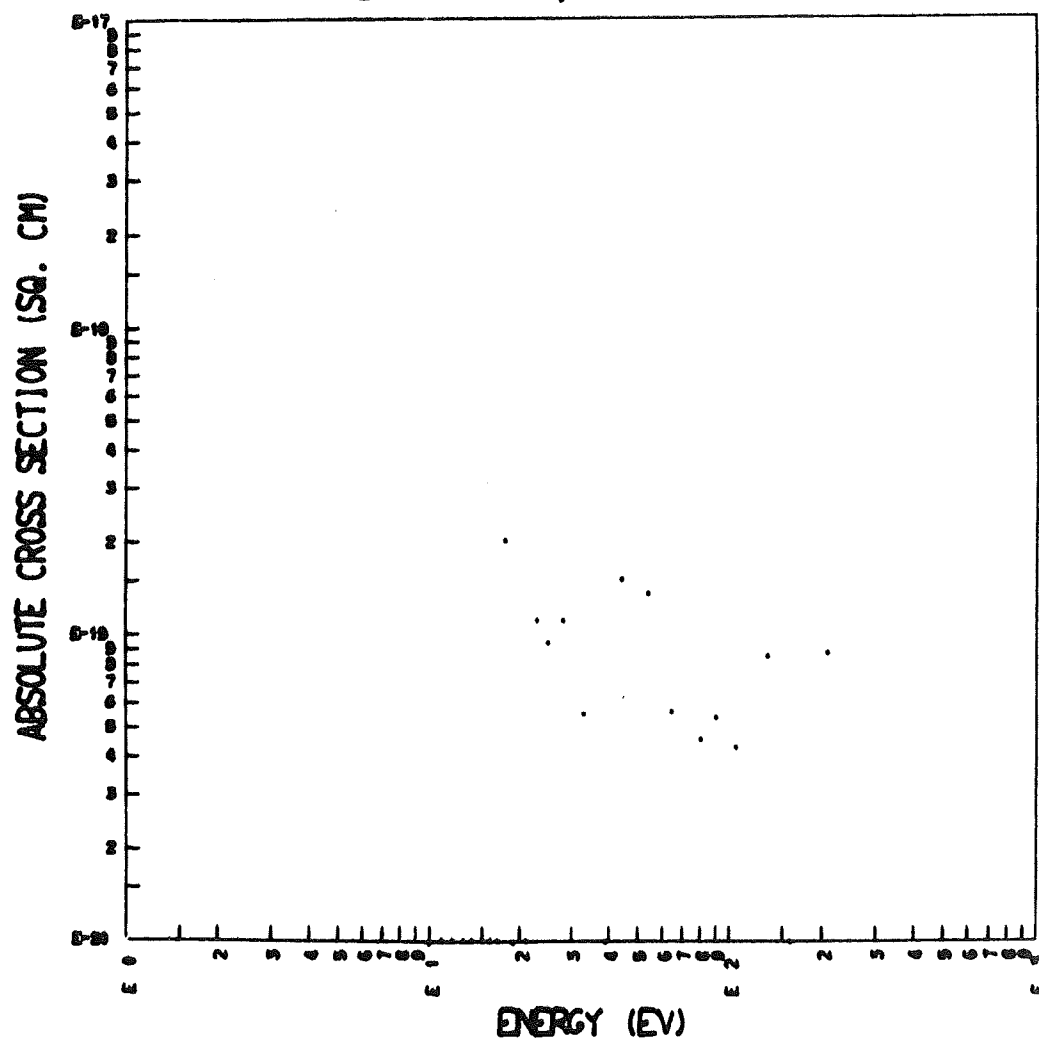
EMISSION CROSS SECTION OF
THE 1429A (2, 1) LBH BAND
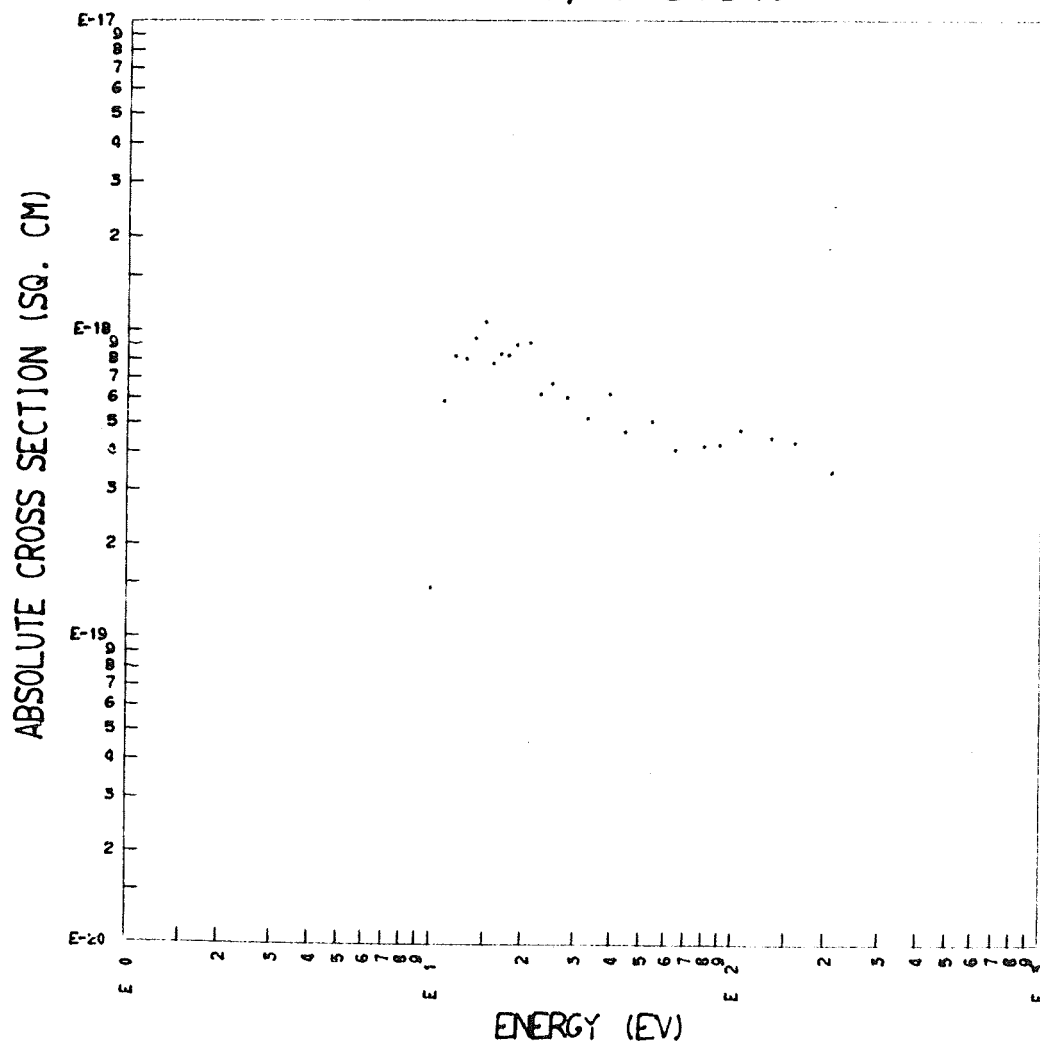
EMISSION CROSS SECTION OF
THE 1444A (3, 2) LBH BAND

ABSOLUTE CROSS SECTION (SQ. CM)

ENERGY (EV)
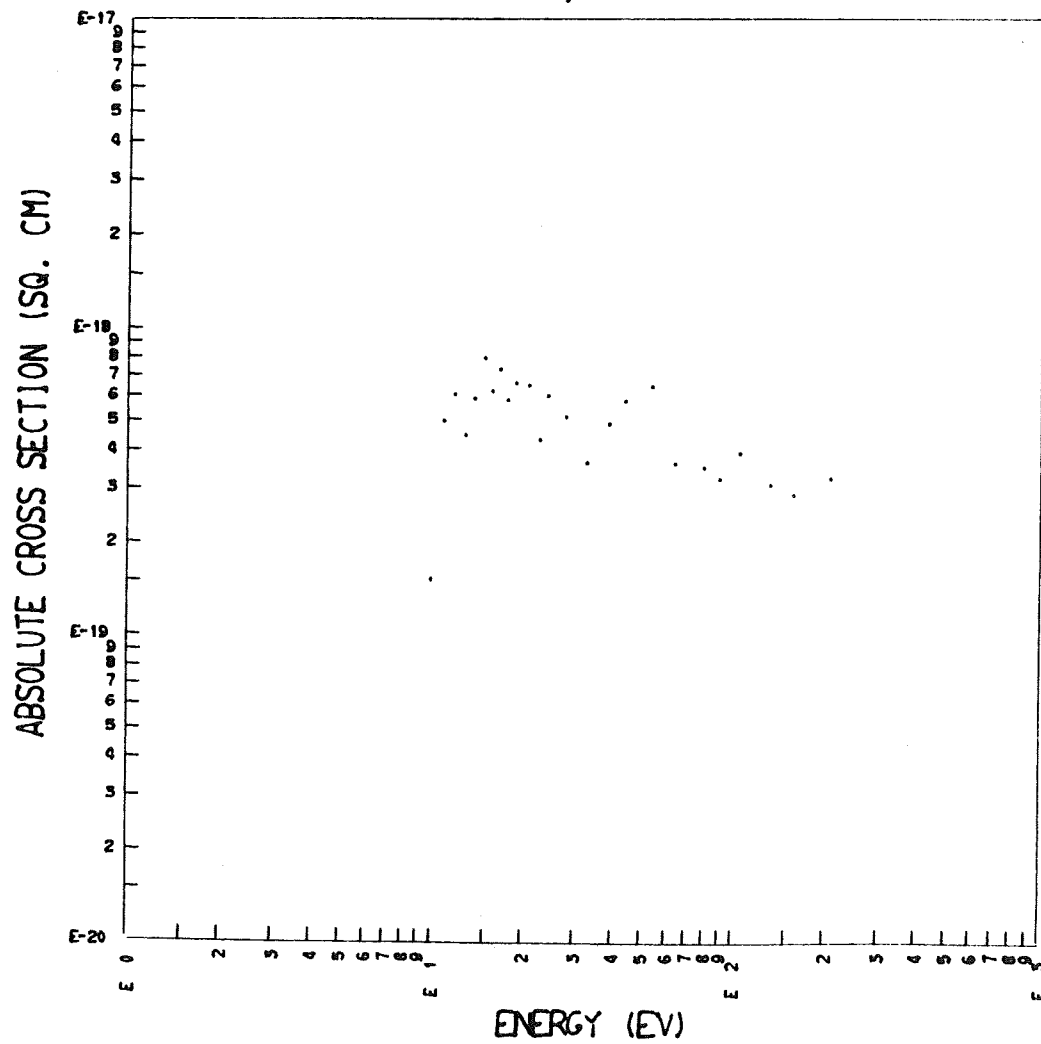
EMISSION CROSS SECTION OF
THE 1450A (0, 0) LBH BAND

ABSOLUTE CROSS SECTION (SQ. CM)

ENERGY (EV)
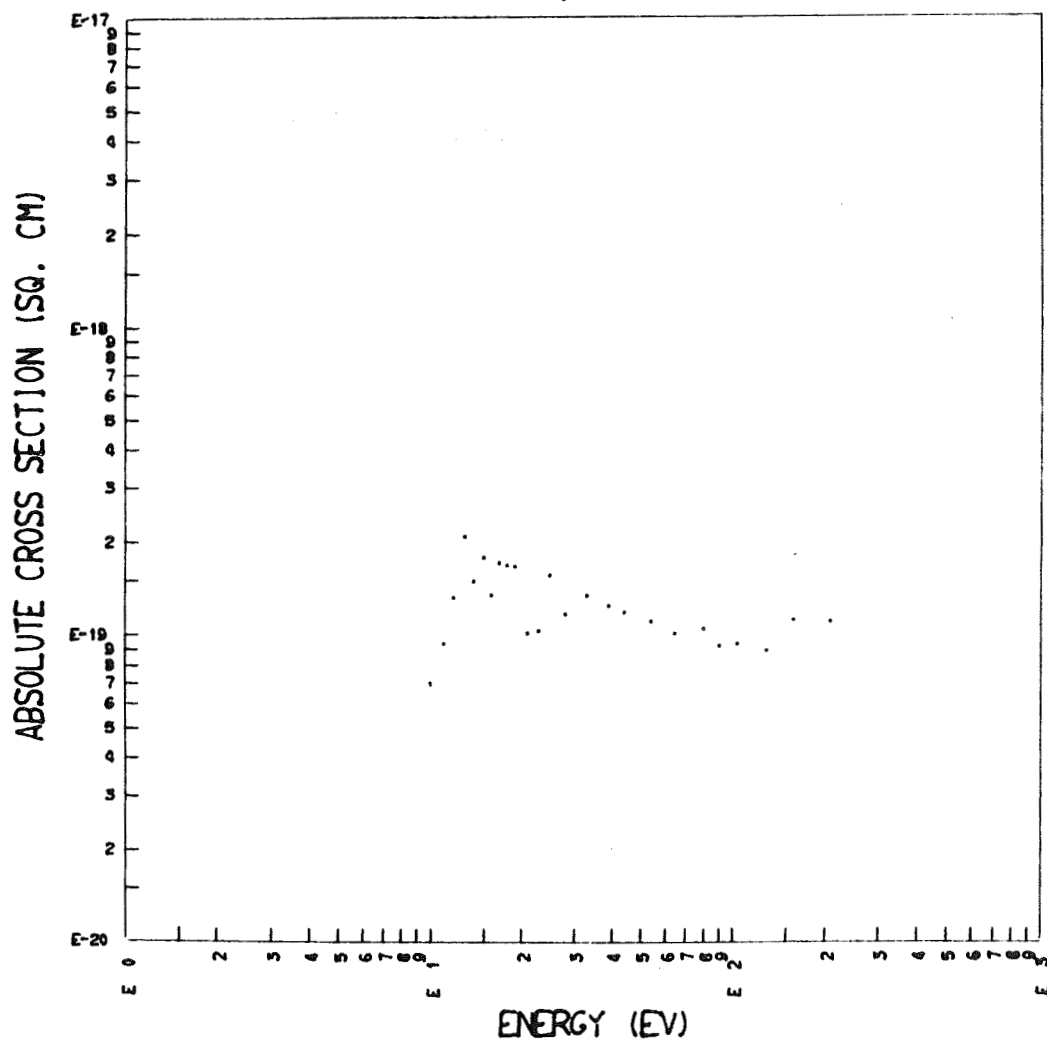
EMISSION CROSS SECTION OF
THE 1464A (1, 1) LBH BAND
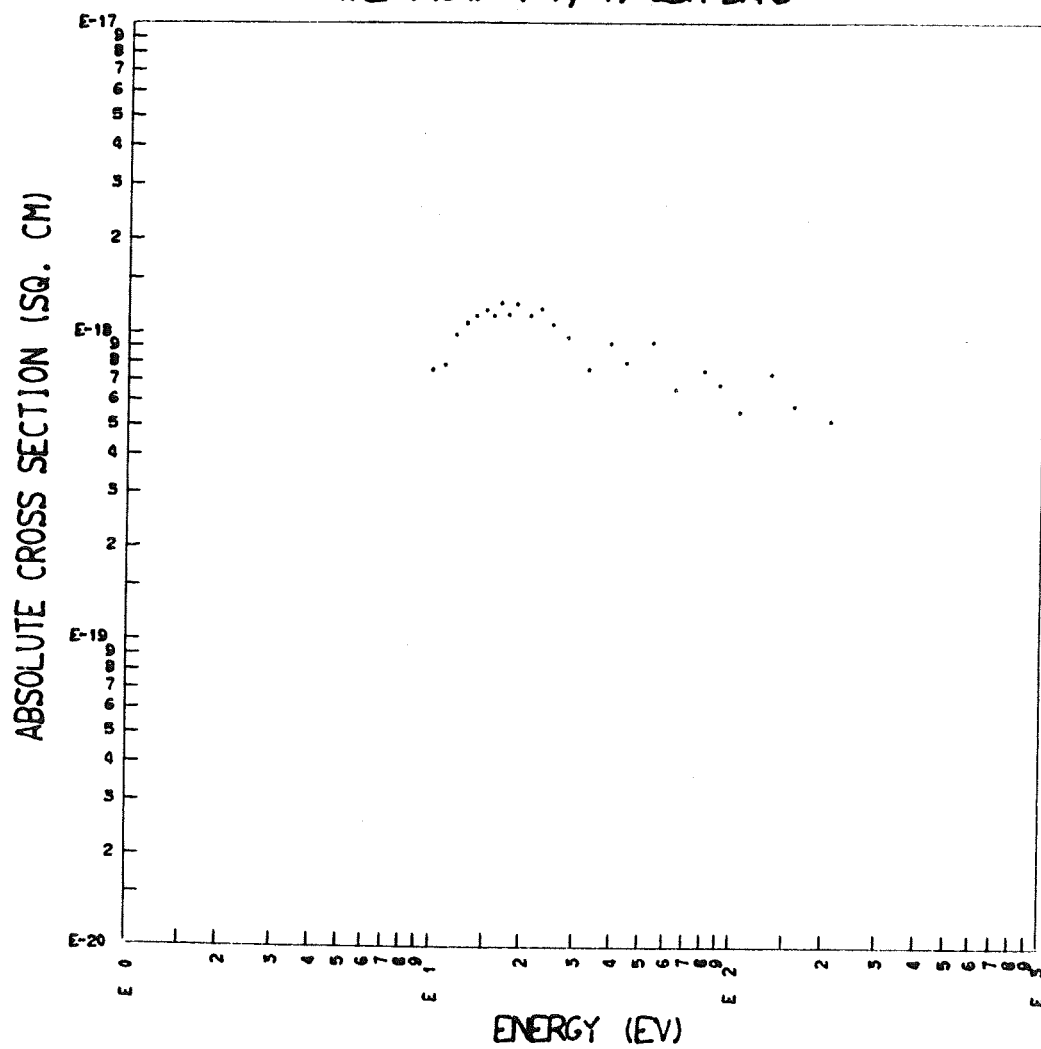
EMISSION CROSS SECTION OF
THE 1473A (5, 4) LBH BAND
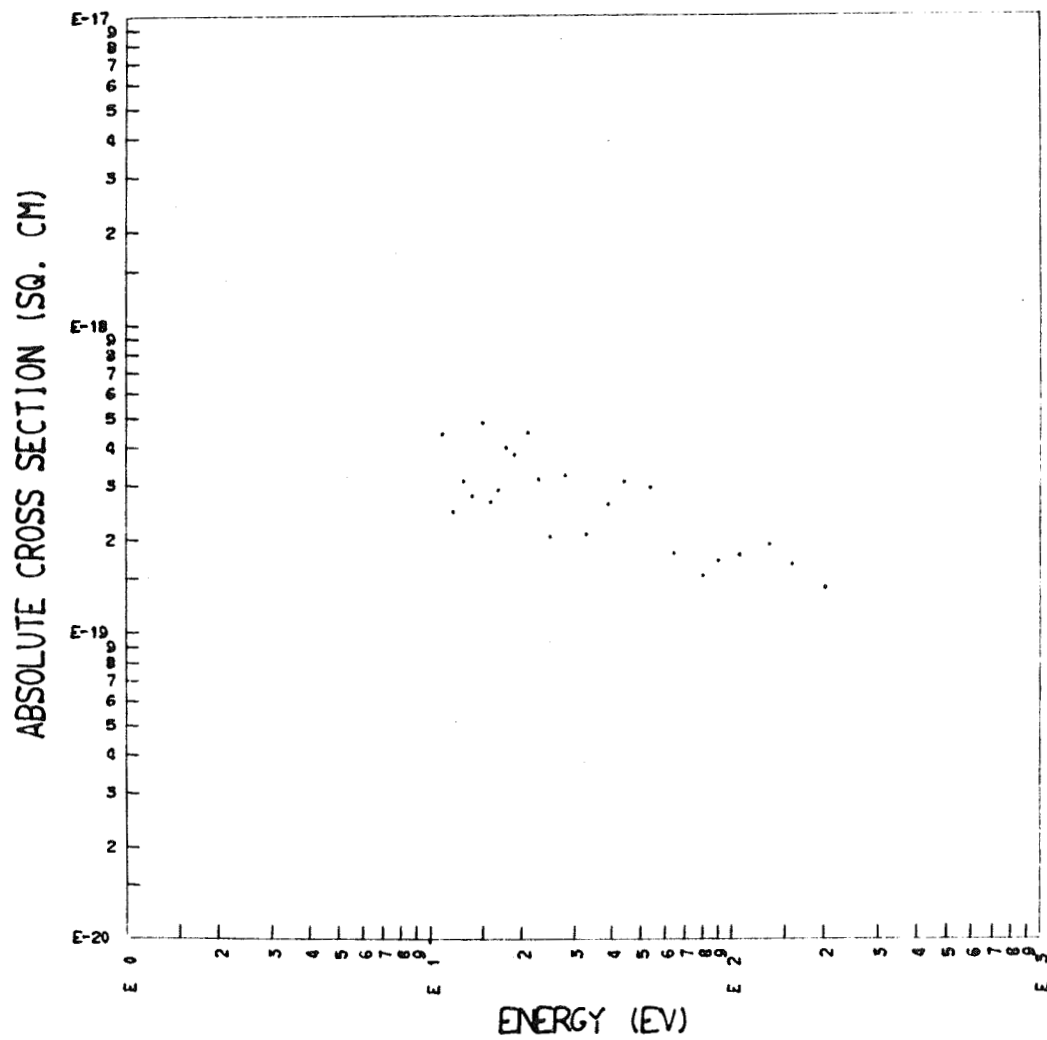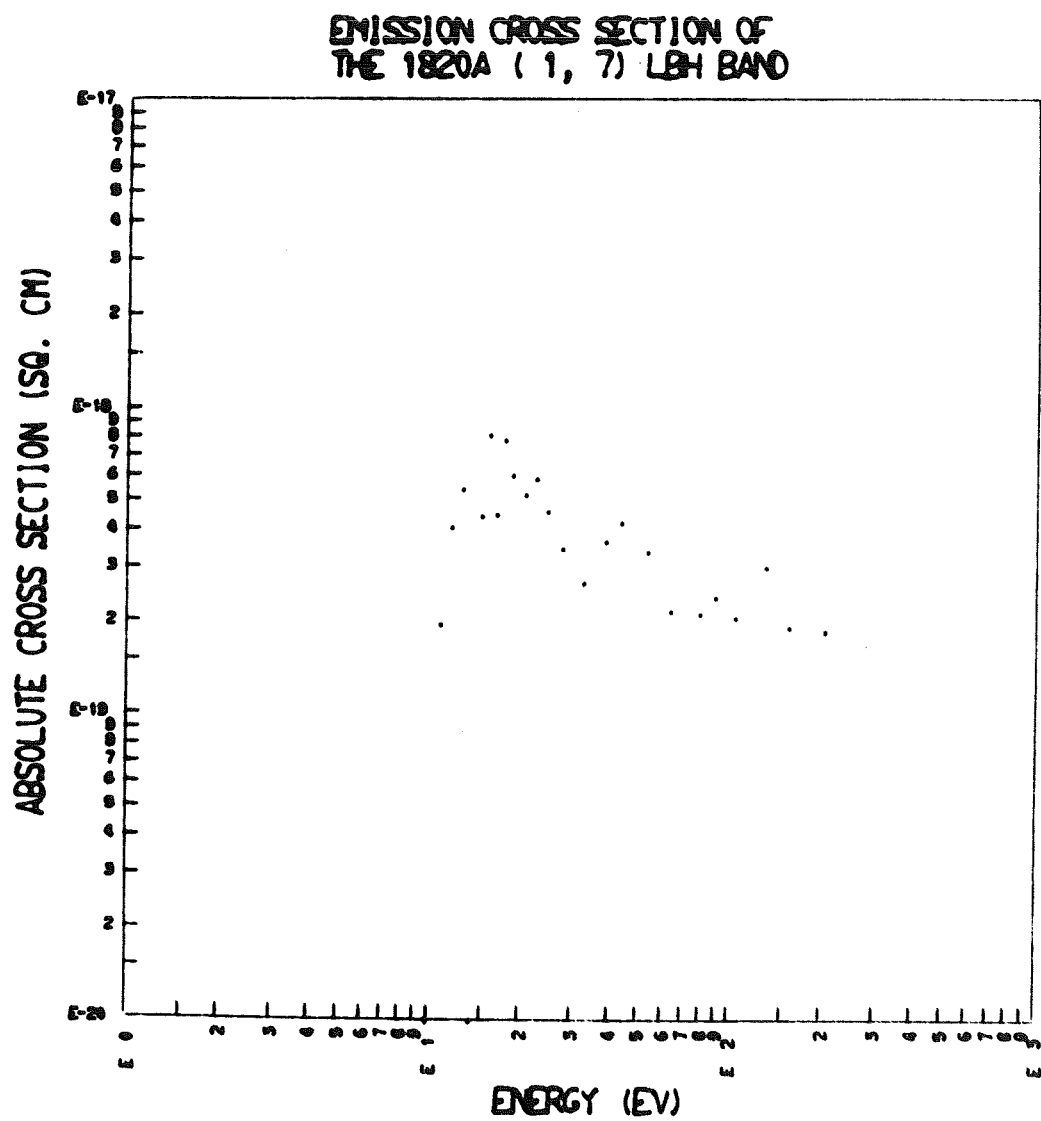
EMISSION CROSS SECTION OF
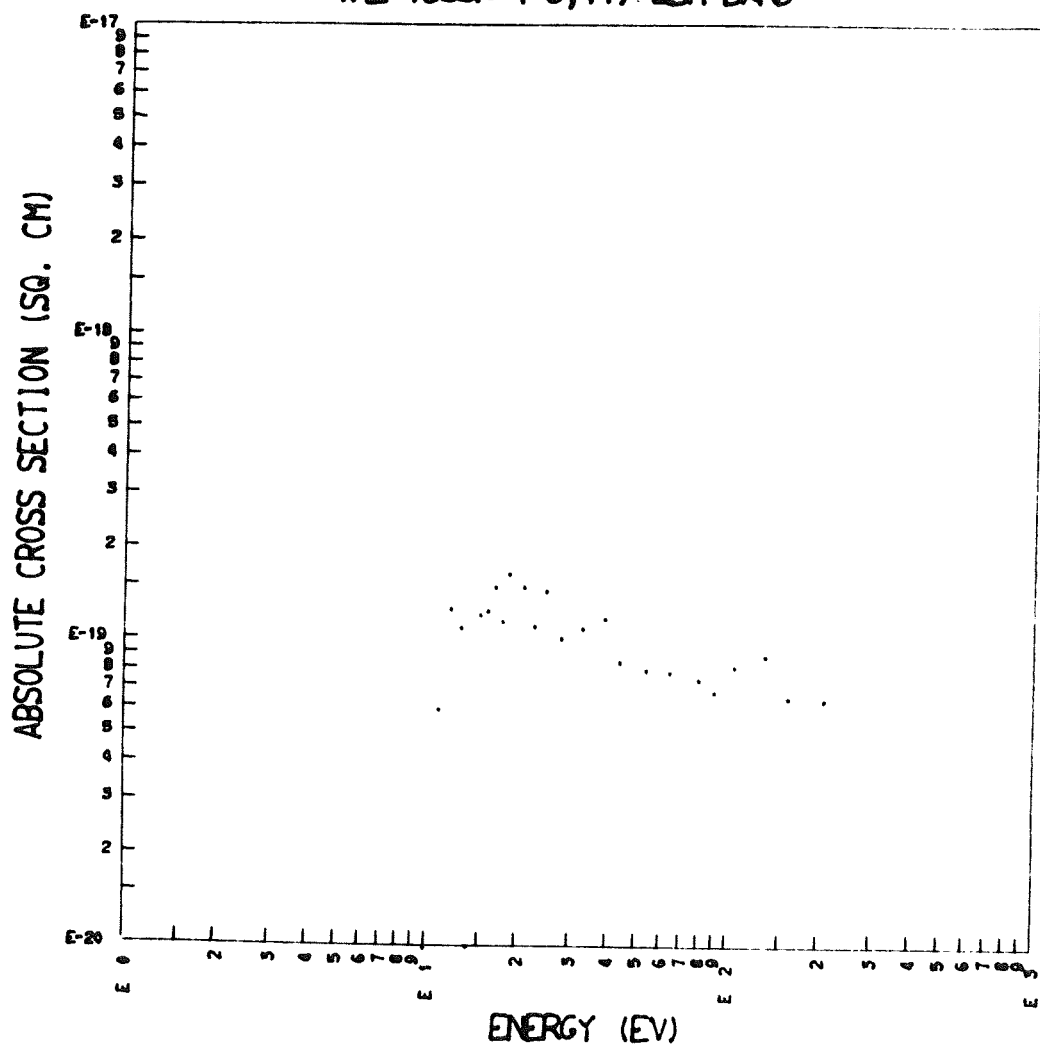THE 1488A (6, 5) LBH BAND
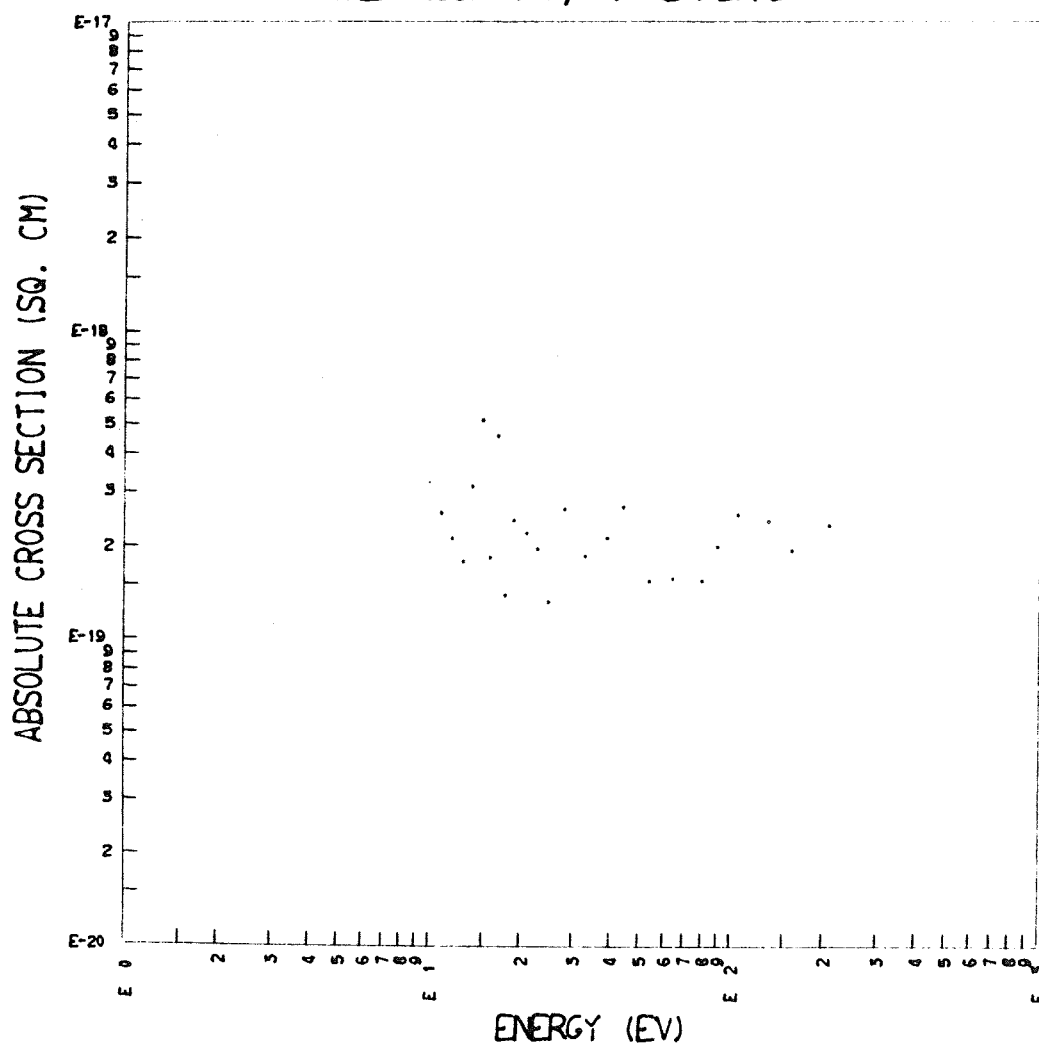
EMISSION CROSS SECTION OF
THE 1493A (3, 3) LBH BAND
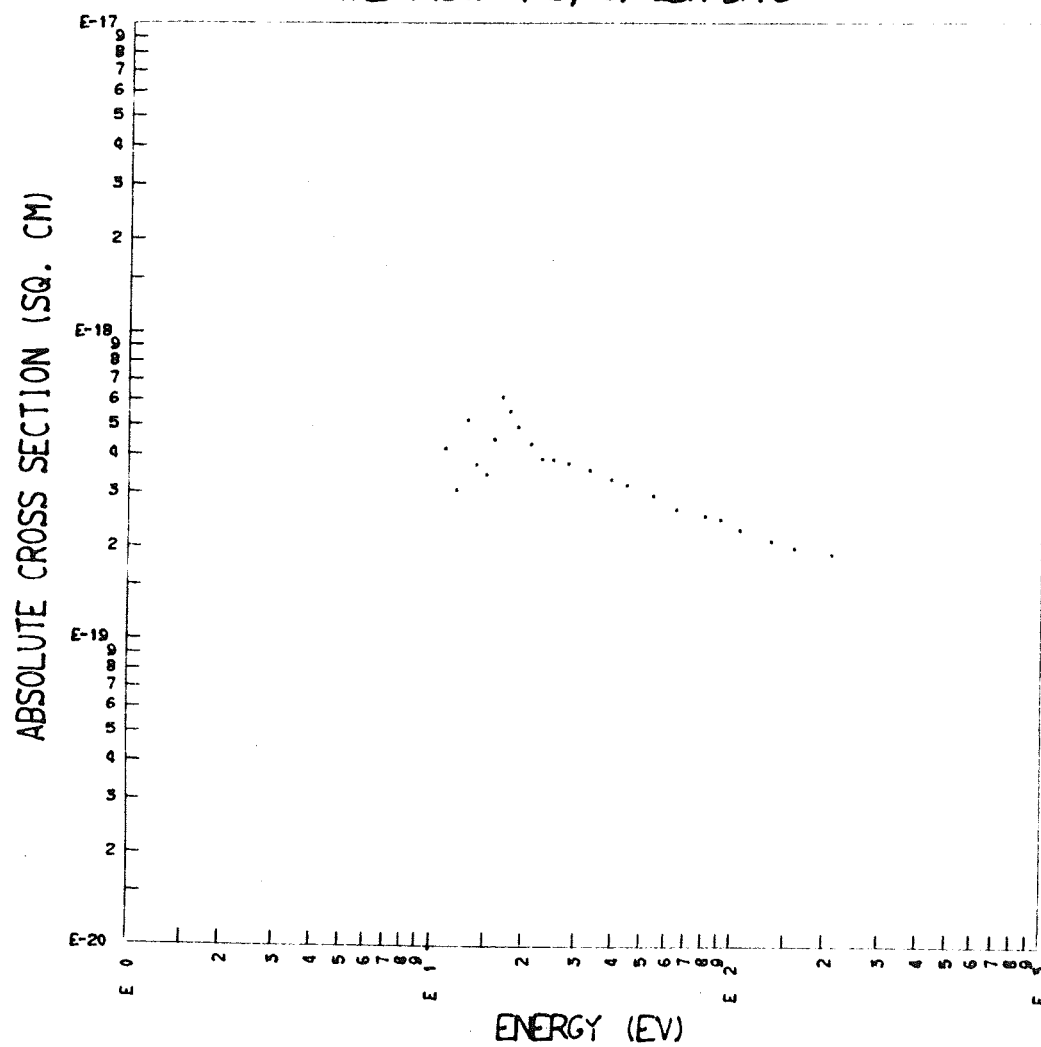
EMISSION CROSS SECTION OF
THE 1500A (0, 1) LBH BAND

ABSOLUTE CROSS SECTION (SQ. CM)

ENERGY (EV)
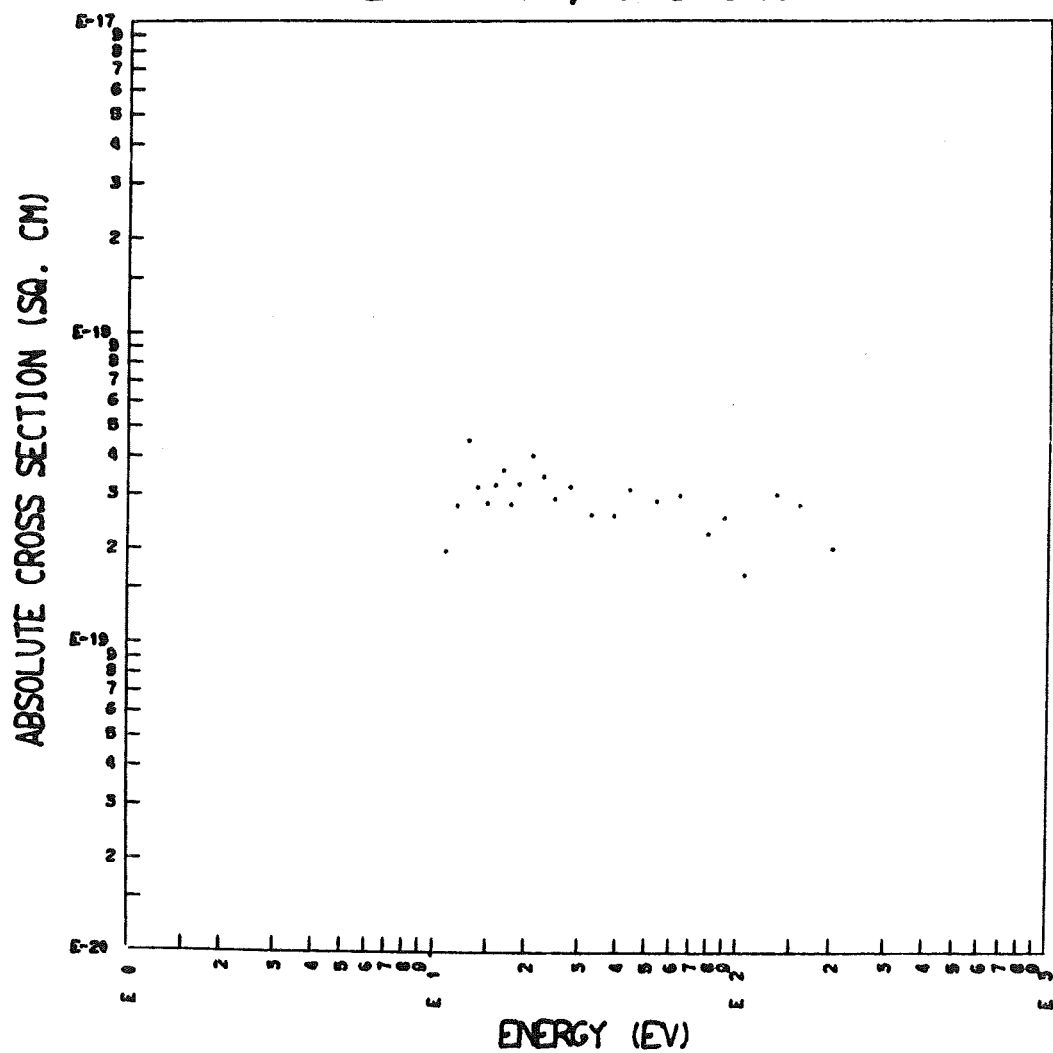
EMISSION CROSS SECTION OF
THE 1508A (4, 4) LBH BAND
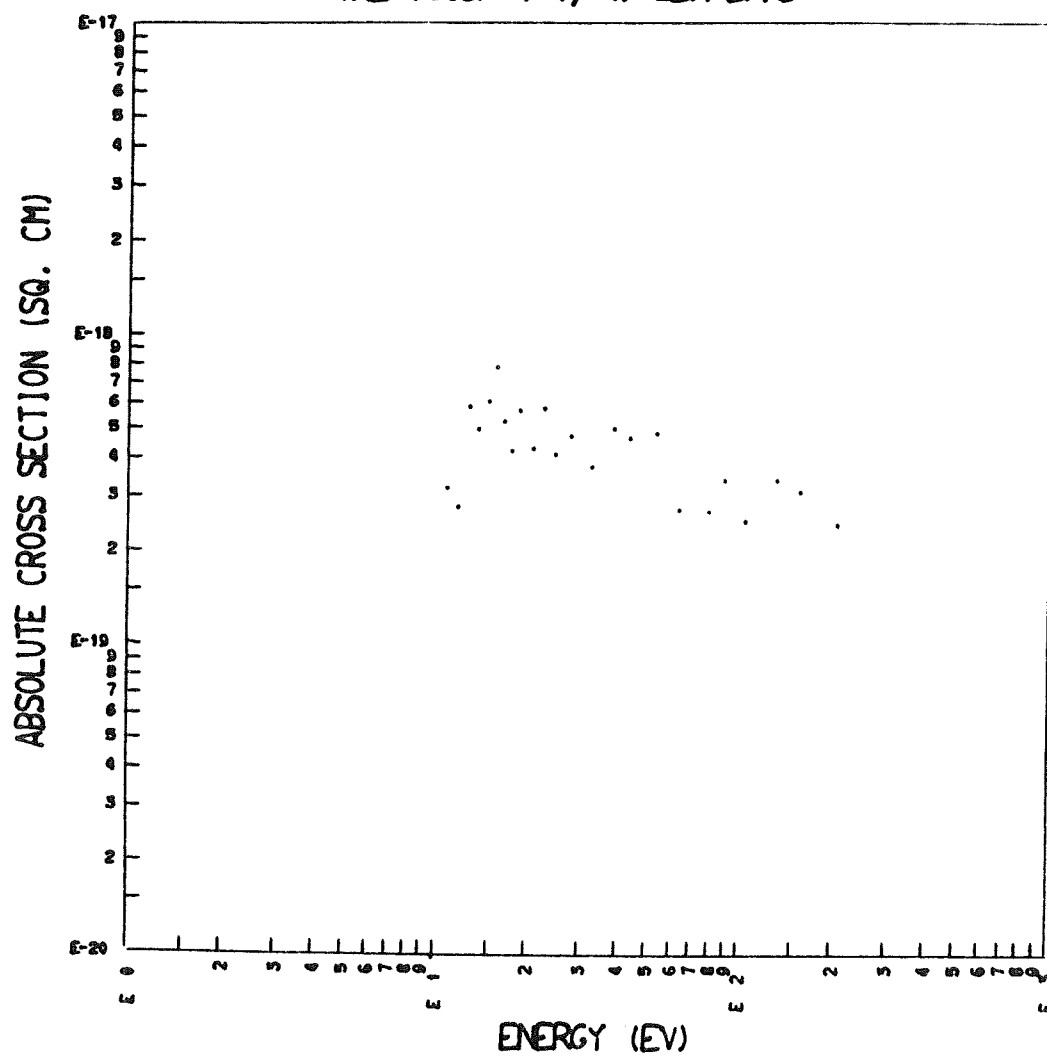
EMISSION CROSS SECTION OF
THE 1515A (1, 2) LBH BAND

ABSOLUTE CROSS SECTION (SQ. CM)

ENERGY (EV)
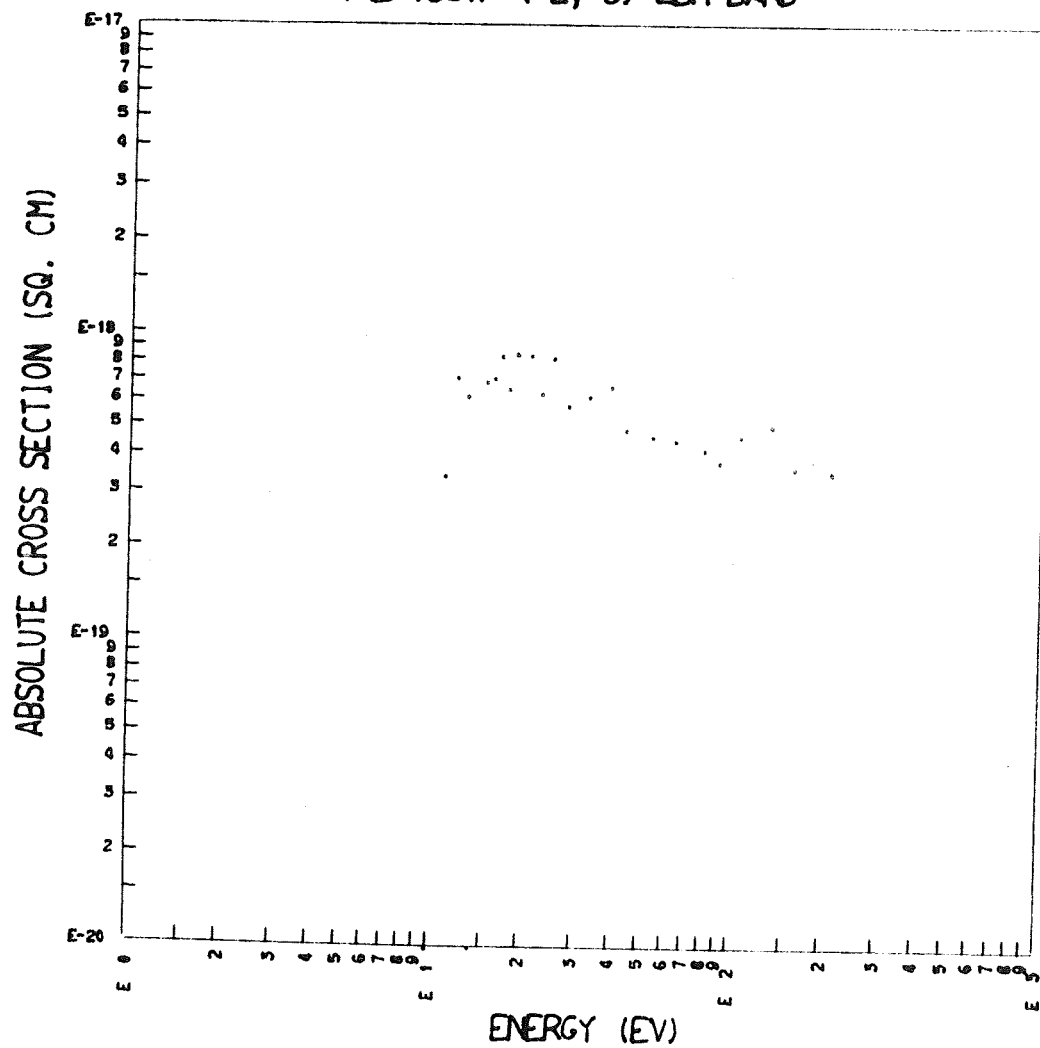
EMISSION CROSS SECTION OF
THE 1529A (2, 3) LBH BAND
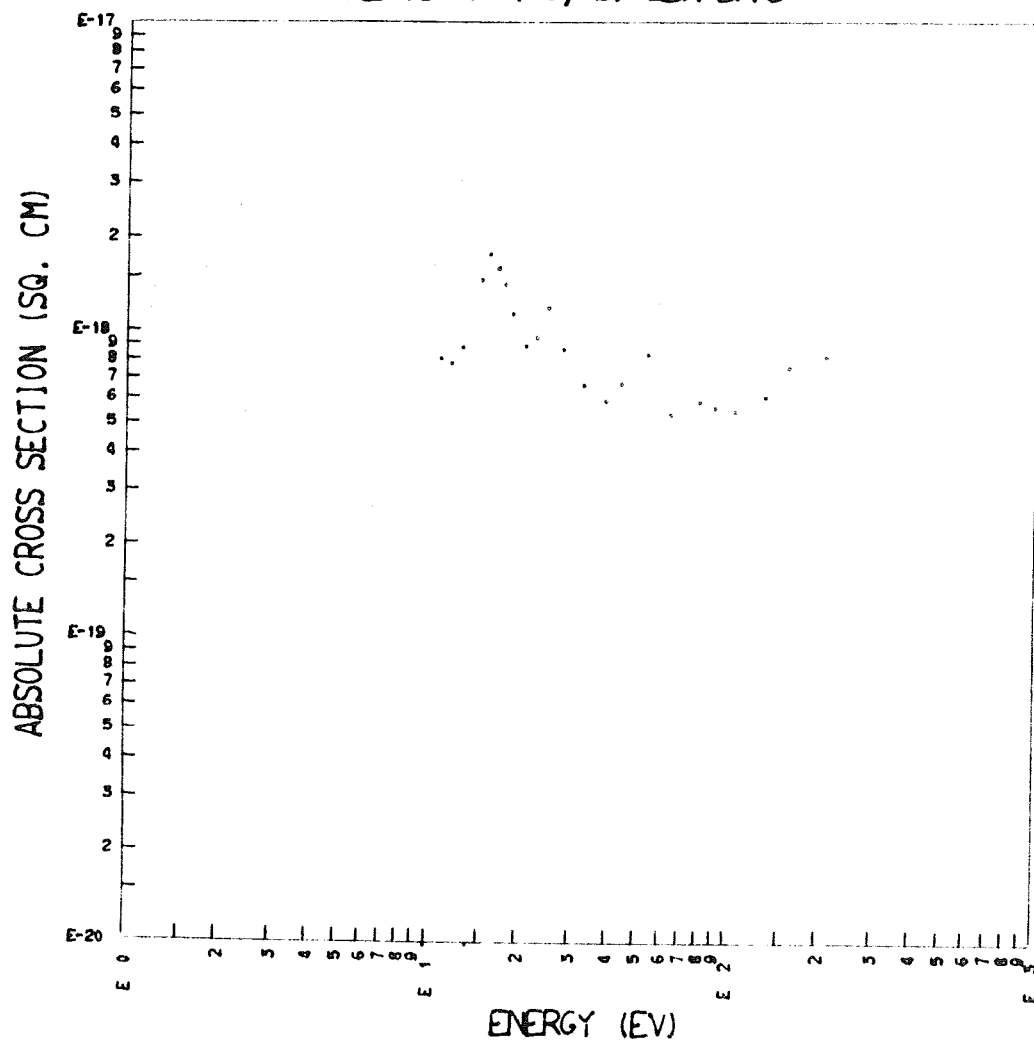
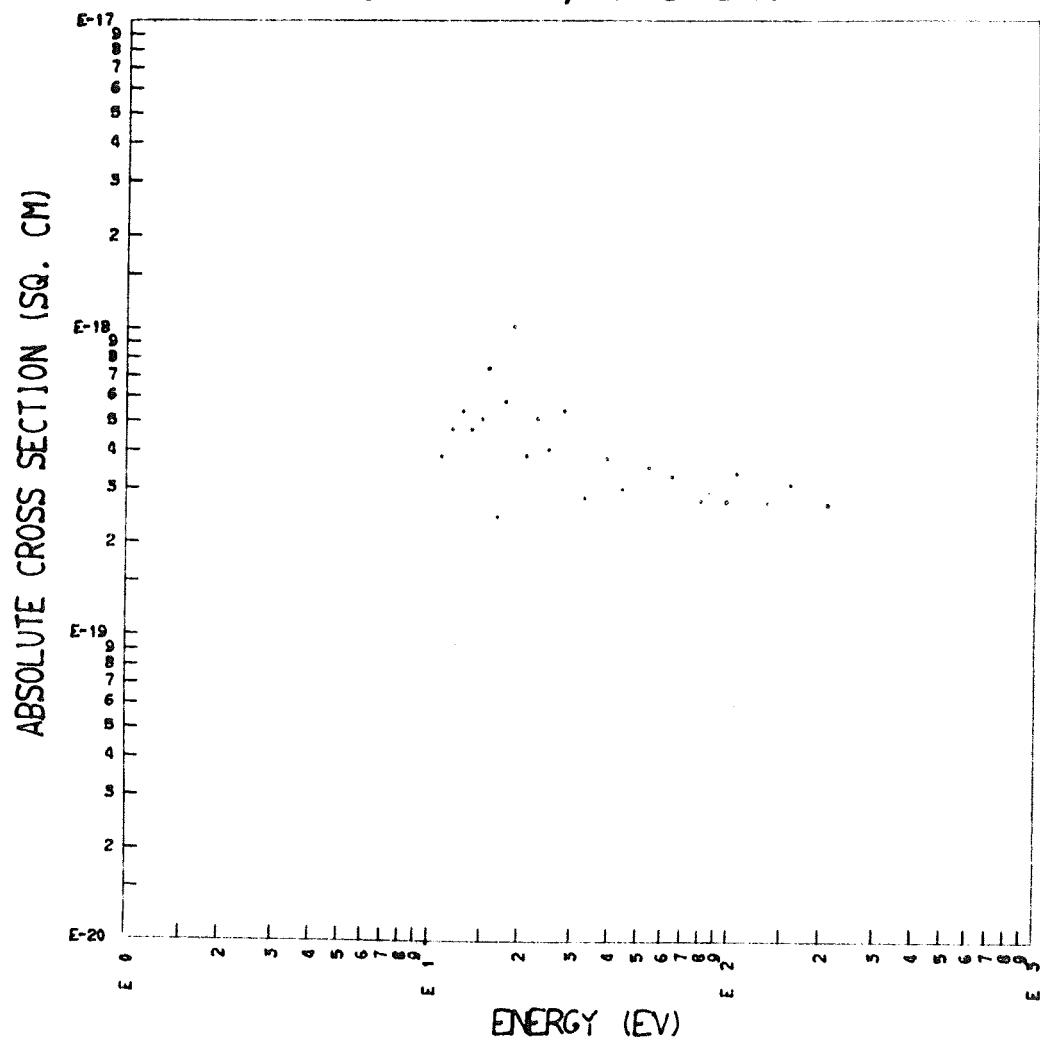EMISSION CROSS SECTION OF THE 1554A (0, 2) LBH BAND
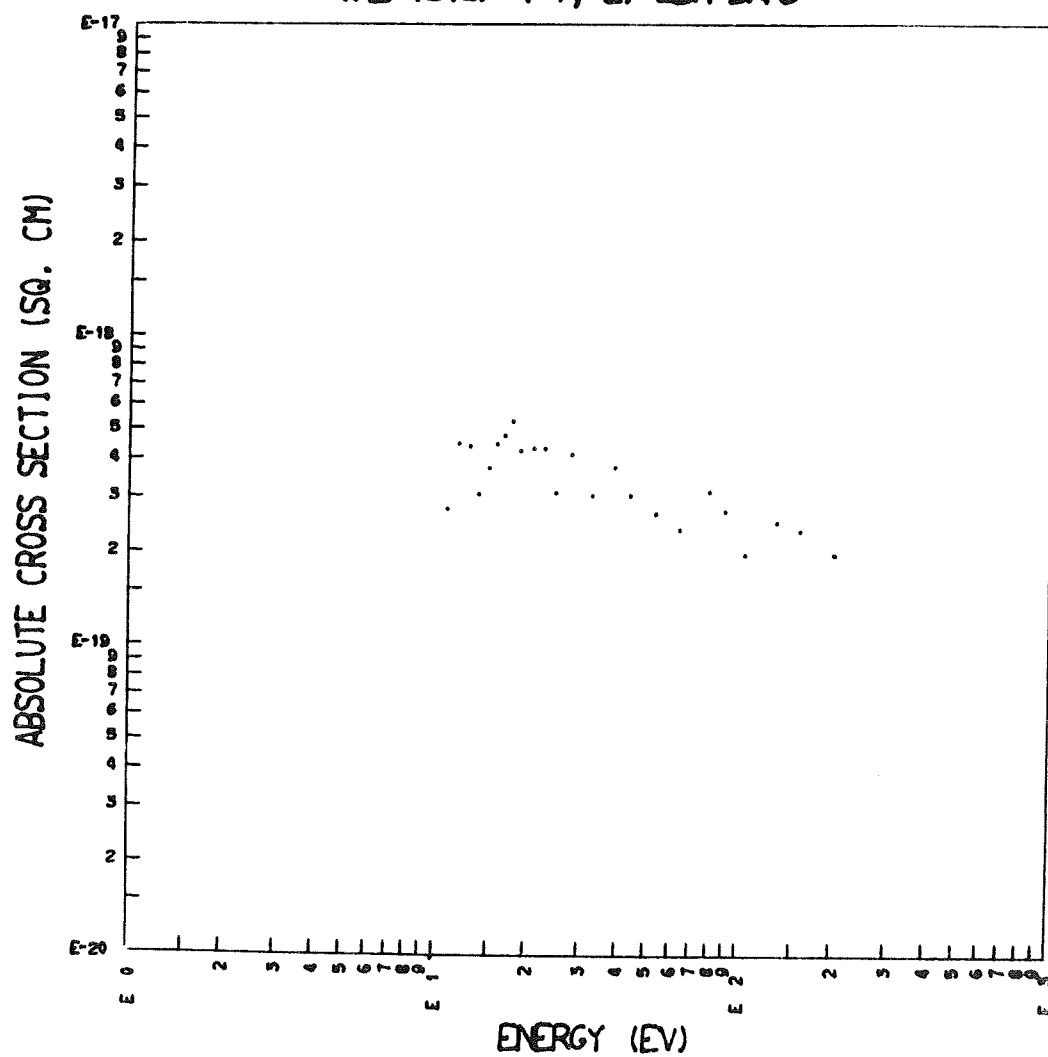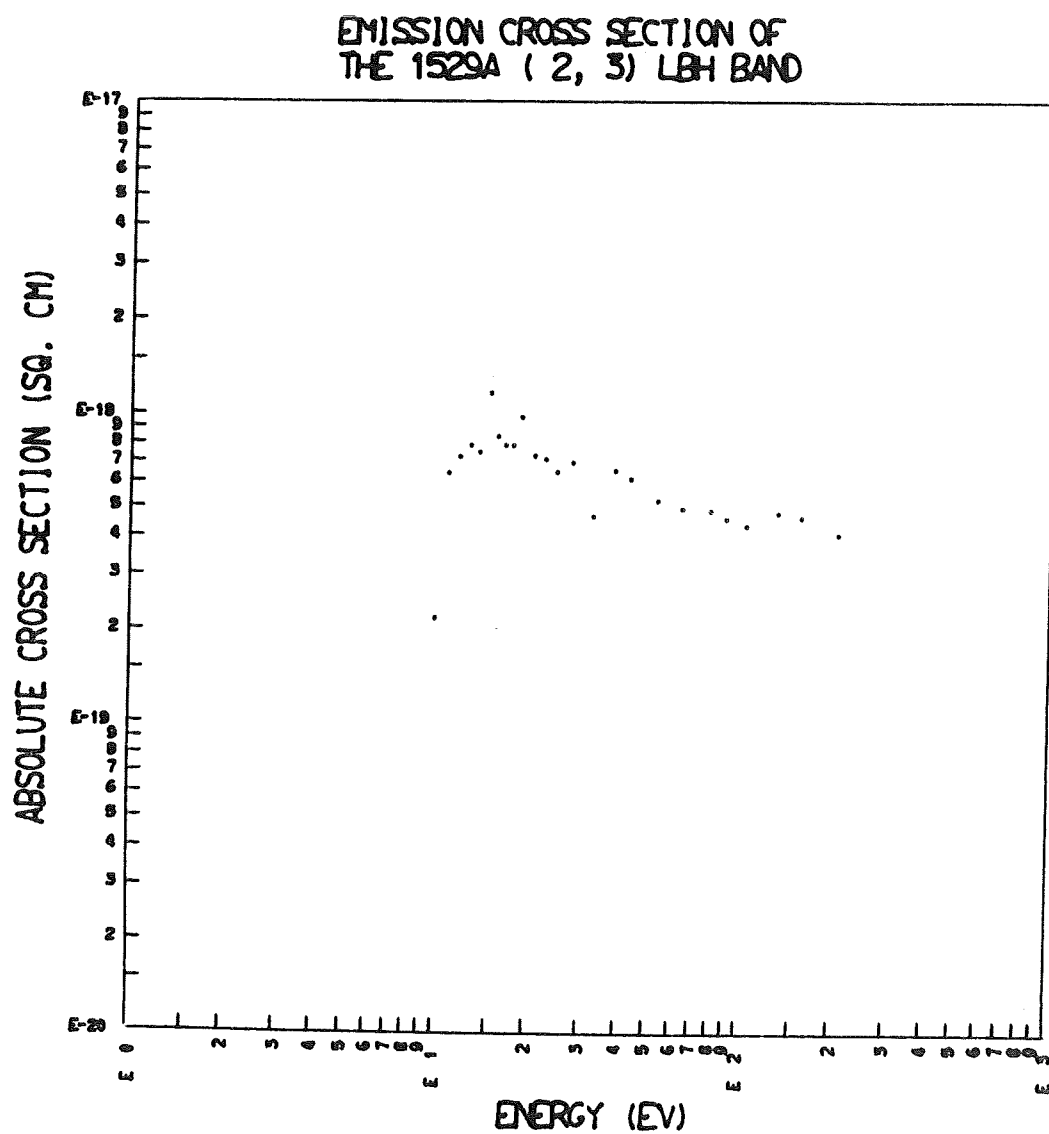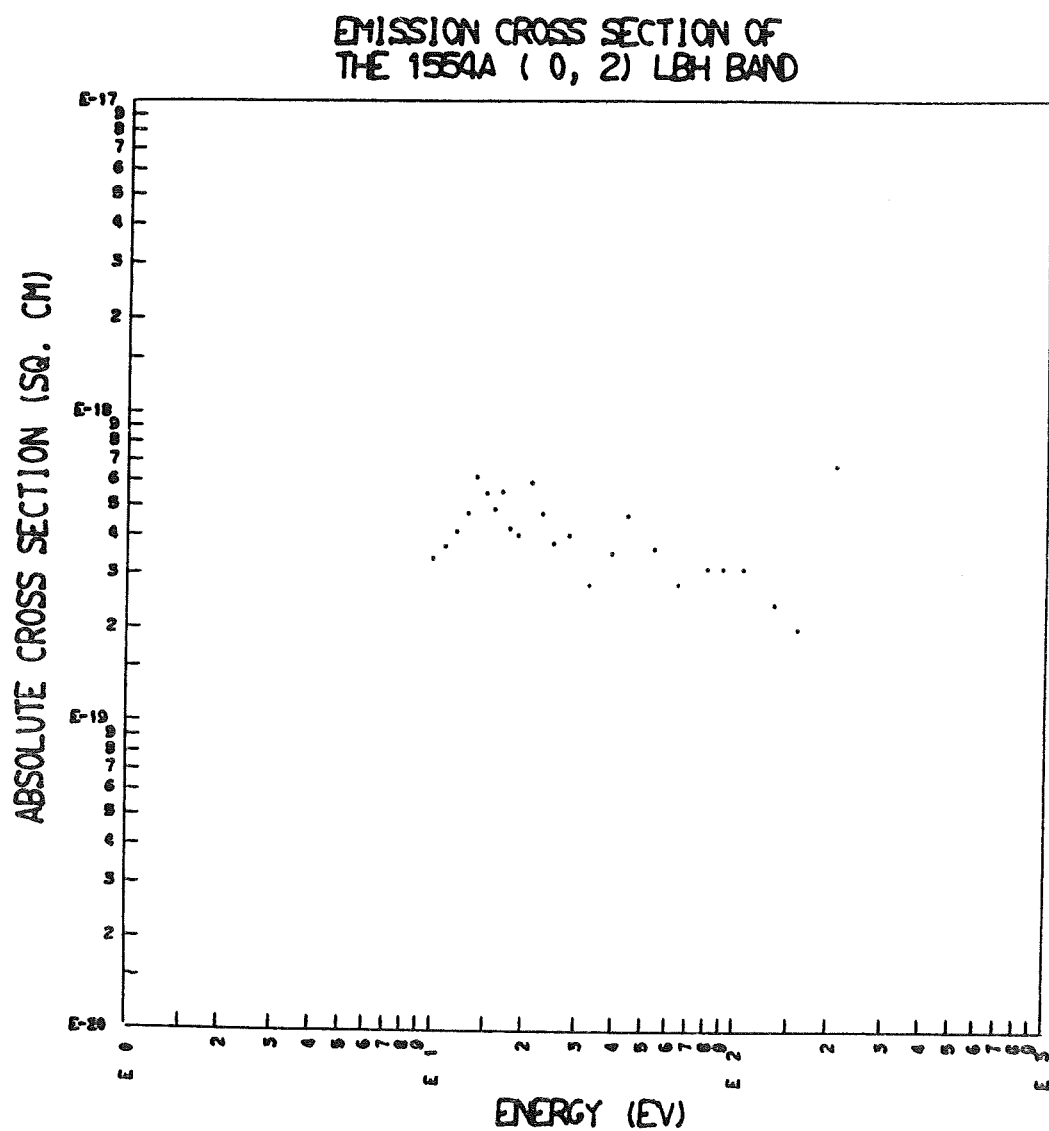
EMISSION CROSS SECTION OF
THE 1560A (4, 5) LBH BAND

ABSOLUTE CROSS SECTION (SQ. CM)

ENERGY (EV)

EMISSION CROSS SECTION OF
THE 1575A (5, 6) LBH BAND

ABSOLUTE CROSS SECTION (SQ. CM)

ENERGY (EV)
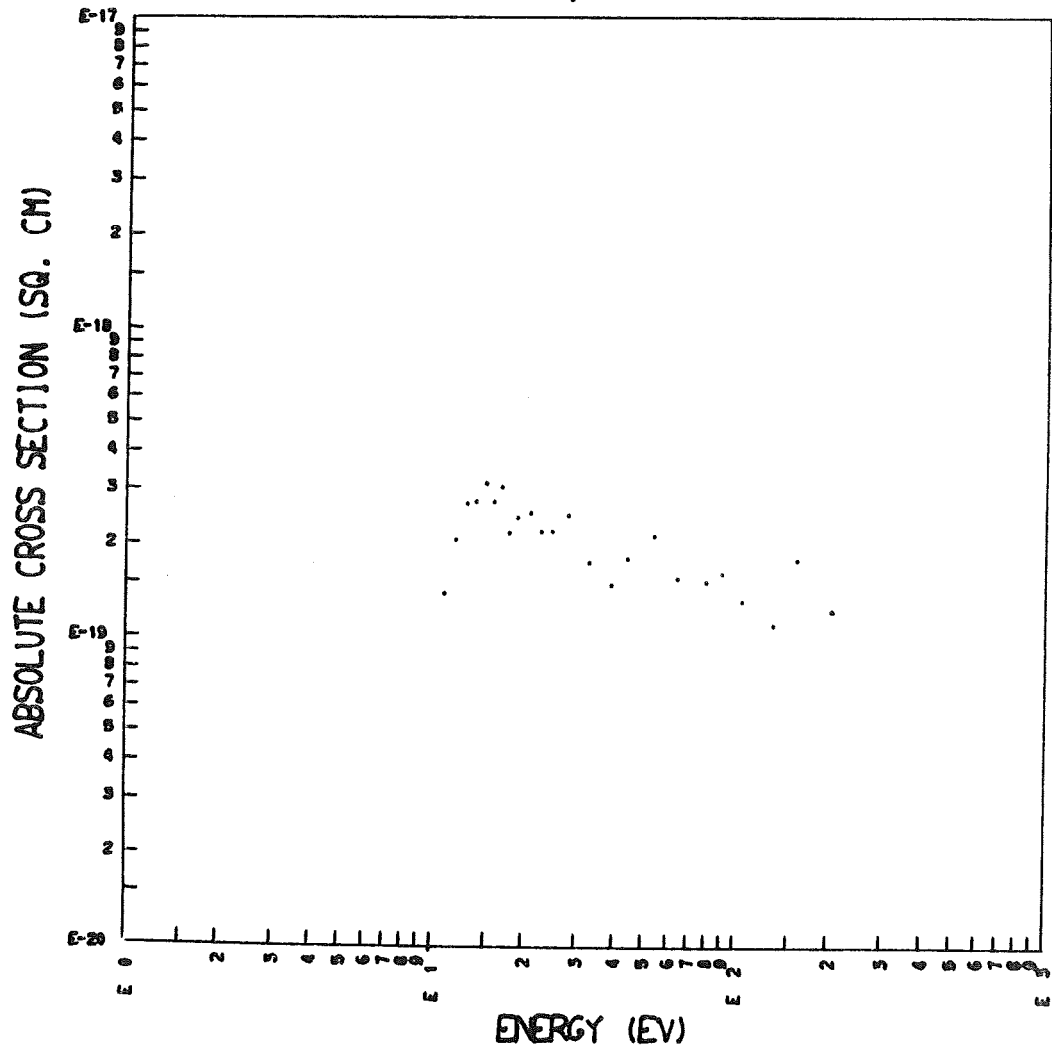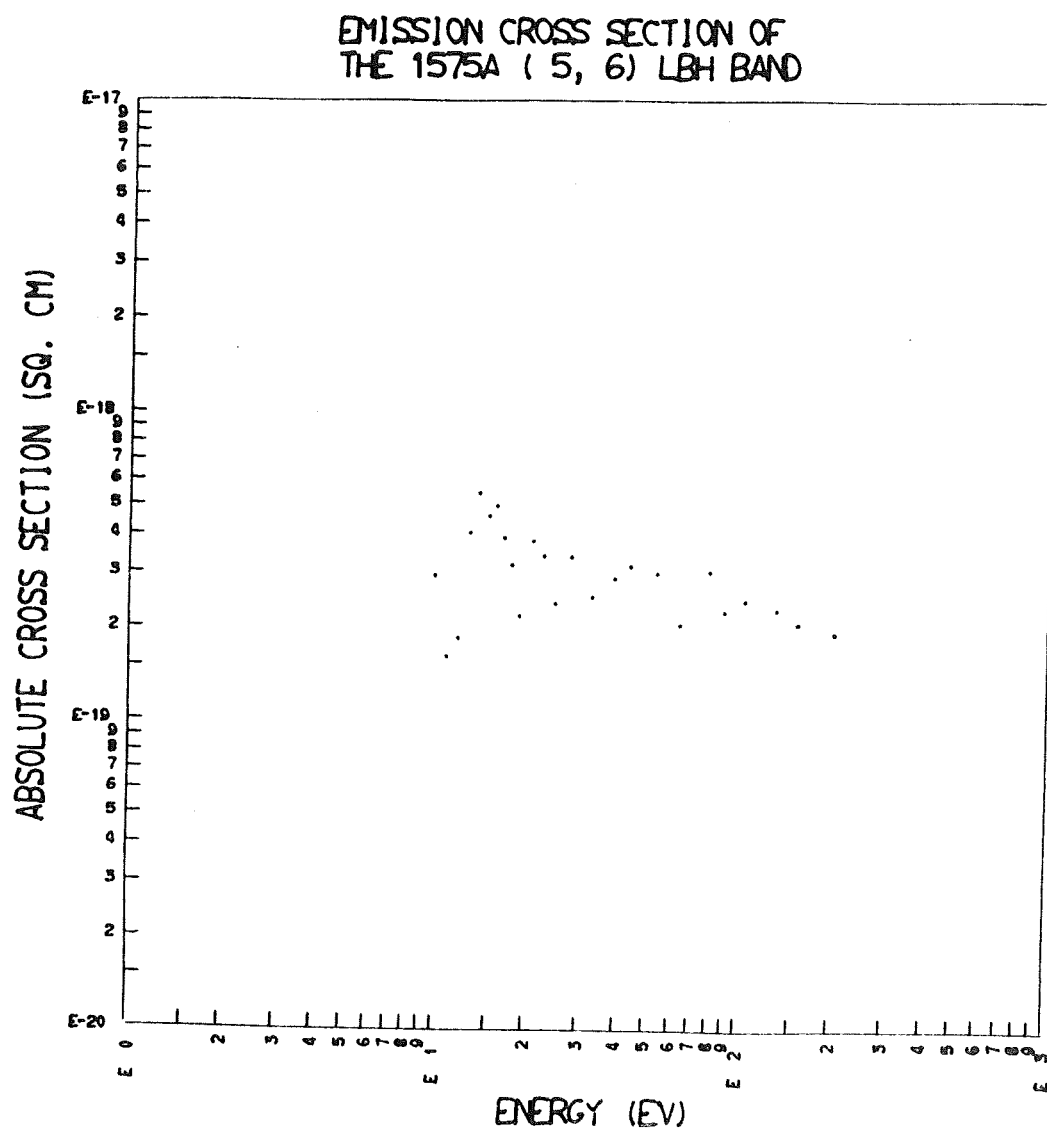
EMISSION CROSS SECTION OF
THE 1584A (2, 4) LBH BAND
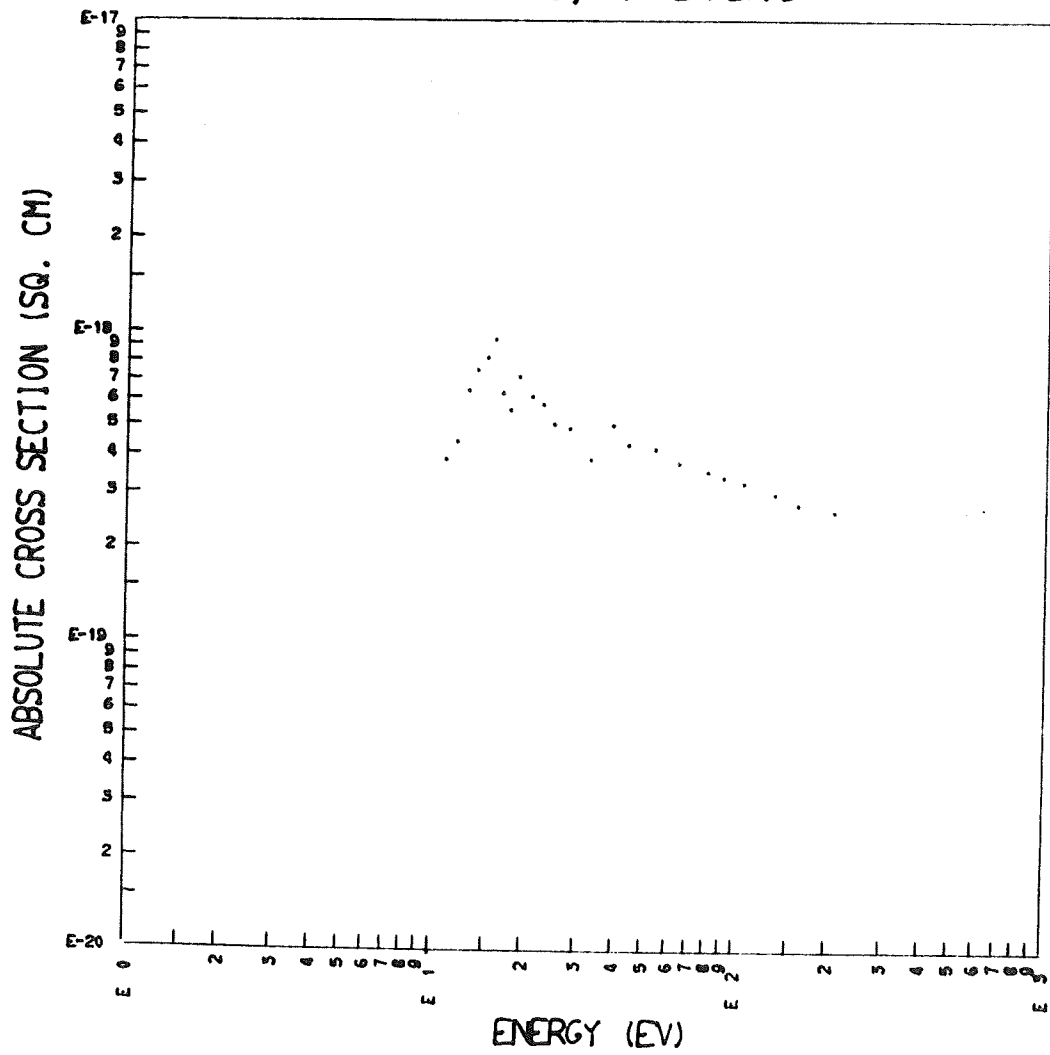
EMISSION CROSS SECTION OF
THE 1591A (6, 7) LBH BAND

ABSOLUTE CROSS SECTION (SQ. CM)

ENERGY (EV)
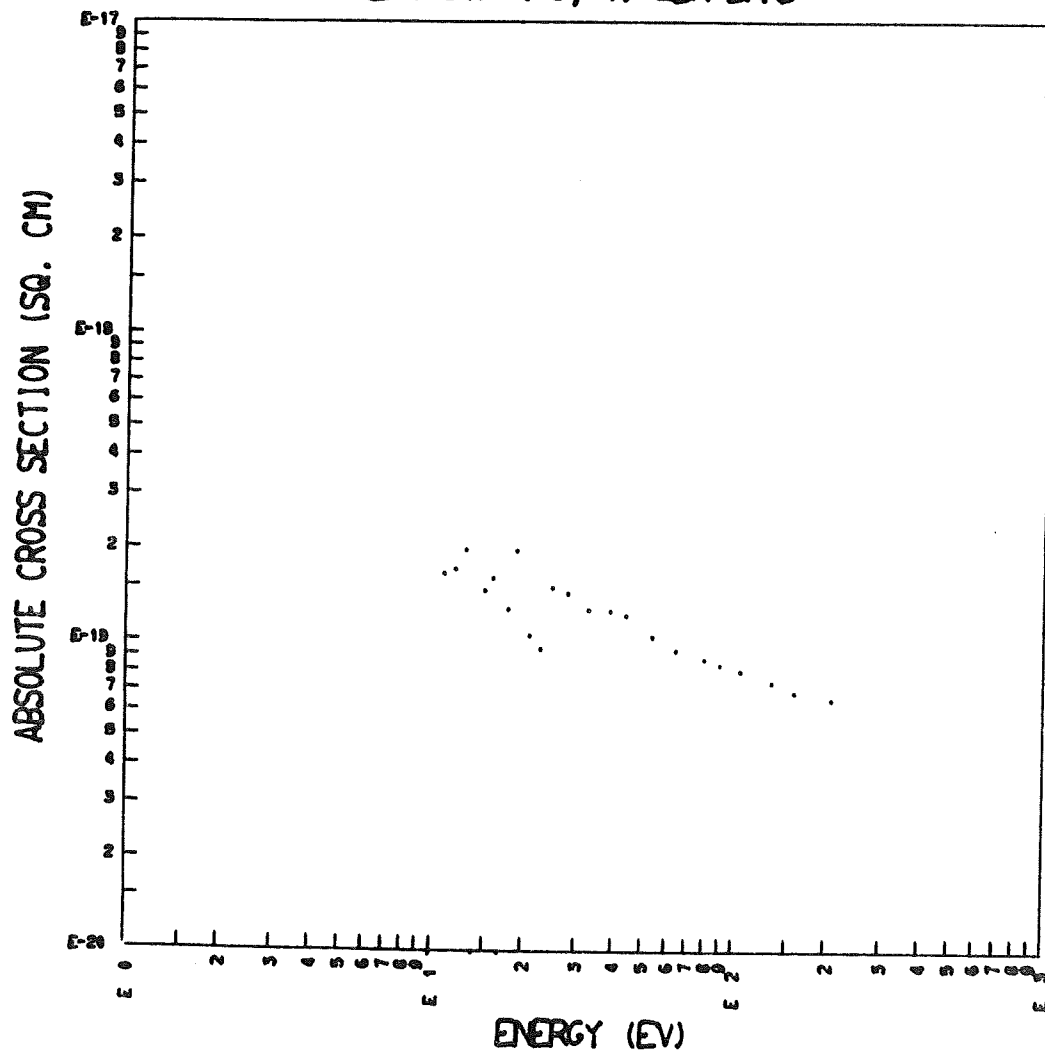
EMISSION CROSS SECTION OF
THE 1599A (3, 5) LBH BAND
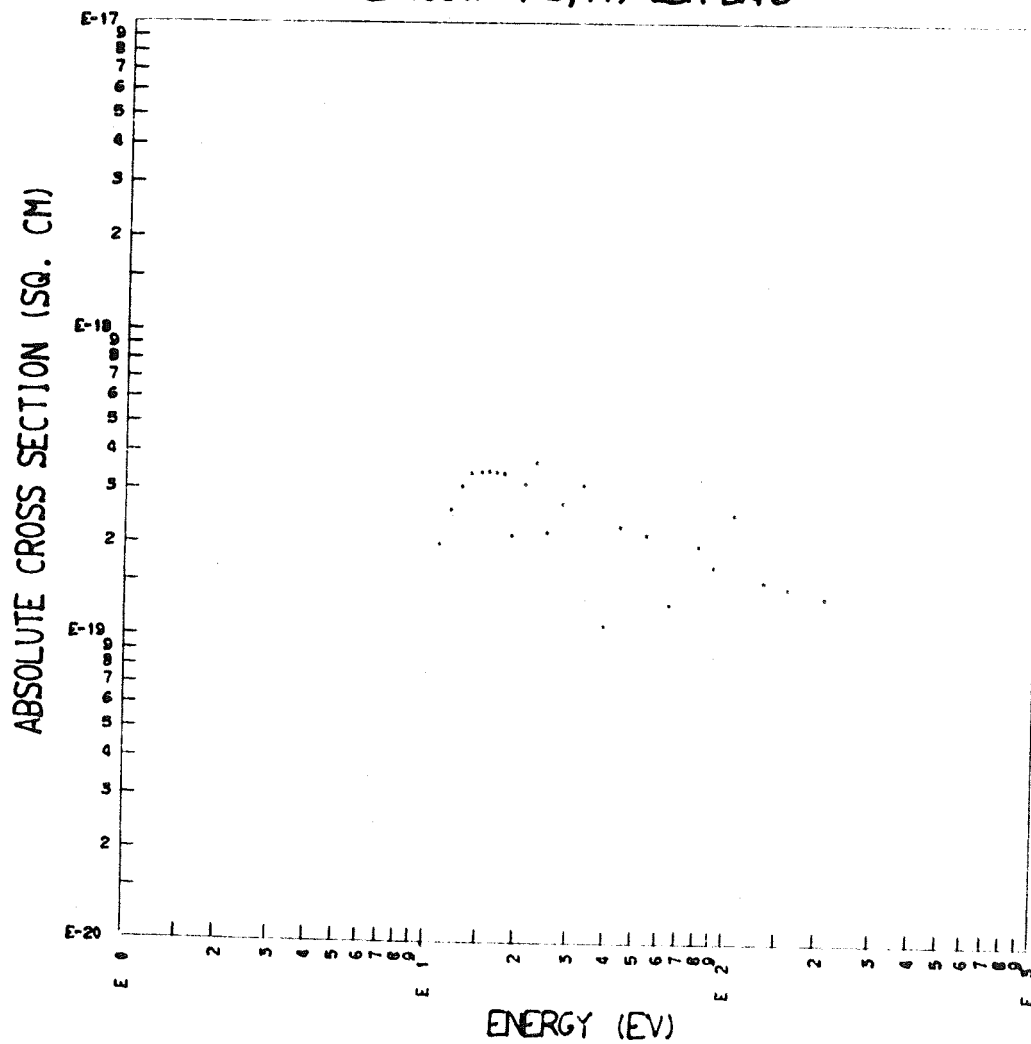
EMISSION CROSS SECTION OF
THE 1611A (0, 3) LBH BAND
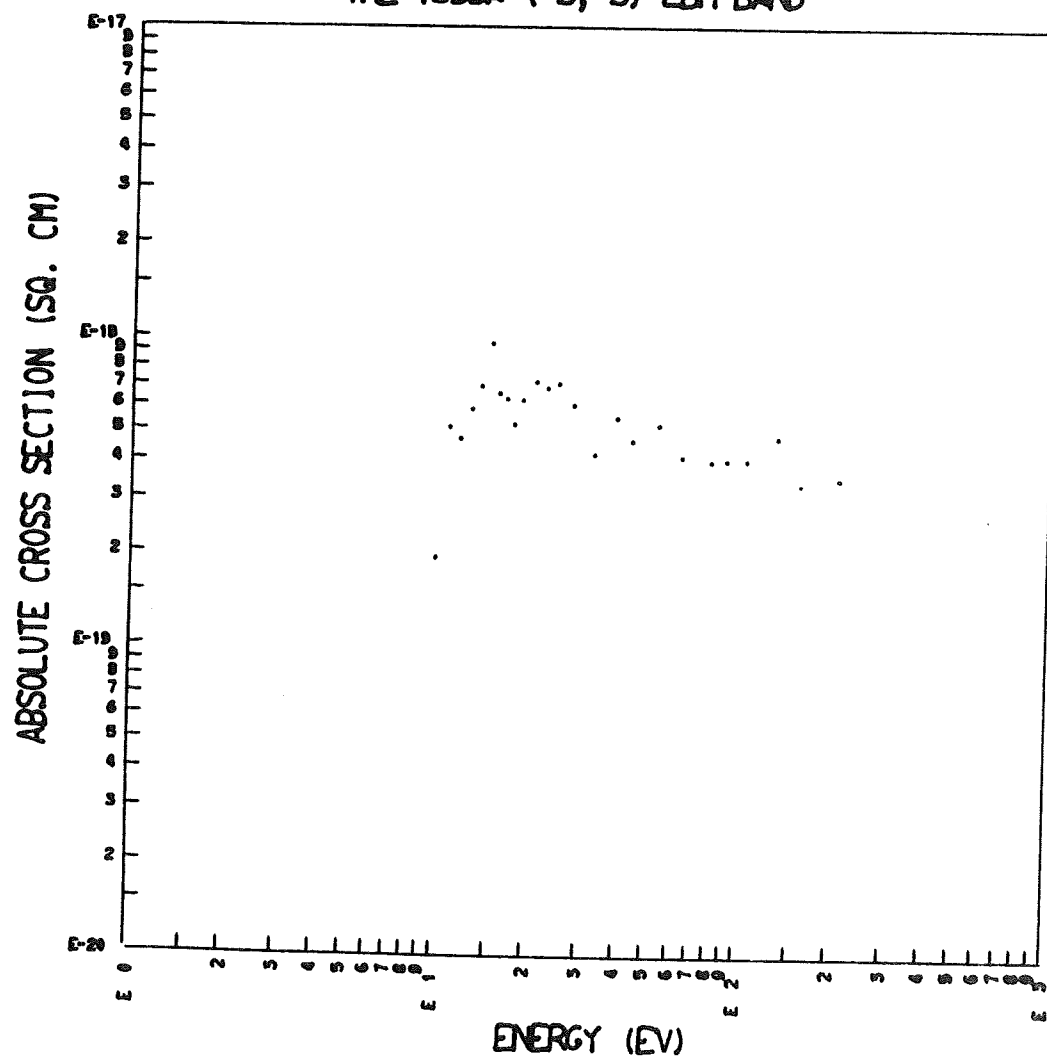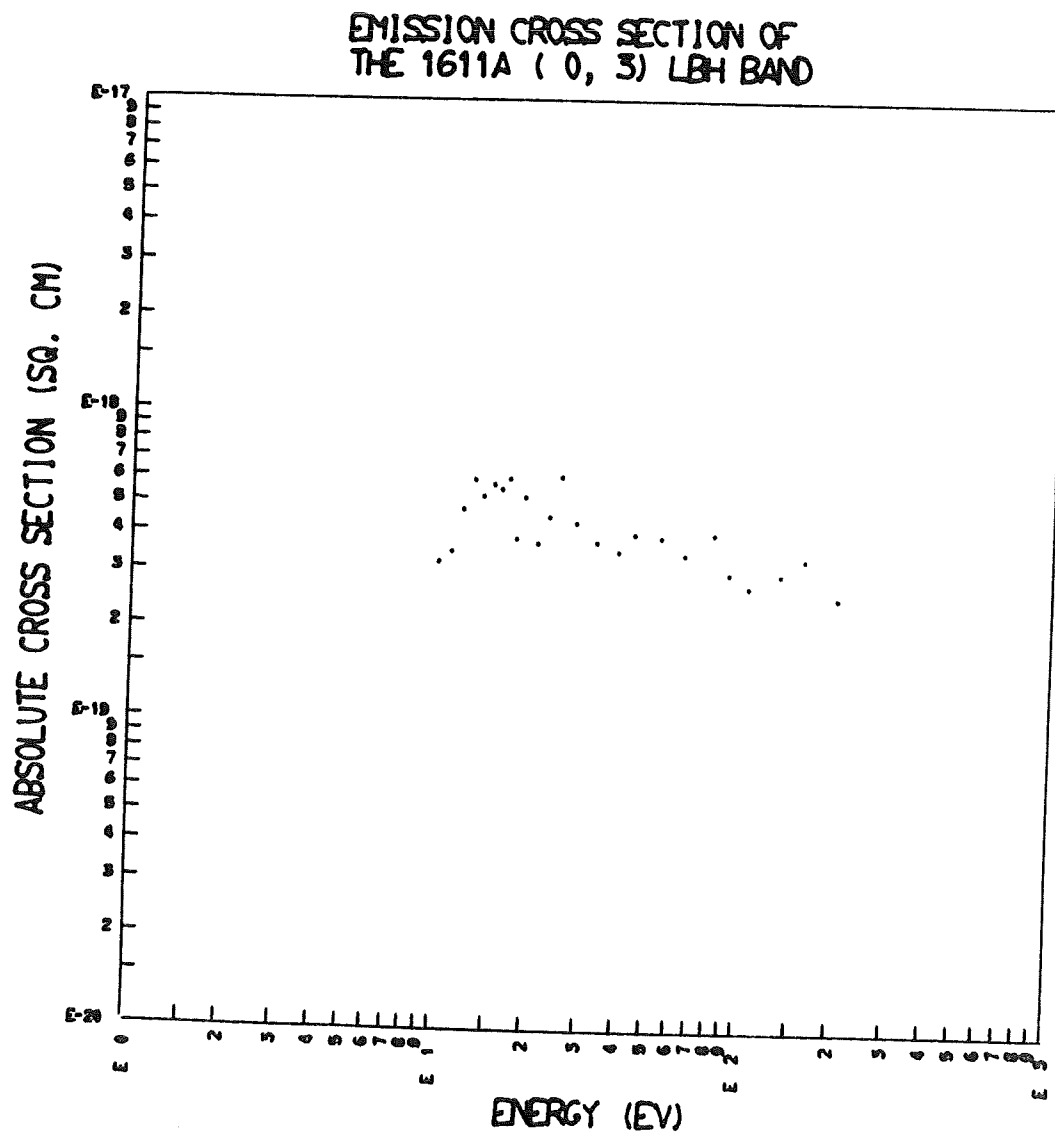
EMISSION CROSS SECTION OF
THE 1615A (4, 6) LBH BAND
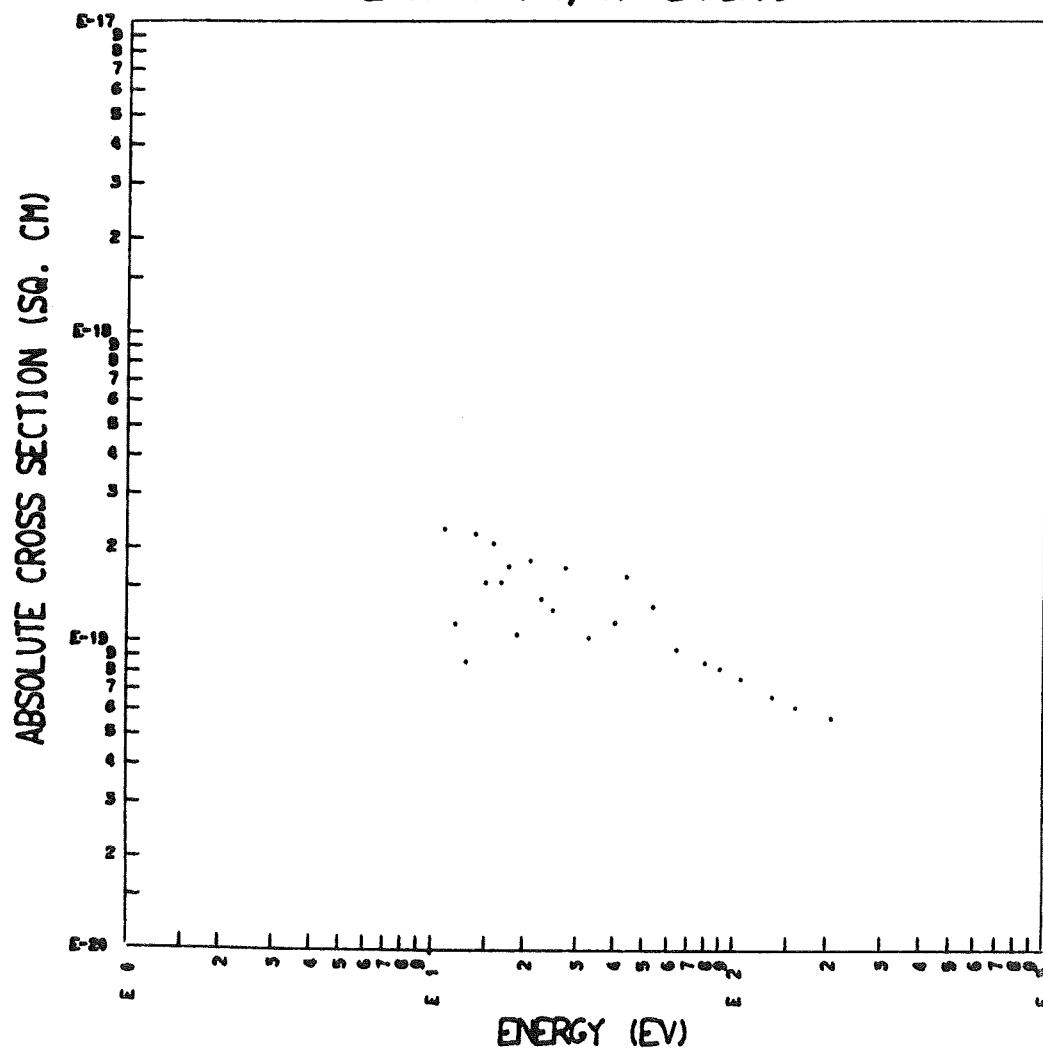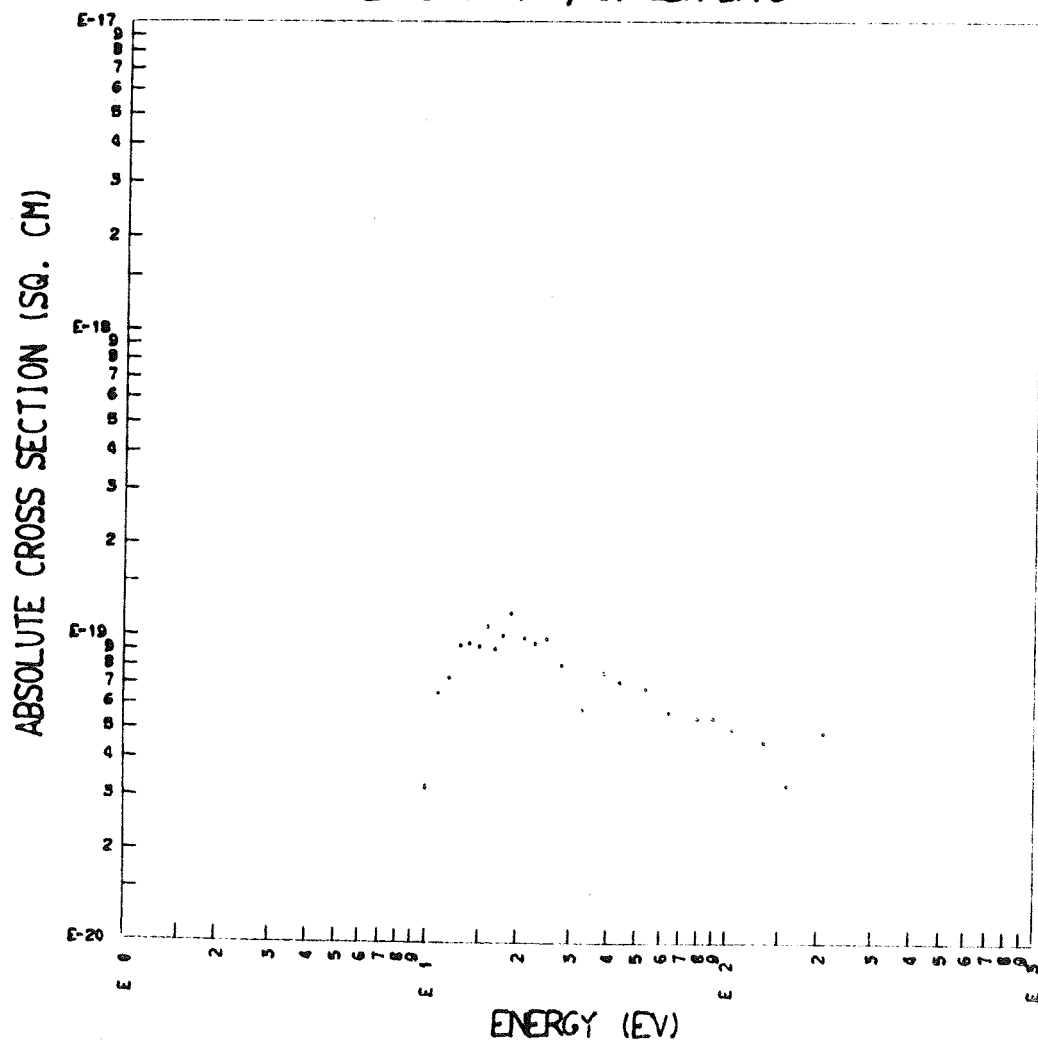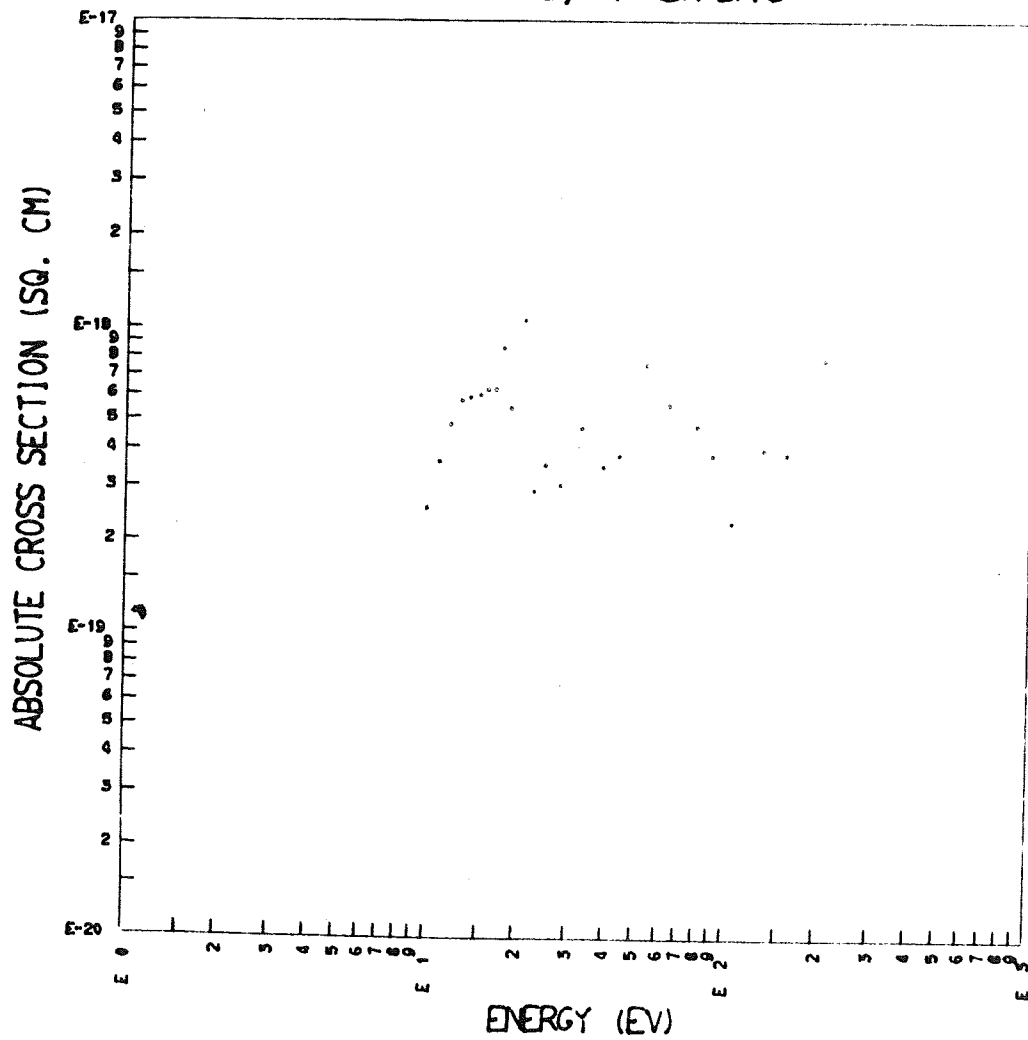
EMISSION CROSS SECTION OF
THE 1631A (5, 7) LBH BAND
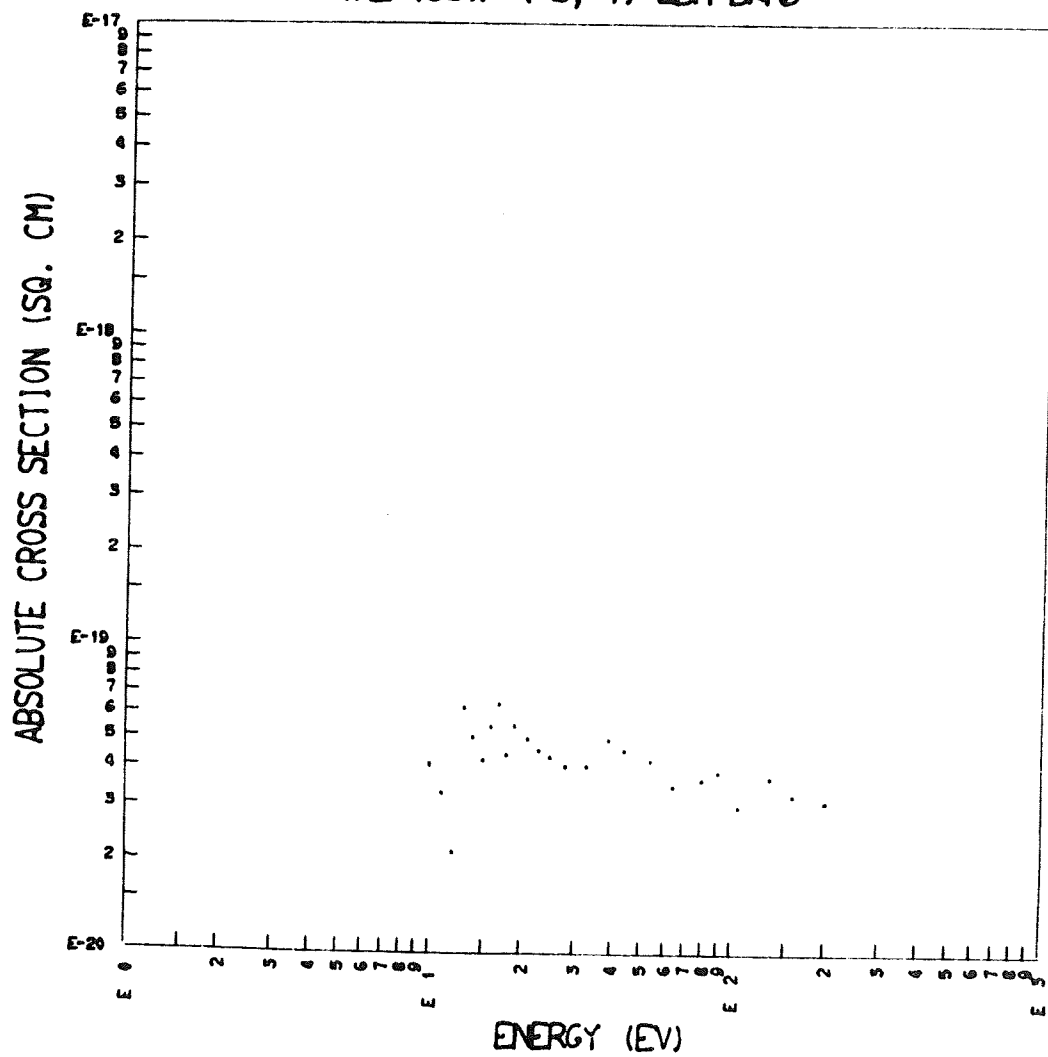
EMISSION CROSS SECTION OF
THE 1647A (6, 8) LBH BAND
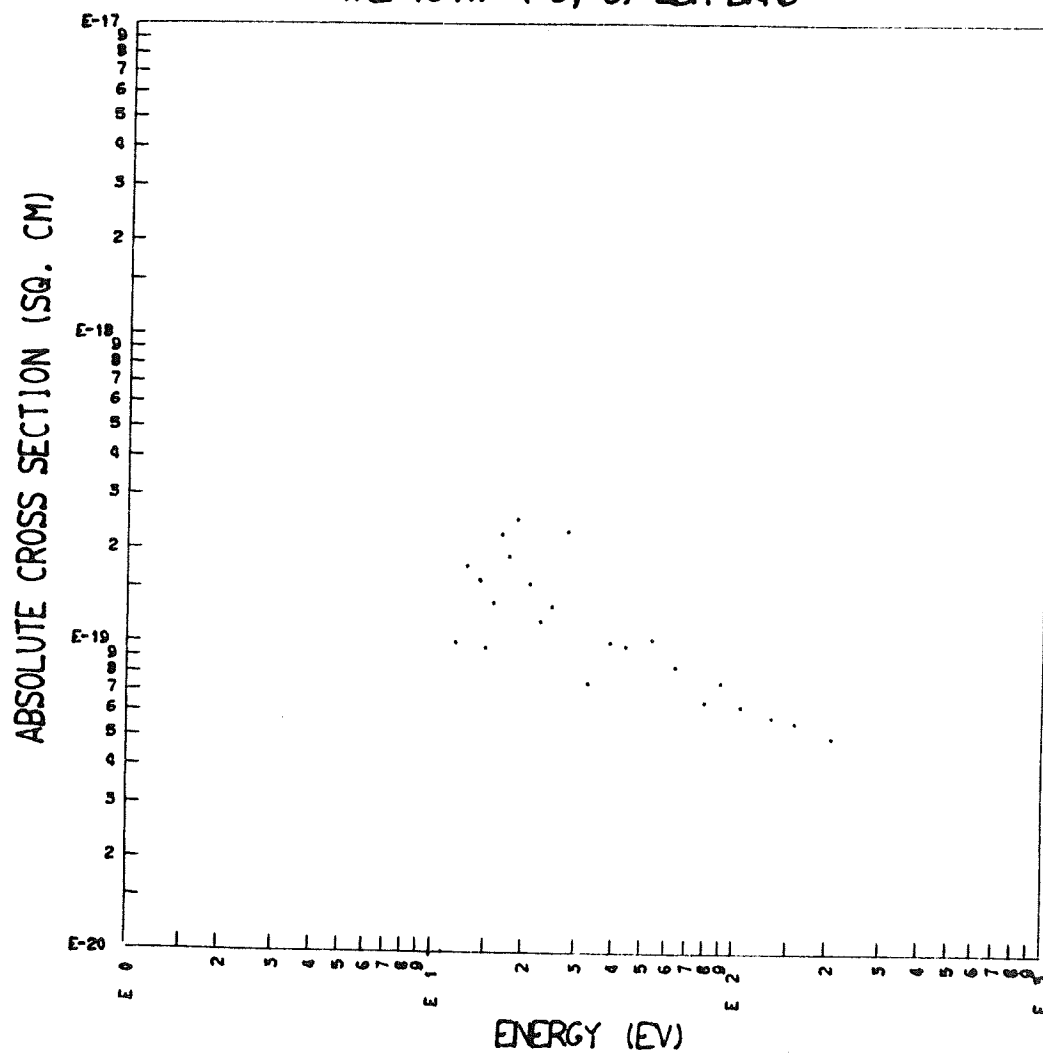
EMISSION CROSS SECTION OF
THE 1657A (3, 6) LBH BAND
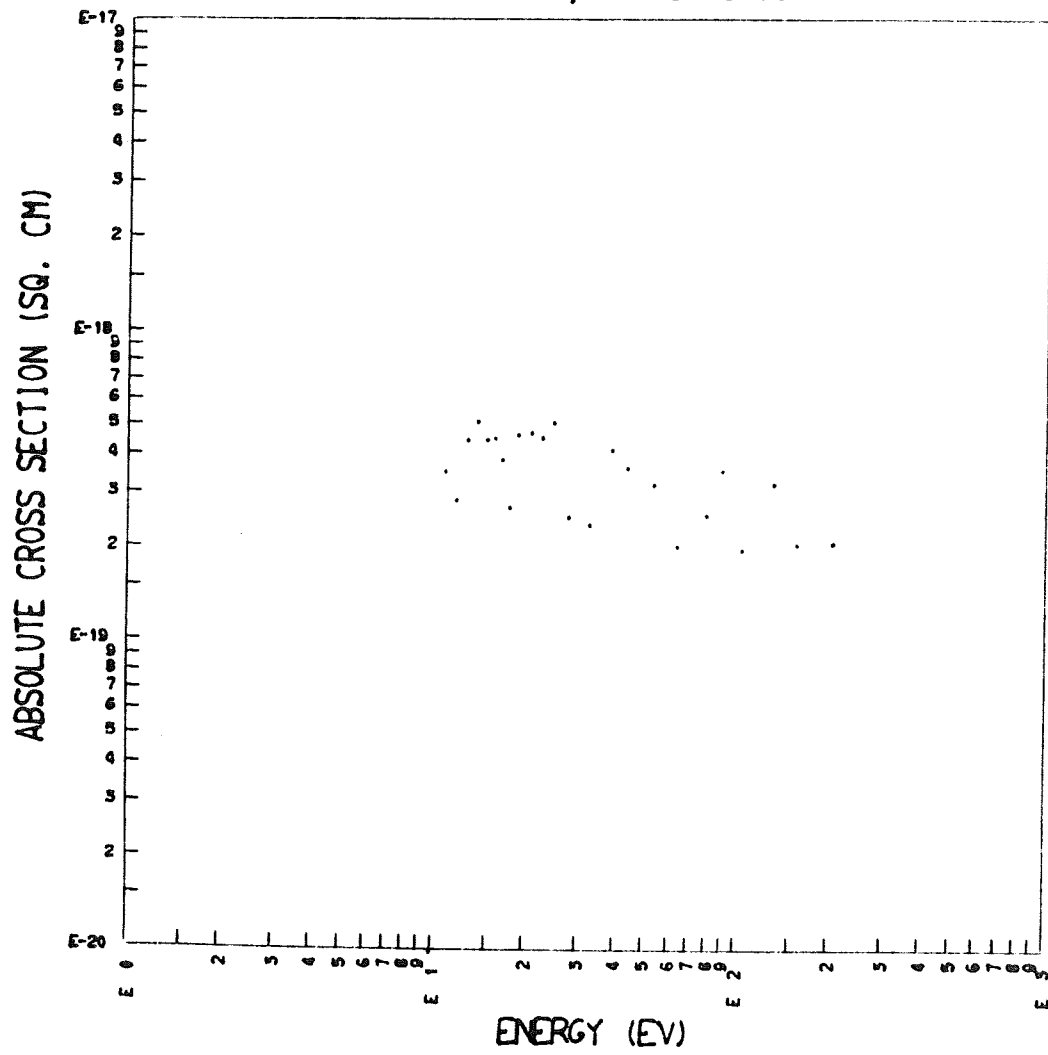
EMISSION CROSS SECTION OF
THE 1671A (0, 4) LBH BAND

ABSOLUTE CROSS SECTION (SQ. CM)

ENERGY (EV)
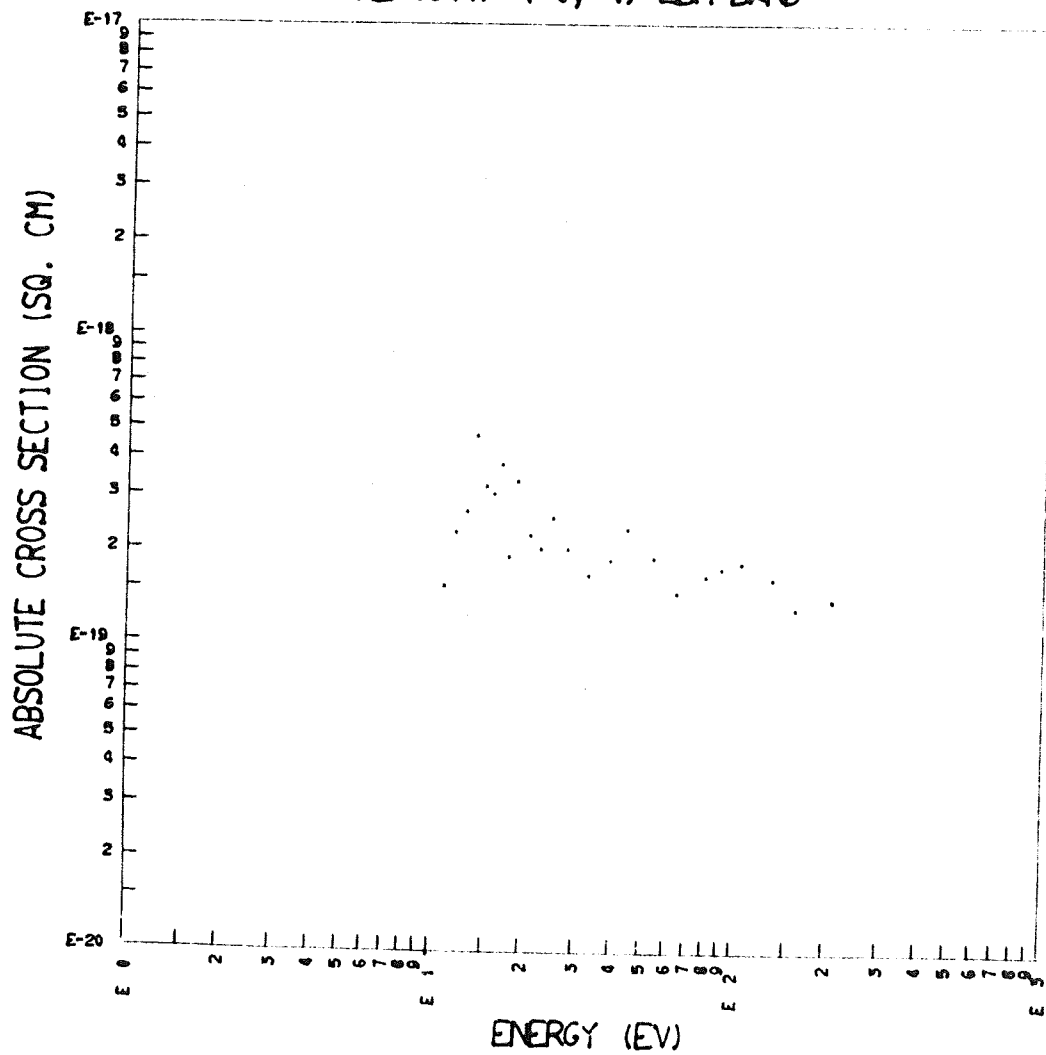
EMISSION CROSS SECTION OF
THE 1673A (4, 7) LBH BAND

ABSOLUTE CROSS SECTION (SQ. CM)

ENERGY (EV)
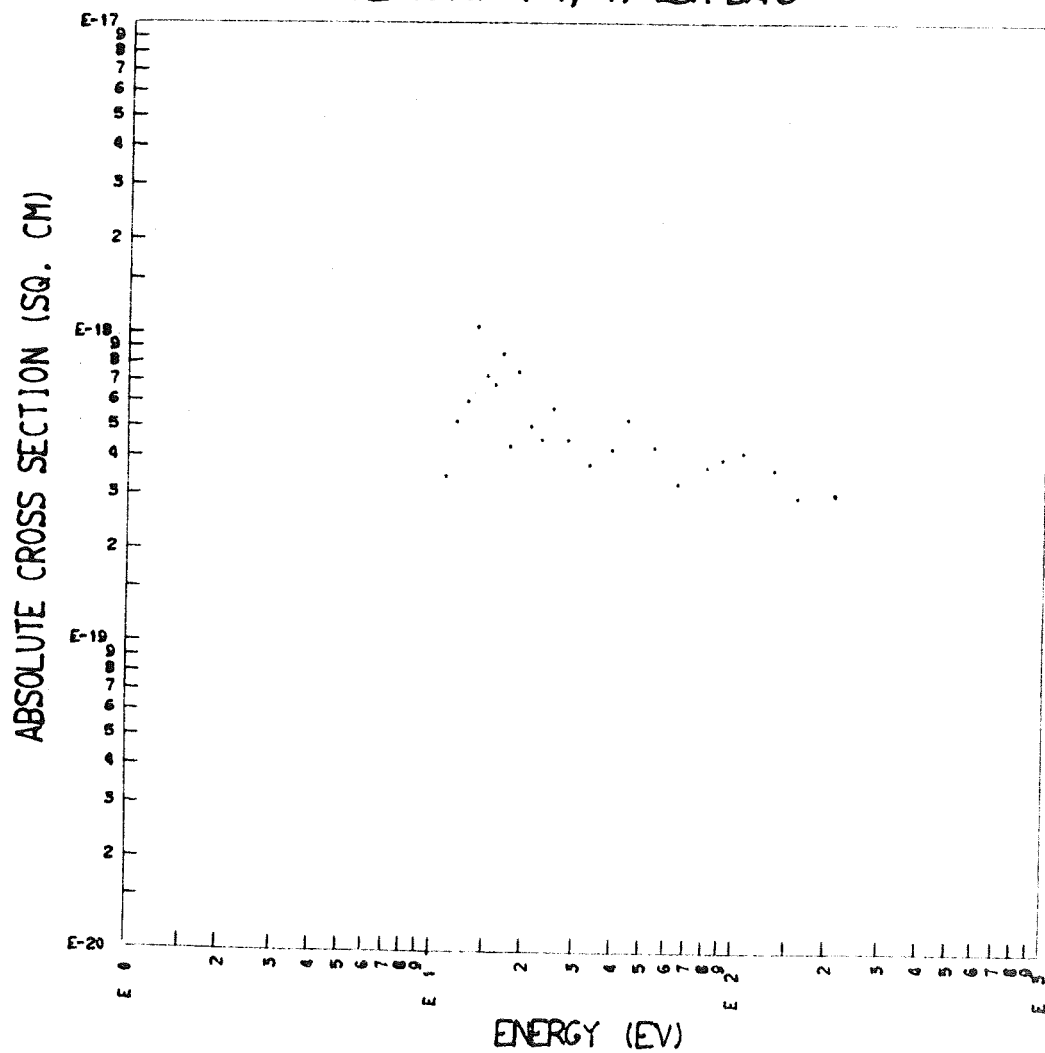
EMISSION CROSS SECTION OF
THE 1687A (1, 5) LBH BAND
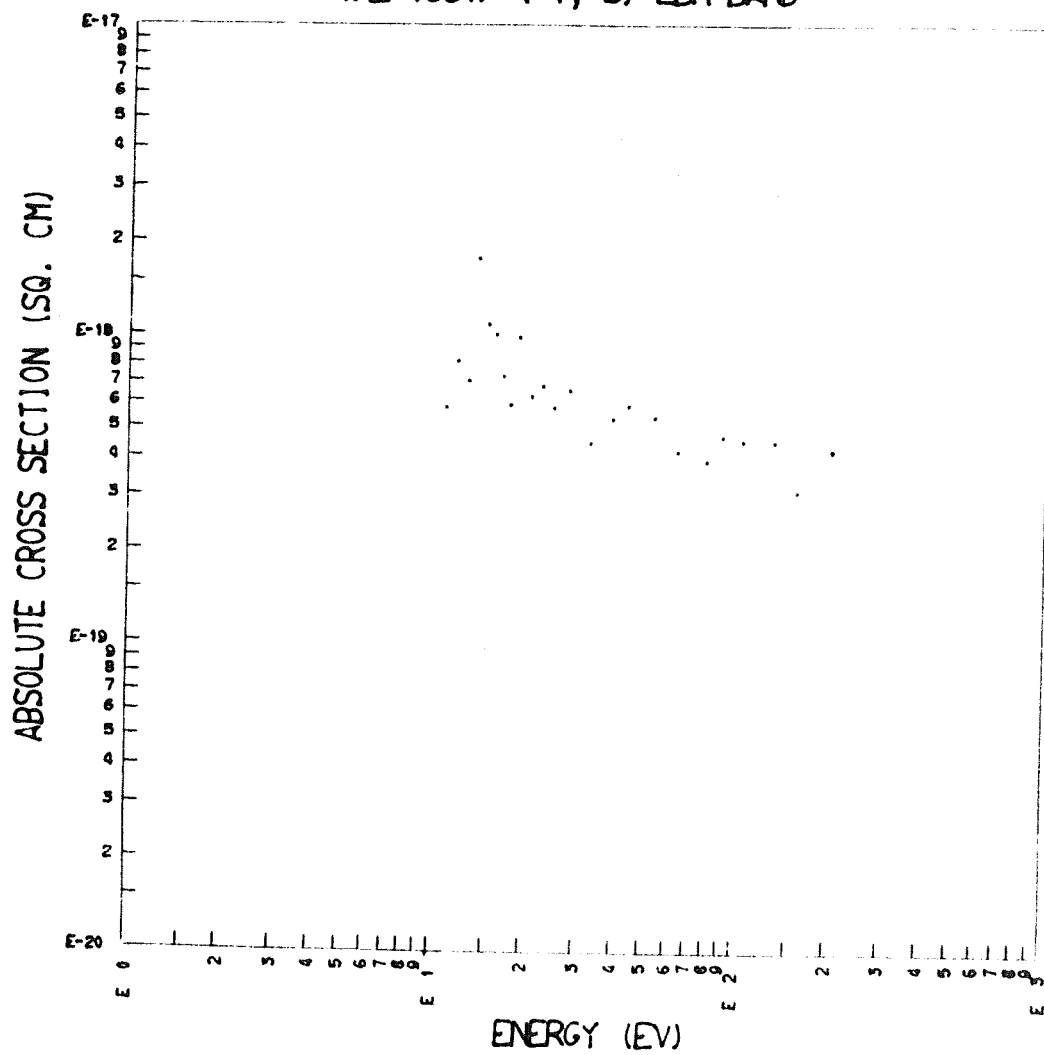
EMISSION CROSS SECTION OF
THE 1689A (5, 8) LBH BAND

ABSOLUTE CROSS SECTION (SQ. CM)

ENERGY (EV)
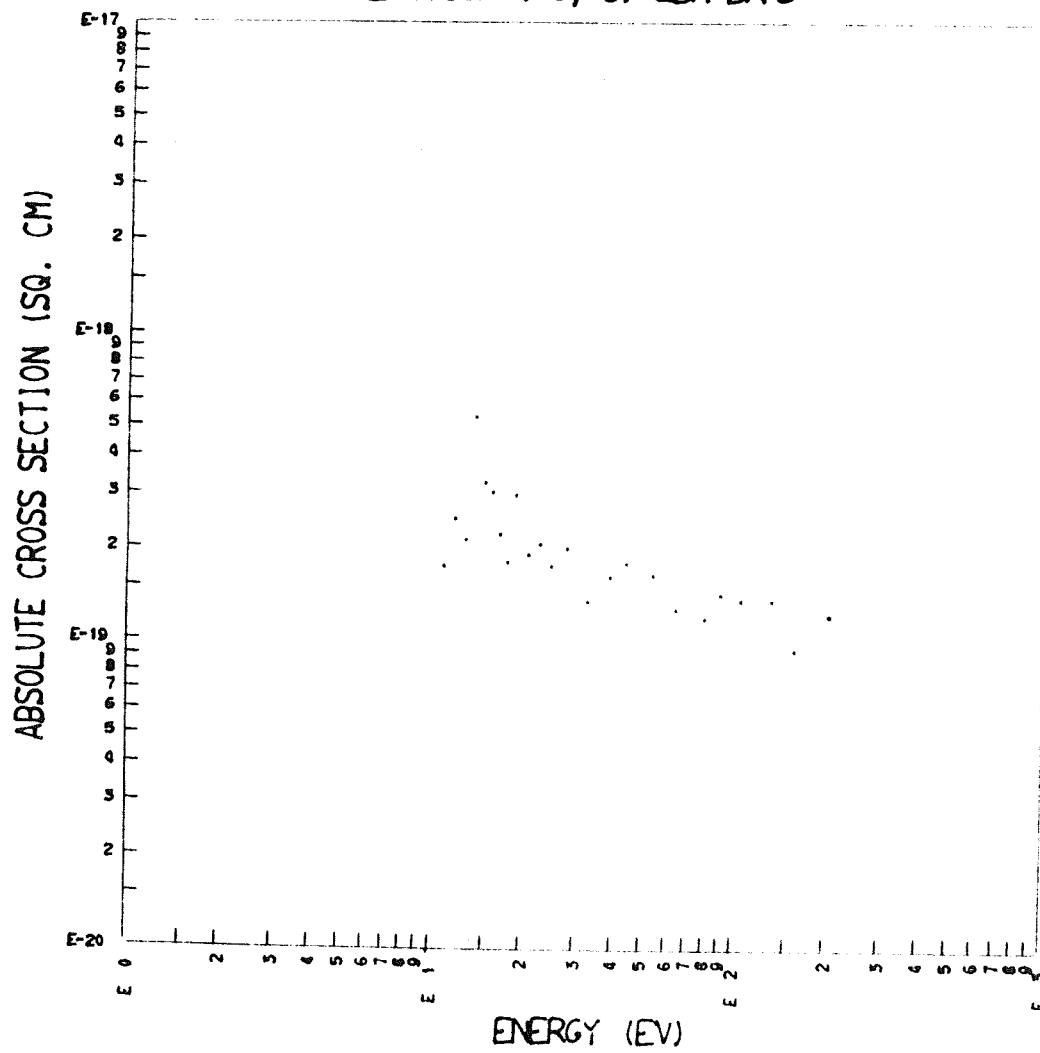
EMISSION CROSS SECTION OF THE 1703A (2, 6) LBH BAND
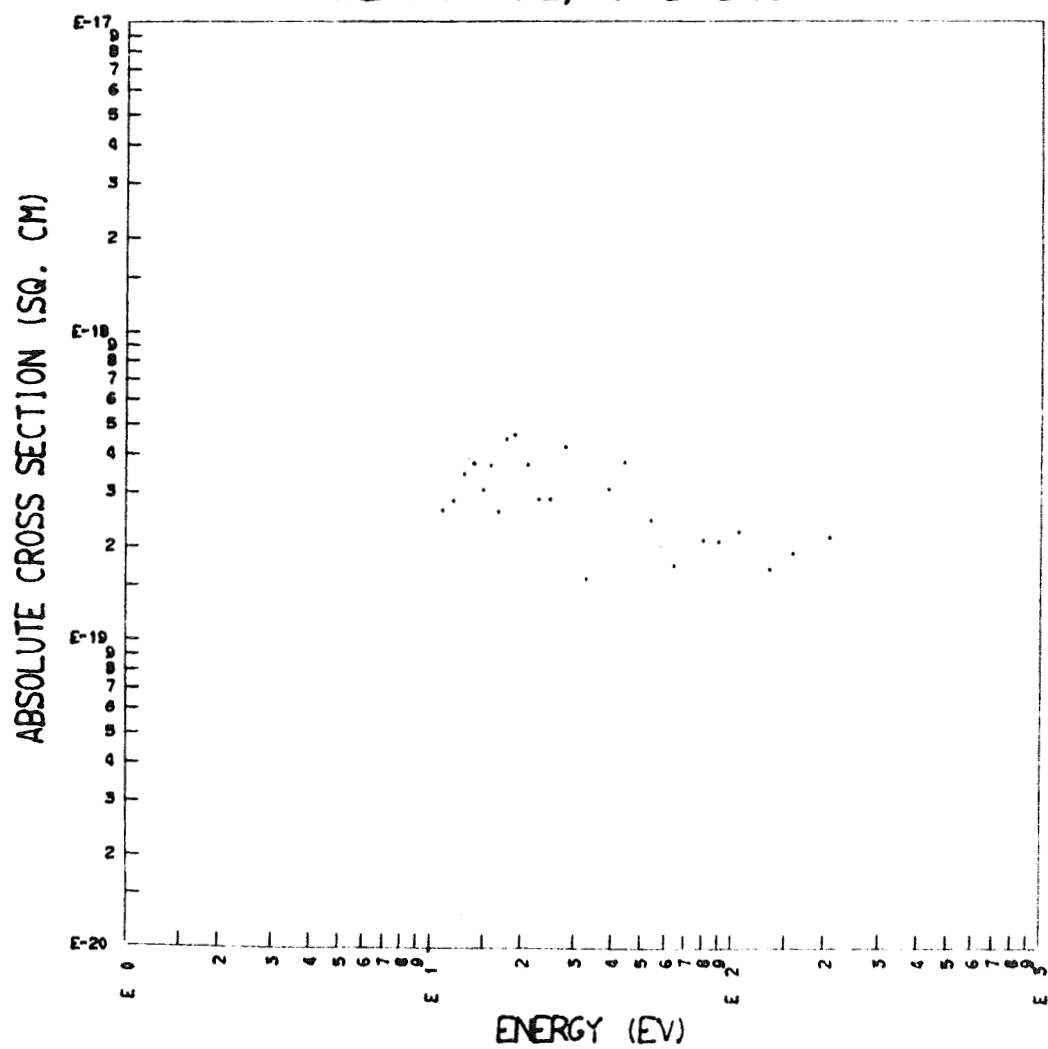
EMISSION CROSS SECTION OF
THE 1755A (4, 8) LBH BAND

ABSOLUTE CROSS SECTION (SQ. CM)

ENERGY (EV)
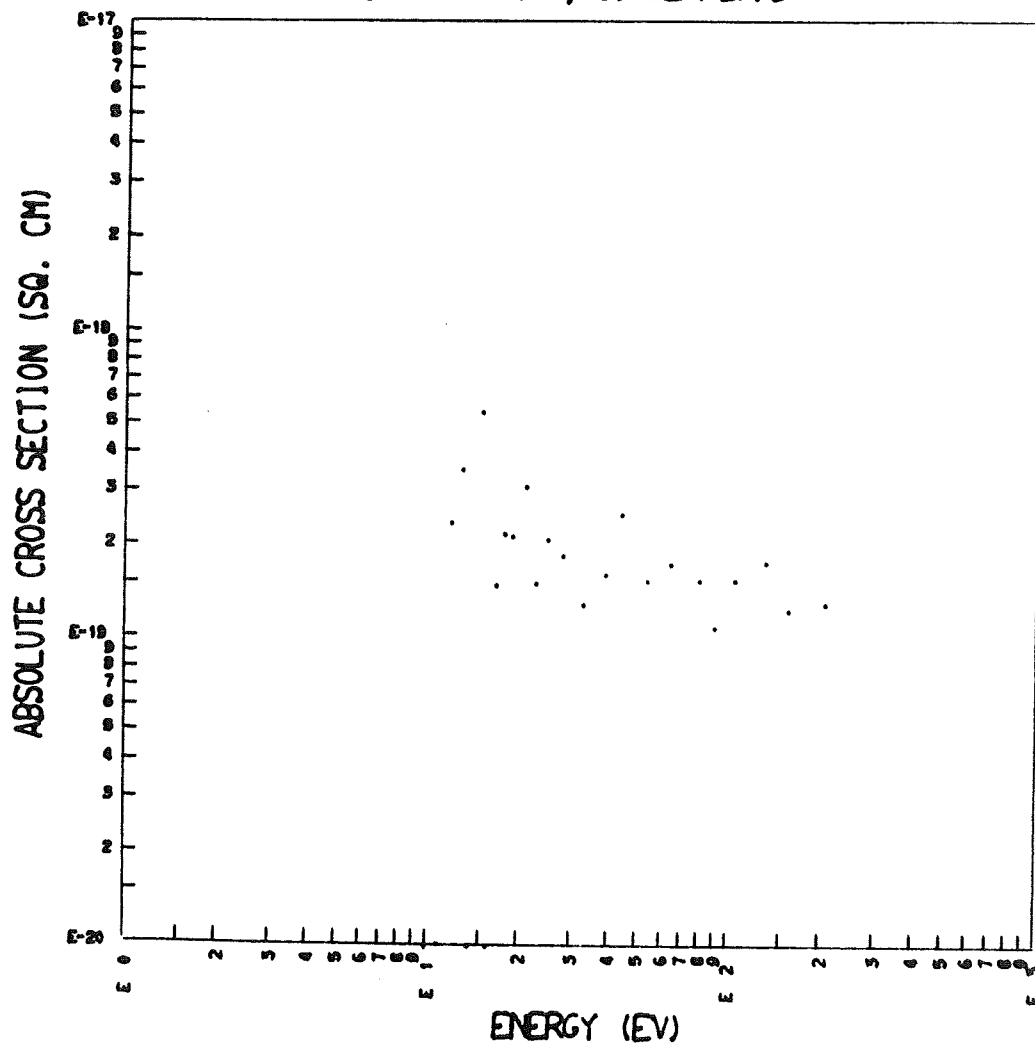
EMISSION CROSS SECTION OF THE 1756A (0, 5) LBH BAND

EMISSION CROSS SECTION OF
THE 1751A (5, 9) LBH BAND

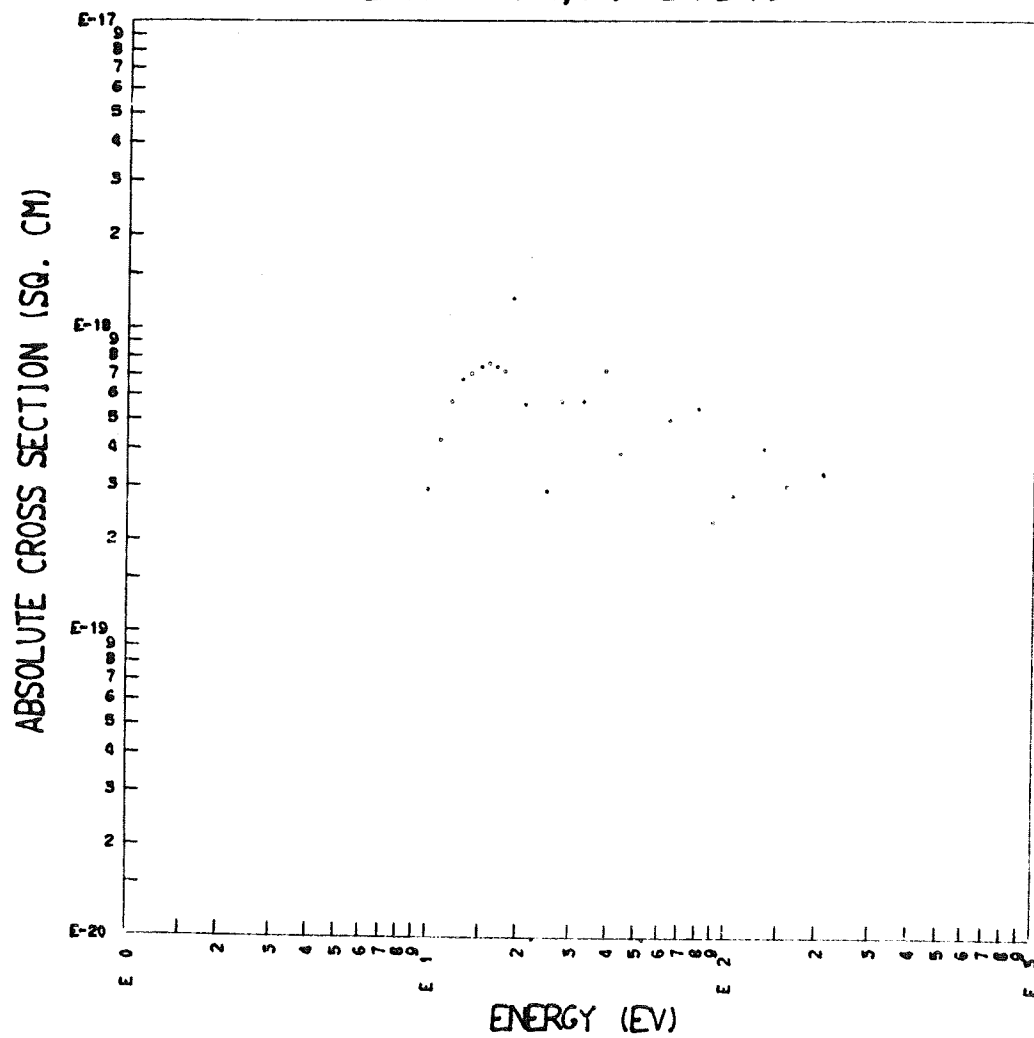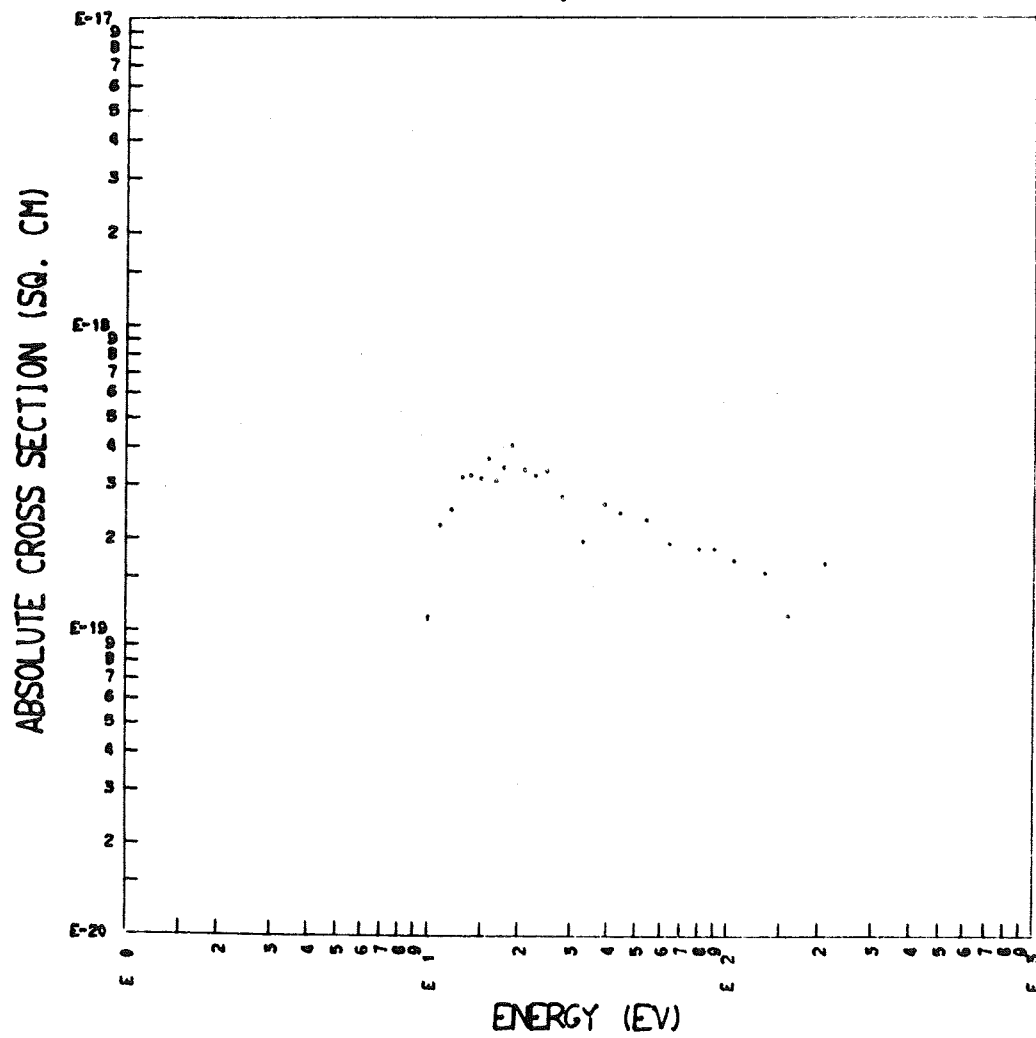EMISSION CROSS SECTION OF
THE 1752A (1, 6) LBH BAND

ABSOLUTE CROSS SECTION (SQ. CM)

ENERGY (EV)

EMISSION CROSS SECTION OF
THE 1768A (2, 7) LBH BAND

266

EMISSION CROSS SECTION OF THE 1769A (6,10) LBH BAND

EMISSION CROSS SECTION OF
THE 1784A (3, 8) LBH BAND

ABSOLUTE CROSS SECTION (SQ. CM)

ENERGY (EV)

EMISSION CROSS SECTION OF
THE 1801A (4, 9) LBH BAND

EMISSION CROSS SECTION OF
THE 1804A (0, 6) LBH BAND
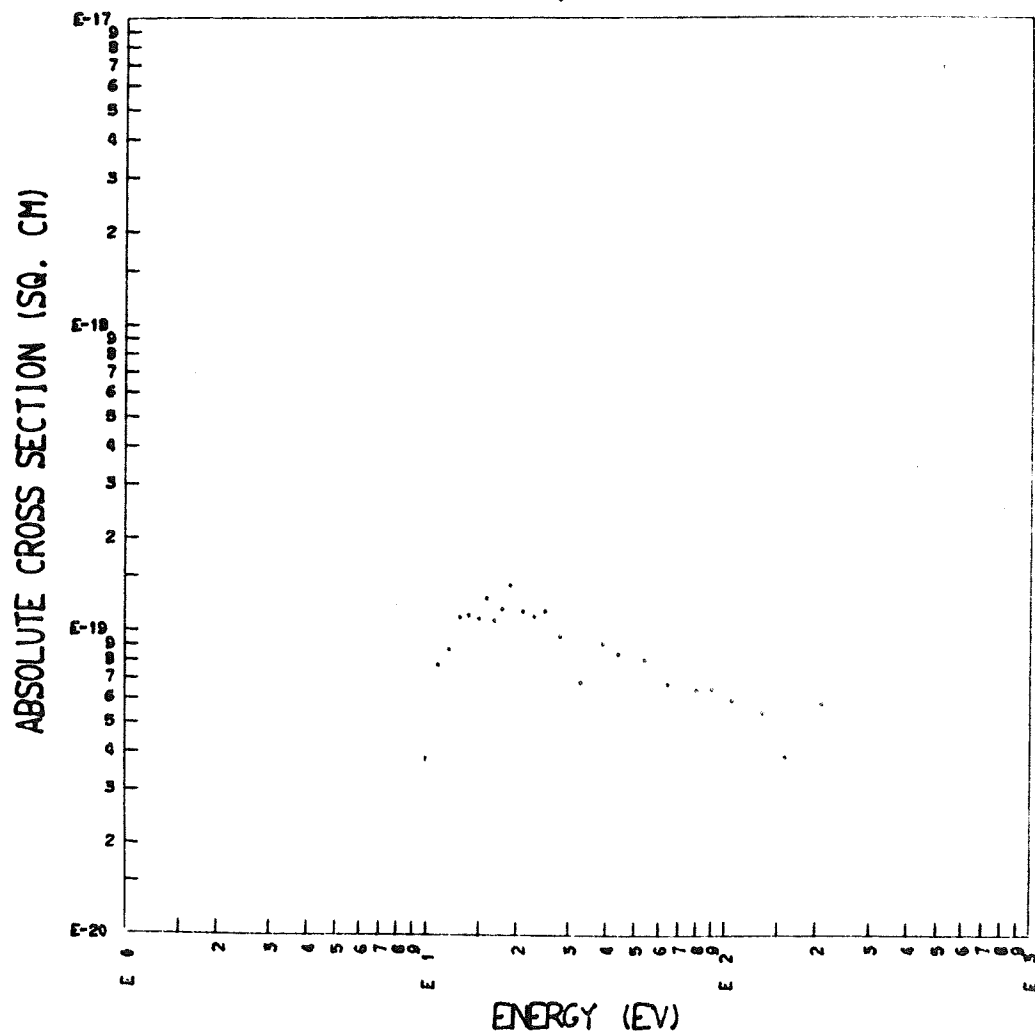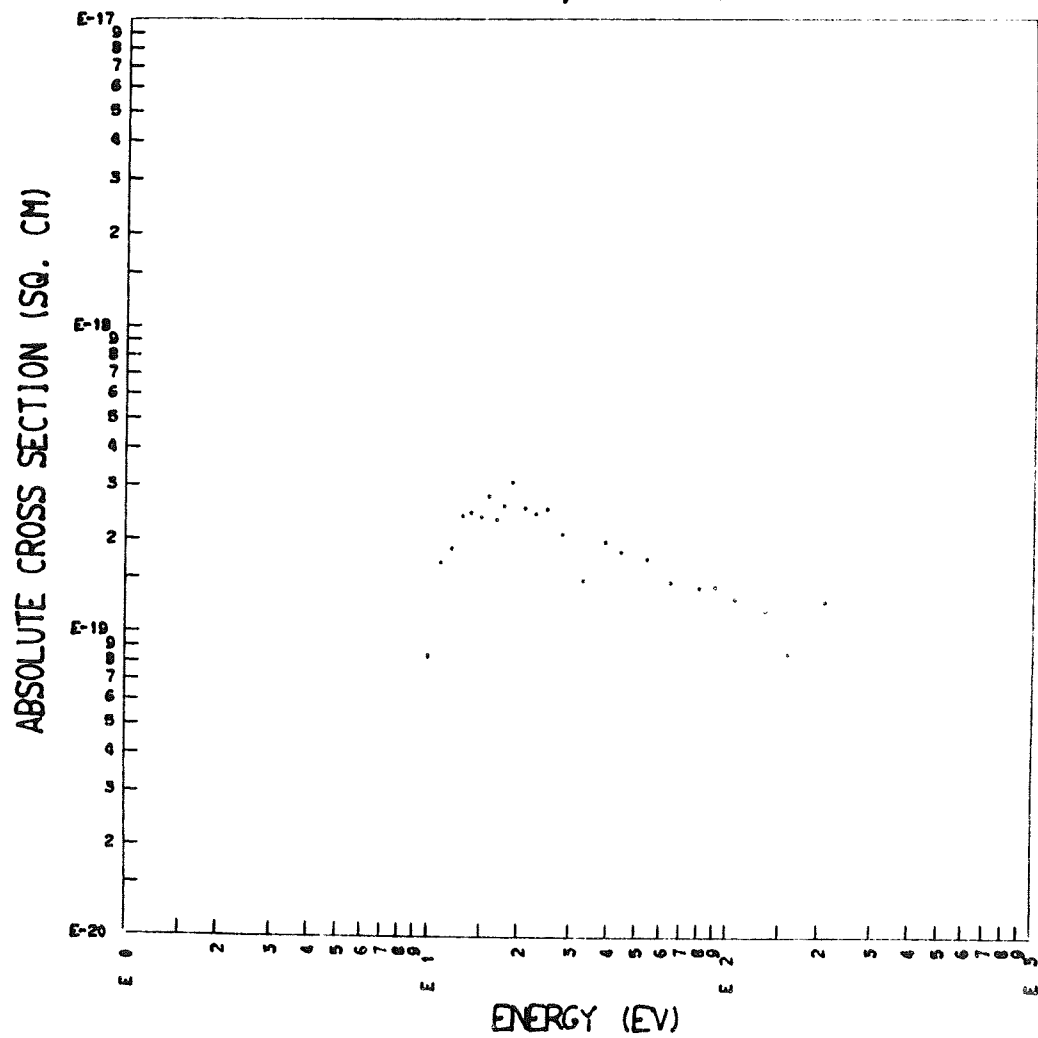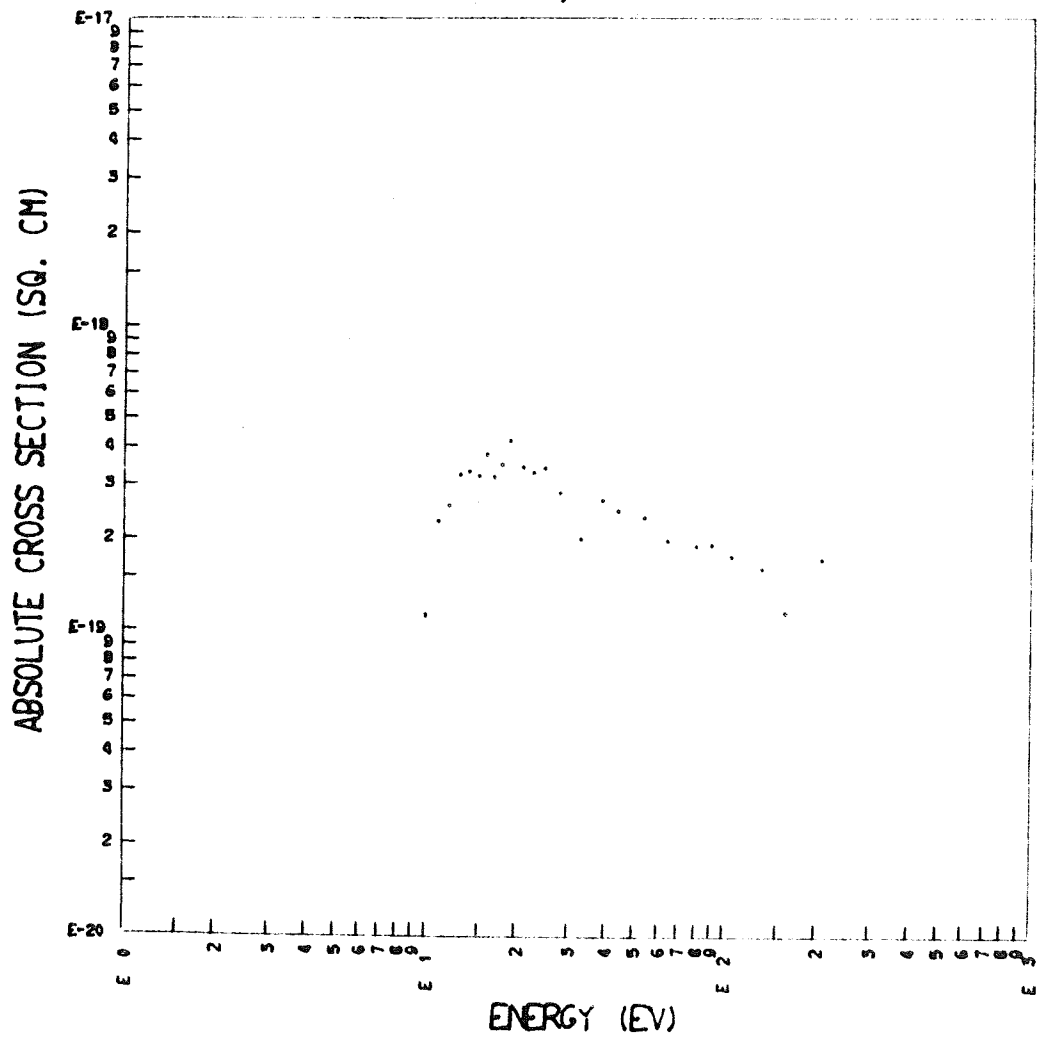
EMISSION CROSS SECTION OF
THE 1820A (1, 7) LBH BAND

ABSOLUTE CROSS SECTION (SQ. CM)

ENERGY (EV)

EMISSION CROSS SECTION OF
THE 1855A (6,11) LBH BAND

ABSOLUTE CROSS SECTION (SQ. CM)

ENERGY (EV)

EMISSION CROSS SECTION OF
THE 1857A (2, 8) LBH BAND

EMISSION CROSS SECTION OF
THE 1853A (3, 9) LBH BAND

ABSOLUTE CROSS SECTION (SQ. CM)

ENERGY (EV)

EMISSION CROSS SECTION OF THE 1870A (4,10) LBH BAND

ABSOLUTE CROSS SECTION (SQ. CM)

ENERGY (EV)

EMISSION CROSS SECTION OF
THE 1887A (5,11) LBH BAND

ABSOLUTE CROSS SECTION (SQ. CM)

ENERGY (EV)

EMISSION CROSS SECTION OF THE 1894A (1, 8) LBH BAND

EMISSION CROSS SECTION OF
THE 1910A (2, 9) LBH BAND

ABSOLUTE CROSS SECTION (SQ. CM)

ENERGY (EV)

EMISSION CROSS SECTION OF
THE 1927A (3,10) LBH BAND
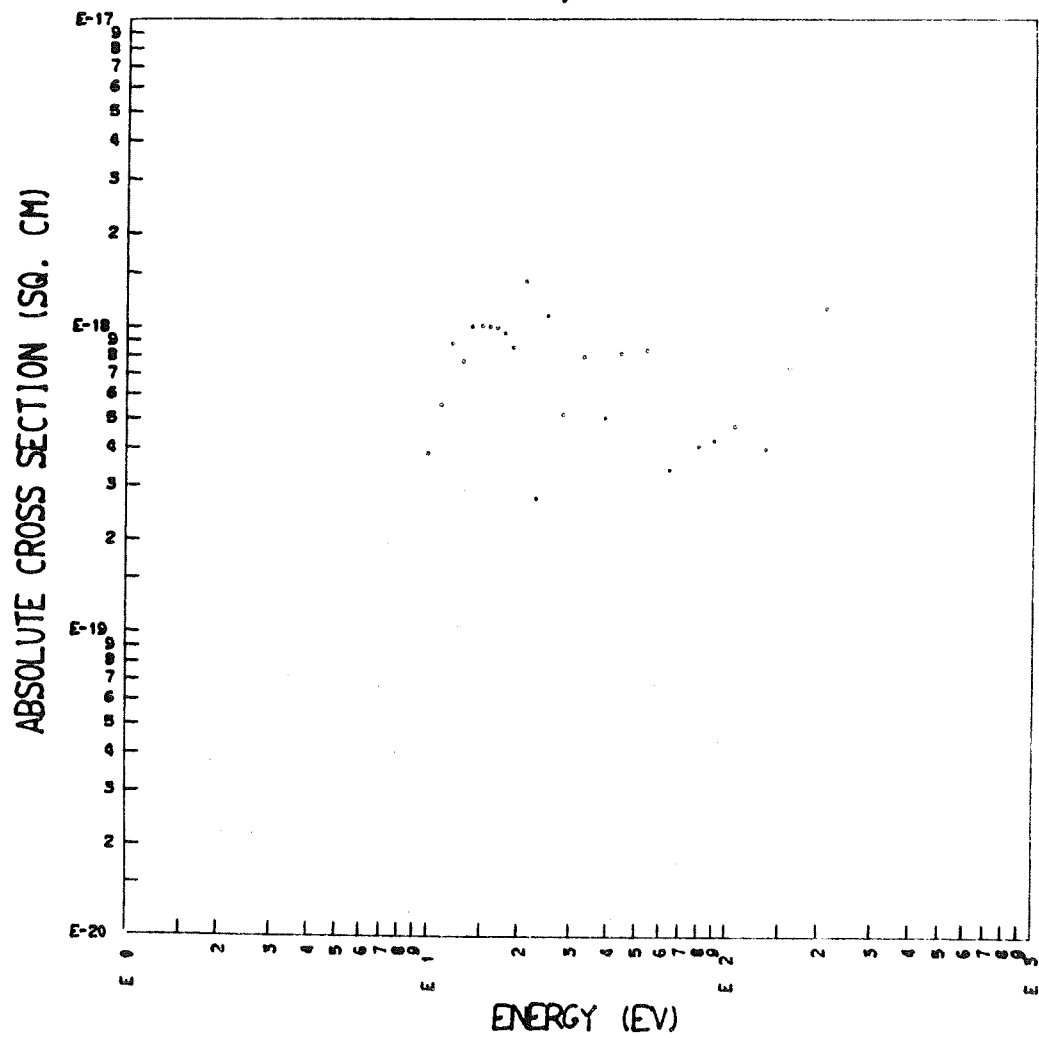
EMISSION CROSS SECTION OF THE 1945A (4,11) LBH BAND

ABSOLUTE CROSS SECTION (SQ. CM)

ENERGY (EV)

EMISSION CROSS SECTION OF
THE 1962A (5,12) LBH BAND

EMISSION CROSS SECTION OF
THE 1980A (6,13) LBH BAND
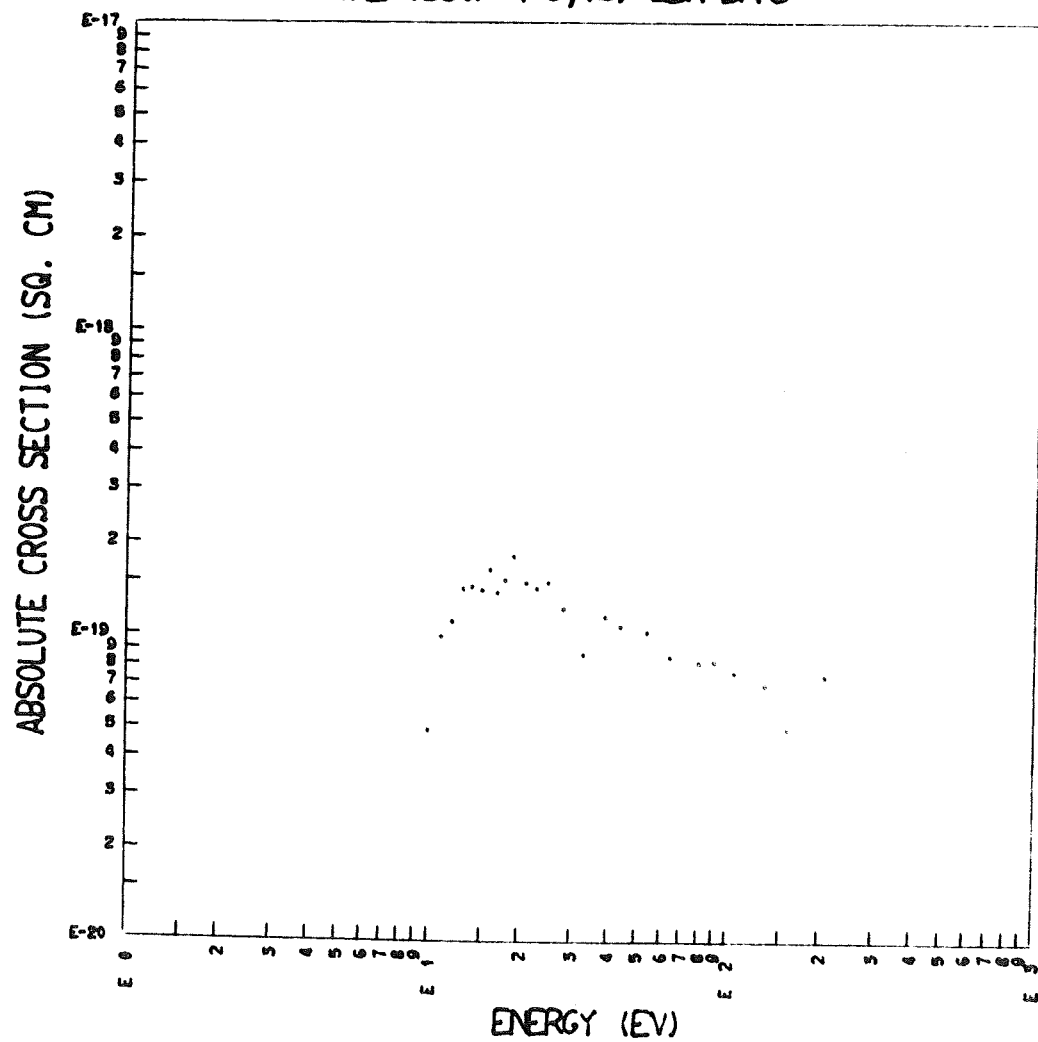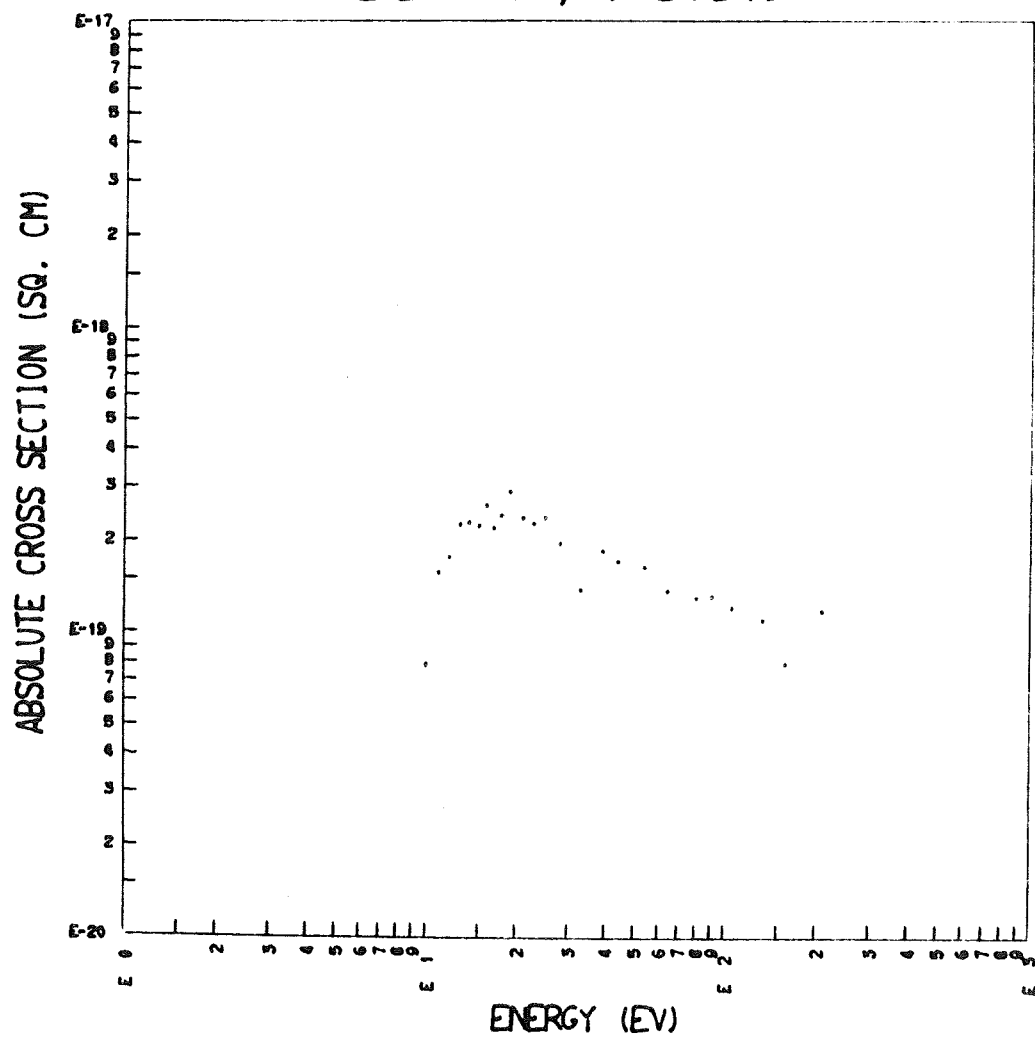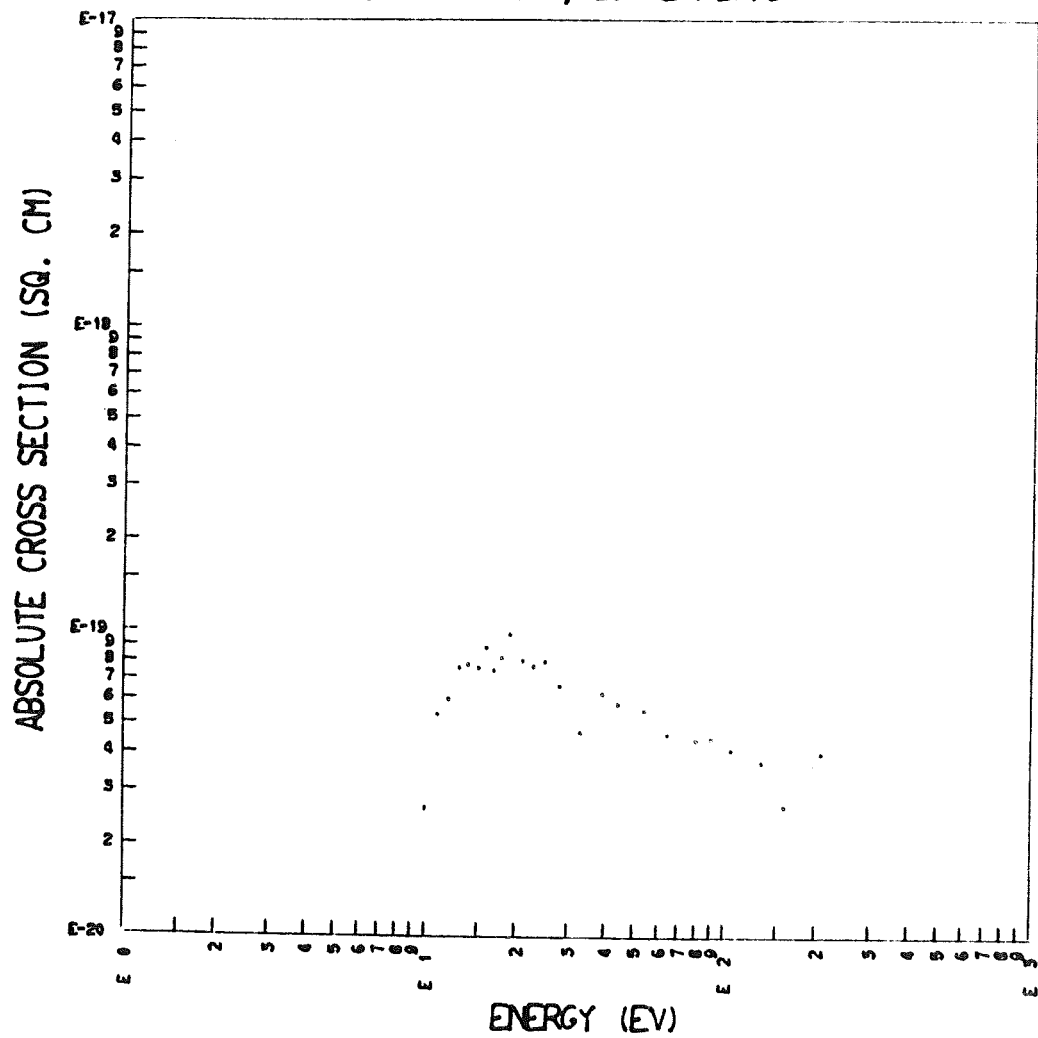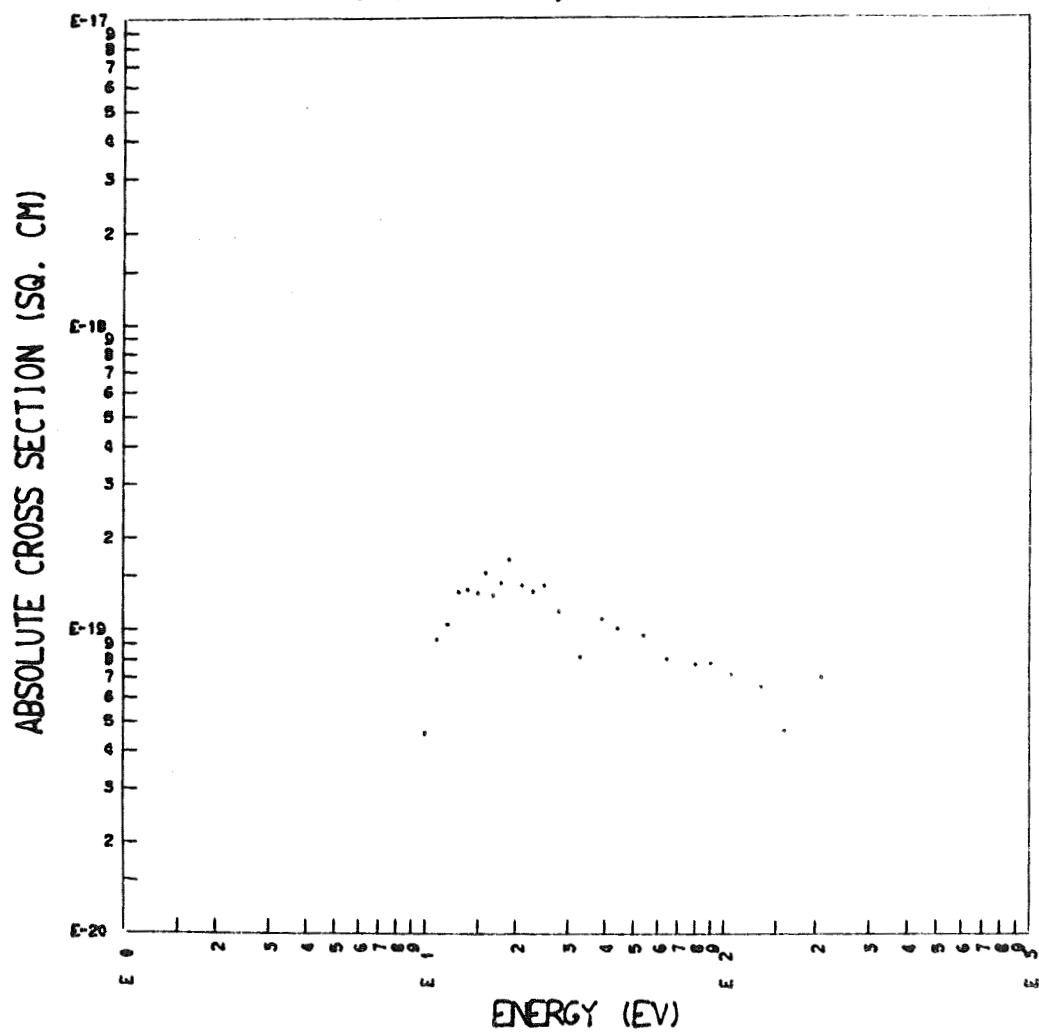
EMISSION CROSS SECTION OF
THE 1989A (2,10) LBH BAND

ABSOLUTE CROSS SECTION (SQ. CM)

ENERGY (EV)

EMISSION CROSS SECTION OF
THE 2006A (3,11) LBH BAND

ABSOLUTE CROSS SECTION (SQ. CM)

ENERGY (EV)

EMISSION CROSS SECTION OF
THE 2024A (4,12) LBH BAND

EMISSION CROSS SECTION OF
THE 2041A (5,13) LBH BAND

ABSOLUTE CROSS SECTION (SQ. CM)

ENERGY (EV)

EMISSION CROSS SECTION OF
THE 2059A (6,14) LBH BAND

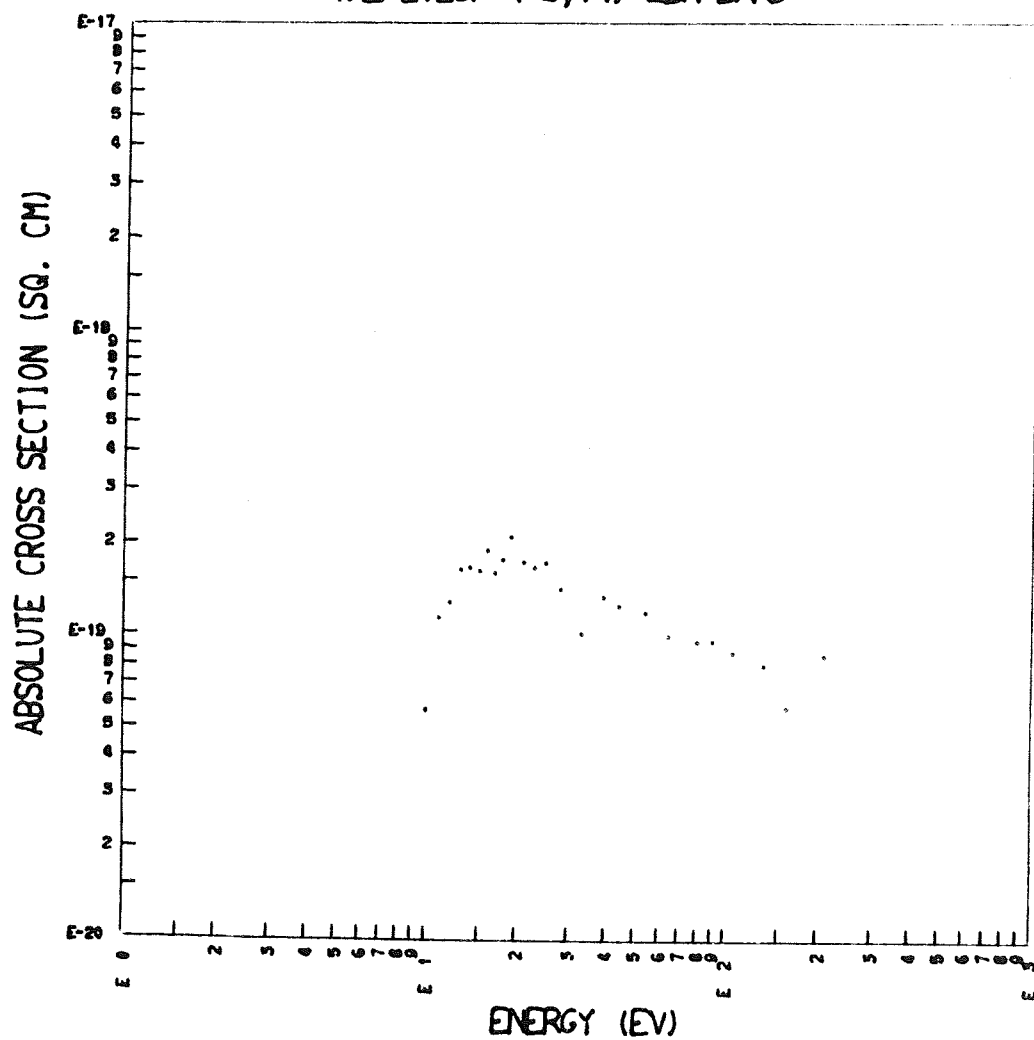ABSOLUTE CROSS SECTION (SQ. CM)
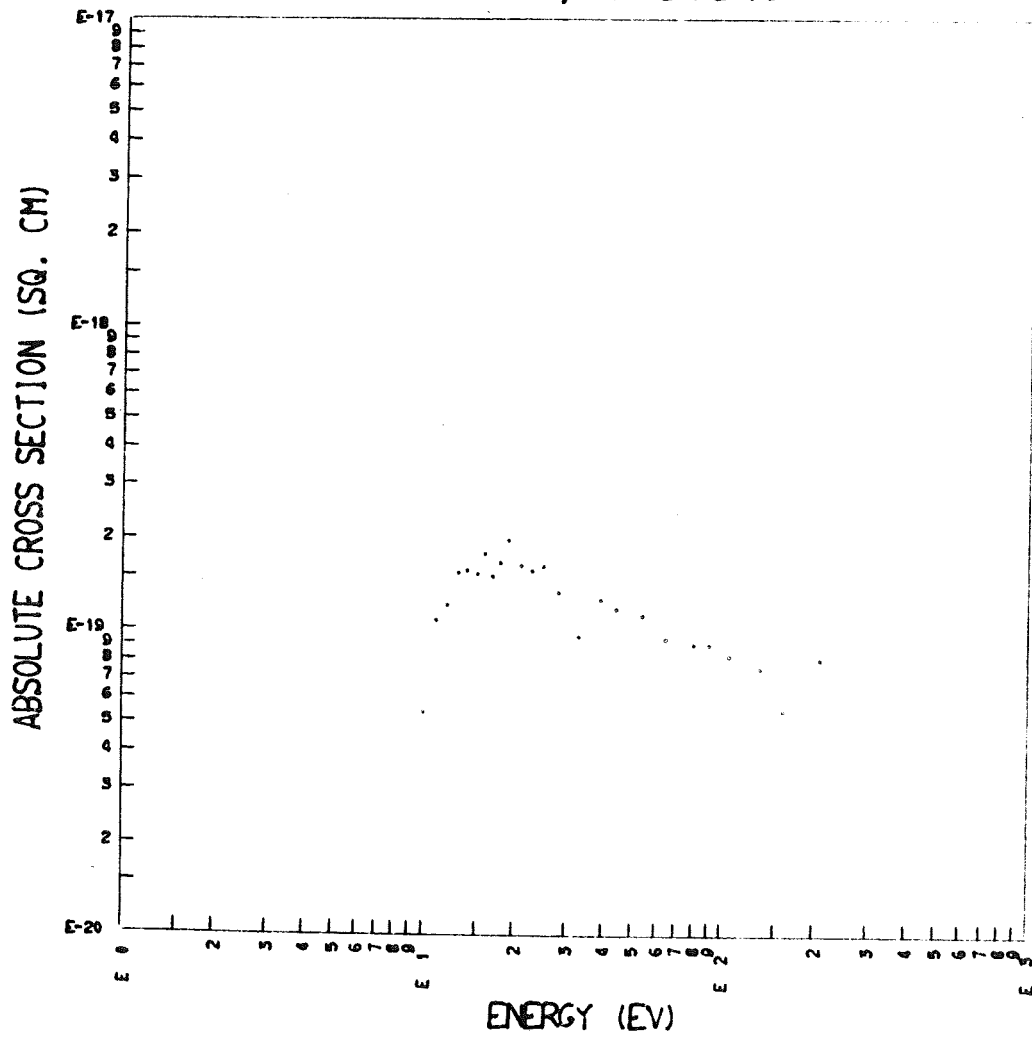
ENERGY (EV)

EMISSION CROSS SECTION OF
THE 2091A (3,12) LBH BAND
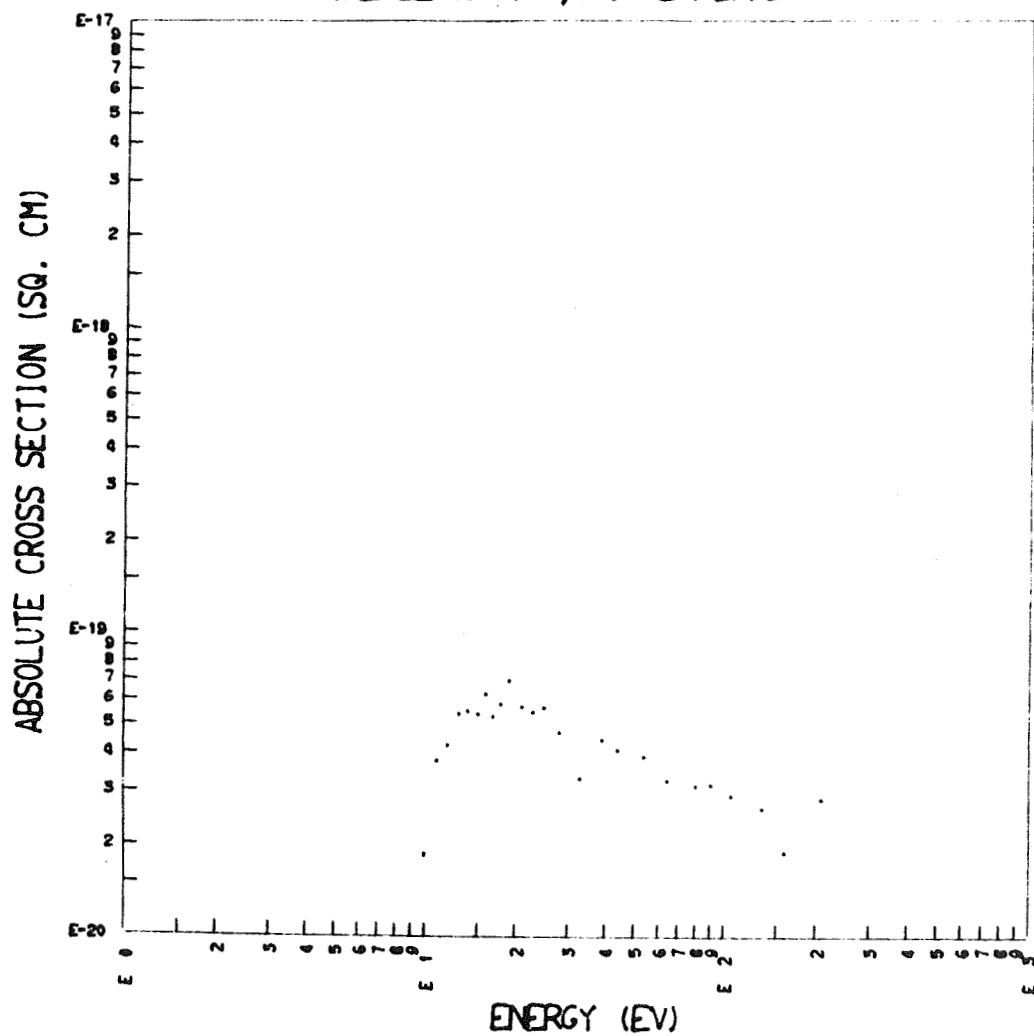
EMISSION CROSS SECTION OF
THE 2108A (4,13) LBH BAND

EMISSION CROSS SECTION OF
THE 2126A (5,14) LBH BAND

ABSOLUTE CROSS SECTION (SQ. CM)

ENERGY (EV)

EMISSION CROSS SECTION OF
THE 2144A (6,15) LBH BAND

EMISSION CROSS SECTION OF
THE 2216A (5,15) LBH BAND

EMISSION CROSS SECTION OF
THE 2234A (6,16) LBH BAND